(Bah)

International Atomic Energy Agency

INDC/156

NUCLEAR DATA FOR REACTORS

(Nuclear Data - Microscopic Cross Sections
and other Data Basic for Reactors)

Supplement to the Proceedings of a Conference
Paris, 17-21 October 1966

(66 PARIS)

International Atomic Energy Agency
Vienna 1967

NUCLEAR DATA FOR REACTORS

Nuclear Data - Microscopic Cross Sections and other Data Basic for Reactors

IAEA, 1967

Nuclear Data - Microscopic Cross Sections and other Data Basic for Reactors

This volume contains the full texts of those papers that for lack of time and to obtain a suitable geographical distribution could not be orally presented at the Conference. The papers are directly reproduced from authors' submitted manuscripts, and no editing or re-typing has been done. This volume is being made available on the recommendation and under the auspices of the International Nuclear Data Committee. It can be requested from the IAEA Nuclear Data Unit, Kaerntnerring 11-13, 1010 Vienna, Austria.

Paper no.	Title	Author(s)
CN-23/7	The fission cross-sections of some plutonium isotopes in the neutron energy range 5-150 keV	W.B. Gilboy, G.F. Knoll
8	Measurements of Effective (Resonance-shielded) Neutron Cross Sections in the keV Region	H. Miessner, E. Arai
11	A Novel Method for Very High Resolution Cross-Section Measurements	S. Cierjacks et al.
12	Measurements of 14 MeV Neutron Induced Reaction Cross Sections Using Enriched Isotopes of Calcium	P.N. Tiwari, E. Kondaiah
14	Basic Nuclear Data for Fast Reactor Calculations	M. Segev et al.
18	The (n,2n) cross sections of ^{9}Be and D in the threshold regions	M. Holmberg, J. Hansén
24	Mechanised Evaluation of Neutron Cross Sections	A. Horsley, J.B. Parker
31	Neutron resonance parameters of ^{240}Pu	M. Asghar et al.
37	Elastic and Inelastic Neutron Cross-Sections	D. Wilmore
50	Analytical Description of Neutron Cross Sections and the Effect of their Energy Dependence Upon their 2200 m/sec Values	J.R. Smith
51	Neutron Capture Between 5 keV and 3 MeV	D.C. Stupegia et al.
59	Gamma Rays from Neutron Inelastic Scattering in Germanium	J.F. Barry
64	Dependance de la fonction densite S_o suivant la valeur du spin	J. Julien et al.
66	Etude des spectres de rayonnements gamma de capture á l'aide de détécteurs Ge-Li	H. Jackson et al.

- continued

Paper no.	Title	Author(s)
CN-23/69	Sections efficaces total et de fission du Np-237	D. Paya et al.
73	Table des integrales de resonance	R. Vidal, F. Roullier
80	The Influence of Chemical Binding on Neutron Cross-Sections at Higher Energies	K. Drittler
92	The Role of Isotopic Composition Measurements in Cross Section Evaluation	P.G. Aline
106	Level Density and the Structure of Atomic Nuclei	Yu.N. Shubin et al.
113	The Dependence of the Symmetrical U-238 Fission Cross-Section on Neutron Energy	N.I. Borisova et al.
114	Evaluation of the Elastic and Inelastic Scattering Cross Sections of 14 MeV Neutrons for Even-Even Nuclei	L. Zuffi
127	Integral and Differential Neutron Fission Cross Section of Th-232	S.B. Ermagambetov et al.

INTERNATIONAL ATOMIC ENERGY AGENCY

CONFERENCE ON NUCLEAR DATA - MICROSCOPIC CROSS SECTIONS AND OTHER DATA BASIC FOR REACTORS

Paris, October 17 - 21, 1966

CN-23/7

THE FISSION CROSS-SECTIONS OF SOME PLUTONIUM ISOTOPES IN THE NEUTRON ENERGY RANGE 5-150 keV

W. B. Gilboy[1] and G. F. Knoll[2]
Kernforschungszentrum Karlsruhe[3]

1. Introduction

In the prototype fast reactors presently being planned a large fraction of the neutron population lies in the energy interval between 5-150 keV. Due to technical difficulties however much of the required neutron data in this region is only known to limited accuracy. The present work was undertaken to provide improved fission cross-section data on ^{239}Pu and ^{240}Pu, which sensitively effect the behaviour of plutonium-fuelled fast neutron assemblies. In order to avoid the necessity of measuring the neutron flux in this rather difficult energy region the fission cross-section ratios $^{239}Pu/^{235}U$ and $^{240}Pu/^{235}U$ are actually measured. Plutonium cross-sections can be derived from these ratios by reference to the best available values of the ^{235}U fission cross-section. This indirect approach was chosen since ^{235}U is much more suitable for absolute cross-section measurements and some accurate ^{235}U results which have recently been published [1,2] may be used for this normalization.

---

1) Now at A.W.R.E. Aldermaston, Berks. England.

2) Now at University of Michigan, Ann Arbor, Mich. U.S.A.

3) Work performed within the Association in the Field of Fast Reactors between the European Atomic Energy Community and Gesellschaft für Kernforschung m.b.H. Karlsruhe

2. Apparatus and Method

The pulsed and bunched proton beam from the Karlsruhe 3 MeV Van de Graaff was used to provide 1 ns duration neutron bursts at 1 Mc/s repetition rate via the $Li^7(p,n)Be^7$ reaction. Thick lithium metal targets were employed to give a wide spread in proton energies and a consequent continuous ("white") spectrum of neutrons so that cross-section ratios could be simultaneously measured over a wide energy range which considerable quickened the rate of data acquisition. Two fission counters, containing ^{235}U and ^{239}Pu (or ^{240}Pu) respectively, were placed symmetrically about the pulsed neutron source in order to sample identical fluxes. Runs were repeated with the counters interchanged to average out any slight source asymmetries. Flight paths from 7.5 to 30 cm were chosen to give these best compromise between neutron energy resolution and fission counting rate. With typical proton currents of about 6 μA runs of between 8 and 16 hours were required to attain reasonable statistics.

The fission samples, manufactured in C.B.N.M. at Geel by the electro-spray technique, are detailed in Table I. For ^{235}U and ^{239}Pu a nominal thickness of 1 mgm/cm^2 was specified to keep the self-absorption corrections fairly small, but a thinner sample of ^{240}Pu was necessitated as only a small amount of this material was available.

The fissile samples were mounted in Xenon gas scintillation counters to detect induced fissions. The very short decay time of scintillations in Xenon ($\sim$ 1ns) helps to reduce pile-up of α-pulses from the highly active plutonium and gives fast output pulses which enable the neutron energies to be determined by time-of-flight. The fission counters were fabricated out of stainless steel to the design shown in Fig. 1. To reduce potential poisoning of the gas scintillator no wavelength shifter was used and since the pure Xenon scintillates in the ultra-violet end of the spectrum both the window of the chamber and the photomultiplier (56 UVP) were made of quartz. The distance between the fission sample and the chamber window was 5 cm which gives a total flight path of at least 10 cm for neutrons backscattered from the window and the multiplier. This reduced the time correlated backgrounds at the fission sample to a low level. Using thin lithium targets these backscattered neutrons could be time resolved and a typical value of $\sim$1.5% of the primary neutron intensity was measured which has only a very slight effect on the ratios over the energy range studied. As a further check on this point thick target runs were made at several different flight paths and with various maximum

neutron energies (by altering the accelerator energy) which should alter the effects of time correlated backgrounds. The ratios measured with these different dispositions were always in good agreement showing that spectral distortions due to scattered neutrons were small.

Due to the intense α-activity ($\sim 10^8$ sec^{-1}) in the plutonium chambers it was impossible to take slow (~ 1 μ sec) outputs from these counters in order to measure pulse-height spectra for setting bias levels. Instead fast outputs (~ 5 ns) were used to trigger fast discriminators which operated the START channels of a nanosecond time-sorter; STOP pulses were derived from a beam pick-up aerial near the neutron producing target. In this way time spectra from the two fission chambers were recorded simultaneously on identical time scales. The spectra from both counters were routed to different parts of the memory of a CAE 510 on-line computer in which the data was accumulated and inspected. The raw time spectra were recorded on punched paper tape for later off-line analysis.

Using a single fast bias level the overall time resolution for neutron events was about 3 ns but for some of the measurements a dual fast bias system was adopted which improved the resolution to about 1.5 ns. Figure 2 shows a typical time spectrum from the ^{235}U chamber with the neutron induced counts collected into 10% lethargy intervals which illustrates the relative neutron source intensity in the range 5-150 keV. The small γ-ray peak was found to be due mainly to γ-rays from the lithium target interacting in the quartz window and photo-multiplier. This γ-peak was useful for fixing the zero of the time scale. The counters were usually biased so that there were almost no counts due to α-pile-up events and the random backgrounds under the time correlated events were found to be due mainly to room scattered neutrons most of which had energies above the cadmium cut-off. In the case of ^{240}Pu the random background also contained spontaneous fission events. This clear time discrimination of most types of background events was an important aid to accurate background removal.

The ratio of the counting rates in the Pu and U fission counters as a function of neutron energy can be derived directly from the background subtracted time spectra and is related to the fission cross-section ratio by a factor containing the relative numbers of fissile nuclei in the two counters multiplied by the ratio of their bias levels. These bias factors were obtained in several different ways which are described in the following sections. These factors were fed into a data analysis computer programme which subtracted backgrounds and combined the various runs according to their statistical

weights. The programme also calculated the neutron energies and divided the data up into equal lethargy intervals of any desired width. The programme output tabulated the final cross-section ratios together with their statistical errors as a function of the mean neutron energy in each lethargy interval. The results are shown in Figures 3 and 4.

3. Fission Counter Bias Factors

3.1 $^{239}Pu/^{235}U$: Method A

As only fast output pulses were available from the Pu-counters fission fragment pulse height spectra were obtained by measuring integral bias curves for equal steps in the threshold settings of the fast discriminators on both detectors. For this purpose the fission rates were greatly increased by surrounding each counter by polythene to moderate neutrons into the energy region near thermal where both isotopes have large fission cross-sections. Pulse height spectra were derived from these integral counting rates by differentiation. Since the two counters contain closely similar fissile deposits the fission spectra for both chambers are expected to be almost identical and this was borne out by the measurements. The spectra from the two counters were normalised to each other and the relative efficiency for counting fissions over the bias levels used in the ratio measurements were calculated by integrating areas under the normalised distribution. Due to the greater α-pile-up the Pu chamber was usually biased about twice as high as the U-chamber. The relative numbers of ^{239}Pu and ^{235}U atoms were calculated from the sample masses with allowance for the other isotopes. The Pu-masses in Table I are given to 5% and are only provisional pending a more accurate assay by destructive analysis. Ratio measurements based on this method of defining the biases are shown in Figure 3.

3.2 $^{239}Pu/^{235}U$: Method B

Both of these isotopes have large fission cross-sections near thermal energies and consequently they can be accurately measured. In particular the ratios of these cross-sections have been measured to about 2% accuracy very recently [3] over the range 16-550 meV. Therefore if the present two fission detectors are compared in the same low energy flux their relative bias levels can be calculated from a measurement of their relative counting rates and a knowledge of the fission cross-section ratio at the energy used. This method actualy gives the ratio of the products < Number of fissile nuclei x Fission counting efficiency > so it also obviates the need to know the masses of the two fissile samples. The fission chambers were irradiated with neutrons of precisely known

energies from the crystal spectrometer on the Karlsruhe FR 2 reactor and the counting rate ratio measured for 41 meV neutrons. Another series of Pu/U counting ratios were measured between 41 meV and 271 meV to check for second order neutrons and these produced a small "ghost" peak at 75 meV corresponding to the strong 300 meV resonance in ^{239}Pu. A 2% correction was estimated for the 41 meV ratio due to second order neutrons; higher orders were negligible. The cross-section ratio at 41 meV was derived by using some older measurements [4] normalised to the new data in reference [3]. In order to conveniently refer to the standard bias ratio defined by the 41 meV measurement a relative bias "indicator" was devised. This consisted of a polythene moderator containing a Po-Be neutron source which was placed over each of the counters in turn and the fission rate ratio measured shortly before the 41 meV standardization runs were made. For later runs at the Van de Graaff the same moderated source was used in identical geometry and from the fission rate ratio with this source the new relative bias conditions could be defined with respect to the 41 meV standard. The bias indicator method was used to check the bias conditions during a further set of accelerator runs and the results are shown in Figure 3.

3.3 ^{240}Pu/^{235}U

^{240}Pu has a very small low energy fission cross-section and has a higher specific α-activity than ^{239}Pu. For these reasons it was difficult or impossible to apply the methods described above for fixing the relative bias levels. However, ^{240}Pu is spontaneously fissile and the sample used had a total spontaneous fission rate of $\sim$2.4 sec^{-1}. With the bias set to cut out α-pulses a spontaneous fission rate of about 1 sec^{-1} was observed. Since this is proportional to the amount of ^{240}Pu in the sample it can be shown that it is unnecessary to know either the mass of ^{240}Pu or the efficiency for counting fissions over the bias if the induced fission rate is always measured relative to the spontaneous fission rate. This method also required a knowledge of the spontaneous fission half-life which has been measured to $\pm$ 1% by Watt et al [5]. In this case the absolute efficiency for counting fissions with the ^{235}U counter has to be measured and this was done in the following way. The moderated Po-Be source was used to give a large number of fission events in the ^{235}U chamber and a slow output from the counter was analysed in a multi-channel analyser to display the fission spectrum. This spectrum was fitted with a semi-theoretical spectrum derived by Kahn et al [6] in order to extrapolate to zero pulse height; a correction was also applied for self-absorption in the fissile layer. Once the total fission rate is known for the Po-Be source in its standard moderator geometry

the total fission rate at any other time can be calculated for the same source. The counting rate actually observed with this source gives the fission counting efficiency for the biassing conditions at the time of the measurement. The only other quantity required for the overall bias factor is the mass of the ^{235}U sample which was accurately measured in Geel by careful weighing techniques. The small fission cross-section of ^{240}Pu below 150 keV gave a rather small counting rate and long runs were made at flight paths as short as 7.5 cm in order to achieve reasonable statistics.

4. Discussion of Results

The ^{239}Pu results are shown in Figure 3 together with ratios measured by Allen and Ferguson [7] and by White et al [2,8]. The data are presented in 10% lethargy intervals and no marked structure is apparent beyond the expected statistical fluctuations. The statistical errors rise from about 1% at the higher energies to 5% at 5 keV. There is a further systematic uncertainty in the upper set of points of about 3% due to uncertainties in the bias factors derived from matching the fission pulse height spectra. Another scale uncertainty of 5% arises from the ^{239}Pu mass determination but this should be greatly reduced when the results of the final assays are available. Method B is independent of this mass measurement and an overall uncertainty in the scale factor of about 4% is estimated stemming mainly from the statistical errors in the bias indicator counts. Taking into account the statistical and systematic uncertainties the two sets of ^{239}Pu results agree reasonably well. A weighted mean of these two sets is in excellent agreement with the work of White and agrees well in slope with the measurements of Allen and Ferguson, although lying about 5% lower.

The results for ^{240}Pu are given in Figure 4 with the error flags showing the estimated overall errors. Since the induced fission rate for the ^{240}Pu sample was rather small the counts were combined into 30% lethargy intervals to improve the statistics. Data is only shown down to 15 keV as the statistical errors at lower energies were very large. Included in the assigned errors is a scale factor uncertainty of 5% which is dominated by the statistical errors on the spontaneous fission counts taken to determine the bias. The data is in good agreement with measurements by White et al [2, 9] which are representative of results by other workers [10, 11]. The present results extend to lower energies than previous measurements and indicate a second fission threshold at about 10 keV. Using the ^{235}U fission cross-section [1, 2] the ^{240}Pu fission cross-section derived from the ratios is in good qualitative agreement with a theoretical curve of De Vroey et al [10] which describes the cross-section below 200 keV as being mainly due to p-wave neutrons.

Table I: Details of Fissile Samples

Sample	Total Weight mgm[a]	Density[b] mg cm^{-2}	Isotopic Analysis atom %
Uranium 235	23.62 ± 0.03 (U_3O_8)	1.204	^{235}U ii.505; ^{234}U 0.168 ^{236}U 0.026; ^{238}U 0.301
Plutonium 239	21.59 ± 1.08 (PuO_2)	1.100	^{239}Pu 99.979; Pu^{240} 0.020 ^{241}Pu 0.001
Plutonium 240	5.70 ± 0.25 (PuO_2)	0.290	^{240}Pu 99.60; ^{239}Pu 0.31 ^{241}Pu 0.07; ^{242}Pu 0.02

a Chemical purity of ≥ 99.9% in each case

b Area of fissile deposit 19.63 cm^2 (5.0 cm diameter circle)

References

[1] White, P. H., J. Nuclear Energy A/B 19 (1965) 325

[2] Perkin, J. L., White, P. H., Fieldhouse, P., Axton, E. J., Cross, P., Robertson, J. C., J. Nuclear Energy A/B 19 (1965) 424

[3] White, P. H., Reichelt, J. M. A., Warner, G. P. (see Proceedings of this Conference)

[4] Hughes, D. J., Schwartz, R. B., Brookhaven National Laboratory Report BNL 325, Second Edition (1960)

[5] Watt, D. E., Bannister, F. J., Laidler, J.B., Brown, F., Phys. Rev. 126 (1962) 264

[6] Kahn, S., Harman, R., Forgue, V., Nucl. Sci. Eng. 23 (1965) 8

[7] Allen, W. D., Ferguson, A. T. G., Proc. Phys. Soc. A70 (1957) 573

[8] White, P. H., Hodgkinson, J. G., Wall, G. J., Physics and Chemistry of Fission, Vol, I, I.A.E.A., Vienna (1965)

[9] Ruddick, P., White, P. H., J. Nuclear Energy A/B 18 (1964) 561

[10] De Vroey, M., Ferguson, A. T. G., Starfelt, N., Physics and Chemistry of Fission, Vol. I, I.A.E.A. Vienna (1965)

[11] Nesterov, V. G., Smirenkin, G. N., J. Nuclear Energy A/B 16 (1962) 51

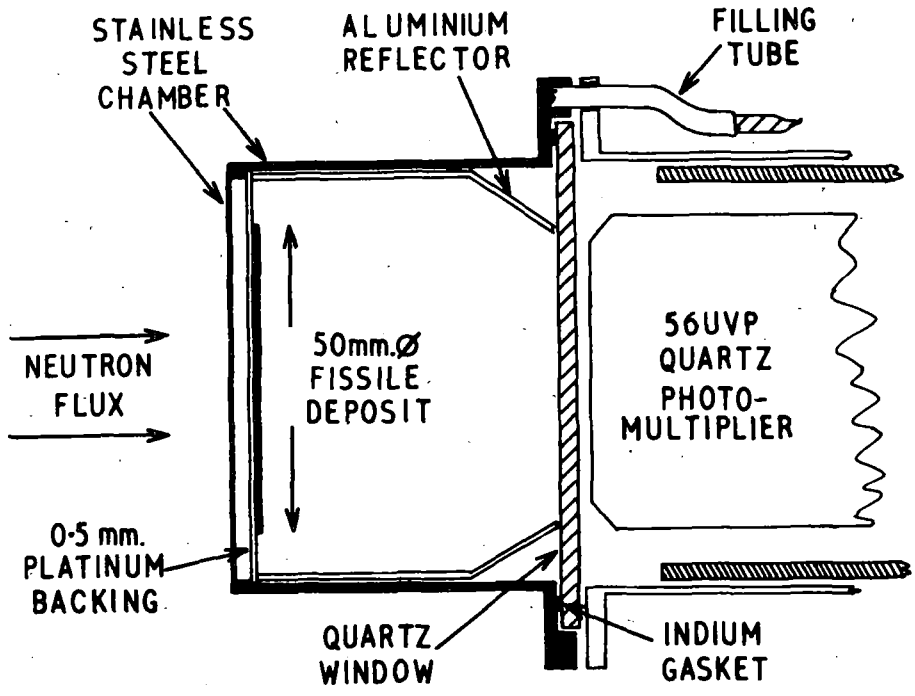

FIGURE 1. GAS SCINTILLATION FISSION COUNTER.

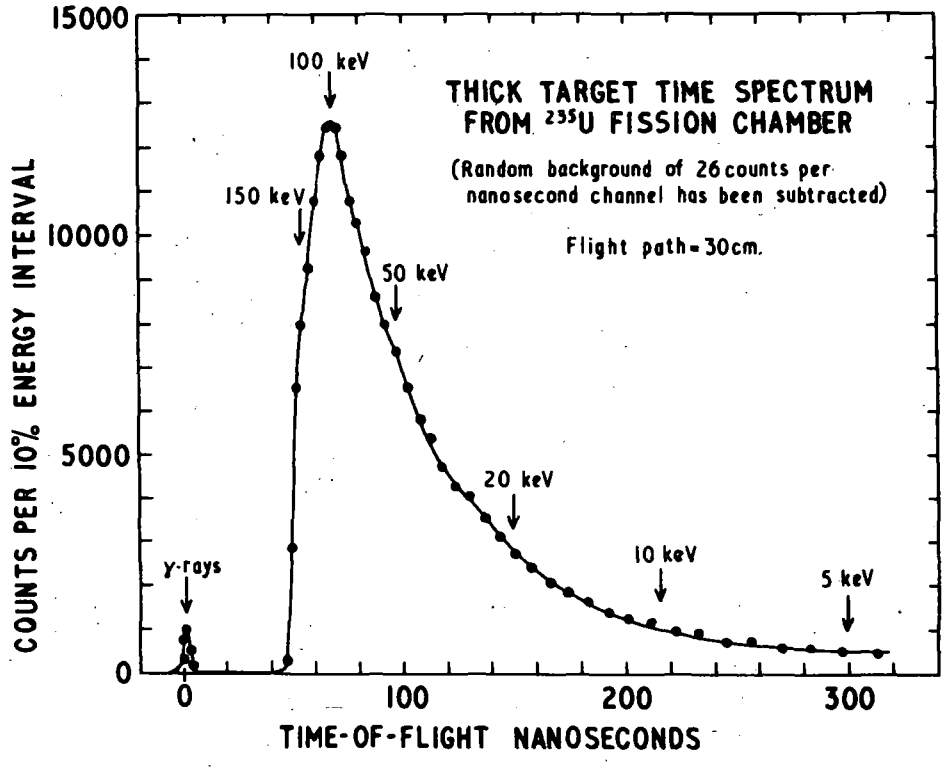

FIGURE 2. TYPICAL THICK TARGET TIME SPECTRUM FROM ^{235}U FISSION COUNTER

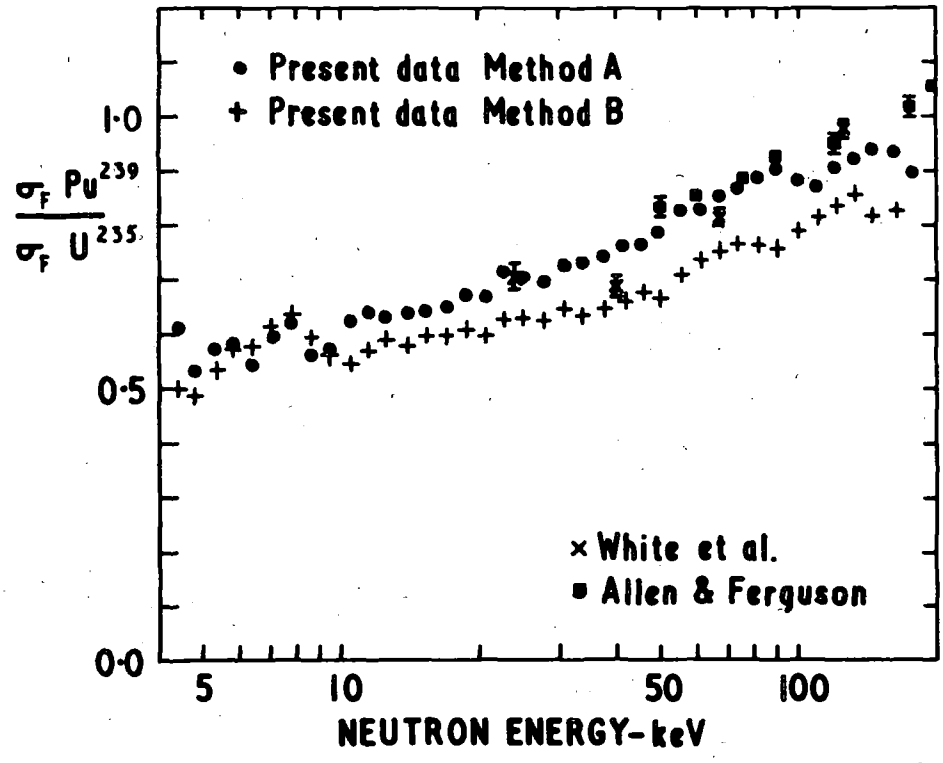

FIGURE 3. $^{239}Pu/^{235}U$ FISSION CROSS-SECTION RATIO at 10 % LETHARGY INTERVALS

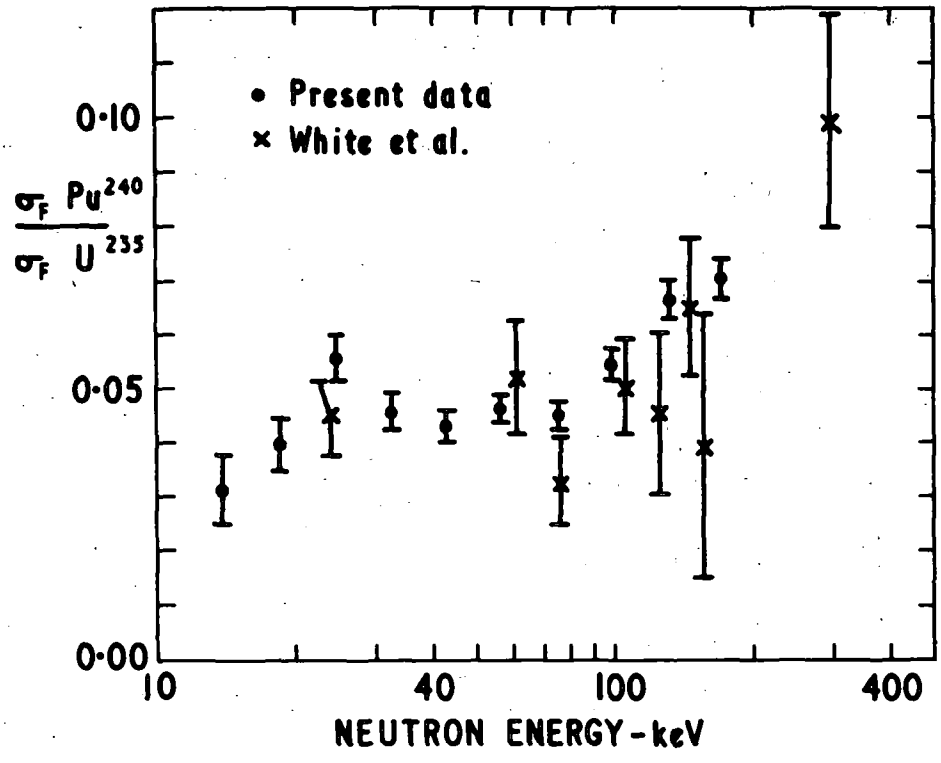

FIGURE 4. $^{240}Pu/^{235}U$ FISSION CROSS-SECTION RATIO AT 30 % LETHARGY INTERVALS

INTERNATIONAL ATOMIC ENERGY AGENCY

CONFERENCE ON NUCLEAR DATA-
MICROSCOPIC CROSS SECTIONS AND OTHER
DATA BASIC FOR REACTORS

Paris, October 17 - 21, 1966

CN-23/8

MEASUREMENTS OF EFFECTIVE (RESONANCE-SHIELDED) NEUTRON CROSS SECTIONS IN THE KEV REGION [1)]

H. Miessner and E. Arai
Kernforschungszentrum Karlsruhe

1. Introduction

The knowledge of effective neutron cross sections is fundamental for Doppler coefficient calculations in fast reactor design. In the low keV region, which is most important for the Doppler effect, the resonances of the cross sections of fertile and fissile materials are narrow and seperated but are still experimentally unresolved.

In the following measurements the pulsed method which has been proved for measuring capture and transport cross sections in the thermal energy range is extended to the keV region. Beghian et al. /1/ used the fast pulsed method to determine nonelastic cross sections in lead, uranium, bismuth, and iron in the MeV range.

2. Principles of Measurement

In the present work, a short burst (1 or 10 ns) of nearly monoenergetic neutrons with energies below the threshold for inelastic scattering is injected into assemblies of lead and

1) This work was performed within the framework of the association EURATOM-Gesellschaft für Kernforschung m.b.H. in the field of fast reactor development.

uranium (parallelepipeds of 10 to 20 cm side length) and the decay of the neutron field in the block is measured. For very heavy materials, moderation effects are negligible, so that the diffusion process can be described by the usual one-group theory and the neutron field decays exponentially with a time constant

$$\alpha_o = v_o \Sigma_a^{eff} + \frac{v_o}{3\Sigma_{tr}^{eff}} B^2 + C_T B^4, \qquad (1)$$

where:

v_o = injection velocity

$$B^2 = \pi^2 \left\{ \frac{1}{(a+1{,}42/\Sigma_{tr}^{eff})^2} + \frac{1}{(b+1{,}42/\Sigma_{tr}^{eff})^2} + \frac{1}{(c+1{,}42/\Sigma_{tr}^{eff})^2} \right\} \qquad (2)$$

the buckling of the assembly (side lengths a,b,c)

$C_T = \frac{v_o}{45 \cdot \Sigma_t^3}$ correction term due to transport theory

Σ_t = macroscopic total cross section

Σ_{tr} = macroscopic transport cross section

Σ_a = macroscopic absorption cross section.

The detailed treatment of the pulsed neutron field including the resonance structure of the cross sections [2] leads to self-shielded cross sections which are identical with effective values defined by Abagjan et al. [3].

$$\sigma_a^{eff} = \frac{\left\langle \frac{\sigma_a}{\sigma_t} \right\rangle}{\left\langle \frac{1}{\sigma_t} \right\rangle} = f_a \cdot \langle \sigma_a \rangle \qquad (3)$$

$$\sigma_{tr}^{eff} = \frac{\left\langle \frac{1}{\sigma_t} \right\rangle}{\left\langle \frac{1}{\sigma_t \cdot \sigma_{tr}} \right\rangle} = f_t \cdot \langle \sigma_{tr} \rangle \qquad (4)$$

The brackets designate averages over an energy interval that is large enough to contain many resonances, but is smaller than the average energy loss per elastic collision. Values of the

self-shielding factors f_a and f_t have been calculated for many nuclides [3].

If the resonance absorber is diluted by a potential scatterer (e.g. Pb), the resonance self-shielding is reduced and can be described by f factors depending on σ_o, which is the potential corss section of the non resonant material referred to a resonance nucleus, that is:

$$\sigma_o = \frac{\Sigma_{pot}}{N_r} - \sigma_{potr} \qquad (5)$$

Σ_{pot} is the macroscopic potential cross section of the mixture, σ_{potr} the microscopic potential cross section of the resonance absorber, N_r the number of resonance nuclei per cm^3. $f_a(\sigma_o)$ and $f_t(\sigma_o)$ are also calculated in Ref. [3].

Eq. (1) is exactly valid only in the absence of moderation effects. It can be shown that, even for materials as heavy as lead and uranium, the moderation is not negligible. According to Eq. (1) the moderation causes a decrease of α with v during the decay, which is therefore not exactly exponential. However, it is possible to calculate the moderation effect and to eliminate it from each decay spectrum. This treatment makes use of the fact that, in the case of heavy materials after pulse injection of nearly monoenergetic neutrons, the spectrum remains sharp during the moderation; its maximum lies near the spectrum-averaged lethargy, which increases with time. It can be shown [2,4] that the decay process can be described as follows

$$N(t) \sim \exp\left[-\left(\alpha_o t + a\frac{t^2}{2} + \ldots\right)\right], \qquad (6)$$

where N(t) is the total (energy-integrated) neutron density, which is measured by a 1/v detector, α_o is the decay constant at injection energy and corresponds to the decay constant that would appear in the absence of moderation. Using a correction function $F(t) = \exp\left(-a\frac{t^2}{2}\right)$ mederation effects are eliminated in the following way:

$$\frac{N(t)}{F(t)} \sim \exp(-\alpha_o t), \qquad (7)$$

where F(t) can be calculated from the buckling, the injection velocity, the mass number of the material and the cross sections. However, for this correction, the cross sections need only be known to first order.

If α_o is measured as a function of the buckling, the cross sections Σ_a^{eff} and Σ_{tr}^{eff} can be obtained according to Eq. (1). The big advantage of this method is that it yields absolute values of the cross sections and no flux determination is necessary.

3. Measurements and Results

The experimental setup is shown in Fig. 1. The neutrons are produced by a pulsed 3-MeV van de Graaff (pulse length 1 or 10 ns, repetition rate 1 or 0,5 Mc/s). The pulsed proton beam passes through an electrostatic pick up system which provides the zero timing pulse. The $Li^7(p,n)\,Be^7$ reaction yields 30 keV neutrons near threshold (the energy spread is $\pm$ 6 keV); the $Sc^{45}(p,n)\,Ti^{45}$ reaction yields neutrons of 7.5 keV with an energy spread of $\pm$ 0.8 keV at the lowest resonance of the(p,n) cross section.

The decay of the neutron field in the assembly is measured with the detector A, which is either a Li^6-loaded glass scintillator (time resolution $\lesssim$ 8 ns) or a LiI crystal (time resolution $\lesssim$ 20 ns) in connection with 56 - AVP photo-multipliers.

The latter detector is used for the measurements on uranium, because of its better discrimination against the gamma radiation from radioactive decay of the uranium. Detector B (Li^6-loaded glass scintillator with a photo-multiplier) as a time-of-flight spectrometer, controls the energy of the neutrons of the Sc reaction.

Measurements of the decay time in assemblies of lead, uranium, and a homogeneous mixture of both have been made.

Fig. 2 shows a typical decay curve of a 30 keV neutron field in uranium. An inspection of the decay curve after background substraction shows that it is not exponential. But the division of the background corrected spectrum by F(t) leads to a decay which is exactly exponential over about 3 decades. However, for the evaluation of α_o, only about 2 decades are used. Within this region, F(t) is smaller than 2 and the accuracy of the Taylor expansion is good enough. Though F(t) is rather large, the difference of the slopes of corrected and uncorrected curve (if we restrict ourselves to the nearly exponential region) is less than 10 %, corresponding to an α correction of the same order. The decay constants obtained have been found to be independent of the detector position.

Figs. 3, 4 and 5 are plots of α_o vs B^2 curves for lead at a neutron energy of 30 keV and uranium at 30 keV and 7.5 keV respectively. The full curves are least squares fits according to Eq. (1), where B^2 is an implicit function of Σ_{tr}^{eff} [Eq. (2)]. Σ_a^{eff} and Σ_{tr}^{eff} are obtained from an iterative procedure which yields a best fit for $\alpha_o(B^2)$. Since C is very small, its theoretical value is used.

Table I shows the measured effective cross sections. Since no similar experimental values exist at present, the measured effective cross sections can be compared with $\langle\sigma\rangle$ values of other authors only after division by the calculated self-shielding factors [3] according to Eqs. (3) and (4). Lead shows no resonance self-shielding in the keV region (the number of resonances is too small) and the f factor is equal 1. The capture cross section ($\approx$3 mb) is too small to be measured by this method. The transport cross section conforms very well with other measurements. For uranium the resonance self-shielding is still small at 30 keV ($f \approx 1$) but is already considerable at 7.5 keV. The agreement of the measured effective capture cross sections after division by

f_a is good both for 30 keV and 7.5 keV. The transport cross section at 7.5 keV agrees very well with other measurements, but at 30 keV this cross section is about 10 % higher than other values.

Measurements on diluted systems are not yet concluded. Fig. 6 is a plot of f_a vs σ_o for uranium for 7.5 keV neutrons, calculated from Ref. /3/ using an interpolation formula /13/. The upper abscissa gives the corresponding volume ratios of a U^{238}-Pb mixture related to σ_o by Eq. (5). Preliminary on diluted systems measured f factures, obtained by measured σ_a^{eff} values after division by $\langle \sigma_a \rangle$ given in Ref. /8/ are consistent with Fig. 6.

The effective cross sections measured by the fast pulsed method agree with values computed from calculated f factors and $\langle \sigma \rangle$ values measured by other authors. The present method can be used to determine f factors, if $\langle \sigma \rangle$ values are obtained by other methods. Further it is possible to investigate the self-shielding in mixtures of materials, e.g., a resonance absorber(U^{238}) and a potential scatterer (Pb), which permits the study of dilution effects, or two resonance absorbers (U^{238} and Pu^{239}).

Table I: Comparison of Measured σ^{eff} Values with $\langle\sigma\rangle$ Values of Other Authors

Material	Neutron-energy [keV]	σ_a^{eff} [b]	f_a [3]	$\frac{\sigma_a^{eff}}{f_a}$ [b]	$\langle\sigma_a\rangle$ [b]	σ_{tr}^{eff} [b]	f_t [3]	$\frac{\sigma_{tr}^{eff}}{f_t}$ [b]	$\langle\sigma_{tr}\rangle$ [b]
Pb	30 ± 6	-	-	-	-	10,1±0,2	1,00	10,1	10,0 [5]
U^{238}	30 ± 6	0,50±0,03	0,92	0,54	0,38 [6] 0,47 [7] 0,50 [8] 0,53 [9]	14,65±0,5	0,97	15,1	13,6 [10] 13,4 [8] 13,7 [11] 12,0 [12]
U^{238}	7,5±0,8	0,40±0,02	0,65	0,61	0,63 [7] 0,64 [8]	11,92±0,4	0,75	15,9	15,8 [11] 15,3 [8]

References:

[1] L.E. BEGHIAN, N.C. RASMUSSEN, R.T. THEWS, J. WEBER
Nucl. Sci. Eng. 15, 375 (1963)

L.E. BEGHIAN, A.E. PROFIO, J. WEBER, S. WILENSKY
Nucl. Sci. Eng. 17, 82 (1963)

L.E. BEGHIAN and S. WILENSKY
Pulsed Neutron Research, Proceedings of a Symposium, Karlsruhe.
Vol. II, 511 (1965). IAEA, Vienna.

[2] K.H. BECKURTS Unpublished internal Karlsruhe report (1964).

[3] L.P. ABAGJAN, N.O. BAZAZJANC, I.I. BONDARENKO, M.N. NIKOLAEV Group Constants of Fast and Intermediate Neutrons for the Calculation of Nuclear Reactors, National Committee for the Use of Atomic Energy in the USSR, Physical Energetic Institute, Obninsk, KFK Report tr-144 (1963)
(Transl. from Russ.).

[4] H. MIESSNER, E. ARAI
Nukleonik, to be published.

[5] D.J. HUGHES and R.B. SCHWARTZ
"Neutron Cross Sections", BNL-325, 2nd ed. Brookhaven National Laboratory (1958)

[6] R. HANNA, B. ROSS
J. Nucl. Energy 8, 197 (1959)

[7] C. BILPUCH, Z. WESTON, H. NEWSON
Ann. Phys. 10, 455 (1960)

[8] J.J. SCHMIDT "Neutron Cross Sections for Fast Reactor Materials", KFK Report 120 (EANDC-E-35U) (1962), Kernforschungszentrum Karlsruhe.

[9] V.A. TOLSTIKOV, L.E. SHERMAN and YU.YA. STAVISSKII
Atomnaya Energya 15, 414 (1963).

[10] R.K. ADAIR, H.H. BARSCHALL, C.K. BOCKELMANN et al.
L.A. - 1060 (1950)

[11] C.A. UTTLEY EANDC-UK-35L (1964), AERE Harwell

[12] R.H. TABONY, K.K. SETH, E.G. BILPUCH
to be published, quoted in
J.R. STEHN, M.D. GOLDBERG, R. WIENER-CASHMAN,
S.F. MUGHABGHAB, B.A. MAGURNO and V.M. MAY
"Neutron Cross Sections, Vol. III, Z = 88 to 98", BNL 325, 2nd ed., Suppl. No. 2, p. 92-0-1, Brookhaven National Laboratory (1965).

[13] E. KIEFHABER, K. OTT
unpublished internal Karlsruhe report (1965)

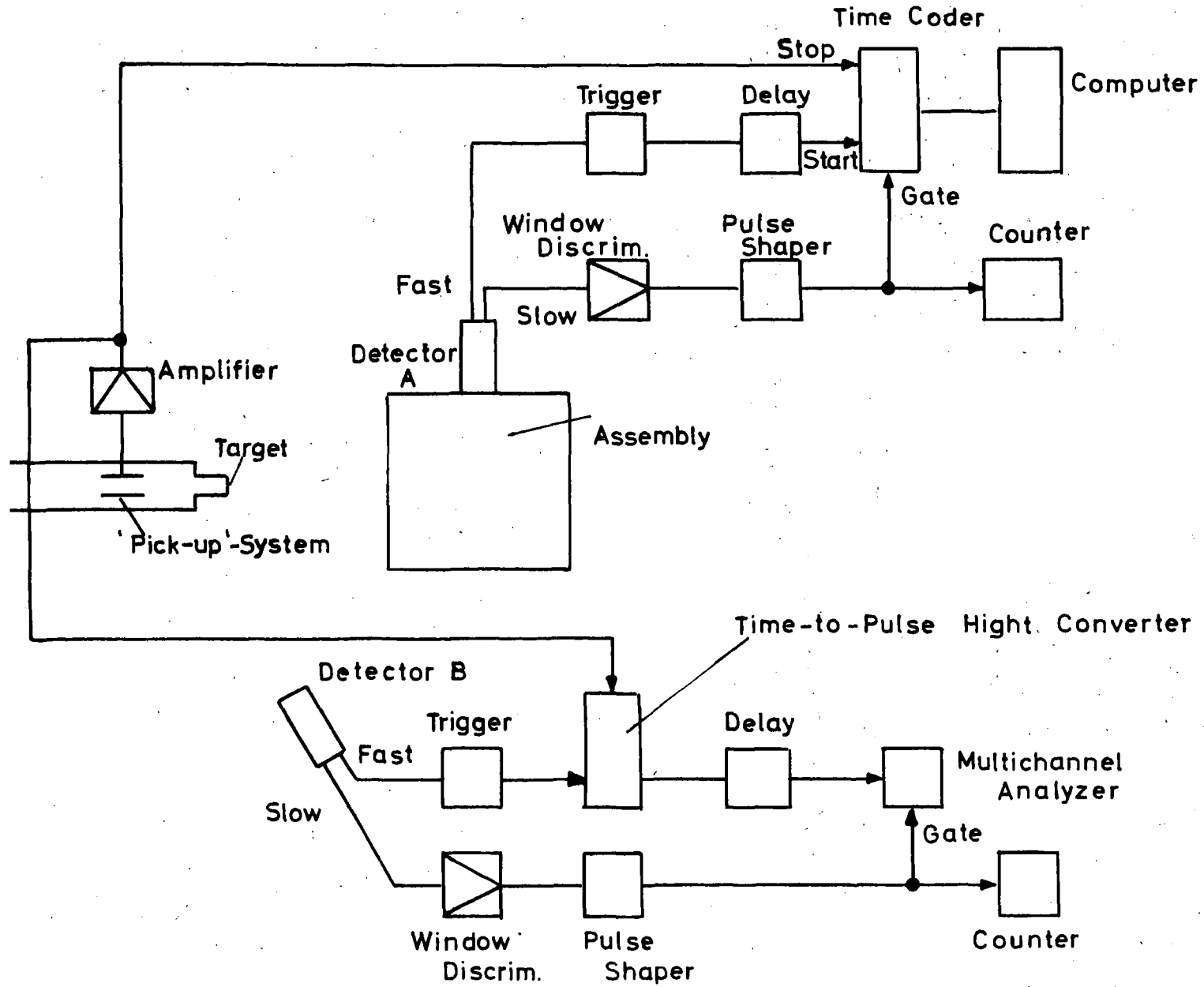

Fig. 1 Experimental Set-up

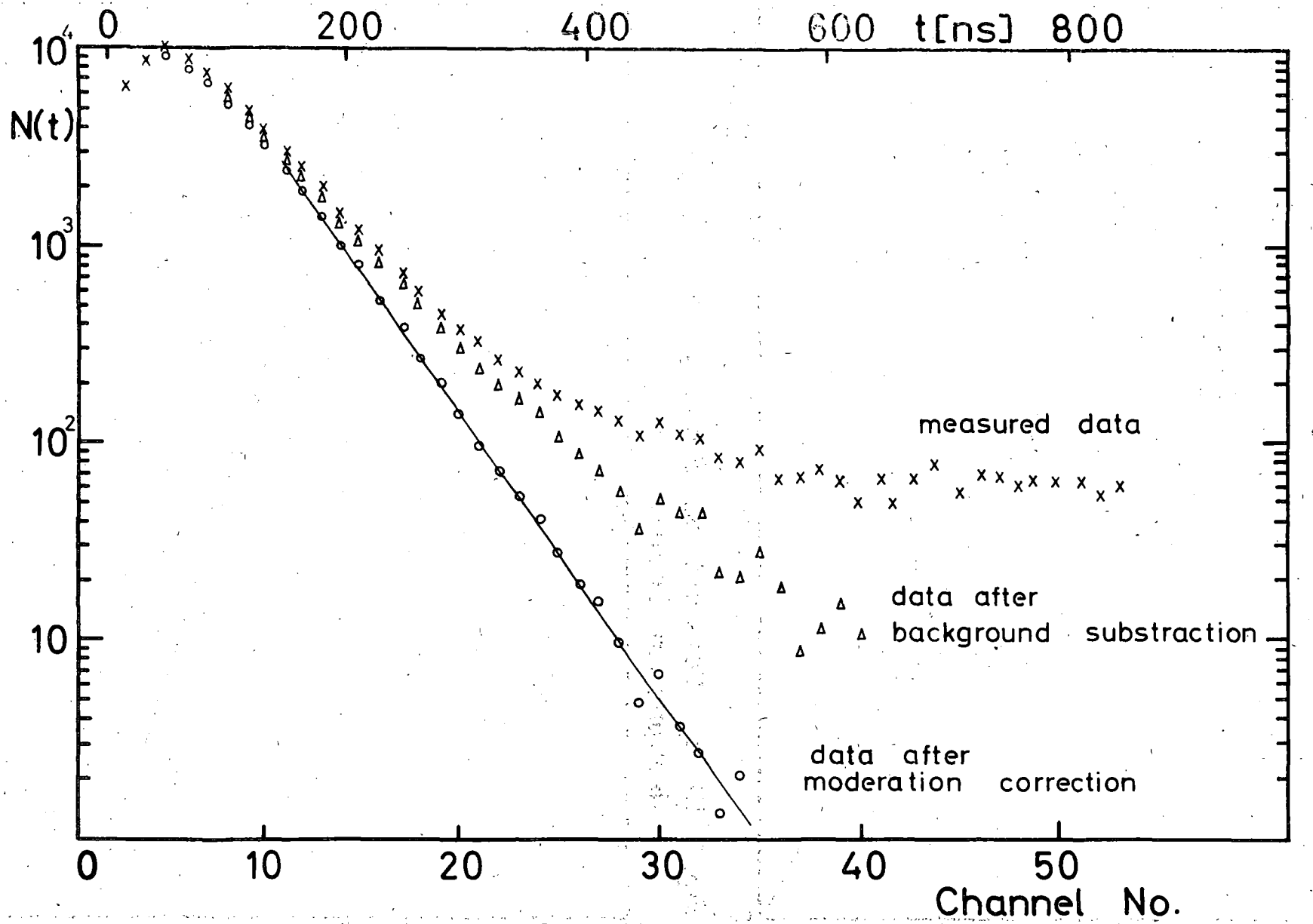

Fig. 2 Decay of a 30 keV Neutron Field in a $15.3 \times 15.3 \times 15.2\ cm^3$ Block of Natural Uranium

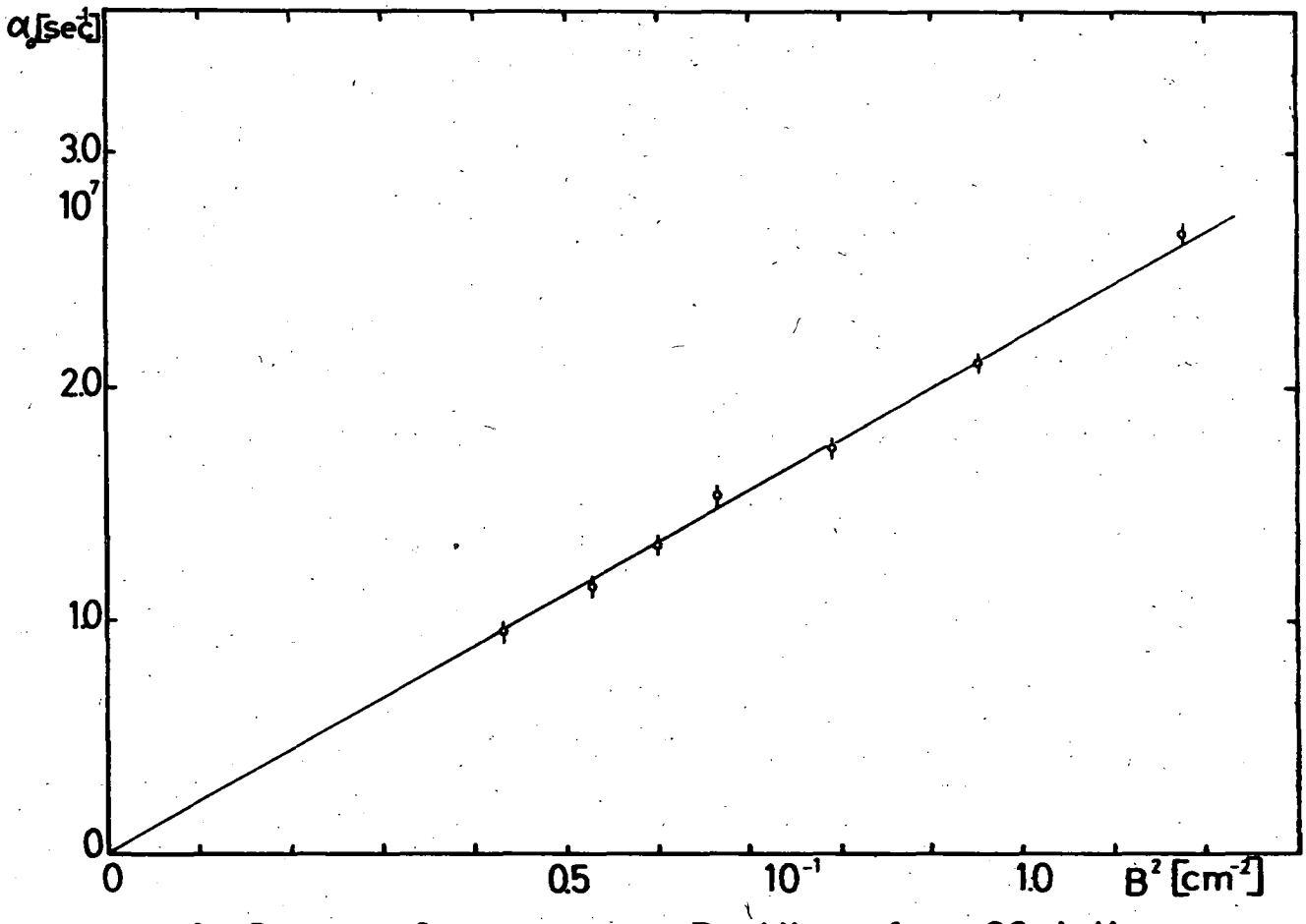

Fig. 3 Decay Constant vs Buckling for 30 keV Neutrons in Lead.

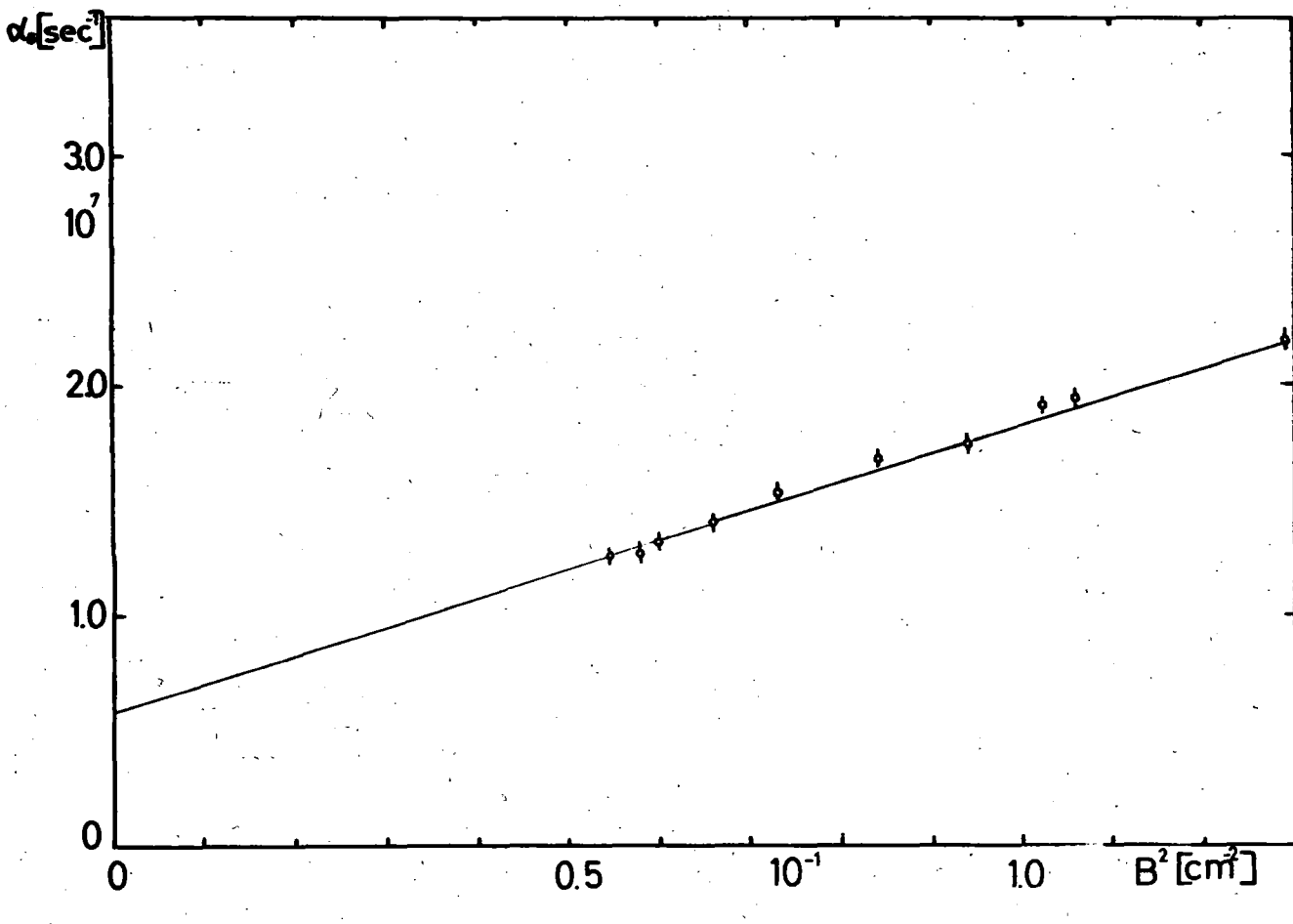

Fig. 4 Decay Constant vs Buckling for 30 keV Neutrons in Natural Uranium.

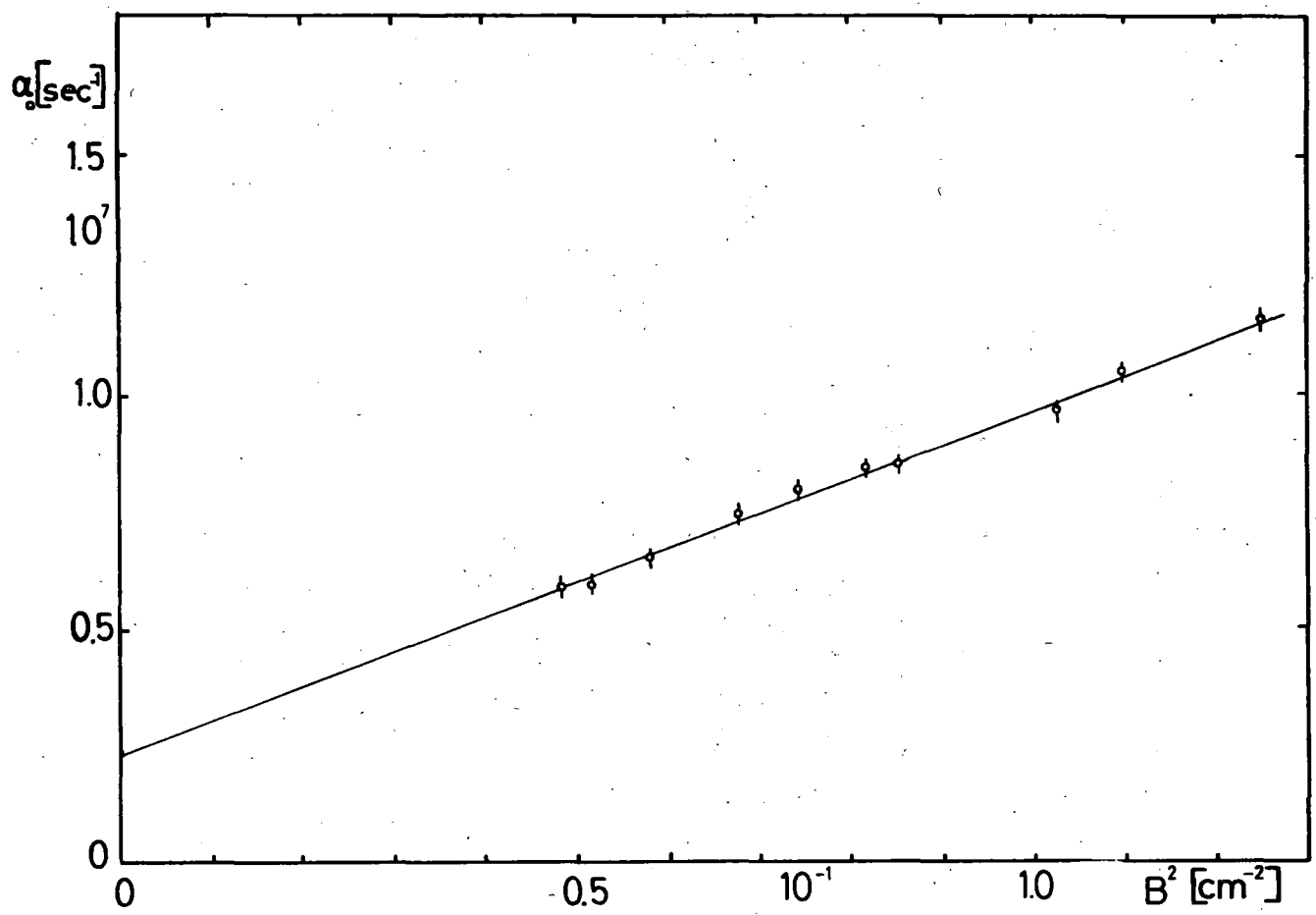

Fig. 5 Decay Constant vs Buckling for 7.5 keV Neutrons in Natural Uranium.

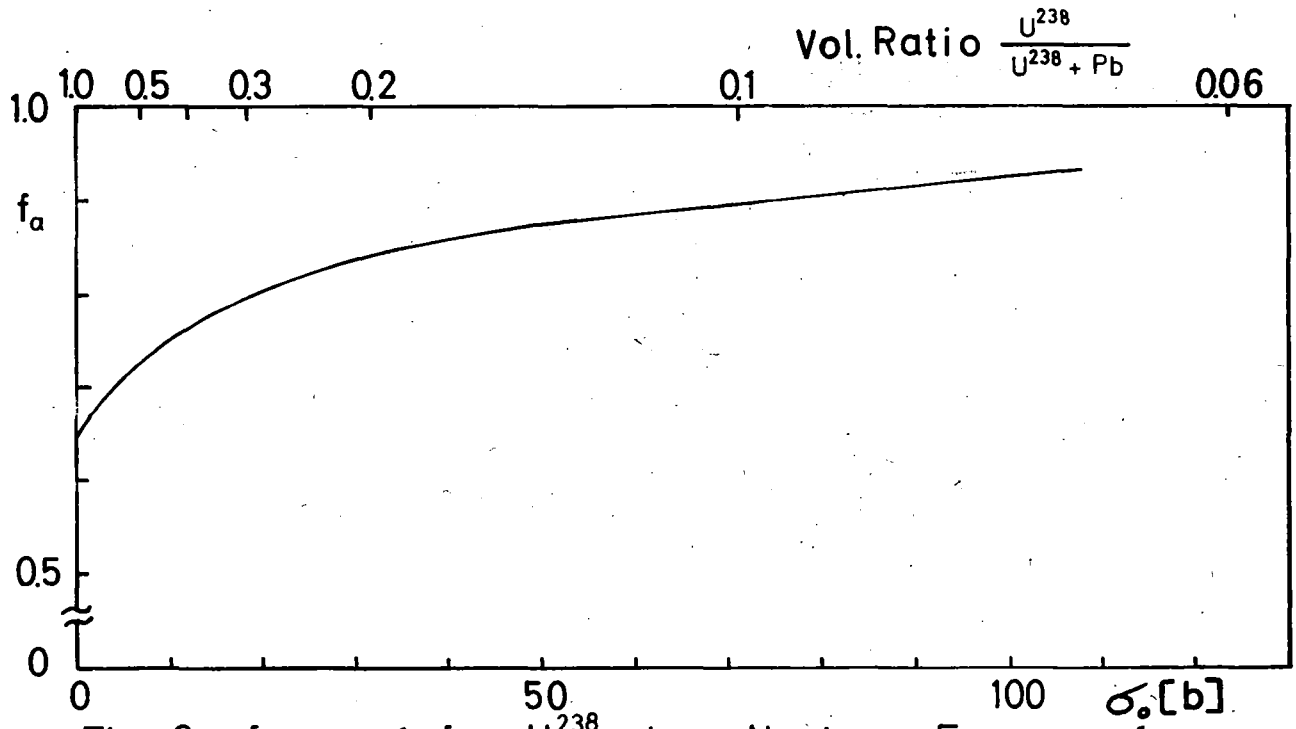

Fig. 6 f_a vs σ_o for U^{238} at a Neutron Energy of 7.5 keV. The Upper Abscissa gives the Corresponding Volume Ratios of a U^{238}-Pb Mixture.

INTERNATIONAL ATOMIC ENERGY AGENCY

CONFERENCE ON NUCLEAR DATA-
MICROSCOPIC CROSS SECTIONS AND OTHER
DATA BASIC FOR REACTORS

Paris, October 17 - 21, 1966

CN -23/11

A NOVEL METHOD FOR VERY HIGH RESOLUTION CROSS-SECTION MEASUREMENTS.

S. Cierjacks, P. Forti, D. Kopsch, L. Kropp, H. Unseld
Kernforschungszentrum Karlsruhe

A neutron time-of-flight spectrometer has been put into operation using the Karlsruhe isochronous-cyclotron as a very intense pulsed neutron source. The very high recurrence frequency of the microstructure bunches from the cyclotron was reduced using a novel "bunching-deflection" system to avoid frame overlap problems while largely preserving the high average neutron intensity available from the internal beam. The performance data of the spectrometer are as follows: flight path 57 m, neutron pulse length 1 ± 0.3 ns full width at half maximum, integrated time averaged neutron flux ($0,2 \leq E_n \leq 50$ MeV) $\emptyset = (5 \pm 2) \cdot 10^4$ n.cm^{-2}s.$^{-1}$ at 57 m, while using a thick natural uranium target and deuterons of (45 ± 5) MeV.

With the present flight path a maximum resolution of 0.02 ns/m has been determined for the spectrometer. The time-of-flight apparatus and the first total cross-section measurements for some light and medium-weight nuclei in the energy region between 0.5 and 10 MeV will be presented.

1. Introduction

In the measurement of nuclear coss-sections basic for reactor various techniques and neutron sources have been involved. In the energy range below several hundred ev one is in the measurement region mainly accessible to crystal spectrometers, choppers and pulsed electron accelerators. Above that energy up to several hundred kev, most cross-section measurements have been made with pulsed Van de Graaff accelerators, linear accelerators, and synchrocyclotrons. Above about 100 kev one is in the most useful region

of the electrostatic accelerator monoenergetic neutron sources.

The best resolution in these measurements have been confirmed to be some tenths of nsec per meter with a lower dispersion limit of about 0.1 ns/m.[1] The limitation in energy resolution in time-of-flight experiments is determined by the maximum total neutron output of the source and the minimum pulse width obtained with the pulsed-beam neutron producing device.

Neutron time-of-flight spectrometers with a resolution up to several tenths of nsec per m, however, work at the extreme limit of their capabilities. Unfortunately the extremely small pulse width obtainable with the pulsed Van de Graaff devices is associated with a limited total neutron output, while for linear accelerators and synchrocyclotrons a moderate pulse length (10 - 20 nsec) is connected with an excellent total neutron output.

Both advantages, an extremely small pulse width and a high total neutron output, can be obtained with isochronous cyclotrons. The disadvantage is however in the high recurrence frequencies of the microstructure pulses of these machines, so that overlap problems arise. By solving the frame overlap problem while largely preserving the high average neutron output obtained from the internal beam, a new method for very high resolution cross-section measurements has been developed at the Karlsruhe isochronous cyclotron. By means of a novel "bunching-deflection" system, described elsewhere,[2] the repetition rate of 33 Mc/s of the microstructure pulses was reduced to 20 kc/s while the neutron intensity was reduced only by a factor of about 30. With this facility a further improvement in resolution of nearly one order of magnitude is envisaged. The useful energy range of the continous neutron spectrum from the source covers an energy region from several hundred kev to more than 10 Mev. This is an essential portion of the energy range which is of interest to reactor physicists. These facts indicate that our spectrometer may represent useful supplement of the existing facilities employed in neutron cross-section work.

The neutron time-of-flight spectrometer will be described in more detail in section 2 of this paper, while in the third section total cross-section measurements for some light and medium-weight nuclei will be presented.

2. The neutron time-of-flight spectrometer

The overall layout of the neutron time-of-flight apparatus is shown in fig. 1. For neutron production a natural uranium target, 10 cm wide, 1 cm in height and thick enough to stop 50 Mev deuterons is used. The two collimators along the flight path have been chosen such that a neutron beam with an angular spread of $\sim 0.5^{\circ}$ is obtained. At the end of the evacuated flight path neutrons are detected by a liquid proton-recoil detector with an effective area of 90 cm^2 and a thickness of 2 cm. For the purpose of neutron beam monitoring a small liquid scintillator is placed in a second neutron beam at an angle of 6° to the main flight path.

A typical neutron spectrum obtained from the uranium target, plotted per unit energy interval, is shown in fig. 2. This spectrum is not corrected for the energy dependent detector efficiency. The high energy part with a broad maximum at about 20 Mev is produced by neutrons from deuteron break-up and possibly stripping reactions. The distribution of low energy neutrons including the maximum at about 1.6 Mev is due to evaporation and fission processes. This part of the spectrum is in a first approximation not very different from a fission spectrum.

The energy resolution of the spectrometer has been determined both by the time distribution of γ-rays within the peak of the promt γ-rays from the target and by measuring the two pairs of closely spaced resonances of Fe^{56} near 512 and 530 kev respectively. The resonances at 512 kev are shown in fig. 3 in comparison with the measurements of Reitmann and Smith[3] which were performed with a resolution of about 0.06 to 0.08 nsec/m. In the measurements of Reitmann and Smith the cross section at 512 kev shows only a weak indication of the presence of two resonances, while in our measurement these two resonances are well resolved.
From the measured half-width of these resonances, the resolution in this energy region seems to be at least equal to or better than 400 ev. From a calculation of the maximum resonance cross-section, an energy resolution of 200 ± 50 ev was deduced assuming the 513 kev resonance to be an s-wave resonance. Similar results were obtained for the case of the resonances at 530 kev. The theoretical value calculated from the neutron pulse width and the length of the flight path is 165 ev.

Because all γ-rays have the same time-of-flight, the width and the shape of the γ-peak reflects the time distribution of the neutron burst at the

target plus any finite time resolution inherent in the recording equipment. With this method a resolution of 0.024 ns/m was determined.

The characteristic features of the spectrometer are shown in table 1.

3. Total cross-section measurements

Transmission measurements have been carried out in the energy range between 0.5 - 30 MeV for the following materials: carbon, oxygen, aluminum, calcium and iron. In the measurements a digital time-sorter (HC 98 Intertechnique) was employed; a range of 4000 channels and 2 ns channelwidth was used. The output signals from the time-sorter were transfered to the Karlsruhe MIDAS Data Aquisitation System. The events were accumulated in an 8 K memory block.

In the carbon transmission experiment a graphite sample (n = 0.2343 at/barn) was used. The total cross-section in the energy range between 2 - 10 MeV is shown in fig. 4. The general behavior is in reasonable agreement with the published [4] cross-sections.

The oxygen transmission was obtained with a distilled water sample (n_{O2} = 0.0835 at/barn) contained in a thin aluminum can. The wall exposed to the neutron beam was only 0.2 mm thick. An identical empty can was put into the sample position during the open beam measurements. The total cross-section for oxygen was obtained from the measurements corrected for the hydrogen content, according to the published [4] total neutron cross-section of hydrogen. The results (fig. 5) have been corrected for the multiple scattering in the sample.

The results for aluminum and iron in the energy range between 0.5 - 10 MeV are shown in fig. 6 and 7. For aluminum a sample thickness of n = 0.1508 at/barn and for iron a sample with n = 0.1653 at/barn were chosen. For comparison the recent results of Carlson and Barschall [5] and Reitmann and Smith [3] are included in the figures.

For studying the total cross-section of calcium a granulated metal sample (n = 0.1690 at/barn) was used; it was contained in a thin aluminum can to avoid oxidation effects. As an example the total cross-section in the energy range from 0.4 to 1.4 MeV is shown in fig. 8. This fig. also includes the high resolution measurements carried out by Bowman, Bilpuch and Newson [6].

A punched card data bibliography of all the data available will be prepared.

References:

(1) H.W. NEWSON - Proceedings of the International Conference on the Study of Nuclear Structure with Neutrons, Antwerp, July 1965, North Holland Publ. p. 195.

(2) S. CIERJACKS, B. DUELLI, L. KROPP, M. LÖSEL, H. SCHWEICKERT, H. UNSELD - International Conference on Isochronous Cyclotrons, Gatlinburg, Tennessee.

(3) D. REITMANN and A. SMITH, - WASH-1044, EANDC (US) - 41 "U".

(4) D.J. HUGHES and R.B. SCHWARTZ - Neutron Cross-Sections, BNL 325 (1958).

(5) A.D. CARLSON and H.H. BARSCHALL - International Conference on the Study of Nuclear Structure with Neutrons, Antwerp, July 1965.

(6) C.D. BOWMANN, E.G. BILPUCH and H.W. NEWSON - Ann. of Phys. 17, 3 (1962), 319

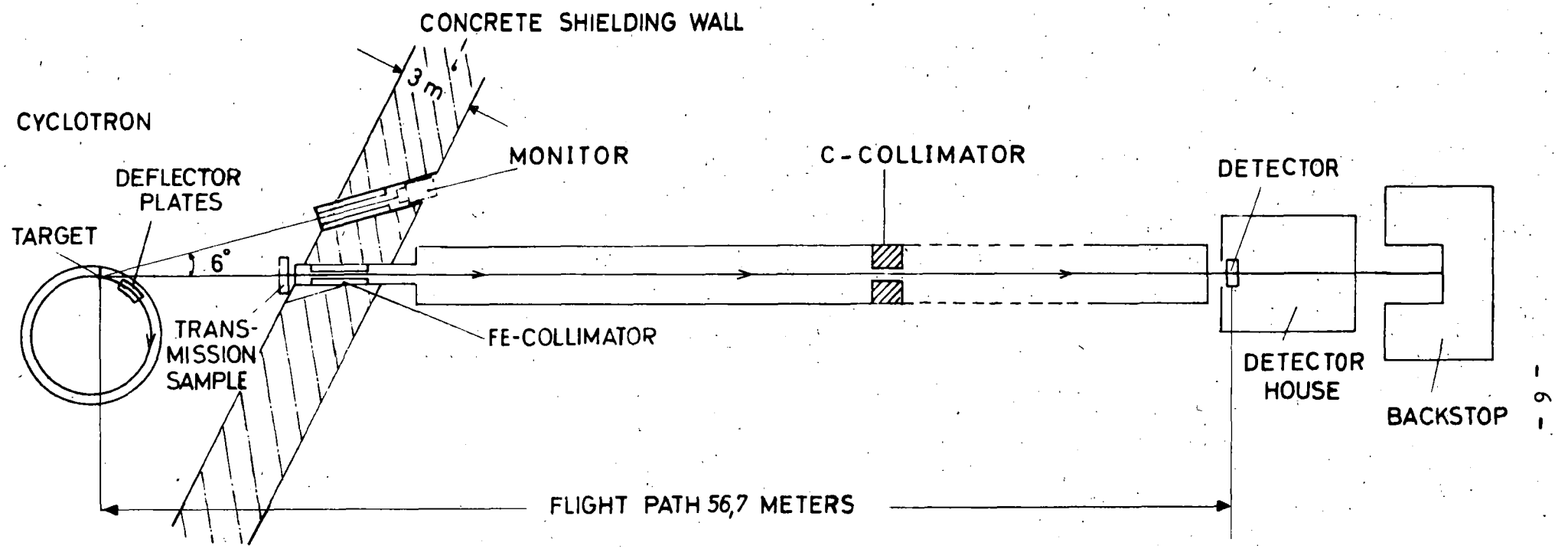

Fig.1: Geometry of the Karlsruhe isochronous cyclotron neutron time-of-flight spectrometer (top view).

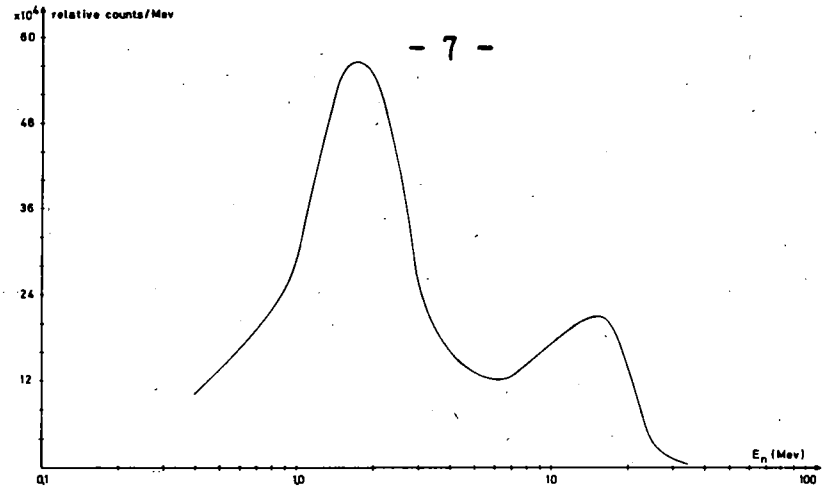

Fig. 2 - Typical neutron spectrum

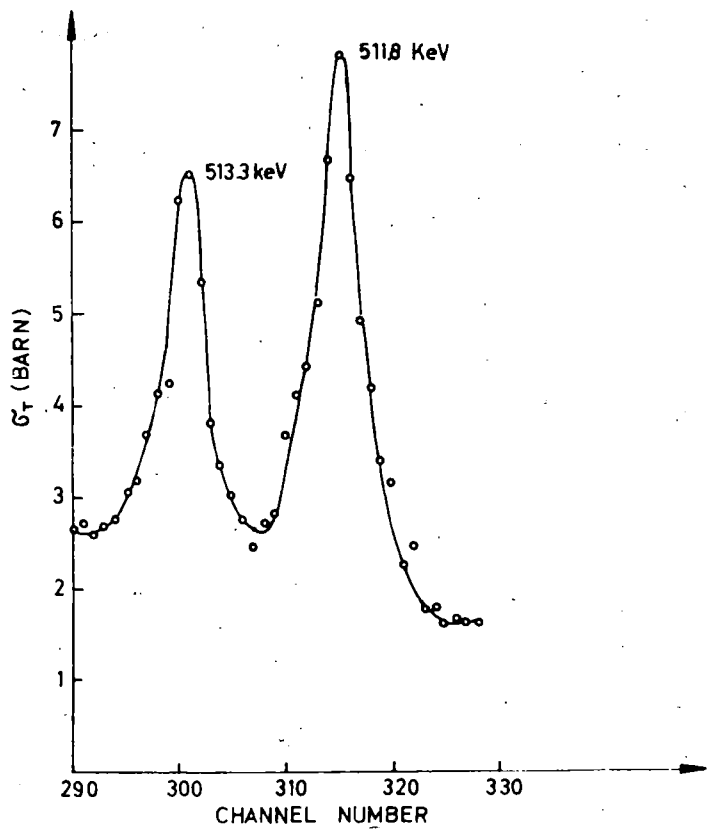

a) Present measurement

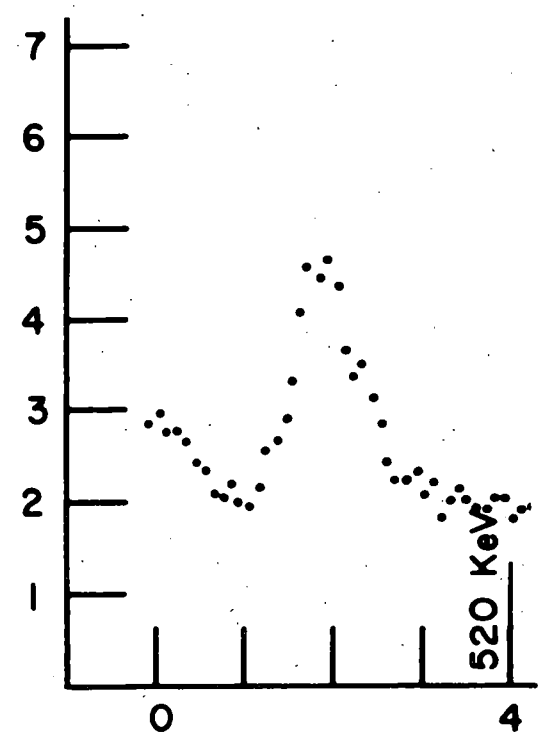

b) Measurement by ref. (3)

Fig. 3 - Fe resonances at 512 Kev

Flight path	56 - 57 m
Deflection radius	0,930 m (40,5 MeV deuterons) to 1,030 m (50 MeV deuterons)
Time resolution	(1 ± 0,3)ns full width half maximum
Energy resolution	200 eV at 0.5 MeV
Resolution of Spectrometer	0,02 nsec/m
Integrated neutron flux at 3 μA target current	$(5 \pm 2) \cdot 10^4$ neutrons cm^{-2} sec^{-1} above 250 keV at 56 m

Table I - Time-of-flight apparatus

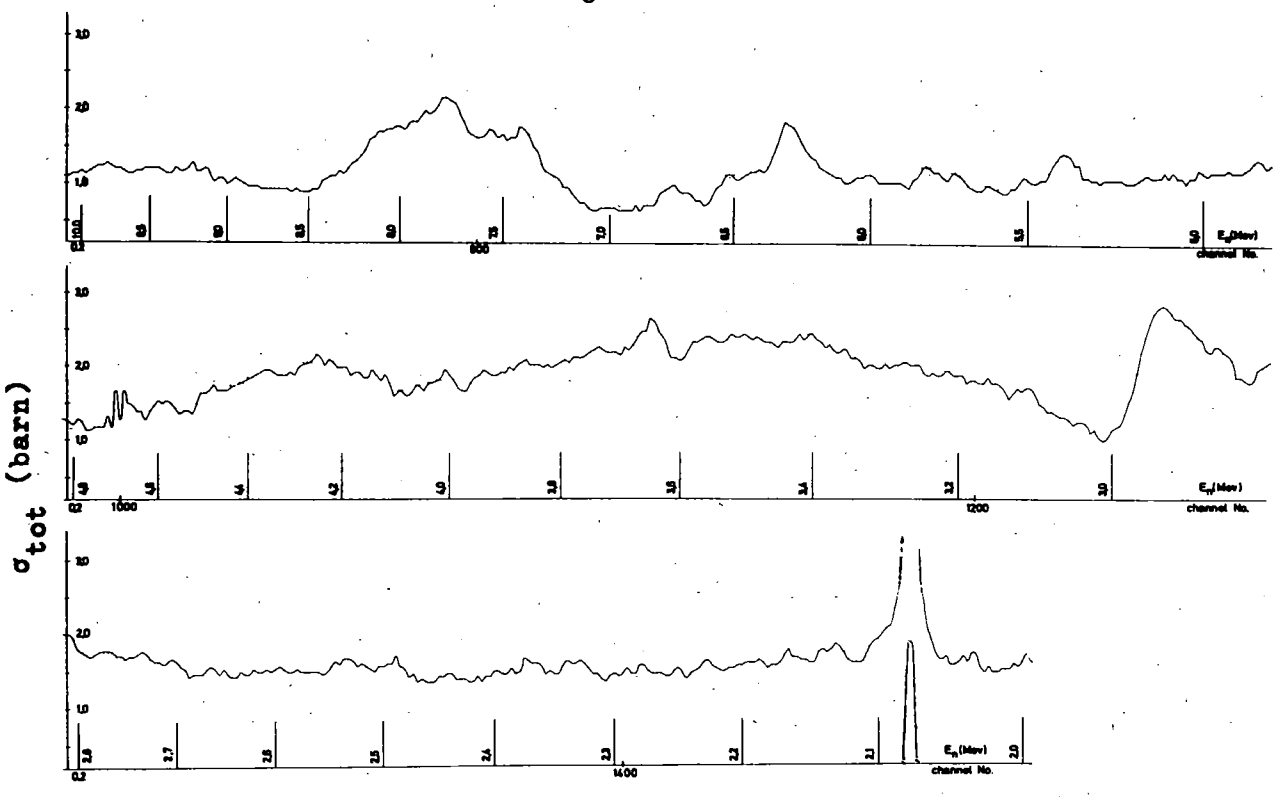

Fig. 4 - The total neutron cross-section of Carbon

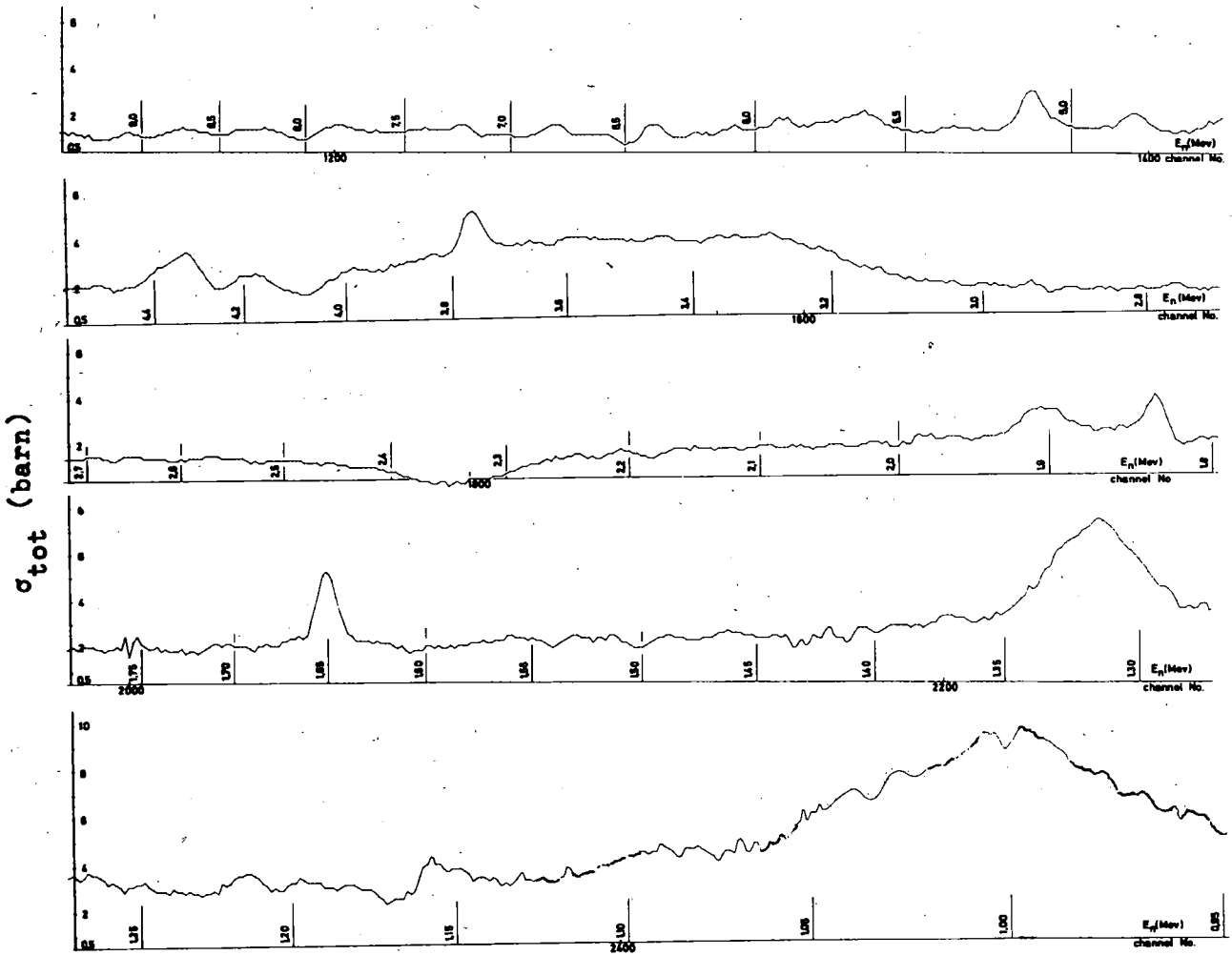

Fig. 5 - The total neutron cross-section of Oxygen

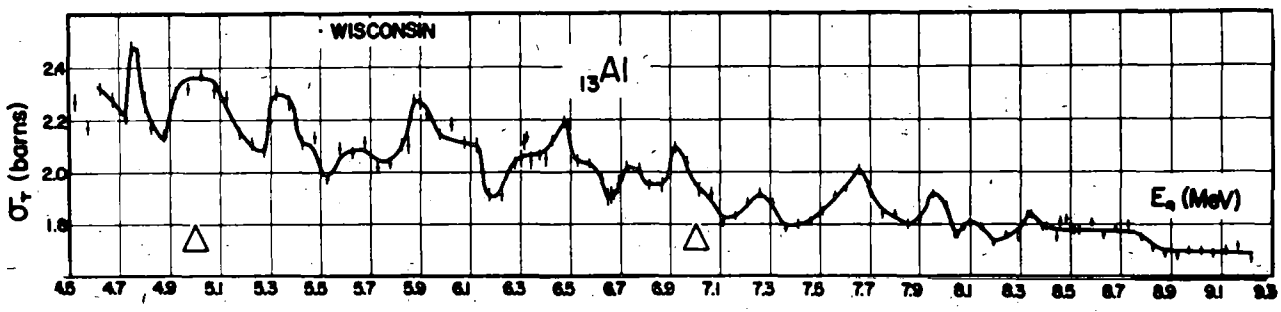

a) Measurement by ref. (5)

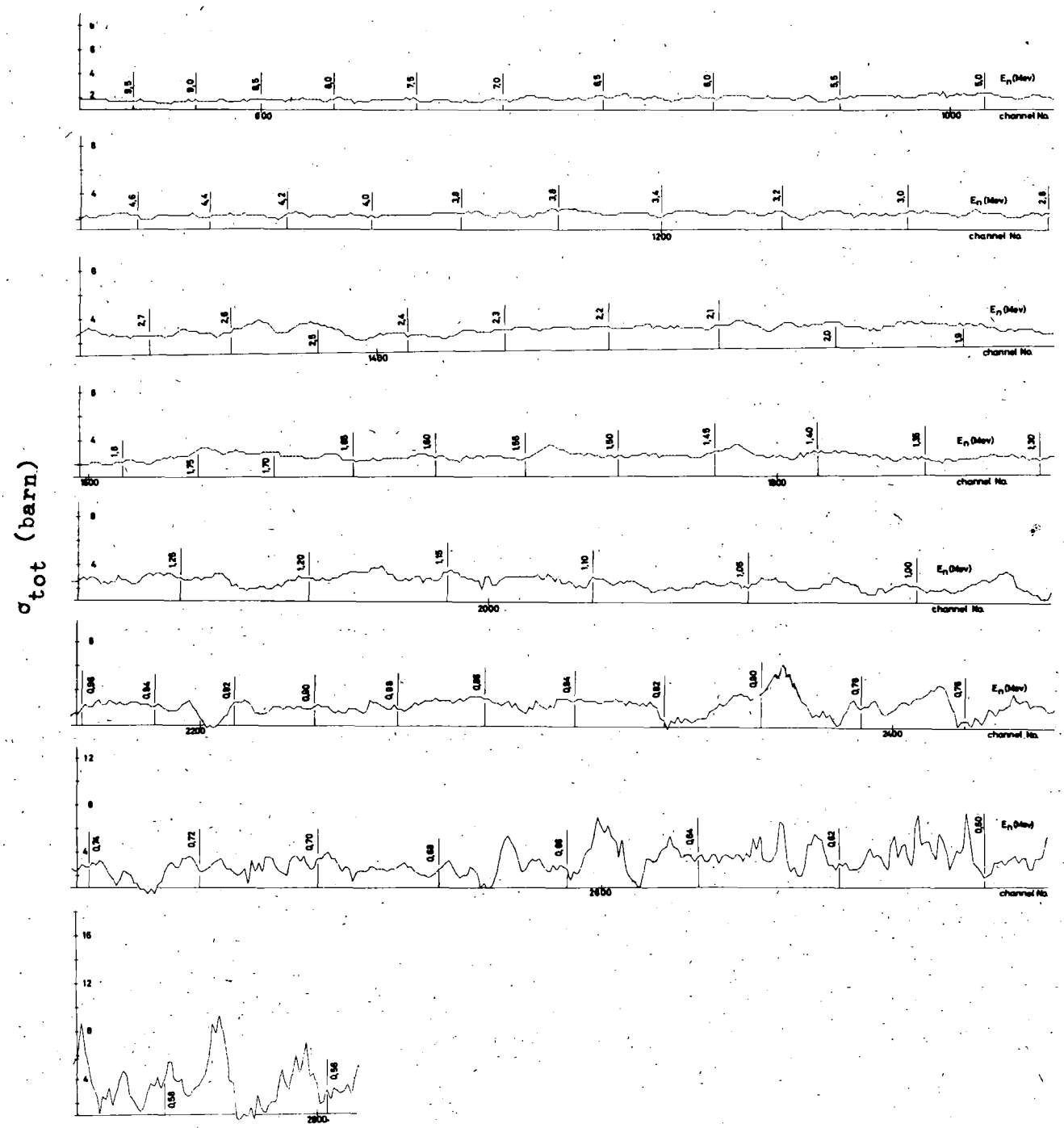

b) Present measurement

Fig. 6 - The total neutron cross-section of Aluminum

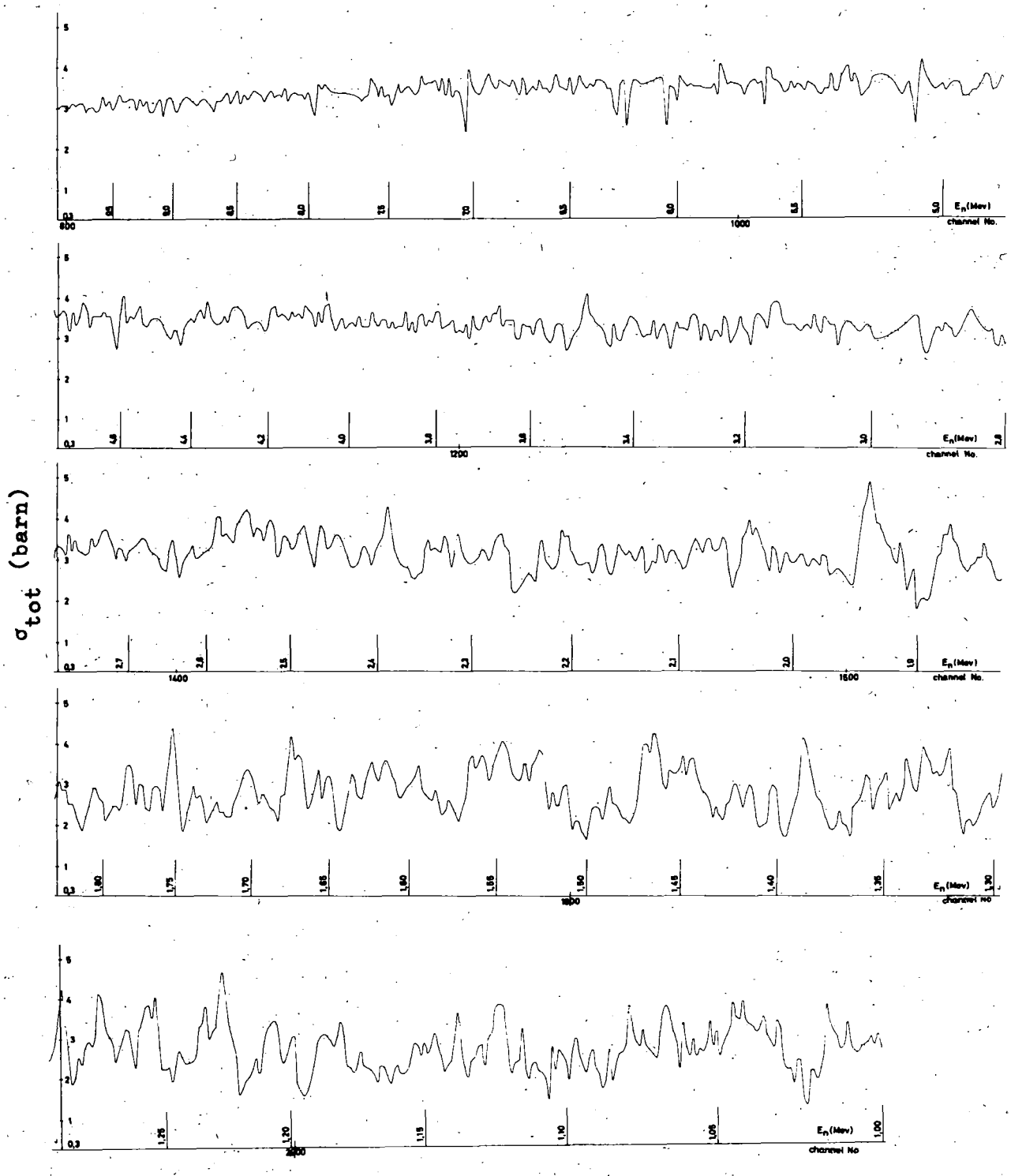

a) Present measurement

Fig. 7 - Total neutron cross-section of Iron (high-energy part)

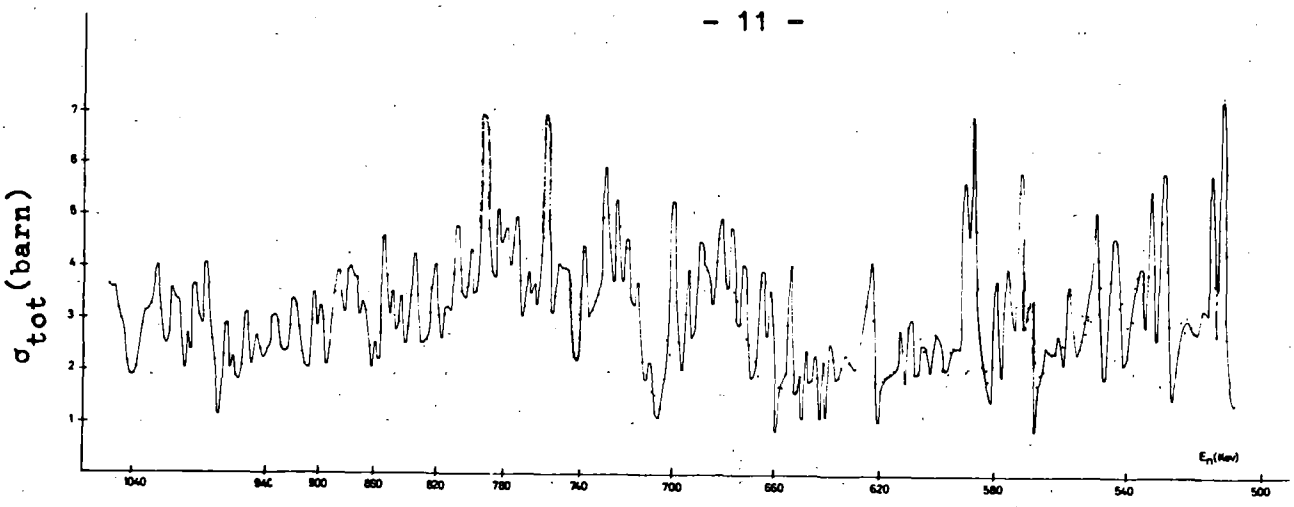

a) Present measurement

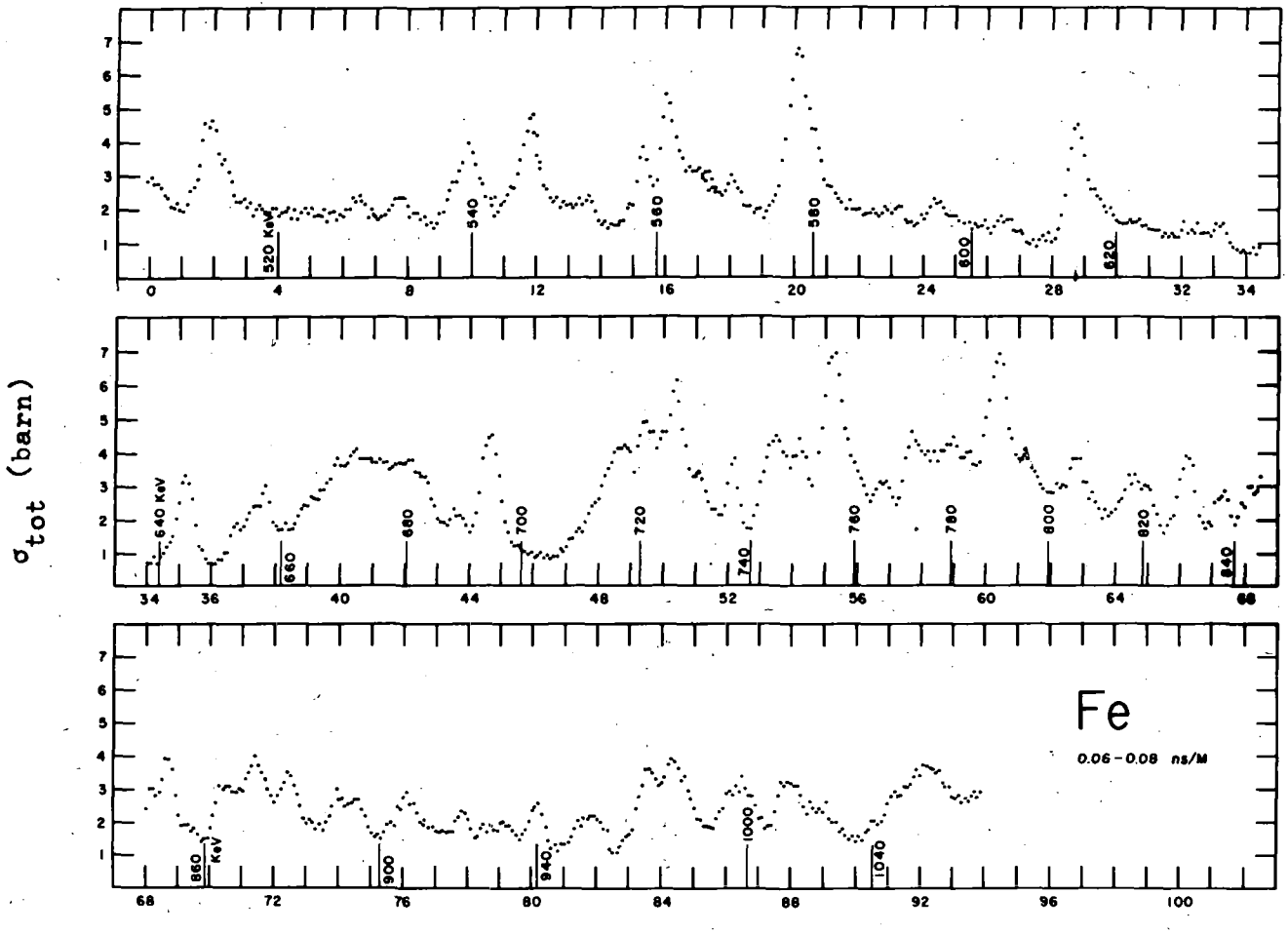

b) Measurement by ref. (3)

Fig. 7 - Total neutron cross-section of Iron (low-energy part)

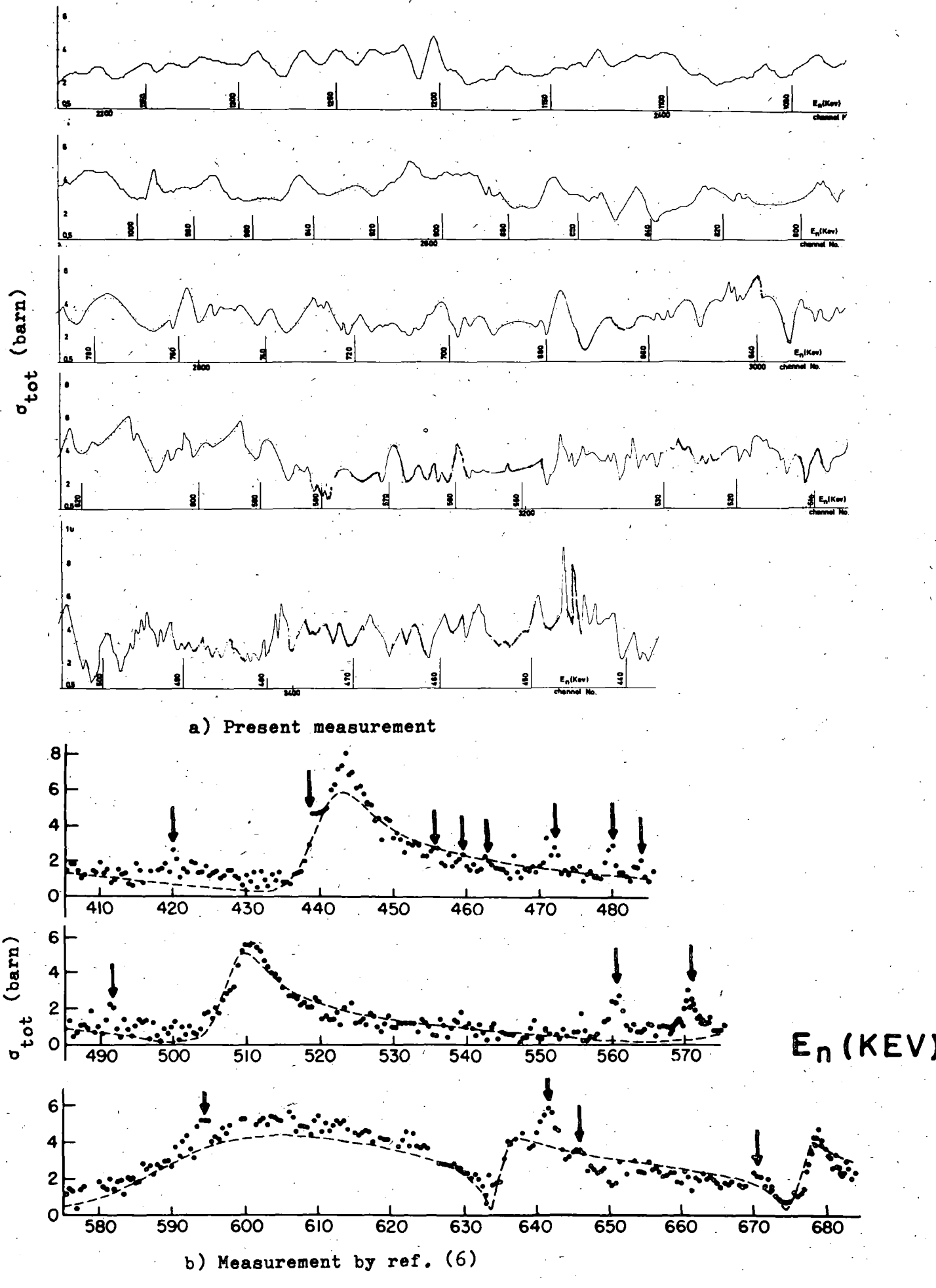

Fig. 8 - Total neutron cross-section for Calcium

CN-23/12

Measurements of 14 Mev neutron induced reaction cross sections using enriched isotopes of calcium

P.N. Tiwari* and E. Kondaiah

Tata Institute of Fundamental Research, Colaba, Bombay - 5

Introduction

Even though most of the (n,p), (n,α) and (n,2n) reaction cross sections have been measured by activation technique only a few cross sections for the rare reactions like (n,t) and (n,d) have been determined by this technique. Because the activities produced in these reactions are small and therefore difficult to measure.

In order to be able to measure small cross sections by activation technique one should do the following things apart from the use of higher flux and longer period of irradiation and counting:

1. Use of large material for irradiation
2. High efficiency of detection
3. Low background of the counting set up

Large material for irradiation can be used in gamma counting. The efficiency of detection can be improved by nearly 4 π counting employing well type of crystals. The background can be reduced by proper shielding.

---

*on leave from Banaras Hindu University

Experiment

A specially shielded gamma counting set up has been built [1] employing well type NaI (Tℓ) crystal. The sensitivity of this set up is such that with a neutron flux of $\sim 10^7$ to 10^8 neutrons per sec per cm^2, cross sections of the order of micro-barns per gram of the irradiated sample can be measured. Cylindrical sources are used with well type of crystals in order to take large material for counting. But there is very little information on the total and photopeak efficiencies of the well type crystals for cylindrical sources. Therefore these efficiencies of the well type NaI (Tℓ) crystal employed in our counting set up have been measured [1].

The cross sections for (n,d) reactions are expected not to be too small ($\sim$ few mb). Still many such cross sections have not been measured, because in many cases the product nucleus of (n,d) reaction is the same as that of (n,p) reaction on the next lower isotope. From the knowledge of (n,p) cross section one can subtract its contribution from the combined activity and get the contribution of (n,d) reaction alone. But such a subtraction is meaningful only when both the contributions are comparable. This will not be so unless the abundance of the next lower isotope is much smaller as compared to the isotope on which the (n,d) cross section is to be measured. In order to make such subtraction meaningful one may have to use enriched isotopes in general. The use of enriched isotope may become essential even for the measurements of other cross sections on the isotope whose natural

abundance is extremely small. Based on these consideration enriched calcium isotopes were used in this work for the cross section measurements.

Reaction cross section can be measured by using either total or photopeak efficiencies. We have used photopeak efficiencies in these measurements because it provides double check of peak position and half-life on the activity under measurement. The samples were irradiated in 14.2 ± 0.2 Mev neutrons. In each case the duration of irradiation was so adjusted as to produce optimum activity of interest as compared to interfering activities.

The samples to be irradiated were in the powder form. They were shaped into cylinders by enclosing them into polyethylene tubes. These tubes did not give any activity when counting was started after a minute from the end of irradiation. In each case the gamma ray spectrum and the half-lives of the produced activities were measured. They were found to be in agreement with the earlier measurements except in the case of K^{38g} for which the earlier reported half-life is 7.66 minutes [2] whereas we found it to be 9.5 minutes. Al^{27} (n, α) Na^{24} reaction with σ = 115 ± 6 mb at E_n = 14.2 ± 0.2 Mev has been used as the standard reaction in this work. The results of the measurements are given in table I.

The cross section for Al^{27} (n,p) Mg^{27} reaction has been well measured [3]. It was measured in this work to give an overall check to our measuring set up. There are no

earlier measurements for the cross section of (n,d) reactions on Ca^{43} and Ca^{44}. In other cases our measurements agree with the earlier measurements except with that of Khurana and Govil [4] as can be seen from table I.

Conclusion

This work suggests that it is possible to measure many (n,d) cross sections that have not yet been measured using about 10 mg of highly enriched isotope and low counting set up [1].

REFERENCES

(1) TIWARI, P.N., KONDAIAH, E., Nucl. Instr. and Meth. 42 (1966) - under publication.

(2) Nuclear Data Sheets, Nucl. Data group. Nat. Acad. Sci. Nat. Res. Council, Wash.

(3) GARDNER, D.G., Nuclear Physics 29 (1962) 373.

(4) KHURANA, C.S., GOVIL, I.M., Nuclear Physics 69 (1965) 153.

(5) NAGEL, W., ATEN Jr., A.H.W., Physica 31 (1965) 1091.

(6) LEVOKOVSKII, V.N., Soviet Physics JETP 18 (1964) 214.

(7) BORMANN, M., Nuclear Physics 65 (1965) 257.

(8) HUGHES, D.J., SCHWARTZ, R.B., BNL-325 (1958).

TABLE I

Reaction studied	Material used	% enrichment of isotopes	σ obtained by us	σ Exp. given in literature
$Al^{27}(n,p)Mg^{27}$	Al foil, 0.0512 g	Natural	71 ± 10.6 mb	50 mb to 115 mb, 80 ± 10 mb [3]
$Ca^{40}(n,t)K^{38g}$	$CaCO_3$, 0.9362 g	Natural	190 ± 30 μb	20000 ± 4000 μb [4]
$Ca^{42}(n,p)K^{42}$	$CaCO_3$, 0.0215 g	Ca^{42}-93.7	190 ± 30 mb	182 ± 27 mb [5] 160 ± 30 mb [6]
$Ca^{43}(n,p)K^{43}$	$CaCO_3$, 0.0336 g	Ca^{44}-70.54 Ca^{44}-17.59 Ca^{42}-1.5	93 ± 15 mb	110 ± 13 mb [5]
$Ca^{43}(n,d)K^{42}$	"	"	1.3 ± 7 mb	-
$Ca^{44}(n,p)K^{44}$	$CaCO_3$, 0.1225 g	Ca^{44}-98.6 Ca^{43}-0.06	20 ± 8 mb	37 ± 7 mb [6] 91 ± 20 mb [4]
$Ca^{44}(n,\alpha)Ar^{41}$	"	"	35 ± 4 mb	35 ± 10 mb [3] 113 ± 20 mb [4]
$Ca^{44}(n,d)K^{43}$	"	"	2.64 ± 4 mb	-
$Ca^{48}(n,2n)Ca^{47}$	$CaCO_3$, 0.0442 g	Ca^{48}-95.64	900 ± 135 mb	1070 ± 360 mb [7] 920 ± 184 mb [7]
$K^{39}(n,2n)K^{38g}$	K_2CO_3, 0.9272 g	Natural	2.6 ± .4 mb	2.7 ± .15 mb [7]
$K^{41}(n,p)Ar^{41}$	"	"	50 ± 7 mb	81 ± 33 mb [3]
$K^{41}(n,\alpha)Cl^{38}$	"	"	46 ± 7 mb	50 ± 25 mb [8]

CN-23/14

BASIC NUCLEAR DATA FOR FAST REACTOR CALCULATIONS

M. Segev, S. Yiftah and L. Gitter

Israel Atomic Energy Commission
Soreq Nuclear Research Centre

1. Introduction

In the last few years discrepancies have been found between the reactivity effects in fast reactors as evaluated by different groups [1]. The cause for these discrepancies is being sought both in differences in calculation methods and in basic nuclear data [2,3]. In the course of this search a comparison has been made of the reactivity effects predicted on the basis of different group cross sections sets [2,3,4]. Recently Greebler and Hutchins [5] established required accuracies in the measured basic data in the energy range 10 eV to 100 keV. In the present work we are concerned with the following specific questions:

a) The dependence of the criticality factor on variations in average cross sections (the Doppler and sodium void effects are less sensitive to uncertainties in average cross sections than is the criticality factor [5]).

b) Uncertainties in the Doppler and sodium void effects caused by uncertainties in resonance parameters and self-shielding factors.

c) Defining basic data from the viewpoint of basic nuclear theory.

2. Method of Calculation

Calculations were made on a critical reflected 2500-liter core with PuO_2-UO_2 fuel containing no higher Pu isotopes [6]. This system corresponds to a prototype fast reactor. Changes in criticality were calculated with the Philco-212 code DIFLEA, using the revised 16-group set YOM-64 [7]. The change in k was obtained each time for a change in a specific cross section of a specific element, with all other cross sections kept constant. To evaluate the Doppler and sodium void effects successive k calculations were performed. Uncertainties caused by resonance parameter variations were calculated using cross section differences as obtained from differences in self-shielding factors, the latter being the output of another Philco-212 code - SHIFTOR.

3. Results

The results of the calculations are given in Figs. 1 to 3 and Tables I and II.

In obtaining the results of Figs. 1 and 2 the same percentage change of cross sections was applied to the full energy range of the core. As long as the changes in k are small they are quite linear with the changes in cross sections, even if the latter are large.

The research reported in this paper was supported in part by the KBB (Karlsruhe) - Euratom Association on Fast Reactors, Kernforschungszentrum , Karlsruhe.

Raising σ_c reduces, of course, the criticality factor, as raising $\nu\sigma_f$ increases it. The amount of Δk caused by $\Delta\sigma_c$(Fe) is comparable with that evaluated by Kusters [3]; the Δk caused by $\Delta\sigma_f$(Pu) is, however, higher in the present case, probably because we calculated a less dilute system. The behaviour of Δk with $\Delta\sigma_{el}$ is the combined effect of two opposing tendencies: one - to lower leakage and increase k, and the other - to increase elastic moderation and soften the spectrum thus decreasing k. The lower the isotope mass, the stronger is the second tendency and therefore in Fig. 2, Δk goes from positive values for Fe to negative ones for C*. The inelastic scattering cross section is, on the average, much lower than the elastic one, so that changes in σ_{in} reflect mostly the degradation (as opposed to the leakage) effect, with negative Δk as a result. Changes in the energy spectrum of inelastically scattered neutrons from U and Pu were examined for scattering at energies above 2 MeV. The effect on the criticality factor is very small: augmenting the parameter a in the evaporation formula from 22 to 38 [8] lowers k by 0.05%.

Self-shielding factors, although not basic data in themselves, depend heavily on resonance parameters and frequently serve as basic input for Doppler calculations [9]. It was therefore thought worthwhile to calculate the changes in Doppler and sodium void effects caused by altering the differences $(f_{900}-f_{300})$ and $(f_{1500}-f_{300})$, where f stands for the shielding-factor. The same percentage change was applied to these differences in the full Doppler energy range (0.1 - 20 keV). The results are summarized in Fig. 3. An increase in the values of (f_T-f_{300}) is the result of a decrease in the overlapping between resonances or a decrease in the background cross section. Thus the shielded cross sections for T = 900° and T = 1500° become higher and, as in Fig. 3, the rate of change of the criticality factor increases for fission and decreases for capture.

A more straightforward dependence of the Doppler and sodium void effects on changes in the resonance parameters of U-238 and Pu-239 is provided by Tables I and II. The corresponding changes in Δk are now composite results of variations in the average (infinite dilution) values of the cross sections and in the self-shielding factors.

4. Basic Data: Needed and Available Accuracies

According to Greebler [5] and R. D. Smith [11] the required accuracy in the calculated criticality factor for large fast reactors is 0.5% k. For the total voiding of Na, required accuracy, as given by Greebler [5], is 0.1% k, and for the Doppler effect it is 5%, which amounts to about 0.025% k for our system.

The required accuracies in cross sections, as obtained from Figs. 1 and 2 according to the above criteria, are compared in Table III with the accuracies in the available data. The latter accuracies are either strictly experimental or are estimated from discrepancies in reported data.

In Tables I and II the changes in resonance parameters reflect uncertainties either as summed up by J. J. Schmidt [16] or as estimated by us. Most of these changes induce uncertainties in the Doppler effect beyond the permitted ones. In U-238 the Doppler effect is sensitive to the values of $D_{J=1/2}$, Γ_γ, S_o and $D_{J=3/2}$. In Pu-239 it is sensitive

---

* Δk for changes $\Delta\sigma$(C) are calculated for a 2500-liter PuC-UC system.

to the values of S_o, $D_{observed}$, $\Gamma_f(J=0)$ and the number of degrees of freedom of the fission width distribution - ν (the transition from high to low ν renders the Doppler effect less positive, as expected by Greebler [2]).

To sum up - the average cross sections listed in Table III need to be measured to better accuracies than have been achieved so far, and, on the whole, better resonance statistics are needed to improve the calculation of the Doppler effect in U-238 and Pu-239.

The call for better basic data assumes that each individual cross section uncertainty exerts its full influence on the reactivity effects in the core. Taken together, of course, uncertainties which induce changes of opposite sign in k may reduce to some extent the overall absolute error in k, as for example in calculating criticality factors [5]. Such an occurrence is, however, incidental and does not lessen the need for better measured cross sections.

5. The High Pu Isotopes

The criticality factor and the coolant void effect are more sensitive to inaccuracies in the cross sections of Pu-240 and Pu-241 than would be expected from the relative density of these isotopes in the fuel [5]. However, wide gaps exist in the experimental basic data on Pu-240 and Pu-241 other than the fission cross sections, and these gaps cannot be simply bridged unless rough interpolations and crude theoretical arguments are applied [17,18]. In the resonance region the basis for predicting resonance parameters for Pu-240 and Pu-241 was hitherto poorer than that for U-238 and Pu-239. The statistical accuracy is now being much improved by nuclear explosion measurements [19,20].

6. Some Remarks on Basic Nuclear Data from the Viewpoint of Reactor Theory

The parameters appearing in the equations used in reactor calculations constitute the basic nuclear data required for the calculations. These parameters vary according to the equations used, and thus the type of equations determines what will be considered "basic nuclear data". In the framework of multigroup diffusion the basic input data are the group cross sections for absorption, fission and transport, and the intergroup transfer elastic and inelastic cross sections. Recently a rigorous formulation of multigroup equations has been completed [21,22] and we mention here several of its implications that concern the definition and use of basic data.

a) The definition of the transport cross section as a reciprocal-type average over the constituents of a mixture has already raised the question of how to decompose it to microscopic contributions from the various isotopes in the mixture [23]. A further complication arises if σ_{tr} is to be given as an energy dependent cross section, because the latter does not really exist. The definition of $1/\sigma_{tr}$ as

$$1\Big/\left[\sigma_t\left(1 - \frac{\sigma_s}{\sigma_t}\mu\right)\right]$$

only holds for monoenergetic problems, while for

energy degradation ones the true definition is for a group g

$$\frac{1}{<\Sigma_{tr}>_g} = \frac{<1/\Sigma_t>_g}{1 - <\frac{\Sigma_s}{\Sigma_t}>_g \mu(g,g)}$$

where $\mu(g,g)$ is the average cosine in scattering within group g. This excludes the possibility of obtaining $<\Sigma_{tr}>_k$ as an average over some elemental $\sigma_{tr}(E)$. Compilations of $\sigma_{tr}(E)$ data [24] should therefore be used with care.

b) the measured elastic differential cross sections are frequently given in the form of energy dependent coefficients of a Legendre expansion [25]. Among other uses, these coefficients have been put into series descriptions of $\xi(E)$ and $\mu(E)$ [26,27], respectively the average lethargy gain per elastic scattering and the average laboratory cosine in this scattering. In some cases, however, instead of calculating ξ and μ by such series (a procedure that involves a consideration of where to terminate the series) the following approximate formulae can be applied [22]

$$\xi = \frac{\alpha}{2}(1 - <\mu_c>) + \frac{\alpha^2}{8}<(1 - \mu_c)^2> + O\left(\frac{5}{A^2}\right) \quad \text{for } A \geq 10$$

$$\mu = <\mu_c> + \frac{1 - <\mu_c^2>}{A} + O\left(\frac{1}{A^2}\right) \quad \text{for } A \geq 10$$

where α is $\frac{4A}{(A+1)^2}$ and μ_c is the cosine in center-of-mass coordinates. It is proposed that for $A \geq 10$ the quantities $\xi(E)$ and $\mu(E)$, calculated in this way, could be included as basic data stemming from the analysis of angular distributions.

c) The two foregoing remarks represent achievements in reactor theory. The present one is concerned rather with a shortcoming. It is that slowing down theories do not describe to a sufficient accuracy the gross variation of the reactor flux with energy. Due to the fact that different weighting fluxes for core and blanket produce significant changes in the elastic moderation cross sections [3] and that the low energy tail is underpredicted by present elastic moderation cross sections, it is proposed that flux-shapes for different reactor types should be measured and considered as basic data.

7. Conclusion

The calculations performed in the present study, although of rather limited range, fit in with the findings of Greebler [5] and Hummel [4] as to the inadequacy of much of the available cross section data from the standpoint of accuracy in reactor calculations. It has also been shown that the resonance parameters for Pu-239 and U-238 still lack the required accuracy for predicting the Doppler effect. Some remarks are made on the question of basic data as from a theoretical point of view.

TABLE I

Change in the Doppler and sodium void effects caused by changes in resonance parameters of U-238

No.	Change in resonance parameter	Change in Doppler effect (% k)		Change in Na void effect (% k)	
		900°	1500°	900°	1500°
1	$S_o(ev^{-\frac{1}{2}})$: $0.9 \times 10^{-4} \rightarrow 1.0 \times 10^{-4}$	-0.016	-0.030	-0.012	-0.023
2	$S_1(ev^{-\frac{1}{2}})$: $2.5 \times 10^{-4} \rightarrow 3.0 \times 10^{-4}$	-0.006	0	-0.005	0
3	$D_{J=1/2}(ev)$: $20.8 \rightarrow 22.8$	-0.044	-0.123	-0.011	-0.078
4	$D_{J=3/2}(ev)$: $11.4 \rightarrow 12.5$	-0.011	-0.021	-0.008	-0.015
5	$\Gamma_\gamma(mV)$: $25 \rightarrow 31$	-0.041	-0.074	-0.024	-0.049

TABLE II

Change in the Doppler and sodium void effects caused by changes in resonance parameters of Pu-239

No.	Change in resonance parameter	Change in Doppler effect (% k)		Change in Na void effect (% k)	
		900°	1500°	900°	1500°
1	$S_o(ev^{-\frac{1}{2}})$: $1.07 \times 10^{-4} \rightarrow 1.20 \times 10^{-4}$	+0.029	+0.043	+0.008	+0.016
2	$D_{obs}(ev)$: $2.3 \rightarrow 2.8$	+0.025	+0.053	+0.008	+0.022
3	$\Gamma_{f,J=0}(ev)$: 2800 – 1000	+0.019	+0.038	+0.006	+0.015
4	$\Gamma_{f,J=1}(ev)$: 57 → 86 for 0.1 keV 70 → 105 for 1 keV 83 → 125 for 10 keV	+0.008	+0.014	+0.003	+0.003
5	$\chi_\nu(\Gamma_{f,J=1})$: $\nu = 1 \rightarrow 2$	+0.033	+0.046	+0.010	+0.016

TABLE III

Comparison of available and required accuracies in basic data

Basic data	Required accuracy	Available accuracy
σ_f (Pu-239)	2%	25% [5,12]*
σ_c (U-238)	3%	25% [3,5,12]
σ_f (U-238)	5%	20% [14]
σ_{el} (Fe)	8%	10% [5]
α (Pu-239)	10%	50% [5,14]
σ_c (Fe)	27%	40% [2,3,5,15]
Γ_γ (Na resonance)	30%	30 - 200% [3,5]

* The 10% accuracy which is achieved in the bomb measurements [13] is still higher than required.

References

[1] OKRENT, D.,"Summary of Intercomparison Calculations Performed in Conjunction with the Conference on Safety, Fuels and Core Design in Large Fast Reactors", ANL-7120.

[2] GREEBLER, P. et al., "Calculated Physics Parameters and their Uncertainties in a 1000-MW(e) Fast Ceramic Reactor", ANL-7120.

[3] KUSTERS, H. and METZENROTH , M., "The Influence of Some Important Group Constants on Integral Fast Reactor Quantities", ANL-7120.

[4] HUMMEL, H. H.,"Sensitivity of Fast Reactor Parameters to Cross Section Uncertainties", Conf. on Neutron Cross Section Technology, March 22-24, 1966.

[5] GREEBLER, P. and HUTCHINS, B. A., "User Requirements for Cross Sections in the Energy Range from 100 ev to 100 kev", Conf. on Neutron Cross Section Technology, March 22-24, 1966.

[6] YIFTAH, S. and OKRENT, D., "Some Physics Calculations on the Performances of Large Fast Breeder Reactors", ANL-6212 (1960).

[7] YIFTAH, S. and SEGEV (Sieger), M., "Nuclear Cross Sections for Fast Reactors", IA-980 (1964).

[8] BATCHLOR, R., "The Statistical Model", Conf. on the Study of Nuclear Structure with Neutrons, Antwerp, July 19-22, 1965.

[9] ABAGYAN, C. P. et al., "Group Constants for Nuclear Reactor Calculations", Consultants Bureau (1964)

[10] HUMMEL, H. H. et al., "Recent Investigations of Fast Reactor Reactivity Coefficients", ANL-7120 (1965)

[11] SMITH, R. D. et al., "Theoretical and Experimental Work on the Physics of Fast Reactors", London Conf. on Fast Breeder Reactors, 17-19 May, 1966.

[12] HUMMEL, H. H. et al., "Recent Theoretical Work in the U.S. on Fast Reactor Physics", London Conf. on Fast Breeder Reactors, 17-19 May, 1966.

[13] EDWARD, R. et al., "Fission Cross Section of Pu^{239}, 20 ev to 2 MeV, LA-DC-7620 (1966).

[14] STEIN, W. E. et al., "Relative Fission Cross Sections of U^{238}, Np^{237} and U^{235}", Conf. on Neutron Cross Section Technology, March 22-24, 1966.

[15] GIBBONS, J. H., "Neutron Cross Sections in the Energy Range 100 ev < E_n < 100 kev: Recent Progress, Current Status, Future Outlook", Conf. on Neutron Cross Section Technology, March 22-24, 1966.

[16] SCHMIDT, J. J., "Resonance Properties of the Main Fertile and Fissionable Nuclei", American Nuclear Society National Topical Meeting on Reactor Physics in the Resonance and Thermal Regions , San Diego, Feb. 7-9, 1966.

[17] YIFTAH, S. et al., "Fast Reactor Cross Sections", Pergamon Press, 1960.

[18] DOUGLAS, A. C., "Neutron Cross Sections of Pu^{240} in the Energy Range 1 kev to 15 MeV",AWRE 0-91/64 (1965).

[19] BYERS, D. H. et al., "Capture and Fission Cross Sections of Pu^{240}", Conf. on Neutron Cross Section Technology, 22-24 March,1966.

[20] SIMPSON, O. D. et al., "The Fission Cross Section of Pu^{241} from 20-200 ev as Determined from a Nuclear Explosion", Conf. on Neutron Cross Section Technology, 22-24 March, 1966.

[21] SEGEV, M. and YIFTAH, S., "Multigroup Diffusion and Multigroup Cross Sections", IA-1088 (1966).

[22] SEGEV, M. and YIFTAH, S., "Group Diffusion with Elastic Scattering", IA-1093 (1966).

[23] ZWEIFFEL, P. F. and BELL, G. L., "Group Cross Sections for Fast Reactors", Seminar on the Physics of Fast and Intermediate Reactors, Vienna, 3-11 August, 1961.

[24] SCHMIDT, J. J., "Neutron Cross Sections for Fast Reactor Materials, Part III: Graphs", KFK 120 (EANDC-E-35 U) (1962).

[25] "Reactor Physics Constants", ANL-5800 (1963).

[26] ZWEIFFEL, P. F. and HURWITZ, H. Jr., J. Appl. Phys. 25(10), 1241-245 (1954).

[27] PRITCHARD, W. M. and AHRENS, T., Nucl. Sci. and Eng. 22, 248-252 (1965).

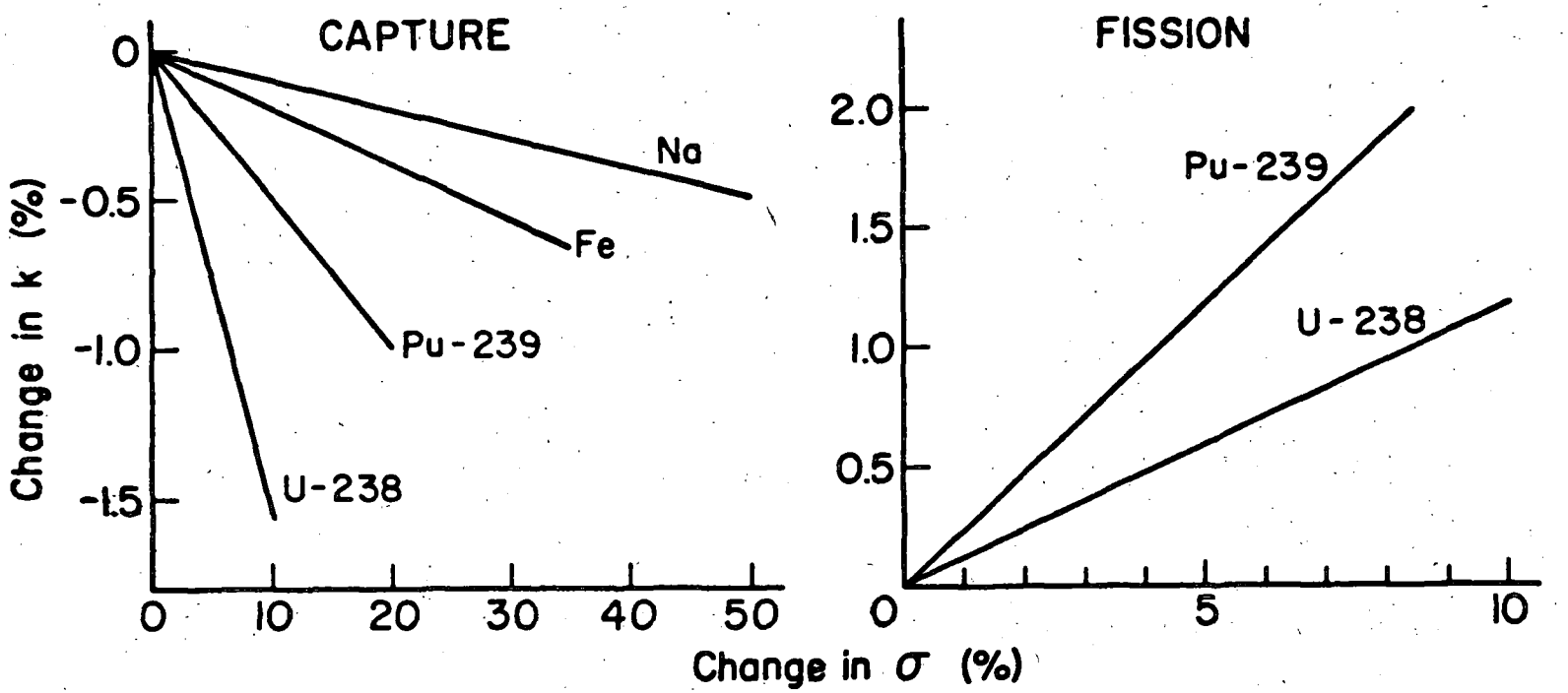

Fig. 1 : Changes in the criticality factor caused by changes in capture and fission cross sections

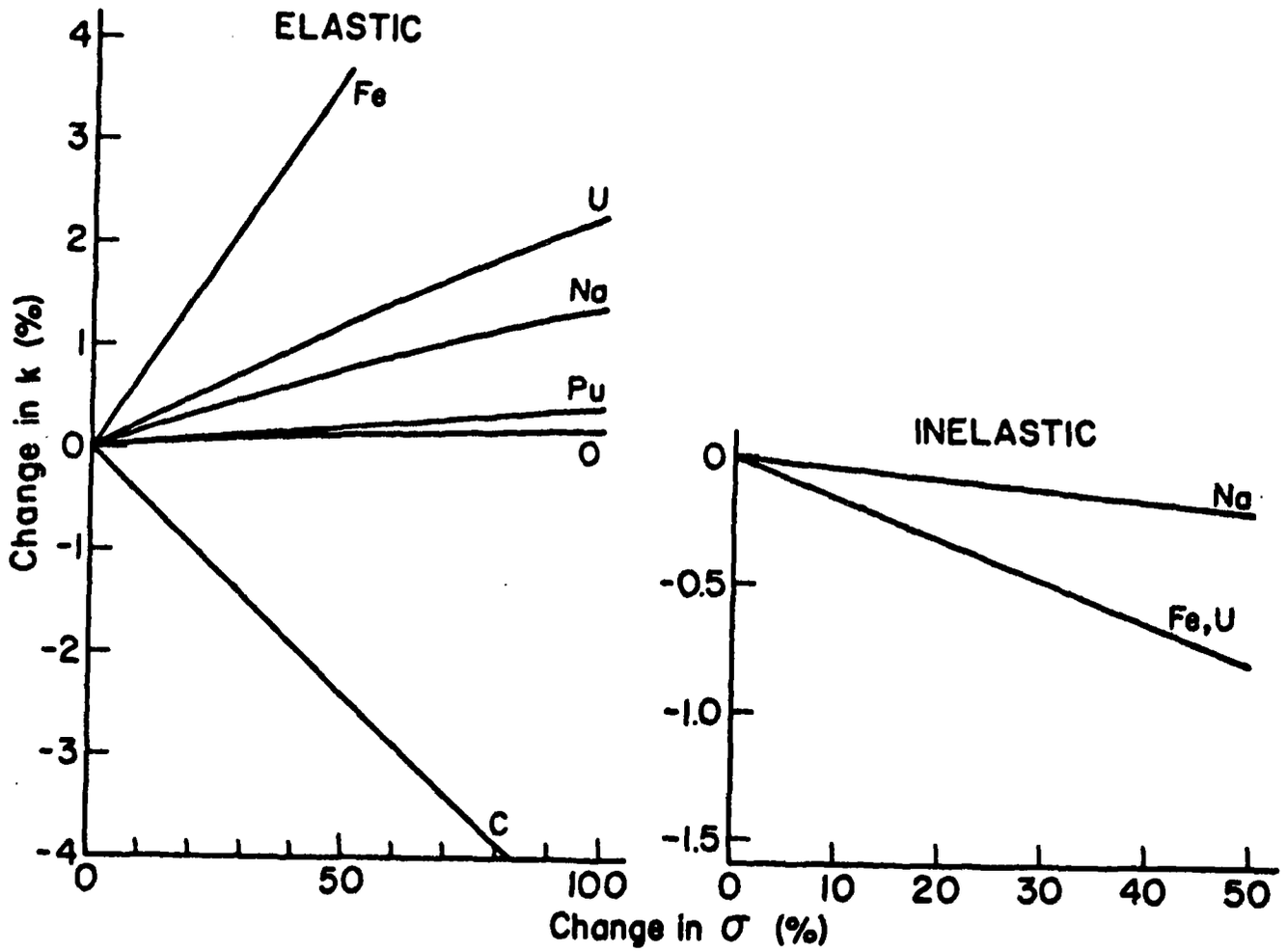

Fig. 2 : Changes in the criticality factor caused by changes in the elastic and inelastic scattering cross sections

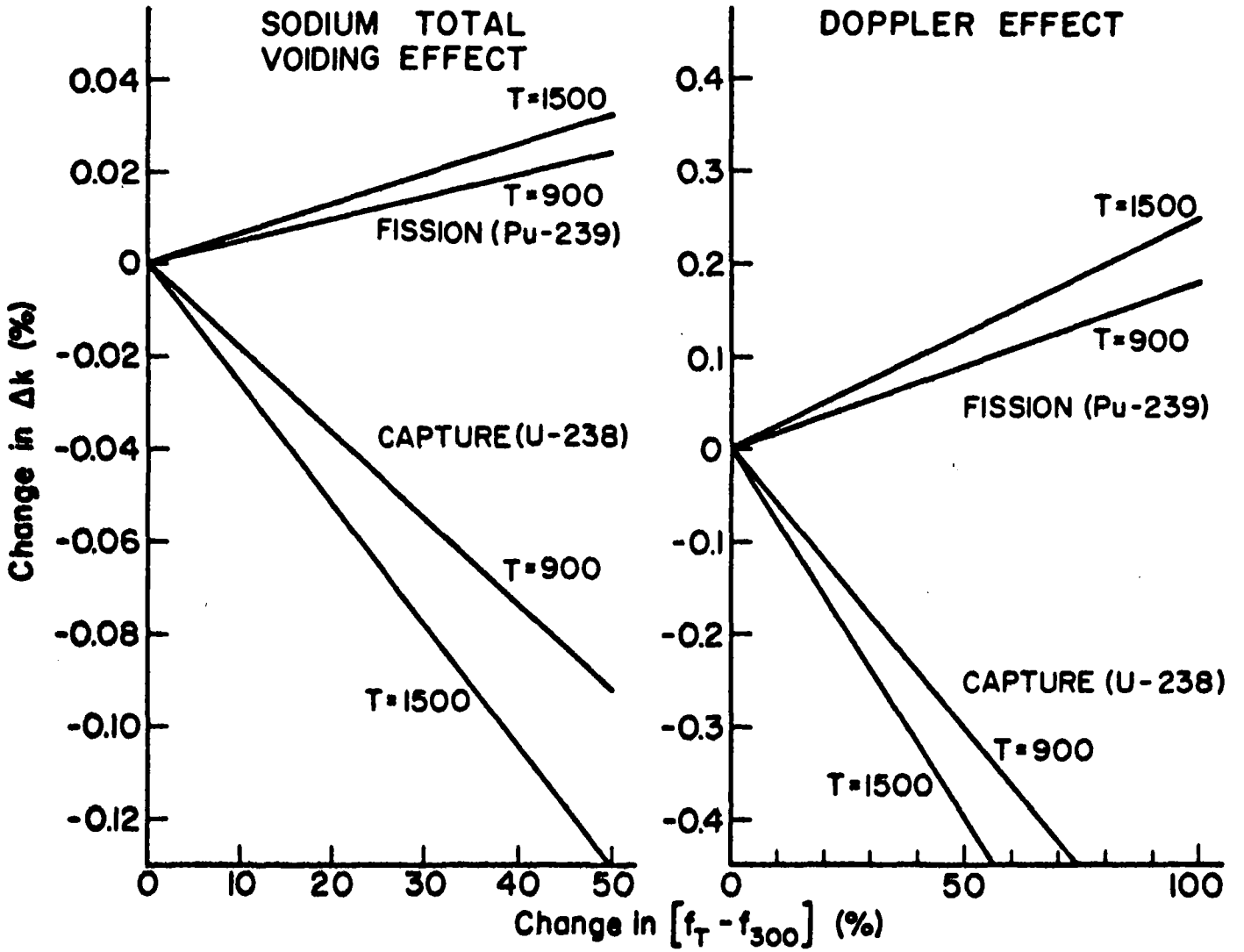

Fig. 3 : Changes in Doppler and sodium void effects caused by changes in self-shielding factors

The (n,2n) cross sections of ^{9}Be and D in the threshold regions

M. Holmberg and J. Hansén
Research Institute of National Defence
Stockholm 80, Sweden

Introduction

This paper gives preliminary data on the (n,2n) cross section of ^{9}Be in the energy region 2 - 6.5 MeV. The shape of the excitation function in this region is of importance for reactor calculations from the viewpoint of neutron economy and helium production.

In addition the cross section of D was measured in the energy region 4 - 6.5 MeV.

It has been known since the work of Fischer [1] that the "effective threshold" for the (n,2n) reaction of Be is at 2.70 MeV. This corresponds to the inelastic scattering to the level at 2.43 MeV of ^{9}Be, which subsequently decays by neutron emission. Above 2.7 MeV the cross section increases rapidly and is about 0.6 b at 4 MeV. Below 2.7 MeV Fischer [1] reported a cross section of 15 mb at 2.57 MeV. However, in the work by Marion et al. [2] the time-of-flight-spectra of the emitted neutrons indicated a contribution from three or four body break-up reactions (thresholds at 1.85 and 1.75 MeV, respectively) or from the inelastic scattering to a level at 1.7 MeV. In fact, Marion et al. [2] concluded that only about half of the (n,2n) cross section at 3.5 MeV arose from the 2.43 MeV level, which indicated that the (n,2n) cross section below 2.7 MeV could be of the order 100-200 mb. This

was also indicated by the revised results [3]. But it should also be pointed out that in the measurement of Wagner and Huber [4] at 3.7 MeV the energy distributions of the emitted neutrons indicated that the levels at 2.43 and 3.1 MeV were entirely dominant.

The measurements of the (n,2n) cross section of Be have been performed with different experimental techniques. Fischer [1] used a neutron regeneration method and Marion et al. [2] combined the time-of-flight measurements with the total minus elastic procedure. The works by Ball et al. [5] and Beyster et al. [6] were made with the sphere transmission method. All these measurements give the total non-elastic cross section or the total non-elastic minus the (n,α) cross section. Direct measurements on the (n,2n) neutrons have been made in the range 6 - 14 MeV by Catron et al. [7] using a large liquid scintillator and in the range 3.2 - 4.5 MeV by Zubov et al. [8] using BF_3-counters.

The aim of the present investigation has mainly been to examine the energy region below 2.7 MeV. A large liquid scintillator was used as detector for the (n,2n) neutrons. However, the experimental method has been somewhat different from that of Catron et al. [7].

Experimental method

The incident neutrons were produced at the 5.5 MeV van de Graaff accelerator at Studsvik. The energy spread of the incident neutrons was about 20 keV for 3 Mev neutrons. The experimental set-up is shown in fig. 1. The large liquid scintillator has earlier been used in $\bar{\nu}$-measurements and is described by Asplund-Nilsson et al. [9]. The tank contained 100 litres of the Gd-loaded scintillator Ne 313.

A fast neutron entering the scintillator gives rise to a prompt pulse due to the n-p scattering, if the neutron energy is above the discriminator setting at about 2 MeV. The neutron is thermalized in a few microseconds and diffuses in the scintillator until it is captured by a Gd-nucleus and a second pulse due to the capture gamma rays occurs. The neutron is captured within 80 μs. With the present method the correlation in time between two successive liquid scintillator pulses was measured. The prompt pulse preceding the capture pulse was first removed. This could be done since the prompt neutron pulse was correlated in time with the pulse from the pick-up tube of the vdG-accelerator. However, for the (n,2n) events there was still

a time correlation between the capture pulses of the two neutrons and this correlation was measured by the use of a time-to-pulse-height converter.

The block diagram of the electronic circuits is shown in fig. 1. The liquid scintillator pulses which passed through the anticoincidence (C) were used both to start and to stop the converter (D). The start pulse was delayed 0.12 μs relative to the stop pulse and with this arrangement the time between two successive pulses could be measured in a time interval of 38.5 μs. For a random distribution of the pulses the probability for a stop pulse to occur in this time interval is given by

$$\int_0^k Re^{-Rt}dt = (1-e^{-Rk}) \approx 0.1 \qquad (R = 2500 \text{ c/s})$$

where R is counting rate and k is the sweep time of the converter (38.5 μs). However, for a (n,2n) event the start pulse is given by the first captured neutron and the stop pulse by the capture of the second neutron. The probability that the stop pulse due to the second neutron occurs within the actual time interval is about 0.9. Accordingly the (n,2n) events could be separated from the random distribution, which in the present experiment was due to the background and the elastically scattered neutrons.

The number of pulses (N) which passed through the anticoincidence circuit was counted by a fast scaler and also the number of output pulses (X) from the converter. For a random distribution of the input pulses to the converter the number of output pulses was given by the expression

$$X_r(T) = \frac{N(1-e^{-Nk/T})}{2-e^{-Nk/T}} \simeq 0.85\,\frac{kN^2}{T} \qquad (1)$$

where X = experimental number of output pulses from the converter. The index r refers to a random distribution

N = total number of input pulses

k = sweep time of the converter

T = time of the experimental run.

The approximation in (1) is valid for the acutal counting rates. An experimental set of values of X_r as a function of N was obtained by measurements on carbon scatterers. When the measurements were extended to scatterers with a nonvanishing (n,2n) cross section this implies $X > X_r$. Hence the number of (n,2n) events was given from the difference $(X - X_r)$, where the proper

value of X_r was obtained by iteration from the experimental value of N. Experimental points of X as a function of N is shown in fig. 2. The spread of the points along the N-axis depends on small changes in the counting rate but also on the fact that samples with different lengths were used. The difference $(X - X_r)$ in fig. 2 corresponds to a (n,2n) cross section of (17 ± 3) mb.

Finally, it should be pointed out that (1) is valid only if the counting rate, R, is approximately constant in the experimental run. This follows from the Schwarz' inequality

$$X_r^{(T)} - 0.85 \frac{kN^2}{T} = 0.85 \left[\int_0^T R^2(t)dt - \frac{1}{T} \left(\int_0^T R(t)dt \right)^2 \right] \geq 0$$

with equality only for R(t) = constant. Therefore, the counting rate was checked during the experimental run by means of a ratemeter and a recorder (fig. 1).

The incident neutron flux was measured by means of a plastic scintillator, the efficiency of which was calculated by a Monte-Carlo program. The efficiency of the large liquid scintillator was determined from the quotient between the observed and the absolute $\bar{\nu}$-value of ^{252}Cf. The absolute value was taken to be 3.772 ± 0.015 [10].

Cross section evaluation and corrections

The (n,2n) cross section, $\sigma_{n,2n}$, was calculated from the expression

$$\frac{\sigma_{n,2n}}{\sigma_t} (1 - e^{-A\sigma_t}) (1 + R) \frac{N_p}{\epsilon_p} \cdot \epsilon_{n;2n} = N_{n,2n} \qquad (2)$$

where σ_t = total cross section

A = number of atoms per cm^2

R = ratio of (n,2n) events produced by elastically scattered neutrons to the (n,2n) events resulting directly from first collisions of incident neutrons

N_p = number of counts registered by the plastic scintillator

ϵ_p = efficiency of the plastic scintillator

$\epsilon_{n,2n}$ = efficiency of the large liquid scintillator for (n,2n) detection

$N_{n,2n}$ = number of (n,2n) events registered by the large liquid scintillator

The total cross section of Be was from the data compilation by Doherty [11]. The multiple scattering correction, R, was calculated by the use of the Monte-Carlo program written by Zetterström [12]. For these calculations the angular distributions of the elastically scattered neutrons were taken from BNL 400. The multiple scattering correction was 12 % at 4.2 MeV and the error was estimated to be less than 2 %. The following corrections were applied to the Be cross sections calculated from equation (2):

1) Variation of neutron detector efficiency with neutron energy. This correction must be calculated on the basis of some assumption about the energies of the emitted (n,2n) neutrons. It was assumed that the (n,2n) reaction above 4 MeV proceeds by inelastic excitation to the levels of ^{9}Be at 2.43 MeV (80 %), 3.04 MeV (15 %) and 5 % by excitation to the 1.7 MeV level or by direct break-up reactions. For the 2.43 MeV level the energy distribution of the first neutron in the laboratory system was calculated using the angular distributions for inelastic scattering to this level measured by Marion et al. [2]. The energy of the second neutron will be less than 1 MeV either this level decays to the ground state of ^{8}Be or via $^{9}Be^{*} \rightarrow {}^{5}He + {}^{4}He \rightarrow 2\,{}^{4}He + n$ [13]. The calculations for the remaining levels were performed in a similar way. It should be pointed out that the correction only is of importance above 4 MeV of incident neutron energy because of the flat energy response of the liquid scintillator below 2 MeV.

2) Absorption of the (n,2n) neutrons by the (n,α) process in the Be sample. This correction was calculated using the above assumptions of the energies of the two neutrons. The correction was 1.5 % at 6.5 MeV.

3) Neutron escape along the axial channel of the scintillator tank. This correction depends on the fact that the (n,2n) neutrons are not emitted isotropically.

4) Spectrum of the incident neutrons. At the higher energies (n,2n) events were induced by low energy neutrons. The correction was (2 $\pm$ 0.5) % at 6.5 MeV.

5) Neutron flux correction. The runs with the plastic scintillator must be corrected for the neutrons which are scattered back to the scintillator by the photomultiplier tube. The correction was 3 % with an estimated error of 1 %.

The data handling procedure for D was close to the above account, valid for the Be data.

Sources of error

The contributions to the absolute error of the cross section at 4.2 MeV are given in Table I. Hence we infer that the error mainly is due to the uncertainty in the determination of $\sigma_{n,2n}$, ε_p and N_p. Therefore, the validity of these figures was determined in separate measurements, in which the total (= elastic) cross section of carbon was used as standard. The relative error of $\sigma_{n,2n}$ is mainly due to the errors ascribed to N_p and ε_p in table I. The error in N_p depends mainly on the uncertainty in the determination of the proton recoil spectrum. For small cross sections the absolute error is mainly due to the statistical error of $N_{n,2n}$.

Results and discussion

Only preliminary results exist since all corrections have not been completely examined and in addition we have some discrepancies in the determination of the efficiency of the plastic scintillator. The results for Be are shown in fig. 3 and for D in fig. 4.

The present result for Be at 4.2 MeV is in agreement with the cross section at 4.07 MeV reported by Beyster et al. [6] and at 6.5 MeV there is agreement with the measurement by Catron et al. [7]. However, our results disagree with those of Fischer [1] according to the shape of the excitation function just above the threshold at 2.7 MeV. In fig. 3 is also shown the excitation function recommended in the data compilation by Doherty [11]. The recommended cross section is a compromise between the results of Fischer [1], Levin and Cranberg [3], Beyster et al. [6] and Fowler et al. [14] and the present results confirm the choice.

The most interesting results of the present investigation concern the cross section below 2.7 MeV. It should be noted that the effect of the 2.43 MeV level can be neglected in this region since the level width is ≤ 1 keV. However, the (n,2n) cross section has a value of 25 mb at 2.60 MeV, 13 mb at 2.3 MeV and about 6 mb at 2.2 MeV. Probably this cross section is due to the excitation of the 1.7 MeV level of ^{9}Be. This level has a width of about 200 keV and this implies a threshold at about 2.0 MeV which is in agreement with the present results.

The (n,2n) cross sections for D at 6.2 MeV and 6.5 MeV are somewhat lower than those reported by Catron et al. [7] but the deviation is within the statistical uncertainties. Below 6.1 MeV there are no earlier measurements. The measured cross sections seem to be in reasonable agreement with the shape of the excitation function as calculated by Frank and Gammel [15].

Acknowledgements

The authors wish to thank Dr. H.-O. Zetterström for many fruitful discussions and for performing the Monte-Carlo calculations. The skilful technical assistance of Mr. D. Lundberg and Mr. L.E. Persson is appreciated.

Table I.

The contributions to the error of $\sigma_{n,2n}$ at 4.2 MeV.

	Error (%)
$\epsilon_{n,2n}$	5-6
ϵ_p	4-5
N_p	4-6
$N_{n,2n}$	3
R	1-2
Corrections	2
Total	8-10

References

[1] Fischer, G.J., Phys. Rev. 108 (1957) 99.

[2] Marion, J.B., Levin, J.S. and Cranberg, L., Phys. Rev. 114 (1959) 1584.

[3] Levin, J.S. and Cranberg, L., WASH 1029 (1960) 44; and WASH 1028 (1960) 26.

[4] Wagner, R. and Huber, P., Helv. Phys. Acta 31 (1958) 89.

[5] Ball, W.P., MacGregor, M. and Booth, R., Phys. Rev. 110 (1958) 1392.

[6] Beyster, J.R., Henkel, R.L., Nobles, R.A. and Kister, J.M., Phys.Rev. 98 (1955) 1216.

Beyster, J.R., Walt, M. and Salmi, E.W., Phys.Rev. 104 (1955) 1319.

[7] Catron, H.C., Goldberg, M.D., Hill, R.W., Leblanc, J.M., Stoering, J.P., Taylor, C.J. and Williamson, M.A., Phys.Rev. 123 (1961) 218.

[8] Zubov, Yu.G., Lebedeva, N.S. and Morozov, V.M., "Neitronnaya Fizika", Moscow (1961) 298.

[9] Asplund-Nilsson, I., Condé, H. and Starfelt, N., Nucl.Sci. and Eng. 20 (1964) 527.

[10] Westcott, C.H., Ekberg, K., Hanna, G.C., Pattenden, N.J., Sanatani, S. and Attree, P.M., Atomic Energy Review 3 2 (1965).

[11] Doherty, G., AEEW - M 513 (1965).

[12] Zetterström, H.O., to be published.

[13] Mösner, J., Schmidt, G. and Schintlmeister, J., Nucl.Phys. 64 (1965) 169.

[14] Fowler, J.M., Hanna, S.S. and Owen, G., Phys.Rev. 98 (1955) 249.

[15] Frank, R.M. and Gammel, J.L., Phys.Rev. 93 (1954) 463.

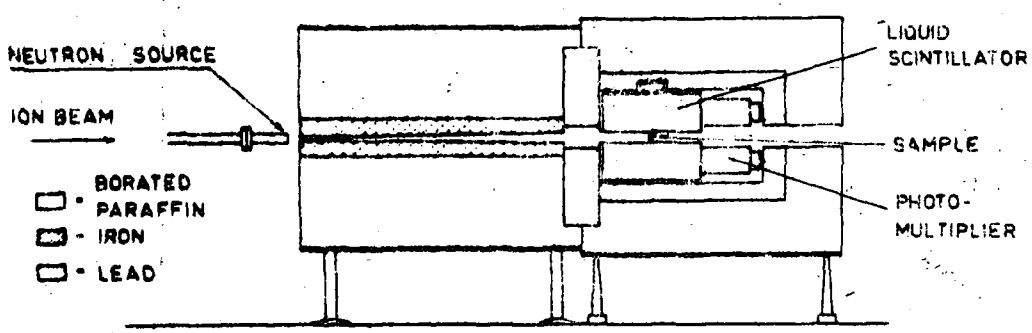

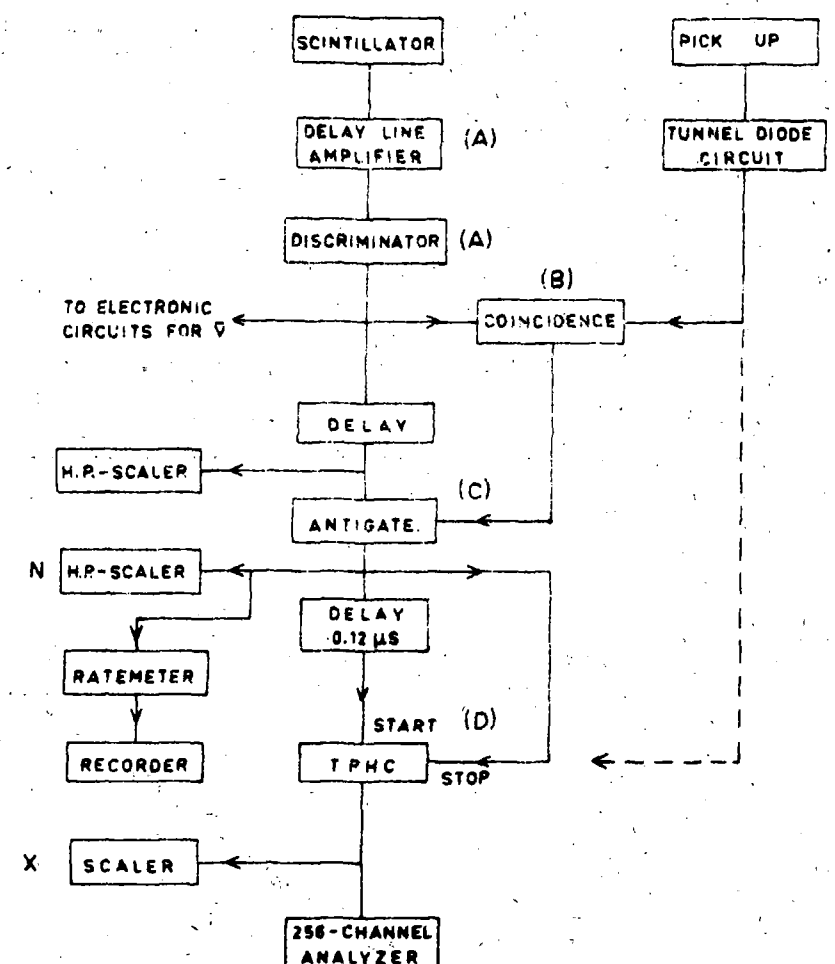

Fig. 1 The experimental set-up and the block diagram of the electronic circuits for the (n,2n) measurement.

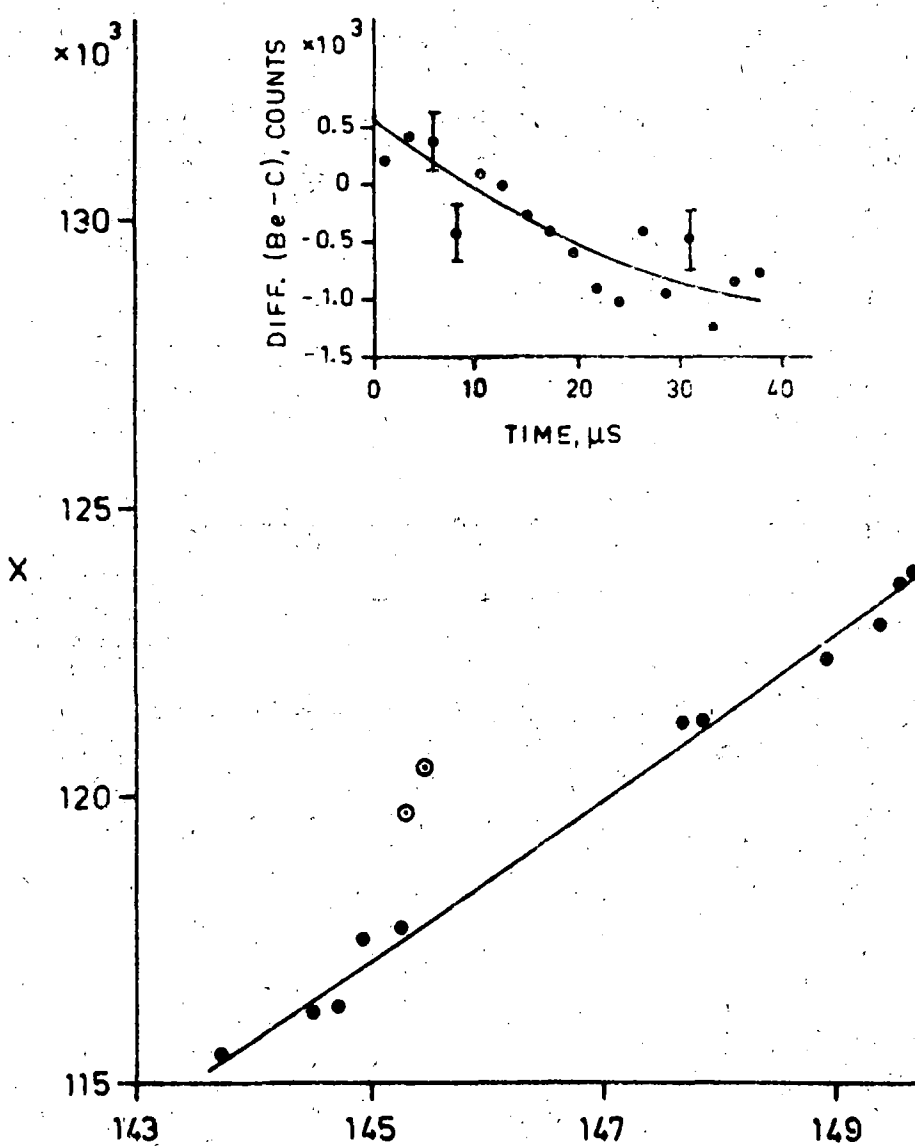
×10^3
130
125
120
115
X
143
145
147
149
×10^3
0.5
0
-0.5
-1.0
-1.5
DIFF. (Be-C), COUNTS
0
10
20
30
40
TIME, μS

FIG. 2

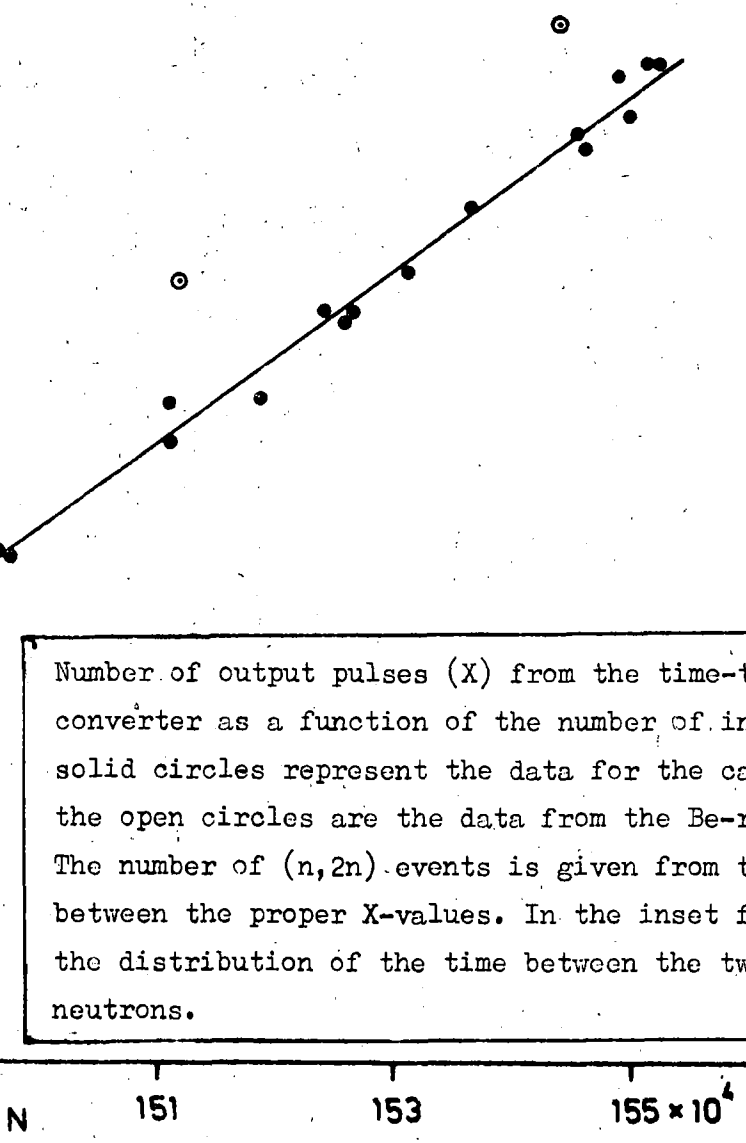

Number of output pulses (X) from the time-to-pulse-height converter as a function of the number of input pulses. The solid circles represent the data for the carbon scatterers and the open circles are the data from the Be-runs at 2.35 MeV. The number of (n,2n) events is given from the difference between the proper X-values. In the inset figure is shown the distribution of the time between the two captured (n,2n) neutrons.

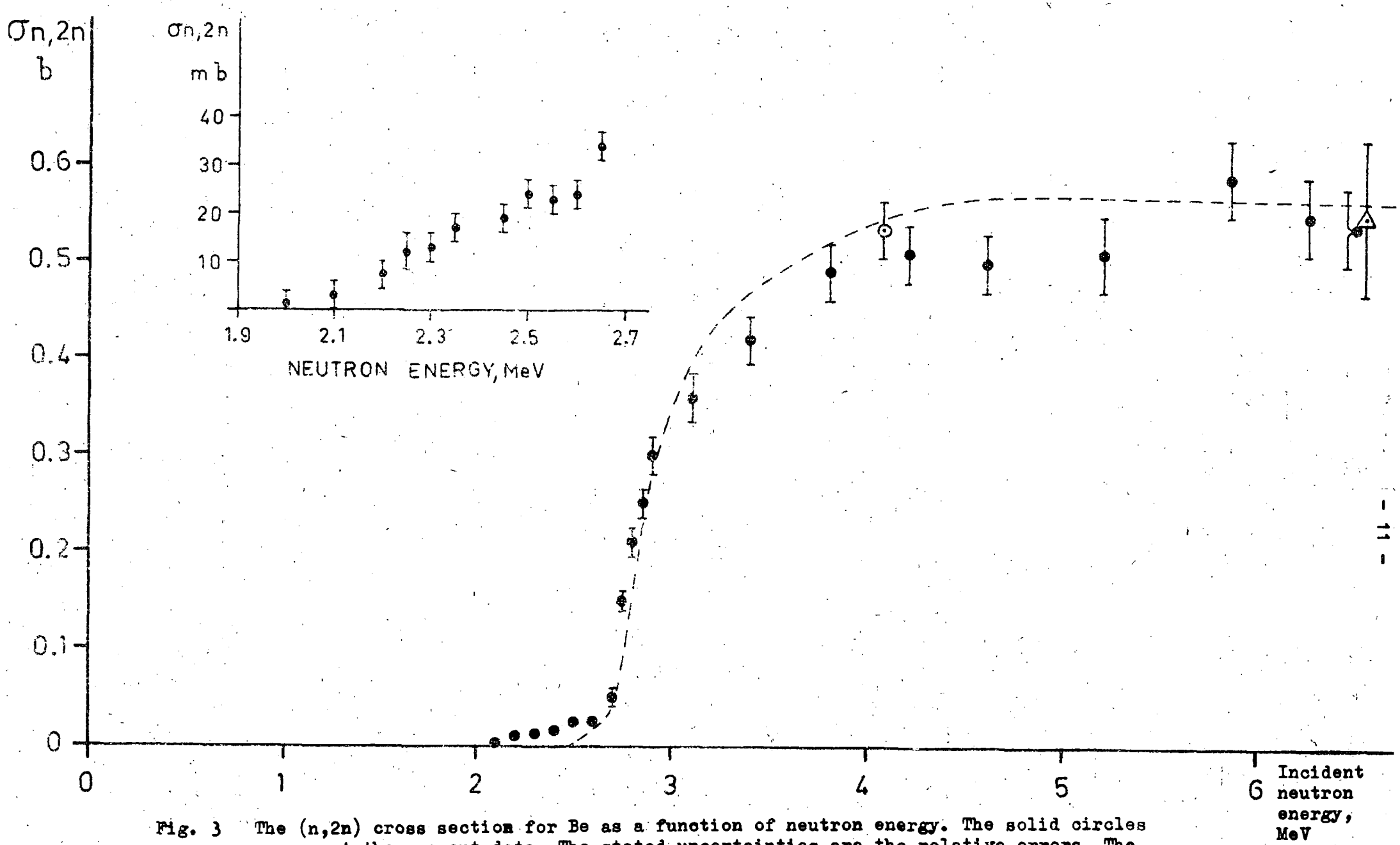

Fig. 3 The (n,2n) cross section for Be as a function of neutron energy. The solid circles represent the present data. The stated uncertainties are the relative errors. The open circle is from Beyster et al. [6] and the open triangle is from Catron et al. [7]. The dashed line is the excitation function recommended in the data compilation by Doherty [11].

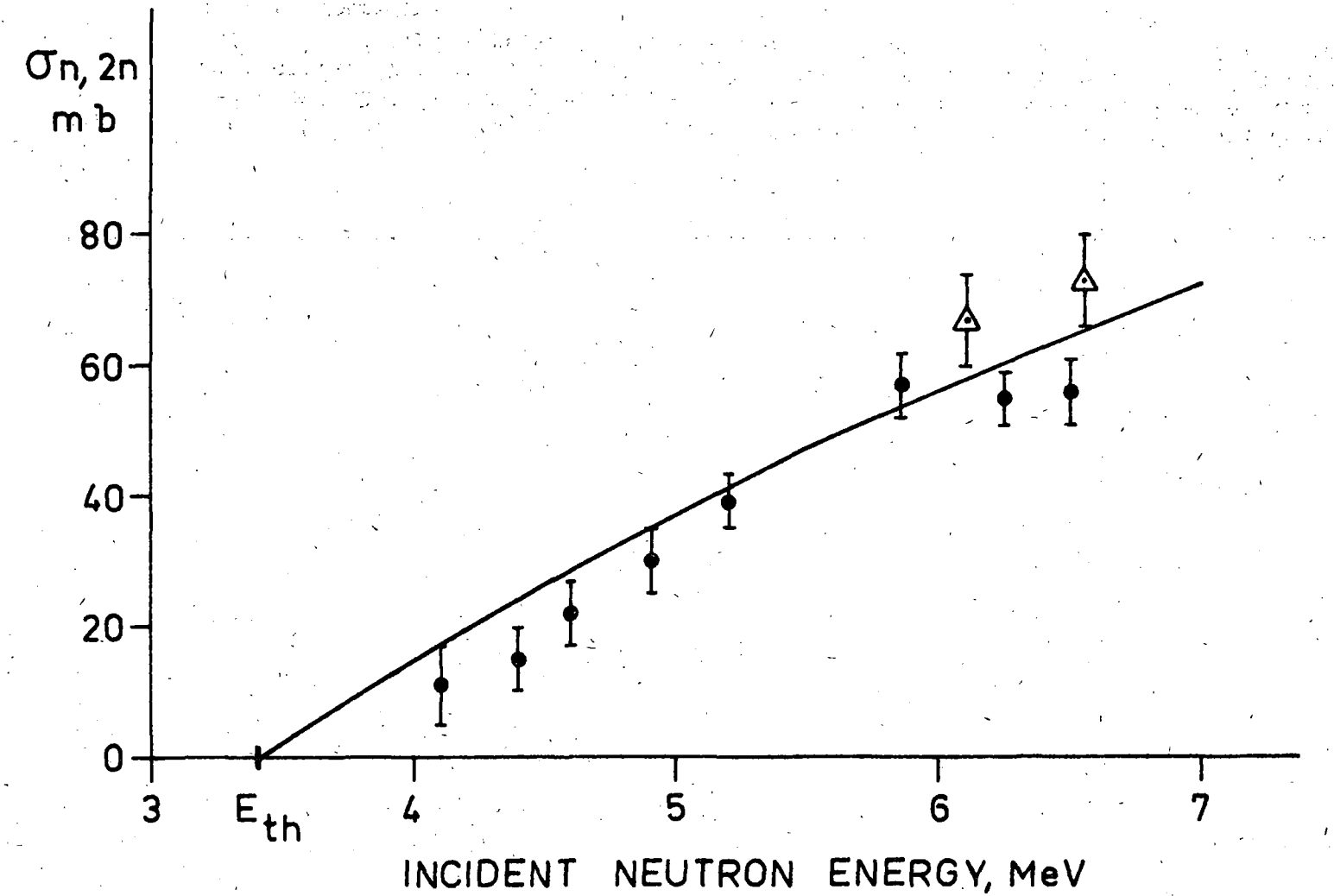

Fig. 4 The (n,2n) cross section for D as a function of neutron energy. The solid circles represent the present data. The stated uncertainties are the relative errors. The open triangels are from Catron et al. [7]. The solid curve is the calculated cross section due to Frank and Gammel [15].

Mechanised Evaluation of Neutron Cross Sections

A. HORSLEY and J. B. PARKER
AWRE, ALDERMASTON, U.K.

1. Introduction

Accurate neutronics calculations depend on good and internally consistent neutron cross section data. In recent years, experimentalists have become very efficient in the measuring of basic nuclear data; so much so, that as Parker [1] and Goldstein [2] have remarked, the available information is by no means being fully exploited.

A radical improvement of this situation can be effected only by mechanising the procedures of evaluation [1]. The problems of collation of the experimental results and speedy access to them should be largely overcome by the SCISRS tape system [3]. It is an easy matter to programme digital computers and graph-plotting machines to display information retained in this form; by such means the labours of evaluation can be greatly reduced.

We examine the problems of mechanised curve fitting of nuclear data and describe a method of graduation based on mathematical spline interpolation used in numerical analysis for approximating to exact functions. This method is extended for application to data subject to statistical error.

2. The curve fitting problems in mechanised evaluation

The two extremes of the many approaches to curve fitting of experimental data are the statisticians', which seeks a fit such that the departures of the data points from the fitted curve are commensurate with the experimental errors, and the more intuitive

approach of the draughtsman which willingly sacrifices non-conforming data to achieve smoothness. The latter, though the less precise, has the virtue of not producing the manifestly absurd results that sometimes bedevil the former. What is needed is a method of curve fitting which combines the virtues of each approach.

Figure 1 is a straightforward, though somewhat extreme, example of a least squares legendre polynomial fit to data for the elastic scattering of neutrons by deuterium. By the criterion of the chi-square test it is a good fit i.e. the deviation from the fit is commensurate with the statistical errors, but, even without knowledge of the physical situation, one would be tempted to regard it as extravagant and unlikely. For when curves are drawn by hand it is probably fair to say that some notions of "smoothness" and "reasonableness" are imposed. That this is so is exemplified in the use of french curves and the draughtsman's spline.

In that most physicists would feel justified in rejecting the above fit it would seem that there is more information available than is contained in the purely statistical details of the data points. Yet, in all likelihood, as much physical information as can be quantified is already contained in the statement that the distribution can be represented as a legendre polynomial expansion.

The additional information is really that, although the approximation to the distribution at the actual data points is good, the extrapolation, and to a lesser degree, the interpolation is very bad; this arises because the representation of a function by legendre polynomials converges very slowly to the function and even more slowly to the derivatives (unless the points fitted are exact function values). This fault is common to all fitting of data points by analytic approximations and occurs because large variations over part of the range (bad data

points) tend to imply similar variations over the remainder of the range. In other words, a few bad data points, when fitted by these means, can spoil the approximation to perfectly good points in another part of the range.

Of course, there are means, subtle and otherwise, of overcoming these difficulties but they are usually very complicated; what is important in mechanised evaluation is that the prescription is simple and that the good data is not lost as a result of there also being bad data.

The other major difficulty in mechanised evaluation of data is the fitting of very complex curves, sometimes over a large energy range. It is easy to point to examples of, say, resonances for which approximation by analytic functions would be hopelessly unwieldy.

We think that the method of interpolation by mathematical splines, discussed by many authors (see, for example; references 4-6), for the representation of exact functions can be developed for use with statistical data to overcome the above difficulties, and we discuss in the next section several approaches which are, operationally, very simple to use.

3. Splines

Our investigations began with the mathematical spline interpolation procedure because it is the analogue of some methods of manual curve fitting. A spline function $S(x)$, of order $2m - 1$, interpolating the values $y_1, y_2, \ldots, y_n$ at $x_1, x_2, \ldots, x_n$ (termed nodes of the spline) has the properties

I(i) $S(x_i) = y_i$ for $i = 1, \ldots, n$

I(ii) $S^{(m-1)}(x)$ is continuous in $[x_1, x_n]$

I(iii) $\int_{x_1}^{x_n} (S^{(m)}(x))^2 \, dx$ exists and is minimised under conditions I(i) and I(ii).

For exact function values $F(x)$ the principal properties of the spline of order $2m - 1$ are its approximation to the function and its derivatives [7]. If we write

$$\Delta = \max(x_{i+1} - x_i)$$

then with conditions I(i) to I(iii) and the requirement that $F(x)$, $F^{(1)}(x), \ldots, F^{(m-1)}(x)$ be absolutely continuous over $[x_1, x_n]$ we have, as the number of nodes is increased such that $\Delta \to 0$,

$$S^{(\nu)}(x) \to F^{(\nu)}(x) \qquad \nu = 0, 1, \ldots, m-1$$

and

$$\int_{x_1}^{x_n} (S^{(m)}(x) - F^{(m)}(x))^2 \, dx \to 0$$

With cubic splines (i.e. interpolating cubic polynomials, $m = 2$) condition I(iii), or similar conditions, can be thought of as a minimising of the overall curvature; the analogy with an "infinitely thin" draughtsman's spline, which achieves a fit through a set of points by minimising its strain energy, is apparent.

Condition I(iii) can be shown to be equivalent to the requirements:

II(i) $S^{(m)}(x)$ is continuous in $[x_1, x_n]$

II(ii) $S^{(m)}(x_1) = S^{(m)}(x_n) = 0$

Using these we may write the equation for a cubic spline in terms of the knots (x_i, y_i) and the second derivatives, g_i, at the knots as

$$S(x) = \sum_{i=1}^{n} \phi_i(x) \left[y_i + x^i \left\{ \frac{y_{i+1} - y_i}{h_i} - \frac{h_i}{6}(g_{i+1} + 2g_i) \right\} + \frac{g_i (x^i)^2}{2} + \frac{g_{i+1} - g_i}{6h_i}(x^i)^3 \right] \qquad (1)$$

where $h_i = x_{i+1} - x_i$ and $x^i = x - \sum_{j<i} h_j$ and

$$\phi_i(x) = 1 \qquad x_i < x < x_{i+1} \qquad i = 1, \ldots, n-2$$
$$\phi_{n-1}(x) = 1 \qquad x_{n-1} < x < x_n$$
$$= 0 \qquad \text{otherwise}$$

From II(i) and II(ii) we have

$$\frac{h_{i-1}}{6} g_{i-1} + \frac{h_{i-1} + h_i}{3} g_i + \frac{h_i}{6} g_{i+1} = \frac{y_{i-1}}{h_{i-1}} - \left(\frac{1}{h_{i-1}} + \frac{1}{h_i}\right) y_i + \frac{y_{i+1}}{h_i} \qquad (2)$$

$$i = 2, 3, \ldots, n-1$$

and

$$g_1 = g_n = 0 \qquad (3)$$

We may write (2) and (3) symbolically as a matrix relationship

$$Ag = By \qquad (4)$$

From (4) we can solve for g in terms of y:

$$g_j = \sum_{k=2}^{n-1} C_{jk}\, y_k + \delta_{j2}\, y_1/h_1 + \delta_{jn-1}\, y_n/h_{n-1} \qquad (5)$$

where

$$C_{ii} = -\frac{1}{4h_i\, h_{i+1}} - \frac{1}{\Delta_1^n}\left\{\Delta_1^{i-1}\, \Delta_{i+1}^n \left(1 + \frac{h_i}{4h_{i+1}}\right) + \Delta_1^i\, \Delta_{i+2}^n \left(1 + \frac{h_{i+1}}{4h_i}\right)\right\}$$

$$C_{ij} = (-1)^{i-j}\, \Delta_1^{i-1}\, h_{i+1} \cdots h_{j-1}\, \Delta_j^n \times \left\{\left(\frac{1}{h_j} + \frac{1}{4h_{j+1}}\right) + \frac{\Delta_{j+2}^n}{\Delta_j^n}\left(h_j + \frac{h_{j+1}}{4}\right)\right\} \qquad j > i$$

and

$$\Delta_i^j = \det \begin{bmatrix} g_i & h_{i+1} & & & & \bigcirc \\ h_{i+1} & g_{i+1} & h_{i+2} & & & \\ & \ddots & \ddots & \ddots & & \\ & & & h_{j-1} & g_{j-1} & h_j \\ \bigcirc & & & & h_j & g_j \end{bmatrix}$$

with the convention $\Delta_i^{i-2} = 0, \Delta_i^{i-1} = 1$; thus the equation of the spline can be written uniquely in terms of the nodes.

A computer programme which uses the above relations to obtain fits to angular distribution data has been described elsewhere by Horsley [8]. It uses a cubic spline fitting procedure by Fowler [14]. This programme takes the given data points as nodes and has a facility for allowing an iterative movement of the actual data points within prescribed limits so as to reduce the overall curvature, thereby "smoothing" the curve. In this programme, instead of the usual least squares legendre polynomial fit to the data points $\sigma(E_j, \mu_r)$ $r = 1, \ldots, R$, (μ_r is the cosine of the scattering angle and E_j the incident energy) the expression minimised is

$$\Delta_j^2 = \sum_{r=1}^{R} \frac{1}{\Delta\sigma_r^2} \left[\sigma(E_j, \mu_r) - \sigma(E_j) \sum_{k=0}^{K} \left(\frac{2k+1}{4\pi} \right) f_k(E_j) P_k(\mu_r) \right]^2$$

$$+ \alpha \left\{ \sum_{t=1}^{T} \left[S(E_j, \mu_t^1) - S(E_j) \sum_{k=0}^{K} \left(\frac{2k+1}{4\pi} \right) f_k(E_j) P_k(\mu_t^1) \right]^2 \right.$$

$$\left. + \sum_{\mu_x = \pm 1} \left[U(E_j, \mu_x) - U(E_j) \sum_{k=0}^{K} \left(\frac{2k+1}{4\pi} \right) f_k(E_j) P_k(\mu_x) \right]^2 \right\} \qquad (6)$$

where α is the weight ascribed to the interpolates and extrapolates.

In (6) $S(E_j, \mu_t^1)$ $t = 1, \ldots, T$ are interpolates obtained from the spline fit and $U(E_j, \mu_x)$ are obtained by extrapolating on a linear-log scale from the data points at the ends of the range using the spline approximation to the 1st derivative. The spline fit to the data of figure 1 is shown in figure 2.

The above method works well when the data is relatively sparse and evenly distributed. When the data is conflicting, as it may be when it comes from several experimenters, it is essential to pay attention to its statistical nature; there are probably many recipes for extending the use of splines to do this and in the remainder of the Section we examine two which appear particularly promising.

First we consider the use of splines with a method of data graduation due to Whittaker [9]. This has been considered independently by Larkin [10] and Schoenberg [11]; the problem is, given the data points (x_i, y_i) $i = 1, \ldots, n$ to find the z_i $(i = 1, \ldots, n)$ which minimise the expression

$$\Delta = \lambda \int_{x_1}^{x_n} \left[S^{(2)}(x) \right]^2 dx + \sum_{i=1}^{n} \frac{1}{\Delta y_i^2} (z_i - y_i)^2$$

where the cubic spline $S(x)$ interpolates the points (x_i, z_i), $i = 1, \ldots n$. It is equivalent to requiring that, writing $\theta(x)$ to represent a step function,

$$\lambda S^{(3)}(x) - \sum_{i=1}^{n} \theta(x - x_i) \frac{1}{\Delta y_i^2} (z_i - y_i) = \text{constant}$$

This leads to the condition

$$\frac{g_{j-1}}{h_{j-1}} - \left(\frac{1}{h_{j-1}} + \frac{1}{h_j} \right) g_j + \frac{g_{j+1}}{h_j} = \frac{1}{\lambda \Delta y_i^2} (z_i - y_i)$$

$$i = 2, \ldots, n-1$$

Thus in addition to the matrix relation 4, viz. $Ag = Bz$ we have a matrix relationship which we write symbolically as

$$Dg = E(z - y)/\lambda$$

Eliminating g we have

$$z = (I - \lambda E^{-1} D A^{-1} B)^{-1} y$$

Figure 3 shows a fit to cross section data obtained from a programme which uses the above technique, written by F. M. Larkin and A. Sykes.

A disadvantage of the above method is that it has as many knots as data points and thus can provide much more "freedom" (in terms of available parameters) than is necessary to fit simple curves. This is also a disadvantage with the computing since more storage space and computing time is used than is necessary.

To overcome these difficulties it seems necessary to eschew using the data points themselves as nodes. In the method we describe below [12], the nodes are placed along the x-axis at x_i, $i = 1, \ldots n$, where they are thought to be needed, being more dense when the structure of the curve to be fitted is more complex. Using the criterion of least squares variation of the data points $(S_j, t_j, \Delta t_j)$, $j = 1, \ldots J$, from the spline curve, it is a linear problem to determine the ordinates of the nodes $y_1, \ldots, y_n$. This problem is most effectively and elegantly solved by using undetermined lagrange multipliers. However, it loses from a pedagogical viewpoint and we give a more simple-minded outline of the problem below.

We may write the equation of the cubic spline in terms of the nodes (x_i, y_i) and the first derivatives at the nodes d_i:

$$S(x) = \sum \phi_i(x) \left\{ y_i + d_i x^i + (x^i)^2 \left[\frac{3}{h_i^2} (y_{i+1} - y_i) - \frac{(d_{i+1} + 2d_i)}{h_i} \right] + (x^i)^3 \left[2 \frac{(y_i - y_{i+1})}{h_i^3} + \frac{(d_{i+1} + d_i)}{h_i^2} \right] \right\} \quad (7)$$

There is an equivalent relationship to (5) between the d_i and y_i so we may write

$$d_j = \sum_{k=1}^{n} e_{jk}\, y_k \qquad j = 1, \ldots, n$$

Substituting in (7) for d_j we have an expression which is linear in g_k and may be written as

$$S(x) = \sum_i \phi_i\,(x) \sum_k \varepsilon_{ik}\,(x^i)\, y_k$$

To find the maximum likelihood values of the y_k we must solve the n linear equations

$$\sum_{j=1}^{J} \frac{(t_j - S(s_j))}{\Delta t_j} \frac{\partial S(s_j)}{\partial y_p} \qquad p = 1, \ldots, n \tag{8}$$

where

$$\frac{\partial S(s_j)}{\partial y_p} = \sum_i \phi_i\,(s_j)\, \varepsilon_{ip}\,(s^j)$$

Powell [13] has pointed out in work on the representation of exact functions that the imposition of the condition $g_1 = g_n = 0$ can lead to considerable errors in the function and derivative values, particularly in the end intervals. According to Powell the virtues of spline fitting may be retained and the errors overcome by relaxing condition II(ii) whilst retaining II(i). With this form of spline various additional conditions may be imposed to obtain a spline fit with various optimal characteristics. For example, to get a very good approximation to d_1 and d_n, as we might wish to do if we were extrapolating, the errors in the approximation to the function at the mid-points of the first and second and the n - 2 and n - 1 intervals might be set equal.

Thus in the case of the first two intervals we would have

$$\sum_i \varepsilon_{1i}^2\left(\frac{h_1}{2}\right) (M^{-1})_{ii} + \sum_i \sum_j \varepsilon_{1i} \left(\frac{h_1}{2}\right) \varepsilon_{1j} \left(\frac{h_1}{2}\right) (M^{-1})_{ij}$$

$$= \sum_i \varepsilon_{2i}^2 \left(\frac{h_2}{2}\right) (M^{-1})_{ii} + \sum_i \sum_j \varepsilon_{2i} \left(\frac{h_2}{2}\right) \varepsilon_{2j} \left(\frac{h_2}{2}\right) (M^{-1})_{ij} \qquad (9)$$

where M is the statistical error matrix. Equation (9) gives a modified expression for the equation of the spline:

$$s(x) = \sum_i \phi_i (x) \sum_k \varepsilon'_{ik} (x^i) y_k$$

but the y_k are obtained in the same manner as in (7).

Powell [13] has shown in his work with exact functions that different intervals are remarkably independent of each other in the sense that, even when large variations are introduced in one interval, they have very little effect on the fit in other intervals. This property of splines together with the prescription that all that needs to be done to cope with very complex data is to introduce more intervals are the primary reasons we submit that the above method is very promising in regard to the mechanised evaluation of data. Of course, the functional form of the curve to be drawn through a cross section is usually not known and the fit has to be an a priori basis. The limitations of fitting by analytic functions in such a situation are well known. The least that can be said of the spline fit is that it is economical and smooth, and the procedures we have outlined may be adapted for arbitrarily complex data.

An additional advantage of splines is that their parameters represent an exceedingly economical method of storing data, say on magnetic tape.

4. Subjective weighting and anomalous data

Figure 4 is included because it shows several experimenters' measurements of the same physical quantity. Needless to say, whether they are measurements of the same physical quantity or not, they are not samples of the same statistical population. This arises because of systematic errors in the procedures of two or more of the experimenters.

The point we wish to make is that implicit in a least squares fitting of such data that does not take account of the populations being different is an a priori assumption that they are all equally likely. In the situation where one cannot renormalise the data we believe that there is a case for introducing subjective weighting of the results of different experimenters. Often this would have to be based on circumstantial evidence, but it must be recognised that to give them all equal weight, as is usually done, is itself a subjective weighting of the points.

A not unrelated problem is the removal of anomalous data from the results of a given experimenter. Again the solution of this problem is somewhat arbitrary. What one might do, for example, is perform a preliminary fit on the data set and reject all data points that are more than twice the claimed standard deviation for the point distant from the fit. The fitting would then be done without the rejected points.

Acknowledgements

We are very much indebted to Mr. M. J. D. Powell of Harwell for many illuminating discussions.

REFERENCES

[1] PARKER, K., "Mechanised Evaluation of Neutron Cross Sections", Conf. Neutron Cross Section Technology, Washington (March 1966) CONF-660303, to be published.

[2] GOLDSTEIN, H., GOLDMAN, D. T., Physics Today (June 1966).

[3] FRIEDMAN, J. M., PLATT M., Scisrs Sigma Center Information Storage and Retrieval System, BNL 883 (T-357) (1964).

[4] CAMPBELL, E. S., "A Smoothest Curve Approximation", Math. Tables and other Aids to Comp. 11 (1957) 233.

[5] SCHOENBERG, I. J., WHITNEY, A., "On Polya Frequency Functions", Trans. Amer. Math. Soc. 74 (1953) 246.

[6] AHLBERG, J. H., NILSON, E. N., "Convergence Properties of the Spline Fit", J. Soc. Indust. Appl. Math. 11 (1963) 95.

[7] SCHOENBERG, I. J., "Spline Interpolation and the Higher Derivatives", Proc. Nat. Acad. Sc., 51 (1964) 24.

[8] HORSLEY, A., "Computer Evaluation of Neutron Scattering Angular Distribution Data", Conf. Neutron Cross Section Technology, Washington (March 1966) CONF-660303, to be published.

[9] WHITTAKER, E. T., Proc. Edinburgh Math. Soc., 41 (1923) 63.

[10] LARKIN, F. M., private communication.

[11] SCHOENBERG, I. J., "Spline Functions and the Problem of Graduation", Proc. Nat. Acad. Sci. 52 (1964) 947.

[12] HORSLEY, A., PARKER, J. B., To be published.

[13] POWELL, M. J. D., private communication.

[14] FOWLER, A. H., WILSON, C. W., Cubic Spline, a curve fitting routine, Union Carbide Report: Y-1400.

LEGENDRE POLYNOMIAL FIT

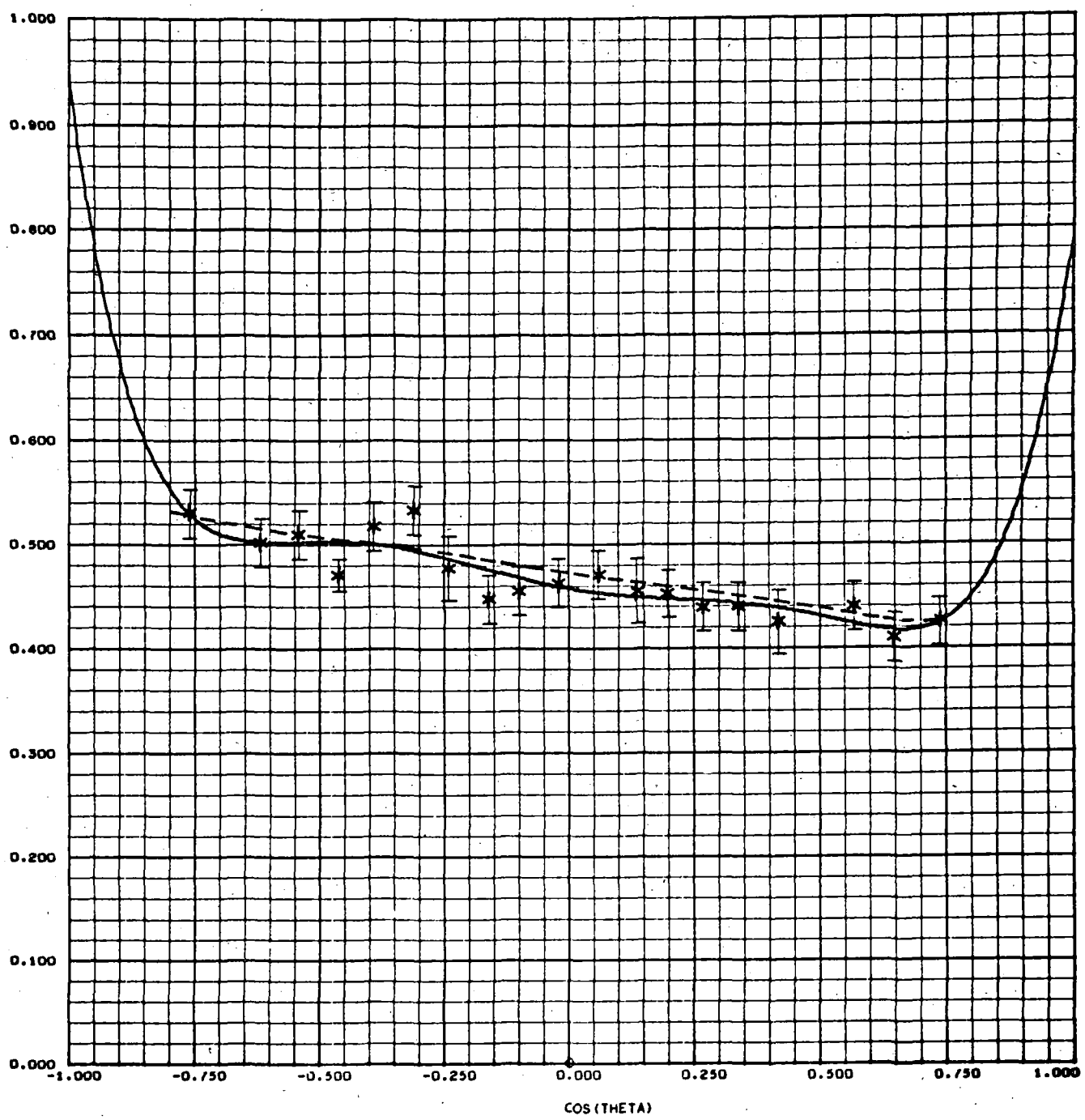

ANGULAR DISTRIBUTION, ENERGY IN MEV 0.10000

FIGURE 1.

LEGENDRE POLYNOMIAL FIT WITH SPLINE

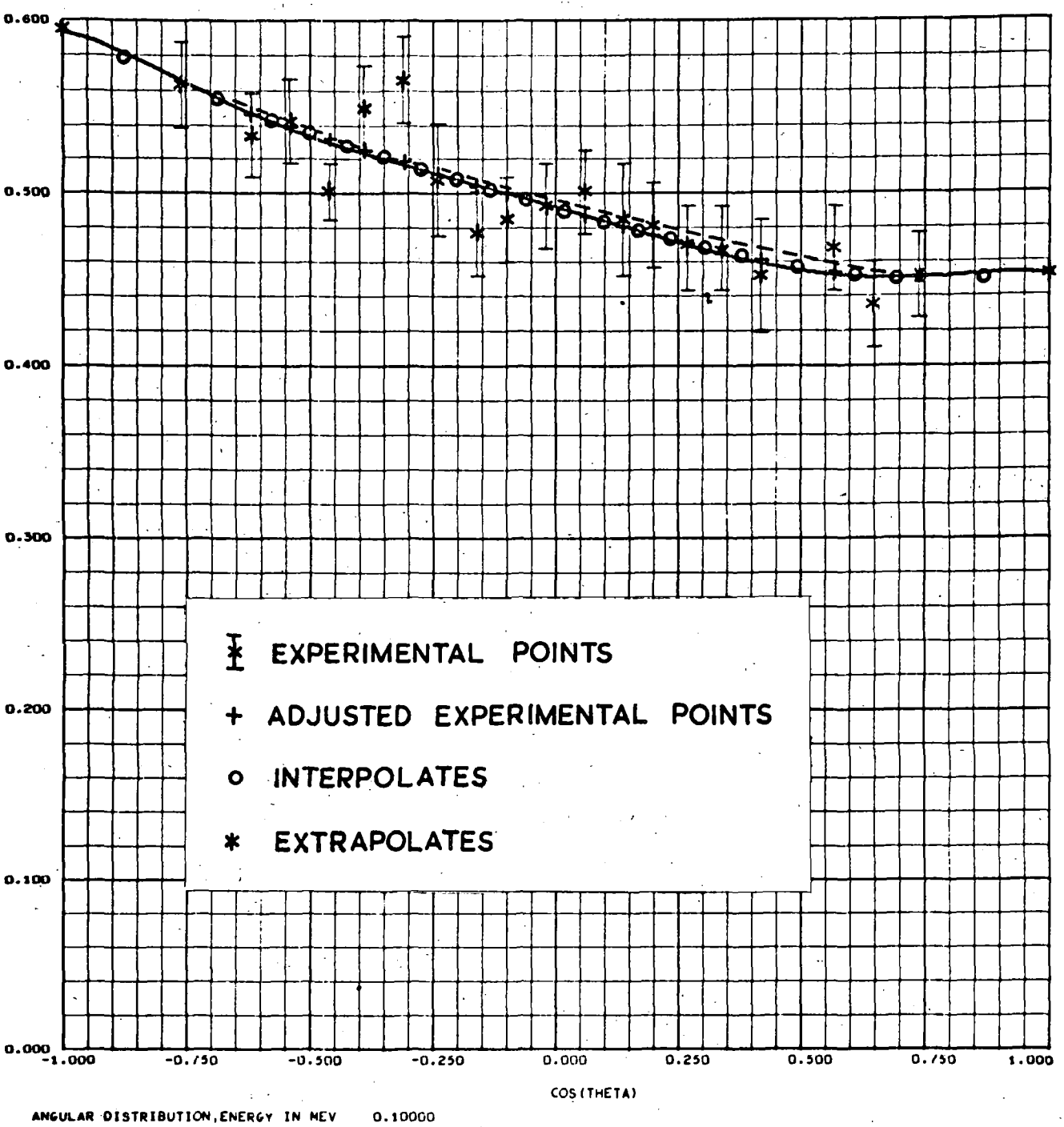

FIGURE 2.

ANGULAR DISTRIBUTION FOR DEUTERIUM DATA AT 0·1 MEV.

W. D. ALLEN ET AL., PROC. PHYS. SOC. A68, 650 (1955)

--- RECOMMENDED BNL 400 CURVE

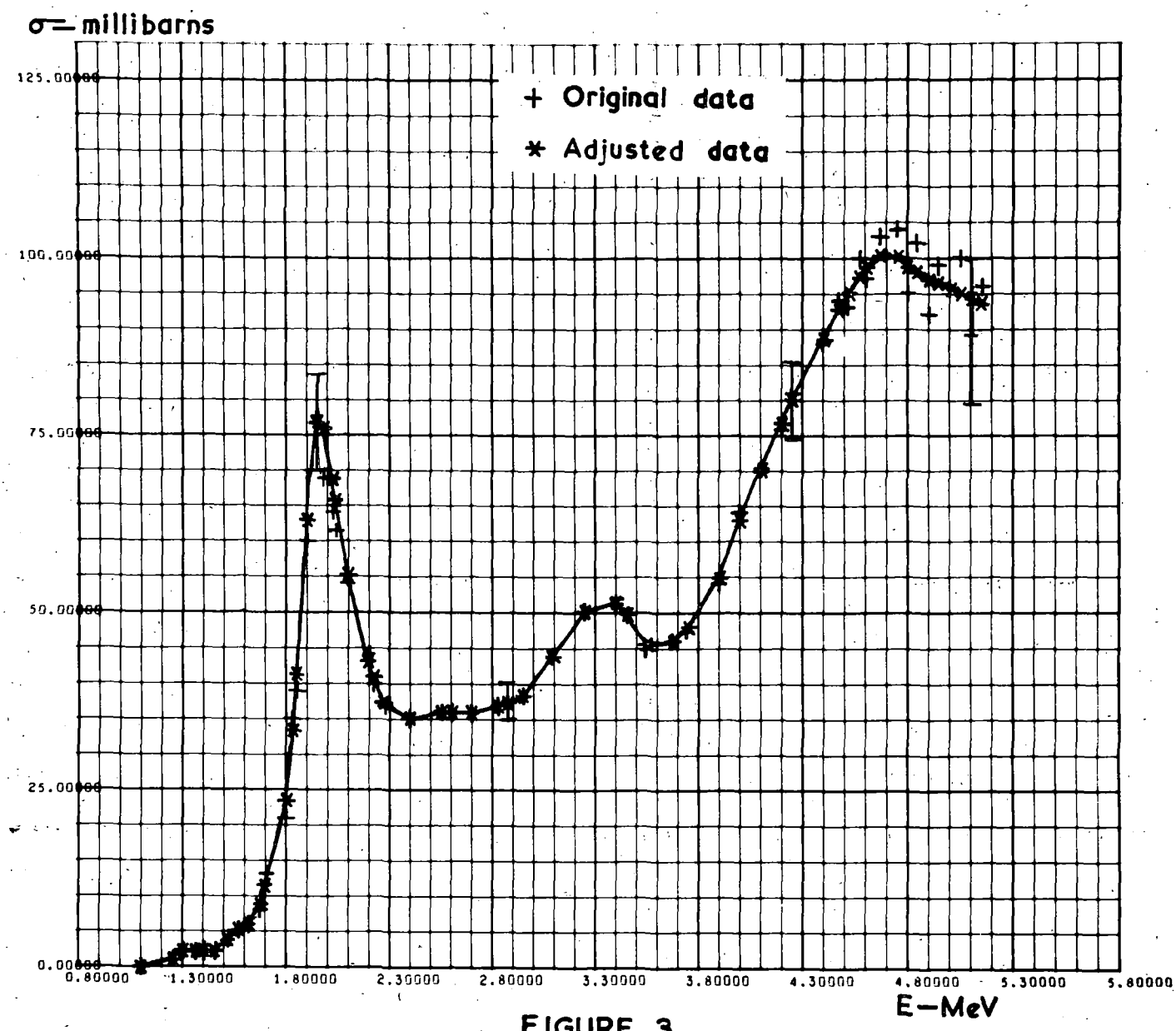

FIGURE 3.

SPLINE FIT TO DATA FOR MEV GAMMA EMISSION IN B^{10}.
DATA AS IN BNL-325

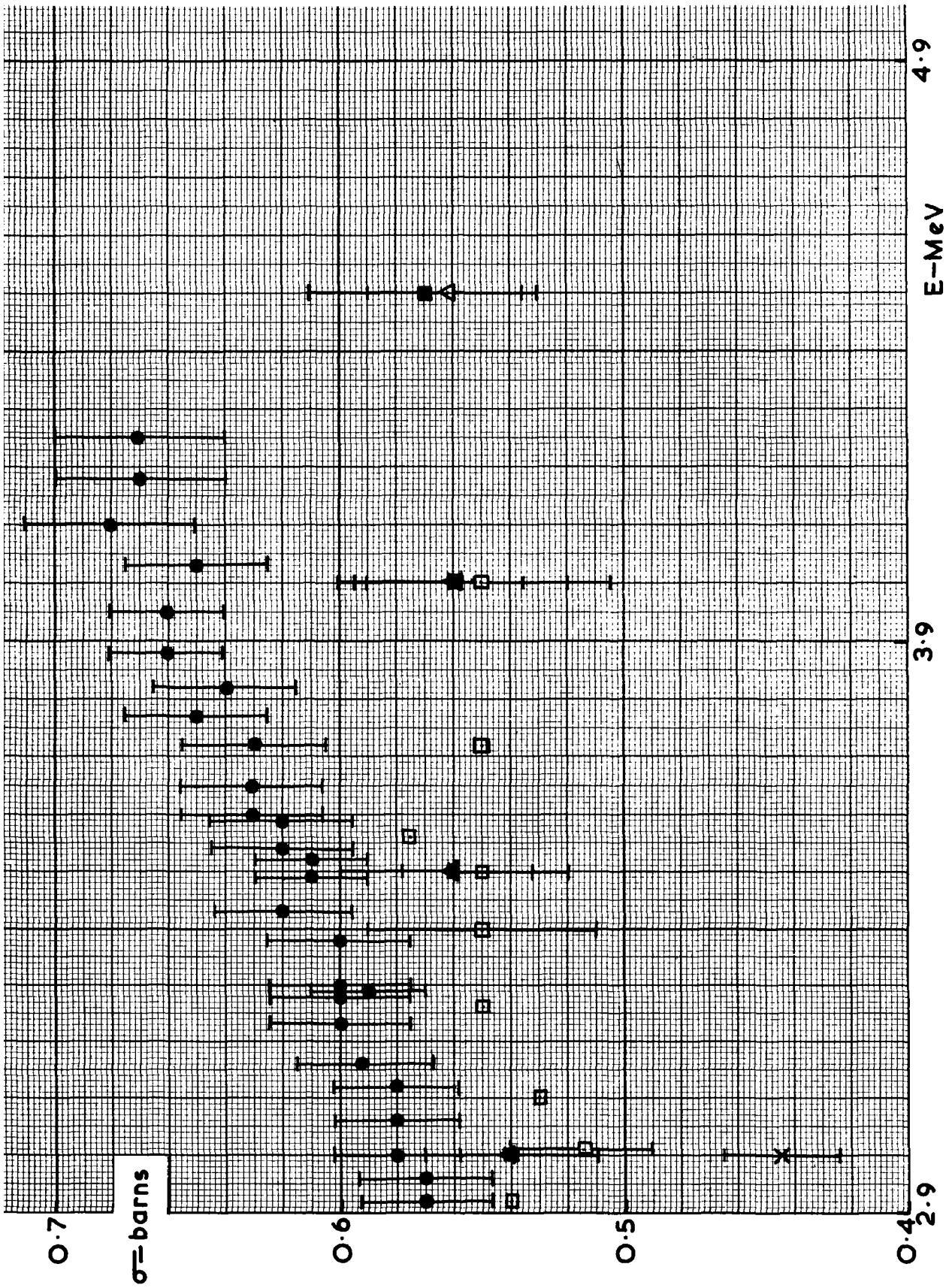

FIGURE 4.

FISSION CROSS SECTION OF U238 FROM 2·9MEV TO 4·9MEV.

CN-23/31

Neutron resonance parameters of ^{240}Pu

M. Asghar*, M.C. Moxon and N.J. Pattenden

Atomic Energy Research Establishment, Harwell,
Didcot, Berkshire, England.

1. Introduction

With the increasing quantities of ^{239}Pu being available from the operation of uranium-fuelled reactors, it is becoming more important to be able to design power-producing reactors which use ^{239}Pu as their primary fuel. In the case of fast reactors a ^{239}Pu-U system is particularly attractive in having a relatively large breeding ratio. Hence a knowledge of the neutron cross sections of ^{240}Pu has acquired a new significance among the many nuclear parameters needed in reactor design.

Little published information has been available hitherto on the ^{240}Pu cross section and resonance parameters, with the exception of the 1 eV resonance, which has been examined in some detail [1, 2, 3]. The resonances at 20 and 38 eV have been studied by Coté et al [1] and Egelstaff et al [4], but the spectrometer resolutions were poor and the ^{240}Pu enrichment in the samples was low.

In this paper, measurements of total, capture and scattering cross sections are described, covering an energy range from about 20 to several hundred electron volts, using samples enriched to 98% ^{240}Pu. Neutron and radiation widths of 16 ^{240}Pu resonances have been obtained by an area analysis method, combining the results from the three types of measurements. The mean values and statistical distributions of the resonance parameters are briefly discussed.

2. Experimental methods

The measurements were carried out using time-of-flight spectrometry on the Harwell 45 MeV electron linac, with the booster target as the pulsed neutron source, and a repetition rate of 190 pulses/sec. The capture measurements were performed on a 32 m flight path, the scattering measurements on a 50 m flight path and the total measurements on a 94 m flight path. The neutron pulse length was about 250 nsec before moderation, and the shortest time channels used were 125 nsec, giving nominal resolutions of 9, 5 and 3 nsec/m for the capture, scattering and total measurements respectively. In all types of measurement, the individual neutron flight times were recorded in 16-bit binary form on

---

*Now at Pakistan Institute of Nuclear Science and Technology, Rawalpindi, Pakistan.

magnetic tape, and the counts per channel were subsequently summed by playing back into a D.E.C. PDP-4 computer. This gave a maximum of 16384 channels per pass of the tape. The contents of the PDP-4 memory were written on to IBM-compatible magnetic tape for reading into an IBM-7030 computer in which further processing was carried out.

2.1 Samples

The samples used in total and scattering measurements were two discs of plutonium-aluminium alloy, sealed in aluminium containers. The discs were prepared at the Los Alamos Scientific Laboratory, New Mexico, U.S.A., under the auspices of the United States Atomic Energy Commission, by groups under the direction of F.W. Schonfeld, C.F. Metz, G.H. Tenney and W.J. Maraman. Both discs were 7.62 cm diameter, with alloy weights of 15.0666 g and 6.4622 g having thickness values 8.150×10^{-4} and 3.496×10^{-4} Pu atom/b respectively. The Pu concentration in the alloy was 98.3 ± 0.5%. Chemical analysis showed that the largest impurity was Ni, with a concentration of 300 parts per million.

The samples used in the capture measurement were in the form of PuO_2 powder deposited on to aluminium foils and held with an organic binder, which was about 15% by weight of the PuO_2. Two samples were prepared, both of 6.75 cm diameter, one containing 4.748 g PuO_2 ($n = 2.788 \times 10^{-4}$ Pu atom/b) and the other containing 2.287 g PuO_2 ($n = 1.33 \times 10^{-4}$ Pu atom/b). The ^{240}Pu enrichment and sample preparation was performed by the Electromagnetic Separator Group at Harwell, under the direction of M.L. Smith.

Isotopic analyses of both sample materials are given in Table I.

TABLE I

Isotopic analyses of ^{240}Pu samples

Isotope	Los Alamos discs	Harwell powder sample
238	0.004 ± 0.002	-
239	1.43 ± 0.02	1.31
240	97.92 ± 0.04	98.48
241	0.52 ± 0.03	0.18
242	0.12 ± 0.01	0.034

2.2 Cross section measurements

A Moxon-Rae capture γ-ray detector [5] was used to measure the capture γ-ray yields, and a ^{6}Li-natural Li glass scintillator detector system [6] was used to measure the scattered neutron rate. Both types of measurement covered the energy range from about 10 eV to 300 eV.

The high natural background produced by the daughter products of ^{240}Pu in the Moxon-Rae detector was reduced by about a factor of four by

surrounding the sample with a 3mm sleeve of lead. The background was still about a factor of 100 greater than that observed with an inactive sample, which increased the minimum capture cross section value which could be measured, and increased the errors on the spectrum normalization by about a factor of two.

The lead sleeve had no effect on the properties of the Moxon-Rae detector, as far as could be measured using radioactive sources and black resonances in Ag, Ta, Pt and Au.

The apparatus for the total cross section measurement has been described elsewhere in this Conference [7]. In this case, two sets of runs were carried out covering different energy ranges. One set, using 4096 channels of 125 nsec duration, covered a range from 160 eV to about 50 keV, and used the aluminium 35 keV resonance as a background normalization point. The other set, using 2048 channels of 250 nsec duration followed by 2048 channels of 500 nsec duration, covered a range from 13 eV to 400 eV, and used the manganese 337 eV resonance as a background normalization point.

3. Results and analysis

The transmissions of the samples of thickness 8.150×10^{-4} and 3.496×10^{-4} Pu atom/b were measured in the 160 eV to 30 keV energy range, and the transmission of the sample of thickness 3.496×10^{-4} Pu atom/b was measured in the 20 eV to 250 eV energy range. A typical section of the run on the sample of thickness 8.150×10^{-4} atom/b showing experimental transmission points as a function of channel number is given in Fig. 1. Area analyses using the Atta-Harvey program [8] were performed on the resonances observed between 20 eV and 950 eV. The program gives the best value of Γ_n for an assumed value of Γ. Since none of the resonances gave zero transmission with these sample thicknesses, the Γ_n values were largely independent of Γ. However, it was not possible to derive Γ (and therefore Γ_γ) values from the analysis. The Γ_n values obtained are shown in Table II.

A typical section of the capture γ-ray yield data is shown in Fig. 2, and a typical section of the neutron scattering yield is shown in Fig. 3. Each set of data was analysed by area techniques developed by Rae et al [9]. Corrections due to resonance self-screening and Doppler broadening were applied to the observed capture and scattering areas of each resonance using the curves of Hughes [10], and a Monte Carlo technique was used with assumed resonance parameters to correct the areas for multiple scattering in the sample. In the case of the scattering data, the total correction on some resonances was very large, being over a factor of 5 in the worst case. The uncorrected and corrected values of $\sigma_0 \Gamma_n$, obtained from the scattering data, are shown in Table III.

4. Combined analysis of all data

The transmission, capture and scattering data all provide different Γ_n, Γ_γ relationships for each resonance, each with an appropriate error. The error is largely due to counting statistics in the case of the transmission data, but for the capture data, systematic errors due to uncertainties in the detector efficiency, resonance self-screening and multiple scattering corrections predominate for some of the resonances. Best values of Γ_n and Γ_γ have been obtained from a combination of all the

data by least-squares fitting, in the way described by Asghar et al [11], and are shown in Table IV. Fig. 4 shows the Γ_n, Γ_γ curves for the 66.65 eV resonance, as an example of the method.

In Table IV the resonance energy values are due to the transmission measurements alone. For the resonances below 140 eV, the data include results from two sample thicknesses each for the capture and scattering measurements, and a Γ_n value from the transmission measurements. Above 140 eV, the scattering data have not been used, and the parameters are due to two capture measurements and two Γ_n values from the two transmission sample thicknesses.

For the 10 resonances below 140 eV, the overall sum of χ^2_{min} is 35.7. The number of degrees of freedom is rather less than this, since for some resonances, the Γ_n, Γ_γ relationship is essentially the same for both samples and hence they cannot be considered as independent determinations.

5. Discussion

The weighted mean value of the radiation widths listed in Table IV is 18.11 meV, with a statistical error of $\pm$ 0.37 meV and a systematic error $\pm$ 1.67 meV. Since the χ^2_{min} value is larger than should be expected, and the corrections to some of the scattering areas are so large, we consider that, until more measurements have been made with a greater range of sample thicknesses, our statistical error should be doubled, to $\pm$ 0.74 meV. Thus our best value for the radiation width is

$$\langle \Gamma_\gamma \rangle = 18.11 \pm 1.81 \text{ meV}$$

This value cannot be reconciled with the measurements on the 1.06 eV resonance [1, 2, 3], which indicate a radiation width of about 31 $\pm$ 3 meV. However, it agrees rather more closely with other recent measurements on neighbouring non-fissile nuclides [11, 12]. The errors on the individual Γ_γ values are too large to permit any conclusions about the shape of their distribution to be drawn. Also, there appears to be some correlation between the size of Γ_γ and Γ_n values, i.e. a resonance with a large Γ_n tends to have a larger than average Γ_γ. This situation might occur if the sample thicknesses for the capture or scattering measurements were in error. Hence, the measurements are at present being repeated with additional samples to provide further evidence on this point. The values reported here must therefore be regarded as preliminary.

If the neutron widths shown in Table IV are taken together with the neutron widths for resonances above 300 eV shown in Table II, the s-wave neutron strength function S_o may be determined, where

$$S_o = \Sigma \Gamma_n^o / (E_2 - E_1),$$

$E_2 - E_1$ is the energy interval between the highest and lowest energy resonances and Γ_n^o is the reduced neutron width of a resonance. The value obtained is $S_o = 0.93 \pm 0.25$.

References

[1] COTÉ, R.E. et al, Phys. Rev. 114 (1959) 505.

[2] LEONARD, B.R. et al, Nuclear Sci. and Eng. 5(1959) 32.

[3] PATTENDEN, N.J. and RAINEY, V.S., J. Nuclear Energy 11 (1959) 14.

[4] EGELSTAFF, P.A. et al, J. Nuclear Energy 6 (1958) 303.

[5] MOXON, M.C. and RAE, E.R., Nuc. Instr. and Methods 24 (1963) 445.

[6] ASGHAR, M. and BROOKS, F.D., Nuc. Instr. and Methods 39 (1965) 68.

[7] MOXON, M.C. and PATTENDEN, N.J., present Conference paper CN-23/27.

[8] ATTA, S.E. and HARVEY, J.A., USAEC rep. ORNL-3205 (1961)(unpublished).

[9] RAE, E.R. et al, Nuclear Physics 5 (1958) 89.

[10] HUGHES, D.J., J. Nuclear Energy 1 (1955) 237.

[11] ASGHAR, M. et al, Nuclear Physics 76 (1966) 196.

[12] ASGHAR, M. et al, Nuclear Physics (submitted for publication).

TABLE II

Neutron width from transmission area analysis

(Γ_γ = 20 meV assumed)					
E_R (eV)	Γ_n (meV)	$\Delta\Gamma_n$	E_R (eV)	Γ_n (meV)	$\Delta\Gamma_n$ (meV)
20.42	2.40	0.33	365.0	30	3
38.26	16.9	3.5	373.2	12	3
41.62	14.8	3.0	406	102	8
66.65	48.0	4.5	451	11	7
72.8	19.0	1.8	501	24	10
90.8	13.0	1.8	516	28	10
92.5	2.8	1.4	526	10	10
105.1	44.5	4.6	549	35	13
121.7	14.3	2.9	555	25	14
135.4	17.0	3.8	569	25	13
152.0	13.2	4.1	599	46	16
163.1	9.0	0.7	610	15	15
170.5	14.0	1.5	668	195	25
186.3	16.5	1.5	681	26	25
239.8	12.6	1.5	753	70	25
260.9	22.4	1.6	814	210	40
287.9	130	5	824	105	30
305.8	6.9	2.0	895	100	46
321.7	14.4	2.5	914	65	42
347.2	14.7	4.3	949	112	50

TABLE III

Corrections to neutron scattering data

E_R (eV)	$n = 3.496 \times 10^{-4}$ atom/b				$n = 8.15 \times 10^{-4}$ atom/b			
	$\sigma_o \Gamma_n$ (b. eV)				$\sigma_o \Gamma_n$ (b. eV)			
	Observed		Corrected		Observed		Corrected	
	Value	Error	Value	Error	Value	Error	Value	Error
20.42	10.9	1.6	24.7	4.2	7.0	1.0	23.3	2.6
38.26	180	5	734	95	89	3	485	100
41.62	151	5	523	52	77	3	525	100
66.65	554	12	1540	140	295	7	1160	150
72.8	226	7	470	50	138	4	380	50
90.8	88	5	124	14	59	3	91	11
92.5	12.7	3.4	15.0	5.0	8.5	1.8	11.0	4.0
105.1	428	13	765	60	272	8	750	60
121.7	75	6	95	10	59	4	93	10
135.4	104	7	128	12	89	5	145	16

TABLE IV

Best values of Γ_n and Γ_γ from the combined analysis

E_R (eV)	Γ_n (meV)	$\Delta\Gamma_n$ stat. (meV)	$\Delta\Gamma_n$ syst. (meV)	Γ_γ (meV)	$\Delta\Gamma_\gamma$ stat. (meV)	$\Delta\Gamma_\gamma$ syst. (meV)	χ^2_{min}	Notes
20.42	2.053	0.043	0.134	20.41	1.89	2.65	2.5	a
38.26	17.79	0.89	1.0	17.06	1.17	2.71	5.8	a
41.62	16.17	0.75	0.67	15.36	1.05	1.50	1.3	a
66.65	50.67	2.43	0.67	22.25	1.71	1.70	3.8	a
72.8	21.27	0.83	0.46	17.59	0.91	1.46	6.6	a
90.8	10.38	0.31	0.30	16.89	1.00	1.48	9.8	a
92.5	2.56	0.14	0.11	12.1	2.3	1.0	0.7	a
105.1	44.94	1.60	0.56	20.95	0.93	1.46	0.6	a
121.7	11.59	0.42	0.38	18.55	1.35	1.68	1.4	a
135.4	15.85	0.60	0.40	19.93	1.39	1.58	3.1	a
152.0	13.2	4.1	0.4	17.0	5.0	1.5		b
163.1	8.8	1.0						c
170.5	15.0	1.0	0.5	14.0	5.0	1.5		d
186.3	17.2	1.5	0.5	15.0	3.0	1.5		d
239.8	12.7	1.5	0.7	15.0	8.0	1.5		d
260.9	22.3	1.6	0.4	18.0	4.0	1.5		d
287.9	130.0		0.0	25.0	4.0	1.5		d

Notes: (a) 1 transmission, 2 capture, 2 scattering measurements.
(b) 1 transmission, 2 capture measurements.
(c) 2 transmission measurements.
(d) 2 transmission, 2 capture measurements.

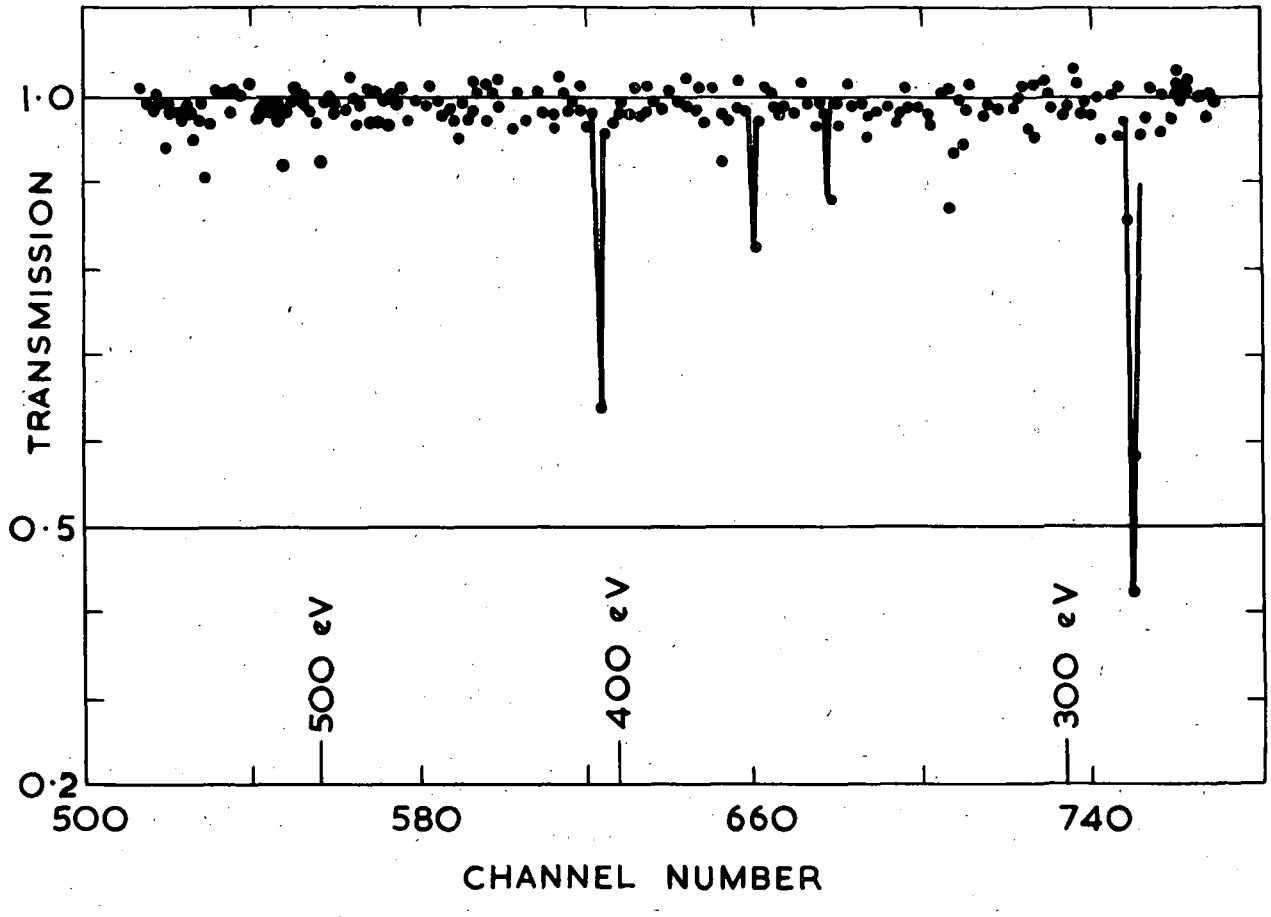

FIG. 1. ^{240}Pu $n = 8{\cdot}15 \times 10^{-4}$ ATOM/B

^{240}Pu experimental transmissions vs. channel number. $n = 8.15 \times 10^{-4}$ Pu atoms/b. The channels are grouped in fours for convenience of plotting.

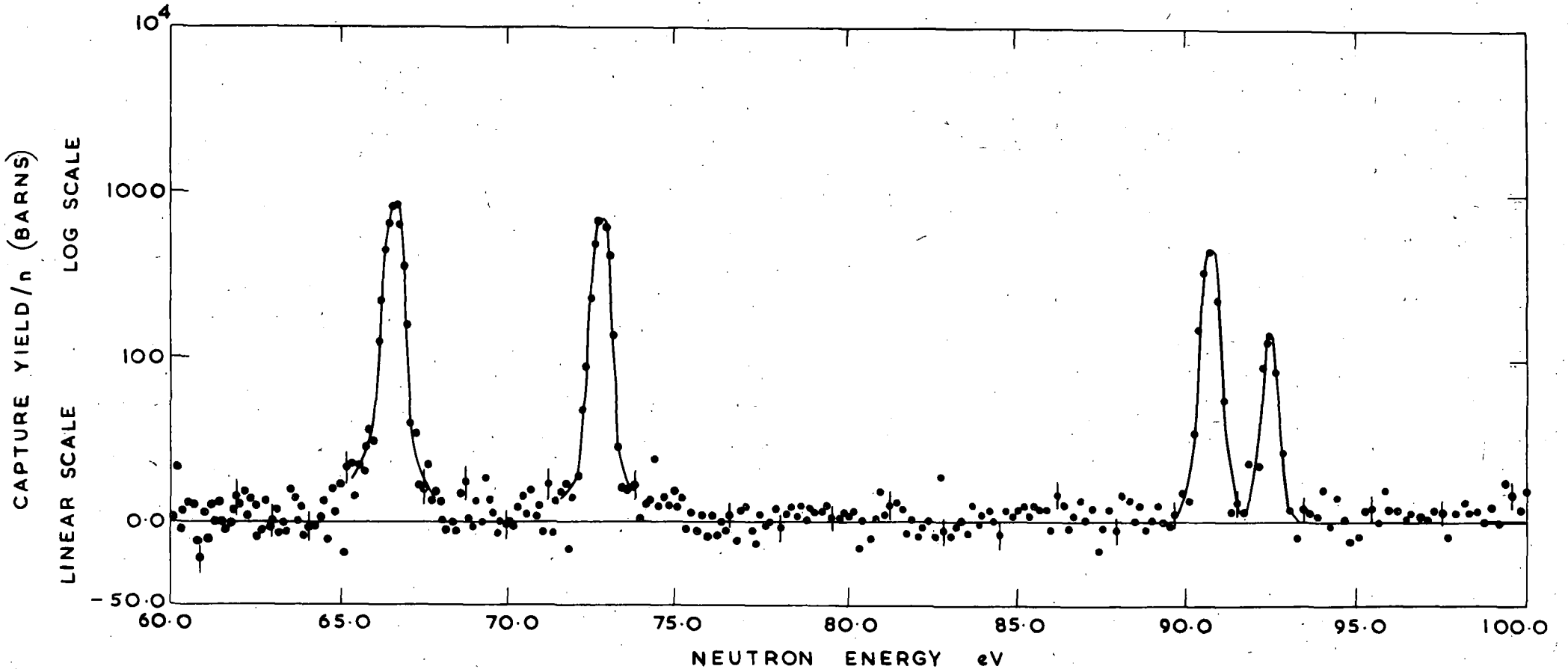

FIG. 2. ^{240}Pu capture γ-ray yield divided by sample thickness ($n = 2.788 \times 10^{-4}$ atom/b) vs. neutron energy.

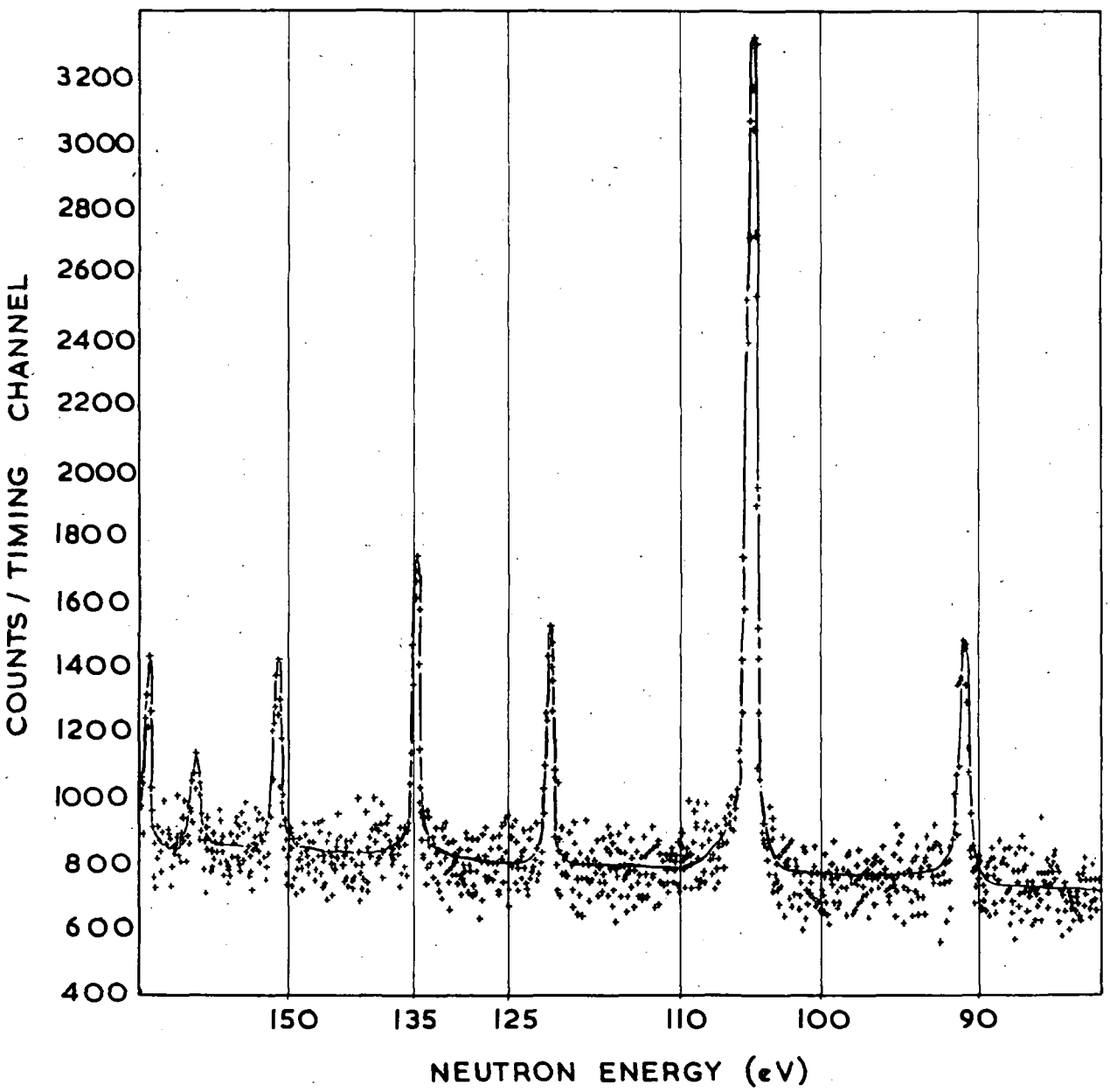

FIG. 3. ^{240}Pu SCATTERING YIELD.

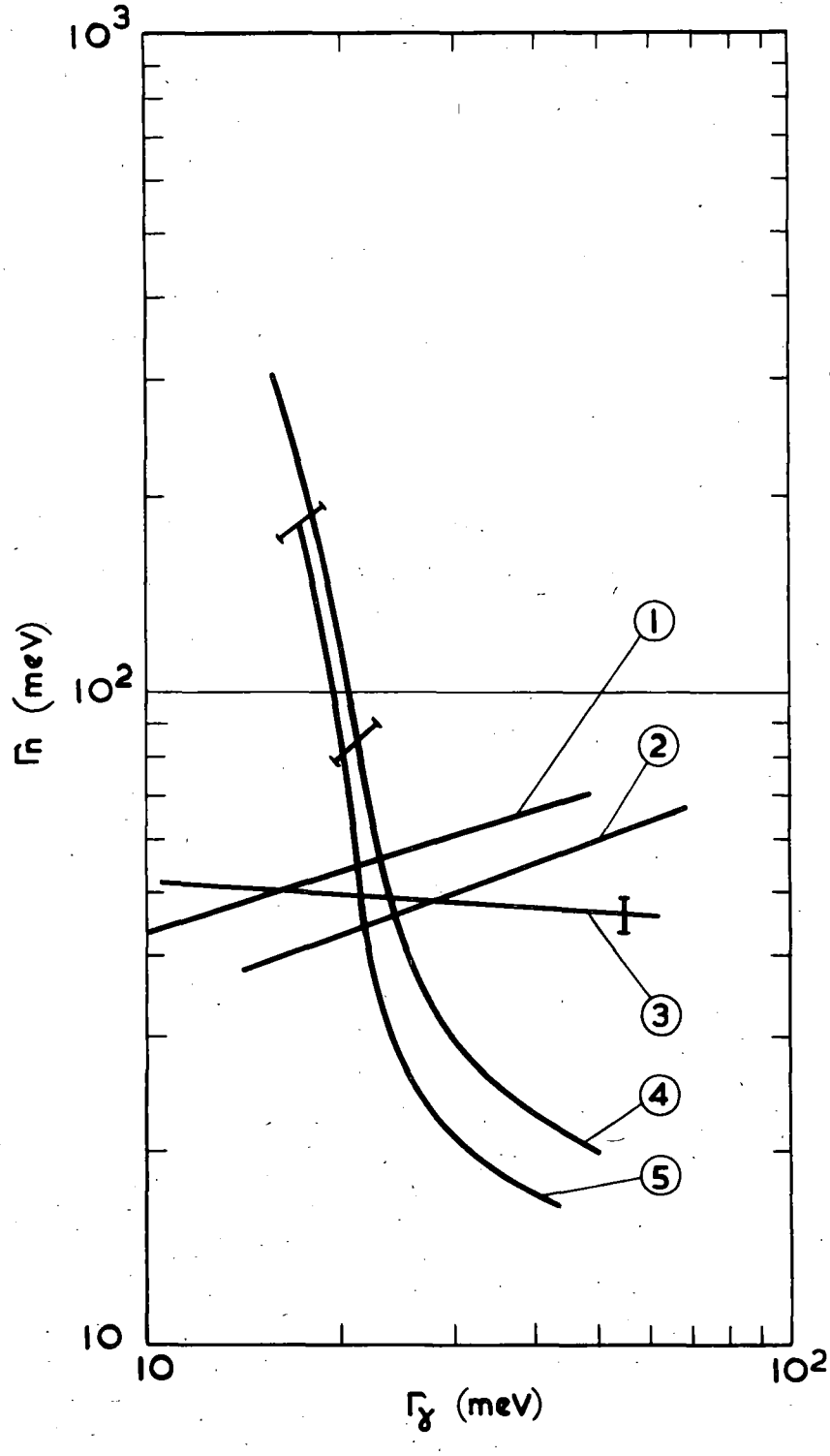

FIG. 4.

^{240}Pu 66.65 eV Resonance Analysis. Γ_n vs. Γ_γ curves of all the data. Curves 1 and 2 refer to scattering data, curve 3 to transmission and curves 4 and 5 to capture.

Elastic and Inelastic Neutron Cross-Sections

D. Wilmore

A.E.R.E., Harwell

1. Introduction

The measurement of cross-sections for nuclear data, is expensive and time consuming. For many purposes theoretical calculations can help by making direct predictions where the required accuracy is not exacting, and by making interpolations and extrapolations of experimental results. Computer programmes are described here which do such calculations for incident neutrons in the MeV region. They are based on the optical model of elastic scattering, which is valid at energies high enough for resonances to have merged together. At somewhat lower energies the model may work if averages over the resonances are required.

When a nuclear projectile is incident at moderate energies on a target nucleus, it is either elastically scattered or absorbed to form a compound nucleus. The compound nucleus then decays into one or other of the energetically allowed exit channels. The entrance channel is itself a possible exit channel and thus elastic scattering may occur by this process. We call such elastic scattering compound elastic to distinguish it from the shape elastic cross-section. The first part of this process we may describe by the optical model with a complex potential to represent the interaction between the target nucleus and the incident particle. This gives rise to shape elastic scattering and also absorption to a compound nucleus. From this model it is possible to calculate the differential cross-section for shape elastic scattering and the absorption or compound nuclear cross-section, which is the total cross-section for all channels into which the compound nucleus can decay.

Hauser and Feshbach[1] showed that, if the processes of formation and decay of the compound nucleus are assumed to be independent, then use of the reciprocity theorem allows the differential cross-sections for all the reactions to be calculated as well. The calculation requires the transmission coefficients for all the inverse reactions, and these may be calculated from the optical potentials appropriate to these reactions.

Three programmes have been written to solve these problems. The first is an optical model programme for the calculation of the shape elastic and absorption cross-sections. It is often necessary to vary the parameters in order to obtain a good fit to the experimental data. The present programme incorporates a multidimensional least squares routine to solve this type of problem. The second programme calculates compound nuclear cross-sections according to the Hauser-Feshbach theory, with or without the level width fluctuation correction. An optical model programme is included to calculate the transmission coefficients. At low energies there may be few open channels, so that there may be a large number of particles re-emitted from the compound nucleus into the elastic channel. Here it is necessary to take into account the compound elastic cross-section when fitting the differential cross-section. A third programme, which is a combination of the first two, has been written to take care of this particular problem.

The programmes are written in the S2 dielect of Fortran for the 7030 computer at Aldermaston. S2 is similar to Fortran 2, except in the use of common storage. A version of the Hauser-Feshbach programme for the Atlas at the Atlas Computer Laboratory, Chilton, is also available[2].

The Optical Model Programme

Here we solve the problem of the scattering of a particle in a complex well. This is described by the Schrodinger equation

$$\nabla^2 \Psi + \frac{2\mu}{h^2}(E-V) \Psi = 0$$

where V is the complex potential and $\mu = A_I A_T/(A_I+A_T)$ is the reduced mass of the incident particle. A_I and A_T are the masses of the incident particle and target nucleus respectively. This equation is solved by making a partial wave expansion and the angular parts may then be evaluated analytically. It is necessary however, to solve the radial equation,

$$\frac{d^2 U_l}{dr^2} + \left\{\frac{2\mu}{\hbar^2}(E - V(r)) - \frac{l(l+1)}{r^2}\right\} U_l = 0$$

using numerical methods. Many computer programmes have used the Runge-Kutta method to solve this equation, but it is preferable to use a method which takes advantage of the absence of a term containing the first derivative of the radial wave function. The present programme uses a method due to Fox and Goodwin[3], that is up to ten times faster than Runge-Kutta. The Coulomb wavefunctions are calculated by a method described by Buck, Maddison and Hodgson [4].

The complex potential has real and imaginary parts U' and W' plus a spin orbit potential, so that $V = U'(r) + i\,W'(r) + V'_{SO}(r)$. The real part of the potential is described by a volume potential of the Saxon Woods form

$$U'(r) = \frac{U}{1 + \exp\left(\frac{r - Ru}{au}\right)}$$

where U is the depth of the potential, $Ru = r_u A_T^{\frac{1}{3}}$ is the radius of the potential and Au is a measure of the surface diffuseness. The imaginary potential may be described by a choice of one of three potentials, a volume potential, and two surface potentials,

$$W'(r) = \frac{W}{1 + \exp\left(\frac{r-R\omega}{a\omega}\right)},$$

$$\text{or} \quad \frac{4W \exp\left(\frac{r - R\omega}{a_\omega}\right)}{\left[1 + \exp\left(\frac{r - R\omega}{a_\omega}\right)\right]^2}$$

$$\text{or} \quad W \exp\left(-\left(\frac{r - r\omega}{a\omega}\right)^2\right)$$

where W is the depth of the potential, $R\omega = r_\omega A_T^{\frac{1}{3}}$ is its radius and a_ω is a measure of the surface diffuseness. These three potentials are called Saxon-Woods (SW), Saxon-Woods derivative (SWD) and Gaussian respectively. The use of the first two is advocated as in the stepwise integration proceedure advantage may be taken of the relation

$$\exp\left(\frac{nr-R\omega}{a\omega}\right) = \left[\exp\left(\frac{r}{a\omega}\right)\right]^n \exp\left(-\frac{R\omega}{a\omega}\right).$$

This saves the calculation of many exponentials which are needed with a Gaussian potential.

The spin orbit form is given by

$$V'_{SO} = -(V_{SO} + i\,W_{SO})\frac{1}{r} \frac{4 \exp\left(\frac{r-R_{SO}}{a_{SO}}\right)}{\left[1 + \exp\left(\frac{r-R_{SO}}{a_{SO}}\right)\right]^2}$$

where V_{SO} and W_{SO} are strengths of the real and imaginary spin orbits potentials, $R_{SO} = r_{SO} A_T^{\frac{1}{3}}$ is the radius and a_{SO} measures the surface diffuseness.

Studies of the theory of nuclear matter show that the optical potential should be non-local in form. This means that $V(\underline{r})\ \Psi(\underline{r})$ should be replaced by $\int V(\underline{r},\underline{r}')\ \Psi(r')\ d\underline{r}'$. Perey and Buck [9] have shown that with certain approximations, this is equivalent to a local potential with energy dependent coefficients. Wilmore and Hodgson[10,11] gave the following form for this energy dependence, which gave good agreement for a wide range of neutron elastic scattering data.

$$U = 47.01 - 0.267E - 0.00118\ E^2,$$

$$W = 9.52 - 0.053\ E \text{ (SWD is used)},$$

$$r_u = 1.322 - 0.00076\ A + (4 \times 10^{-6})\ A^2 - (8 \times 10^{-9})\ A^3,$$

$$r_w = 1.266 - 0.00037\ A + (2 \times 10^{-6})\ A^2 - (4 \times 10^{-9})\ A^3,$$

$$a_u = 0.66 \text{ and } a_w = 0.48$$

The present programme incorporates an option which will automatically use this equivalent potential, either for an ordinary optical calculation, or as a starting point for a least squares fit.

The least squares routine uses a method by M.K. Powell.[5] The initialisation process requires (N+1) optical model calculations, where N is the number of variables. There are then about 3 further optical model calculations per iteration. The total number of calculations necessary before convergence is obtained is usually between 10 and 30.

It is sometimes necessary to take account of the compound elastic cross-section when obtaining a fit. This programme includes the compound elastic cross-section either by assuming it is

isotropic or has a specified shape. If required, the computer will vary the magnitude to obtain the best fit to the experimental data.

When a non zero spin orbit force is used, polarisations are calculated. Experimental polarisations may be supplied as data for a least squares fit, together with the differential cross-section, the total and absorption cross-sections.

For a typical problem 0.5 secs is required for an optical model calculation, while a least squares fit, varying two parameters, will usually converge in 20 secs.

3. The Hauser Feshbach Programme

This programme calculates the cross sections for compound nucleus reactions . The transmission coefficients may be supplied, or can be calculated within the programme by the internal optical model routine. No spin orbit force can be included, but channels for incident particles of any spin and parity are allowed. This makes it possible to include such reactions as (n,n'), (n,p), (n,d), (n,t), (n,α) etc., if the interaction can be described by an optical potential. The programme will calculate the differential and integrated cross-sections in any or all of the possible channels. The method of operation is such that the angular functions are calcualated only once, even for many channels, thus saving computer time.

The Hauser-Feshbach theory does not take into account the structure of the compound nucleus, and a factor which makes a correction for the distribution of level widths in the compound nucleus may be obtained. For any particular entrance and exit channel we may write the cross-section as a sum over Breit-Wigner resonances. This neglects any interference between resonances in the compound nucleus. If we average over these resonances to find the actual cross-sections, expressions of the form $< \frac{\tau_i \tau_o}{\tau} >$ are obtained. We use here

angular brackets to denote an average; τ_i and τ_o are the widths of resonances in the ingoing and outgoing channels respectively and $\tau = \sum_j \tau_j$ is the sum of the widths for all energetically allowed exit channels. The distribution of widths for low energy neutrons has been shown to follow the Porter-Thomas distribution[6] and the use of this distribution enables the average to be computed. The transmission coefficients appear through the relation $T = \frac{\langle\tau\rangle}{D}$, where D is the average level spacing. We obtain an expression which is often known as the level width fluctuation correction,

$$\left\langle \frac{\tau_i \tau_o}{\tau} \right\rangle = T_i T_o \int_0^\infty \frac{(1+2\delta_{io})\, dx}{(1+2T_i x)(1+2T_o x)\prod_j (1+2\, T_j\, x)^{\frac{1}{2}}}$$

where the product over j runs over all open channels. The variable x appears through the substitution $\frac{1}{\tau} = \int_0^\infty e^{-x\tau}\, dx$ which is necessary to evaluate the integral.

For convenience of computation the Hauser-Feshbach expression is written in the following way

$$\sigma(\theta,n,m) = \frac{\pi\lambda\!\!\!^{-2}}{(2\, I_n+1)(2i_n+1)} \sum_{JP} \left[\frac{\sum_{l'j'} \left(\sum_{lj} (2l+1)\, A_J(lj|l'j'|\theta) T_l^n T_{l'}^m \right)}{\sum_{l''j''q} T_{l''}^q} \right]$$

where q labels the channels, (n is the incident and m the exit channel) and with the conditions $\Delta(J,j,l)$, $\Delta(J,j',l')$, $\Delta(J,j'',l'')$, $\Delta(j',I_m,i_m)$ $\Delta(j'', I_q,i_q)$ $\Delta(j, I_n, i_n)$ where $\Delta(a,b,c,)$ means $|a-c| \leq b \leq a+c$.

P is the parity of the compound nucleus and places a restriction on the values of l,l' and l" that are allowed.

This method of reordering the summation makes it difficult to

calculate the limits of summation, but it has the great advantage of making the summations occuring in the square bracket simpler.

The lower summation depends only upon J and P and needs to be calculated only once for each set of these parameters. The central section of the programme includes a loop for different values of m which label the outgoing channel. This makes it possible to calculate $A_J\,(lj|l'j'|\theta)$ once only for all m. When fluctuations are included a list is made of all the $T^q_{l''}$ which appear in the lower summation. The upper summation is done subsequently with reference to this list. The expression when fluctuations are included is

$$\sigma(\theta,n,m)=\frac{\pi\lambda^2}{(2I_n+1)(2i_n+1)}\sum_{JP}\left[\sum_{l_j l'_{j'}} S(2l+1)\,A_J(lj|\,l'j'|\,\theta)T^n_l\,T^m_{l'}\int_0^\infty \frac{dx}{(1+2xT^n_l)(1+2xT^m_{l'})\prod\limits_{l''j''q}(1+2xT^q_{l''})}\right]$$

with the same restrictions as before. The factor S=3 when m=n, l'=l, j'=j; otherwise S=1.

The coefficient $A_J\,(lj|l'j'|\theta)$ is given by

$$A_J(lj|l'j'|\theta) = \frac{(2l'+1)(2J+1)^2}{4\pi}\left|\sum_L C(llL;ooo)W(JJll;Lj)C(l'l'L;ooo)\,W(JJl'l';Lj')\,P_L(\cos\theta)\right|$$

where C and W denote Clebsh-Gordon and Racah coefficients respectively The sum L is defined by $0 \leq L \leq \min(2l, 2l', 2J)$ such that L is even. Both coefficients are calculated using recurrence relationships.

The integral

$$\int_0^\infty \frac{dx}{(1+2xT^n_l)(1+2xT^m_{l'})\prod\limits_{l''j''q}(1+2xT^q_{l''})}^{\frac{1}{2}}$$ is evaluated by

using the transformation $Y = \frac{1}{1+2x\ Tmax}$ where Tmax is the largest transmission coefficient occuring in this channel. The integral then becomes

$$\frac{1}{2\ Tmax} \int_0^1 \frac{dy}{y^2 \left(1+\frac{T^n_l}{Tmax}\left(\frac{1}{y}-1\right)\right)\left(1+\frac{T^m_{l'}}{Tmax}\left(\frac{1}{y}-1\right)\right)\prod_{l''j''q}\left[1+\frac{T^q_{l''}}{Tmax}\left(\frac{1}{y}-1\right)\right]^{\frac{1}{2}}},$$

and is evaluated using Simpson's Rule

The transmission coefficients are evaluated using an optical model routine which is incorporated within the Hauser-Feshbach programme.

If only Hauser-Feshbah calculations are made, the time taken depends mainly on the calculations involved in the angular functions. Since this is done simultaneously for all channels, the time depends more upon the largest level spin involved than the number of levels for which angular distributions are required. If the level width fluctuation correction is included, the integrals have to be done for each level separately, so that time can be saved by not asking for output from some levels. A typical calculation involving 18 levels, the width fluctuation correction and angular distributions for all 18 levels, took 30 secs.

4. Least Squares Fitting with the Inclusion of the Compound Elastic Cross-Section.

The third computer programme is basically a least square fitting programme which calculates the elastic scattering differential cross-section using both an optical model and a Hauser-Feshbach programme. The optical potentials for each of the final states may be given separately. Alternatively any number of them can be specified by the potential in the incident channel and thus have a dependence on the least squares variables.

It would take too much computer time if a Hauser-Feshbach calculation were to be done for each optical model calculation, but fortunately this is not necessary. The compound elastic cross-section is less sensitive than the shape elastic cross-section to the optical potential. A Hauser-Feshbach calculation is only necessary every few iterations of the least squares routine.

5. Examples of the use of these programmes

5.1 Inelastic scattering of neutrons from U^{238}

To calculate the compound inelastic scattering of neutrons from U^{238}, it is necessary to know the optical potential for the scattering of neutrons from the ground and excited states. Since it is difficult to obtain information about neutron scattering from excited states,,the same potential was used for all states. The elastic scattering angular distributions have been measured, and can be used to obtain a least squares fit. Since the compound nuclear cross-section is quite large and anisotropic, having zero ground state spin, it must be taken into account in the fitting procedure. The programme described in section 4, gave fast convergence when U and W were varied. During the fitting procedure only three Hauser-Feshbach calculations were necessary, and, for the lower energies, where only two or three channels are open, the whole calculation took about 20 secs. It was found that the parameters obtained by this method showed no evidence for a systematic energy dependence. Forfurther calculations the mean parameters were therefore used.

The results of calculations using the mean parameters are shown in figures 1 and 2. Figure 1 displays the agreement for the elastic scattering angular distributions while figure 2 shows the fit for a few typical inelastic cross-sections at 90°, as a function of the bombarding energy.

5.2 Neutron cross-sections for light nuclei.

For light nuclei the calculation of elastic angular distributions is difficult as the resonances are not completely smoothed out. This means that the parameters of the optical potential will vary with the nucleus and with energy. Since the potential is largely determined by the properties of the compound nucleus, neutron scattering can be related to proton scattering, provided that the same compound nucleus is involved. In practice this is not usually possible, but in the case of neutrons and protons scattered from closed shell nuclei, the compound nuclei are mirrors of each other. Here we can expect similar structures for the compound nuclei.

The potentials which give agreement for proton scattering on O^{16} have been given by Duke[8] who obtained them by a least squares fit. These potentials were used to calculate the differential elastic cross-sections for neutrons of 3.5 MeV less energy. This gives the same excitation energy in the compound nucleus for both particles. Some of the results are shown in figure 3. The agreement with experiment shows that in difficult cases, this procedure may give better results than using a standard potential, such as the equivalent non-local potential.

6. Regions of validity of the optical model

For the optical model to apply, the energy of the incident neutrons must be sufficiently high for fluctuations in the cross-sections to have dissappeared. At low energies individual resonances are seen. There is an intermediate region where many resonances are present, but statistical fluctuations in the cross-section are seen. These fluctuations are often more prominent in the differential cross-sections than they are in the integrated cross-sections. Before an optical model analysis is performed, it is wise to see that measurements indicate that fluctuations are not present. Fluctuations usually

smooth out at 2 MeV for nuclei in the mass 50 region, and at lower energies for heavier nuclei. At energies above this the equivalent non-local potential usually gives good agreement with experiment if the compound elastic cross-section is taken into account. The compound elastic cross-section is negligible above 5 or 6 MeV for medium nuclei and 1 or 2 MeV for heavy nuclei.

In regions of the periodic table where the nuclei are strongly deformed, the non-local potential may be inadequate. In the absence of a coupled channels programme which takes the deformation into account explicitly, a least squares search usually gives parameters which may be used for a considerable energy range.

7. References

[1] HAUSER,W., FESHBACH H., Inelastic Scattering of Neutrons, Phys. Rev. 87 2(1952) 366.

[2] WILMORE D., A Computer programme for the calculation of compound nuclear cross-sections by the Hauser-Feshbach theory, AERE- R5053, Atlas computer laboratory nuclear physics computing library report No.2.

[3] FOX,L,. GOODWIN E.T., Some new methods for the numerical integration of ordinary differential equations. Proc. Camb. Phil. Soc. 43 3(1949) 373.

[4] BUCK, B. et al. Optical Model Analysis of Nuclear Scattering, Phil. Mag. 5 59 (1960) 1181

[5] POWELL, M.J.D., A method for minimising a sum of square of non-linear functions without calculating derivatives. Computer Journal 7 4(1965) 303

[6] PORTER C.E., THOMAS, R.G. Fluctuations of Nuclear Reaction Widths, Phys. Rev. 104 2(1956) 483.

[7] FERGUSON A.J.G., Proc. Int. Conf. on the Study of Nuclear Structure with neutrons (1965) p.63

[8] DUKE C.B.,Optical-Model analysis of elastic scattering of protons on Oxygen at intermediate energies 129 2 (1963) 681.

[9] PEREY F., BUCK B., A non-local model for the scattering of neutrons by nuclei 32 3 (1962) 353.

[10] WILMORE, D., The calculation of neutron cross-sections from the non-local optical model. AERE R4649, EANDC(UK) 36 'U'

[11] WILMORE, D., HODGSON P.E., The calculation of neutron cross-sections from optical potentials. Nucl . Phys. 55 4(1964) 673.

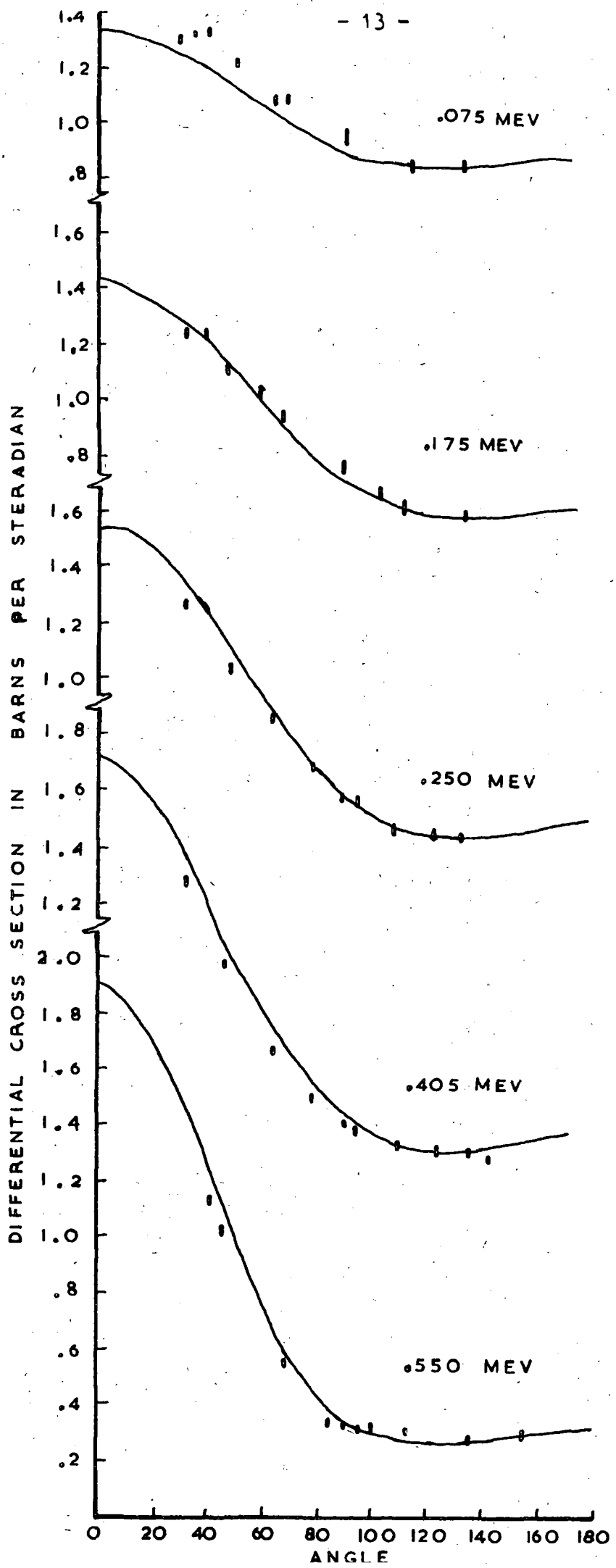

FIG 1

Angular - distributions of neutrons elastically scattered from ^{238}U. Solid line shows calculated shape+compound

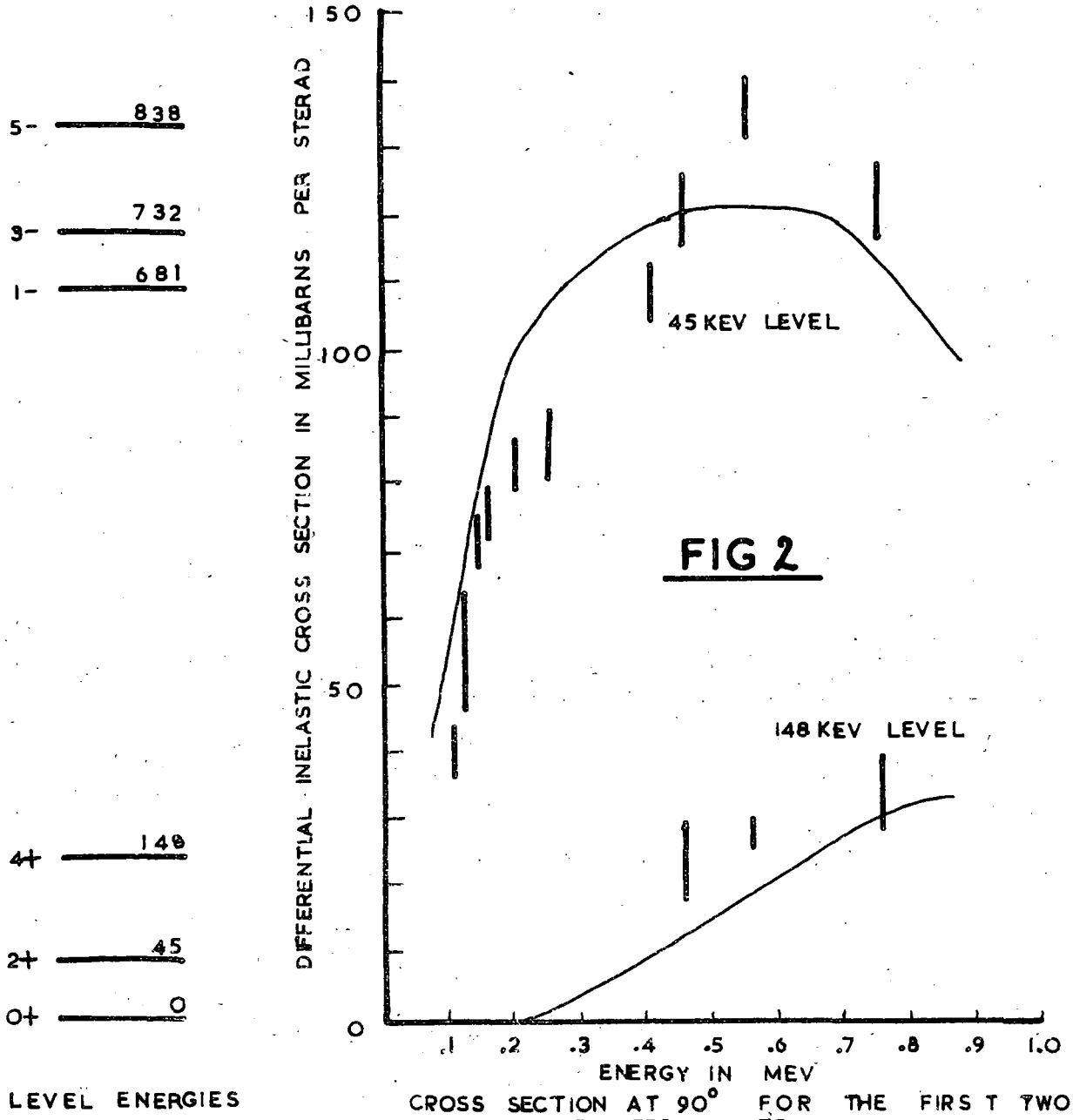

CROSS SECTION AT 90° FOR THE FIRS T TWO EXCITED STATES

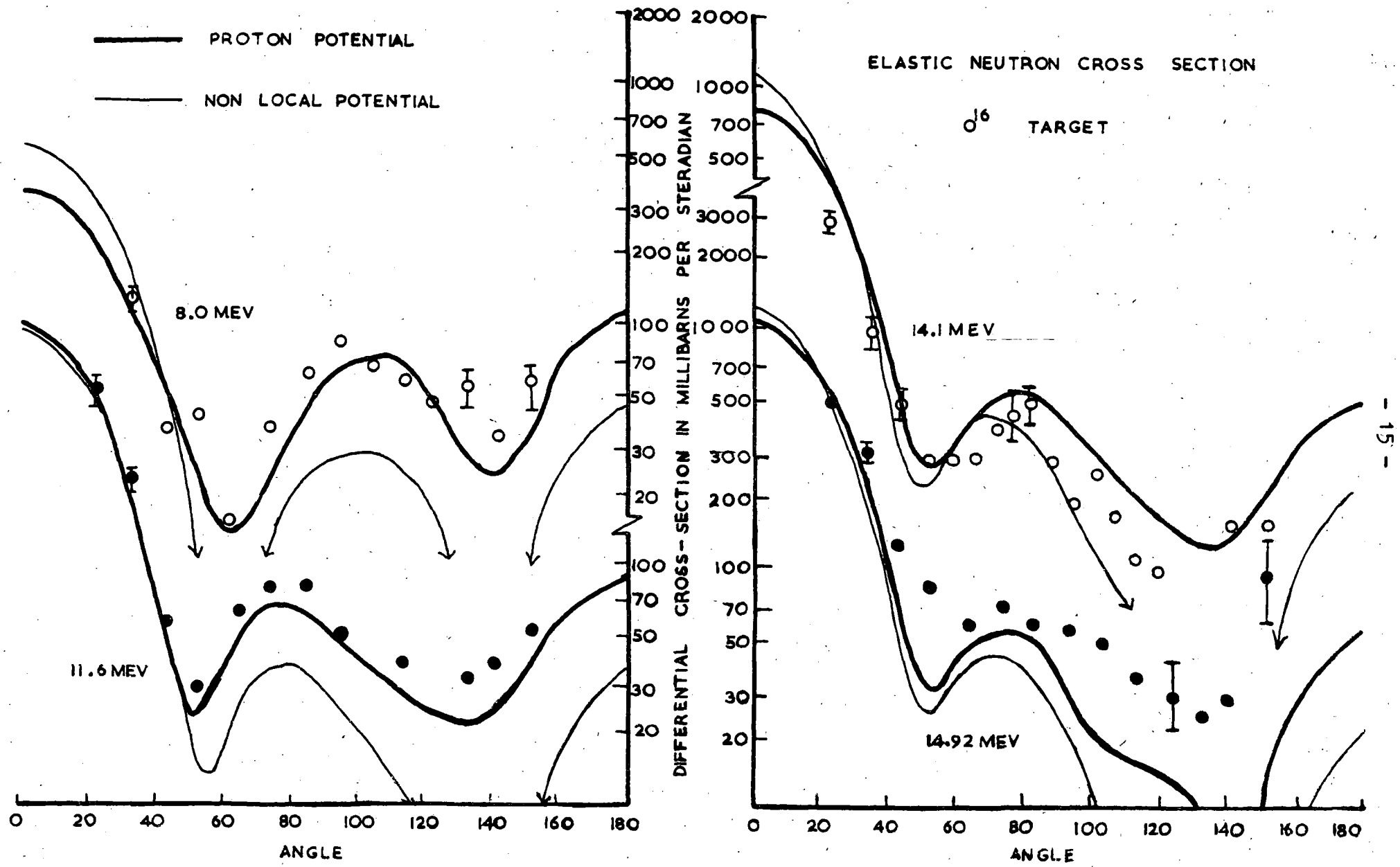
PROTON POTENTIAL
NON LOCAL POTENTIAL
ELASTIC NEUTRON CROSS SECTION
O^{16} TARGET
8.0 MEV
11.6 MEV
14.1 MEV
14.92 MEV
DIFFERENTIAL CROSS-SECTION IN MILLIBARNS PER STERADIAN
ANGLE
ANGLE

FIG 3

CN-23/50

Analytical Description of Neutron Cross Sections and the Effect of their Energy Dependence Upon their 2200 m/sec Values*

J. R. Smith
Idaho Nuclear Corporation, Idaho Falls, Idaho

Introduction

The need for precision in the values of the 2200 m/sec constants of the thermal fuels, ^{233}U, ^{235}U, ^{239}Pu, and ^{241}Pu, has prompted studies of the problem by the method of least squares [1-2]. In the course of such studies it is necessary to reduce to 2200 m/sec values those data which were measured at other neutron velocities or in a spectrum of neutron velocities. In the former case reduction to the 2200 m/sec value is accomplished by direct application of the curve describing variation with energy of the quantity being measured. In the latter case, the correction is often applied by means of Westcott's formalism [3], using his "g" and "s" parameters. These are themselves calculated from the energy variation curves. In either case the accuracy of the conversion depends upon the precision with which the energy variation is established.

Difficulties Associated with Normalization to 2200 m/sec Values

The energy commonly selected for specification of absolute values of nuclear parameters corresponds to a neutron velocity of 2200 m/sec, or 0.0253 eV neutron energy. This seemed a convenient energy when it was chosen and perhaps remains so from the point of view of reactor measurements. From the point of view of those making measurements with fast choppers and crystal spectrometers, however, it is doubtful that a more inconvenient energy could have been chosen. These instruments have provided a large proportion of the existing cross

*Work performed under the auspices of the U. S. Atomic Energy Commission.

section data in the thermal energy range, and both encounter systematic difficulties close to 0.0253 eV. Fast choppers are usually designed to operate primarily at higher energies. They are likely to run into problems associated with the rotor cutoff function at low energies, and counting rates drop to low values. Moreover, the usual problems associated with fission foil nonuniformity are compounded by the inhomogeneity observed in chopped neutron beams [4]. Crystal spectrometers have problems with beam contamination by neutrons from higher order Bragg reflections. Even when a velocity selector is used to cut out the higher order neutrons, a problem remains due to competition between planes of the crystal monochromator [5]. Many monochromators have a large dip in their response function very close to 0.025 eV. Such dips can cause a loss of 50% of the Bragg beam intensity, and are to be avoided where possible.

When all instrumental problems are solved there still may be ambiguities introduced into the data by coherent scattering effects in the sample itself. Consider for example the two sets of measurements of the total cross section of ^{197}Au ($\sigma\sqrt{E}$), shown in Fig. 1. The open circles represent data taken with the Materials Testing Reactor (MTR) fast chopper. The closed circles represent data taken with the MTR crystal spectrometer, using a velocity selector to eliminate order effects. The two sets of data agree well except near 0.0253 eV. Bragg cutoff for the ^{240}Au planes occurs at 0.0247 eV and leads to a fluctuation in the cross section. These two sets of data were taken with different Au samples. The chopper experiment used a stack of 0.005 in. Au foils, while the crystal spectrometer experiment used a single block of gold. Both samples were about 0.080 in. thick. Because of the difference in mode of preparation of the samples the molecular arrangements and hence the coherent scattering effects differed. It would appear that if normalization of these curves were desired, it should be done at some energy other than 0.025 eV.

These problems are mentioned to point out that precise establishment of an energy dependence of a cross section may be difficult. In some cases it may be impossible, unless the sample form is specified. Ambiguity in the energy dependence is reflected in an uncertainty in the absolute value. The situation would be somewhat better, at least for comparison of cross section measurements, if the reference energy were somewhere between 0.06 and 1.2 eV. Here fast choppers and crystal spectrometers are both operating very efficiently. Counting rates are reasonable, second order fractions are at a minimum, resolution is not a problem, and choppers are farther from their rotor cutoffs. This region lies between the regions complicated by resonance effects on the one hand and coherent scattering effects on the other.

Least-Squares Analysis

A change in the reference energy would make comparisons of data somewhat more straightforward, but the problem of establishing the curve shape in the low energy regions would remain. The many individual points comprising the energy variation data constitute an overdetermined system. To extract the "best" set of values for descriptive parameters of such an

overdetermined system, the least-squares technique is well suited. In order to apply this technique to data taken at different energies it is necessary to assume an analytical function through which the data points are related. The R-matrix formulation of resonance theory [6] thrusts itself forward as a likely candidate to provide this function. It has been proved highly successful in describing the cross section behavior in the resonance region [7]. It has a sound theoretical basis, and offers the hope that extrapolations may be made with confidence beyond the region where data exist. Spurious wrinkles in data due to instrumental effects might also be ironed out. Yet these apparent advantages may not be fully realized. In the low energy region the data are affected by negative energy resonances, whose parameters can be only partially inferred from their effect on the data. The R-matrix description remains limited by the quality of the experimental data. For the low energy regions this formalism offers only slight theoretical advantages over a polynomial description, and this advantage is obtained at the cost of considerably greater difficulty in calculation.

An alternative multilevel description has been proposed by Adler and Adler [8]. These authors have shown that the effects of interference in fission can be described by an expression containing a set of symmetric and unsymmetric single-level terms plus a polynomial in powers of the neutron energy. The polynomial represents the residual effects of resonances lying outside the energy region under consideration.

Using an Adler-type formula, Fluharty et al [9] made least-squares fits to the fission and absorption cross section data for the four thermal fuels in the energy region below 0.5 eV. They chose to split off the energy region below 0.1 eV from the rest of the data and represent it by a polynomial alone. For the region 0.1 - 0.5 eV a resonance term was added. Each of the nuclei considered has a single resonance in this energy region. The analytical expressions used were:

$$\sigma\sqrt{E} = A + BE + CE^2 \qquad 0.02 < E < 0.1 \text{ eV} \tag{1}$$

$$\sigma\sqrt{E} = \frac{\alpha + \beta(E-E_o)}{(E-E_o)^2+\Gamma^2/4} + D + FE + GE^2. \qquad 0.1 < E < 0.5 \text{ eV} \tag{2}$$

The constants α and β give the relative magnitudes of the symmetric and unsymmetric resonance terms, respectively. The unsymmetric term represents the effects of interference in the fission process. E_o is the resonance energy and Γ the width of the resonance.

By fitting selected sets of data to these expressions by a least squares technique, Fluharty et al derived the sets of parameters shown in Table I. The corresponding curves are illustrated in Figs. 2 through 5. The analytical forms appear to fit the data well. From these simple expressions it is easy to calculate not only the cross section at any energy in the region covered, but also Westcott's Maxwellian spectral factor "g". Table II shows Westcott "g" factors calculated from the

Fluharty fit curves for several values of the neutron temperature. Errors in these factors are due to shape uncertainties in the energy variation of the cross sections, and have not been satisfactorily treated theoretically. The estimates shown are based on the standard deviations shown in the "g" values as calculated from fits to separate sets of data. These can be only rough estimates, since many of the data sets do not cover a broad enough energy range to make the calculation of the "g" value valid.

Despite their pleasing appearance, these analytical fits turned out not to give a completely satisfactory accounting for the energy dependence of eta (or alpha) [12]. This limitation indicated a need for greater generality in the analysis. The general procedure desired is one that will allow least-squares fitting of three or more equations simultaneously, with normalization provided where necessary to absolute values at the energies where the values were measured. The least-squares adjustments of absolute values and the precision fitting of the energy variation would thus be accomplished simultaneously for all available related data. A mechanism for accomplishing this objective is to be found in the general least-squares procedure described by Cohen et al [10] and used by them to obtain least-squares-adjusted values for the atomic constants. In the application of this method to the current problem, each experimental data point is considered to be a solution (with residual error) to the appropriate analytical equations. The analytical expressions and energy region division used by Fluharty were retained. The system is thus represented by the following sets of equations:

For the region 0 to 0.1 eV:

Absorption: $$\sigma_a\sqrt{E_m} = A_a + B_aE_m + C_aE_m^2 \tag{3}$$

Fission: $$\sigma_f\sqrt{E_m} = K_n(A_f + B_fE_m + C_fE_m^2) \tag{4}$$

Eta: $$\eta = \nu L_n\left[\frac{A_f + B_fE_m + C_fE_m^2}{A_a + B_aE_m + C_aE_m^2}\right] \tag{5}$$

For the region 0.1 to 0.6 eV:

Absorption: $$\sigma_a E_m = \frac{\alpha_a + \beta_a(E_m-E_{oa})}{(E_m-E_{oa})^2 + \Gamma_a^2/4} + D_a + F_aE_m + G_aE_m^2 \tag{6}$$

Fission: $$\sigma_f\sqrt{E_m} = K_n\left[\frac{\alpha_a + \beta_f(E_m-E_{of})}{(E_m-E_{of})^2 + \Gamma_f^2/4} + D_f + F_fE_m + G_fE_m^2\right] \tag{7}$$

$$\text{Eta:} \quad \eta = \nu L_n \frac{\dfrac{\alpha_f + \beta_f(E_m - E_{of})}{(E_m - E_{of})^2 + \Gamma_f^2/4} + D_f + F_f E_m + G_f E_m}{\dfrac{\alpha_a + \beta_a(E_m - E_{oa})}{(E_m - E_{oa})^2 + \Gamma_a^2/4} + D_a + F_a E_m + G_a E_m^2} \tag{8}$$

Each data point used was expressed as a solution to one of these equations. Four additional equations were inserted to match the value and slope of the absorption and fission functions at the boundary (0.1 eV). The subscripts m denote the points of a data set. The subscripts n characterize complete sets of data from a given experiment. The constants K_n and L_n allow the normalization of the fission and eta data to the absolute value measurements, for which the normalization constant is defined to be unity. Cohen et al [10] describe the method for linearizing the equations, reducing them to a normal set, and solving to extract the values and variances of the parameters.

The computer program to accomplish this least squares adjustment has not been completely developed, and final data cannot be given at this time. However, some preliminary results have been attained for ^{233}U, and these appear promising. The first trials were restricted to the energy region below 0.1 eV, and used the same sets of data as did the Fluharty fit. To these were added relative eta data from BNL [11] and MTR [12], plus the MTR Mn bath absolute value points [13] for normalization. Both linear and parabolic fits were obtained, and these are illustrated in Fig. 6. The parameters are shown in Table III. A comparison of these results with those from the original Fluharty fit shows very little difference for the absorption data. On the other hand, the slope of the fission curve is significantly smaller than that previously obtained without considering the eta data. Standard deviations of the parameters are probably similar to those obtained by Fluharty, although at this stage of development of the program the variances were not printed out.

For the fit of the two regions together, the fission and absorption data used were the MTR data as recorded on the SCISRS tape, vintage December 1965. The absorption cross sections were derived by subtracting 13 b. from the total cross sections listed. The data as used by Fluharty had been averaged and normalized to the 2200 m/sec values given by Westcott [2]. For this fit it was desired to leave the averaging and normalization tasks to the least squares operation. The fission cross section value recommended by Westcott, 527.7 b, was fed in for normalization, and 2.50 was used as an origin value for ν.

The parameters obtained in this fit are shown in Table IV, and the corresponding curves in Fig. 7. The fits look rather pleasing to the eye, but there are some disturbing features. After 10 iterations the fit has not yet satisfactorily converged. The boundary equations failed to force continuity completely and there are discontinuities in the value of the absorption cross section and in the slope of the eta curve at 0.1 eV. Moreover the 2200 m/sec value of the fission cross

section came out 526.3 b instead of the normalization value. The last result is not too surprising, since the other parameters were not normalized to the Westcott values. The set of 2200 m/sec values produced by this analysis are shown in Table IV. Despite the non-convergence, these numbers look quite reasonable.

Some of the above disagreeable effects may be due to a loss of significance in the numbers propagated through the computer. The matrix inversion itself has been carried out in double precision, but the remainder of the calculation has not. The standard deviations indicated for C_a and F_a at this stage in the calculation are rather startling. They indicate that these values have little or no significance. The program is being rewritten to use double precision throughout. It is hoped that this modification will allow convergence of the iterations and significance of the parameters.

Conclusions

While the multi-equation least-squares fitting procedure has not yet produced completely satisfactory results, it promises to have certain advantages. It allows the simultaneous consideration of the maximum amount of information concerning the nuclear interactions. It allows normalization of sets of data to be based on behavior over a wide energy region instead of at just one point. All cross section curves can be fit simultaneously and the fit to each is influenced by its effect on the others. The parameters produced in the fit describe the cross sections in a simple form readily adapted to reactor calculation.

A ifficulty with this method is the problem of assigning weights to the various sets of data. These weights determine which set of data will be fit best, if there are conflicts. However the problem of weight assignment is common to all least squares procedures and is not particularly more troublesome here than elsewhere.

The system at present does not provide for the inclusion of data from measurements made in a spectrum of neutron energies. This limitation need not remain a permanent one, however. If the results of such spectral measurements can be expressed by a set of equations that can be linearized, they may be included in the analysis.

Acknowledgments

The author would like to express his appreciation to Messrs. R. A. Gideon and F. W. Spraktes for their efforts in developing the least-squares program described, to Messrs. N. H. Marshall and H. R. Creasey and Miss B. K. Sidle for additional programming and computational assistance, and to Dr. R. G. Fluharty for advice and counsel.

REFERENCES

[1] SHER, R., FELBERBAUM, J. USAEC Rep. BNL-918 (1965) and BNL-722 (1962).
[2] WESTCOTT, C. H. et al, Atomic Energy Review 3 2 (1965) 3.
[3] WESTCOTT, C. H., WALKER, W. H., ALEXANDER, T. K., Proc. 2nd UN Int. Conf. PUAE 16 (1958) 70.
[4] WATANABE, T., SIMPSON, O. D., USAEC Rep. IDO-16995 (1964).
[5] SPENCER, R. R., SMITH, J. R., BRUGGER, R. M., Pile Neutron Research in Physics, IAEA, Vienna (1962) 433.
[6] WIGNER, E. P., EISENBUD, L., Phys. Rev. 72 (1947) 29.
[7] MOORE, M. S., REICH, C. W., Phys. Rev. 118 (1960) 718.
[8] ADLER, F. T., ADLER, D. B., Trans. Am. Nucl. Soc. 6 (1963) 37; ADLER, D. B., ADLER, F. T., Trans. Am. Nucl. Soc. 6 (1963) 38; and Trans. Am. Nucl. Soc. 5 (1962) 53.
[9] FLUHARTY, R. G., MARSHALL, N. H., SIMPSON, O. D., CONF-660303 (1966) 985.
[10] COHEN, E. R., CROWE, K. M., DUMOND, J. W. M., The Fundamental Constants of Physics, Interscience Publishers, Inc., New York (1957).
[11] PALEVSKY, H., et al, J. Nucl. Energy 3 (1956) 177.
[12] SMITH, J. R., FAST, E., CONF-660303 (1966) 919; also USAEC Rep. IDO-17173 (1966).
[13] SMITH, J. R., REEDER, S. D., FLUHARTY, R. G., USAEC Rep. IDO-17083 (1966).
[14] MOORE, M. S., MILLER, L. G., SIMPSON, O. D., Phys. Rev. 118 (1960) 714; also MOORE, M. S., MILLER, L. G., SIMPSON, O. D., USAEC Rep. IDO-16576 (1959).
[15] BLOCK, R. C., SLAUGHTER, G. G., HARVEY, J. A., Nuc. Sci. Engng. 8 (1960) 112.
[16] SIMPSON, O. D., MOORE, M. S., SIMPSON, F. B., Nuc. Sci. Engng. 7 (1960) 187.
[17] SAPLAKOGLU, A., Nuc. Sci. Engng. 11 (1961) 312.
[18] LEONARD, B. R., Jr., Neutron Physics (YEATER, J. L. ed.) Academic Press, New York and London (1962) 3.
[19] SAILOR, V. L., Proc. Int. Conf. PUAE 4 (1955) 199.
[20] LEONARD, B. R., Jr., Proc. Int. Conf. PUAE 4 (1955) 193 and personal communication (1966).
[21] RICHMOND, R., PRICE, B. T., J. Nucl. Energy 2 (1956) 177.
[22] EGELSTAFF, P. A., GAYTHER, D. B., NICHOLSON, K. P., J. Nucl. Energy 6 (1958) 303.
[23] BOLLINGER, L. M., COTE', R. E., THOMAS, G. E., Proc. 2nd UN Int. Conf. PUAE 15 (1958) 127.
[24] PALEVSKY, H. private communication; listed on SCISRS tape.
[25] SIMPSON, O. D., SCHUMAN, R. P., Nucl. Sci. Engng. 11 (1961) 111; and SIMPSON, O. D., MARSHALL, N. H., USAEC Report IDO-16679 (1961).
[26] LEONARD, B. R., Jr., FRIESENHAHN, S. J., USAEC Report HW-62727 (1959) 32.
[27] CRAIG, D. S., WESTCOTT, C. H., Can. J. Phys. 42 (1964) 2384.
[28] WATANABE, T., SIMPSON, O. D., Phys. Rev. 133 (1964) B390.

TABLE I

Parameters of Fluharty Analytical Fit

Absorption

Parameter	^{233}U	^{235}U	^{239}Pu	^{241}Pu
A	92.36 ± 0.15	115.65 ± 0.16	158.02 ± 1.79	233.36 ± 0.71
B	-26.97 ± 2.31	-319.04 ± 6.26	-93.89 ± 63.49	-709.96 ± 26.11
C	0	879.33 ± 55.13	7329.33 ± 499.19	9168.56 ± 211.46
α	0.0009 ± 0.002	0.335 ± 0.021	6.223 ± 0.316	3.924 ± 0.085
β	0.297 ± 0.088	1.410 ± 0.113	4.038 ± 3.051	-5.218 ± 0.617
Γ	0.080 ± 0.018	0.148 ± 0.003	0.094 ± 0.002	0.115 ± 0.001
E_o	0.173 ± 0.007	0.283 ± 0.001	0.297 ± 0.001	0.259 ± 0.0004
D	92.85 ± 1.68	108.14 ± 1.34	38.25 ± 50.69	146.96 ± 9.52
F	-4.69 ± 12.82	-188.96 ± 15.97	652.64 ± 595.39	-662.24 ± 107.39
G	42.15 ± 19.83	162.29 ± 26.53	-1333.26 ± 1089.72	866.26 ± 187.00

Fission

Parameter	^{233}U	^{235}U	^{239}Pu	^{241}Pu
A	84.86 ± 0.31	99.28 ± 0.70	114.98 ± 2.28	154.92 ± 4.80
B	-36.44 ± 4.94	-306.34 ± 24.91	49.26 ± 80.08	150.71 ± 153.52
C	0	1018.59 ± 196.81	2911.16 ± 635.05	2761.86 ± 1145.64
α	-0.0155 ± 0.010	0.256 ± 0.025	4.818 ± 0.192	2.527 ± 0.109
β	0.389 ± 0.206	1.399 ± 0.136	6.966 ± 1.601	-6.225 ± 0.911
Γ	0.100 ± 0.026	0.154 ± 0.005	0.105 ± 0.002	0.112 ± 0.002
E_o	0.165 ± 0.010	0.285 ± 0.002	0.294 ± 0.001	0.260 ± 0.001
D	85.35 ± 3.63	91.41 ± 1.87	108.83 ± 23.03	94.88 ± 13.85
F	22.80 ± 26.12	-140.28 ± 20.24	-502.28 ± 270.14	-218.74 ± 138.63
G	-19.37 ± 38.64	102.41 ± 32.36	573.07 ± 480.59	163.78 ± 224.61

TABLE II

Westcott "G" Values as Calculated from Fluharty Analytical Fit

Nucleus	T(°C)	g_{abs}	g_{fis}	g_{η}
^{233}U	20	.9970	.9952	.9982
	20.44	.9970 ± .0009	.9951 ± .0008	.9981 ± .0012
	40	.9966	.9943	.9977
	60	.9961	.9935	.9974
^{235}U	20	.9779	.9773	.9994
	20.44	.9778 ± .0010	.9772 ± .0014	.9994 ± .0018
	40	.9733	.9724	.9990
	60	.9690	.9677	.9987
^{239}Pu	20	1.0818	1.0567	.9768
	20.44	1.0822 ± .0012	1.0570 ± .0027	.9767 ± .0030
	40	1.1002	1.0705	.9730
	60	1.1211	1.0862	.9689
^{241}Pu	20	1.0375	1.0495	1.0115
	20.44	1.0376 ± .0027	1.0497 ± .0029	1.0117 ± .0040
	40	1.0456	1.0611	1.0148
	60	1.0552	1.0737	1.0176

Indicated errors are deviations of the mean, derived from the analytical fitting of many data sets.

TABLE III

Parameters for 3-Equation Fit to $\sigma_a\sqrt{E}$, $\sigma_f\sqrt{E}$, and η for ^{233}U

	Parameter	Linear Fit	Parabolic Fit
Absorption	A_a	92.26	91.73
	B_a	-24.86	-1.71
	C_a	0	-206.08
Fission	A_f	84.58	83.85
	B_f	-25.77	12.31
	C_f	0	-359.8
	Westcott g-Values*		
	g_a	.9972	.9970
	g_f	.9962	.9955
	g_{η}	.9990	.9984

*The g-value computations used the parameters from the Fluharty fit above 0.1 eV.

TABLE IV

Analytical Fit Parameters for ^{233}U, 0-0.6 eV
3-Equation, 2-Region Fit

Parameter	Fission		Absorption	
A	84.32	± 0.40	91.91	± .45
B	-21.18	± 14.8	-31.20	± 16.2
C	-103.93	± 120	-10.28	± 1.2×10^3
α	0.008	± .007	0.0009	± .0010
β	0.465	± .155	0.311	± .127
E_o	0.168	± .005	0.171	± .007
Γ	0.098	± .021	0.083	± .021
D	88.19	± 3.53	92.19	± 2.8
F	-17.90	± 25.4	-5.06	± 5.5×10^4
G	50.77	± 28	41.44	± 19.8

Westcott g-Values	Indicated 2200 m/sec Values		
g_a = .9964	σ_a	572.9	± 3.5
g_f = .9954	σ_f	526.3	± 3.5
g_η = .9989	η	2.294	± .005
	ν	2.497	± .004

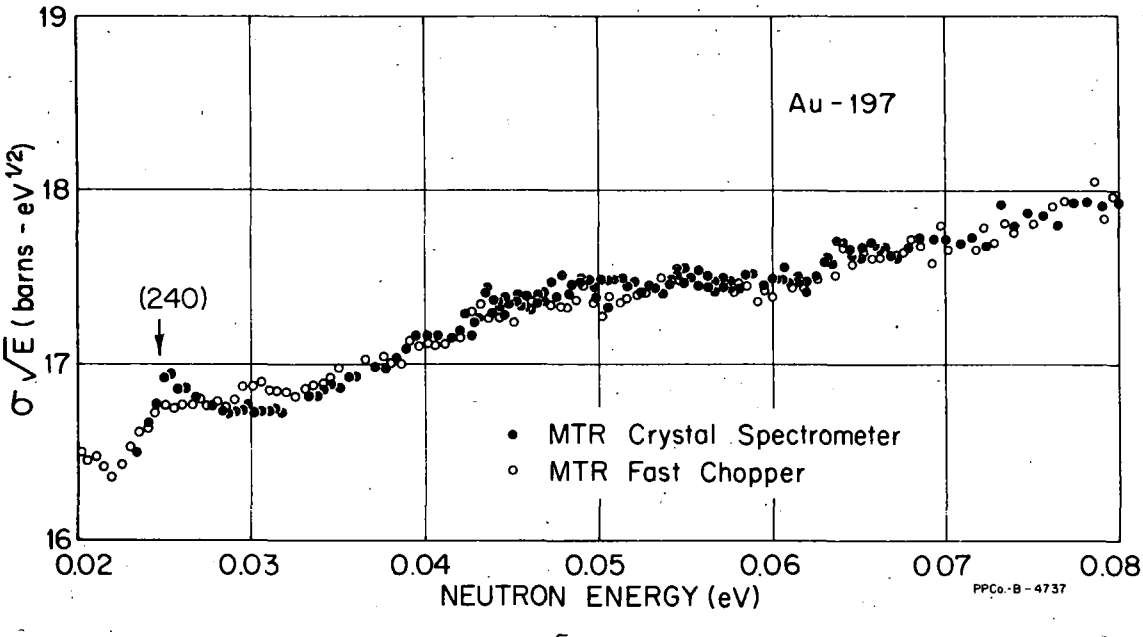

Figure 1 - Total cross section ($\sigma_T\sqrt{E}$) of gold, as measured by the MTR crystal spectrometer and the MTR fast chopper, using different samples. The arrow marks the position of Bragg cutoff for Au (240).

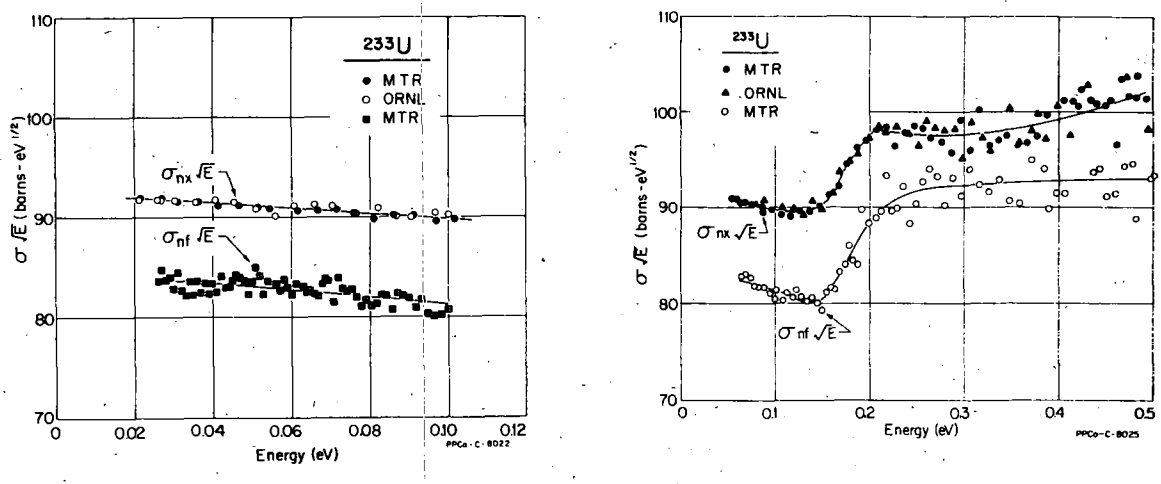

Figure 2 - Fluharty's analytical fit to the ^{233}U absorption and fission cross sections ($\sigma\sqrt{E}$). Data were measured at MTR [14] and ORNL [15].

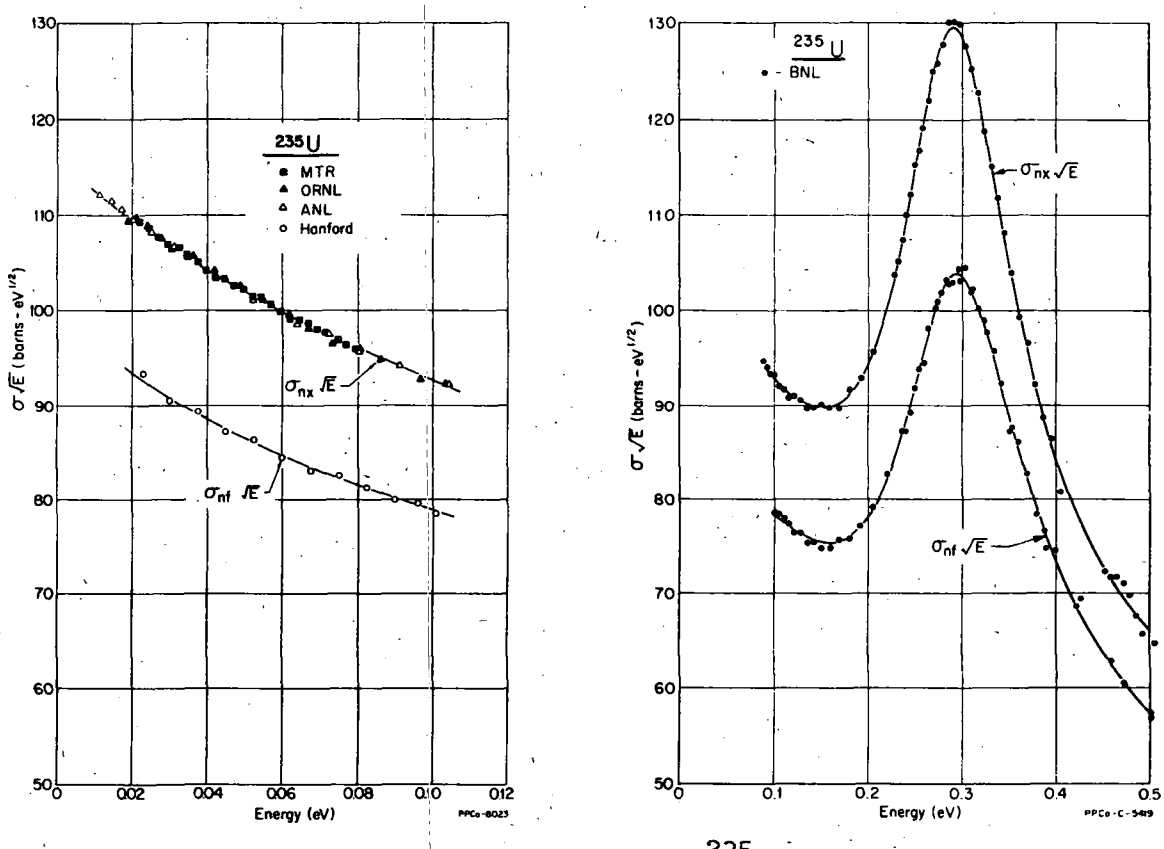

Figure 3 - Fluharty's analytical fit to the ^{235}U absorption and fission cross sections ($\sigma\sqrt{E}$). The measurements were made at MTR [16], ORNL [15], ANL [17], Hanford [18], and BNL [19].

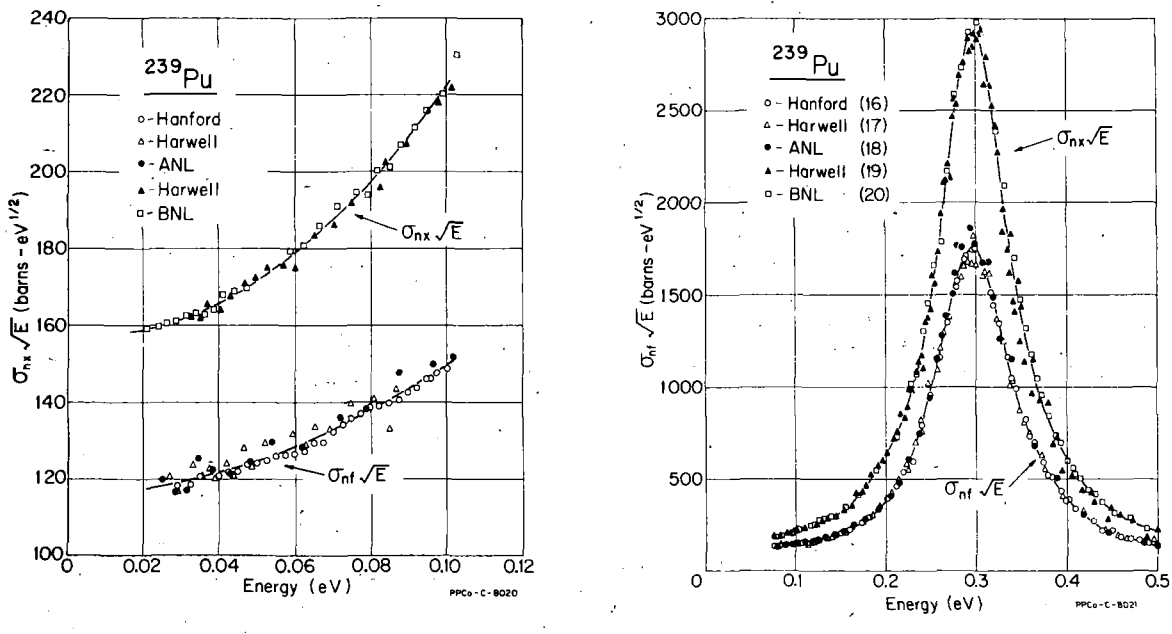

Figure 4 - Fluharty's analytical fit to the absorption and fission cross sections of ^{239}Pu. The data are plotted in the form $\sigma\sqrt{E}$, and were obtained at Hanford [20], Harwell [21,22], Argonne [23], and Brookhaven [24] laboratories.

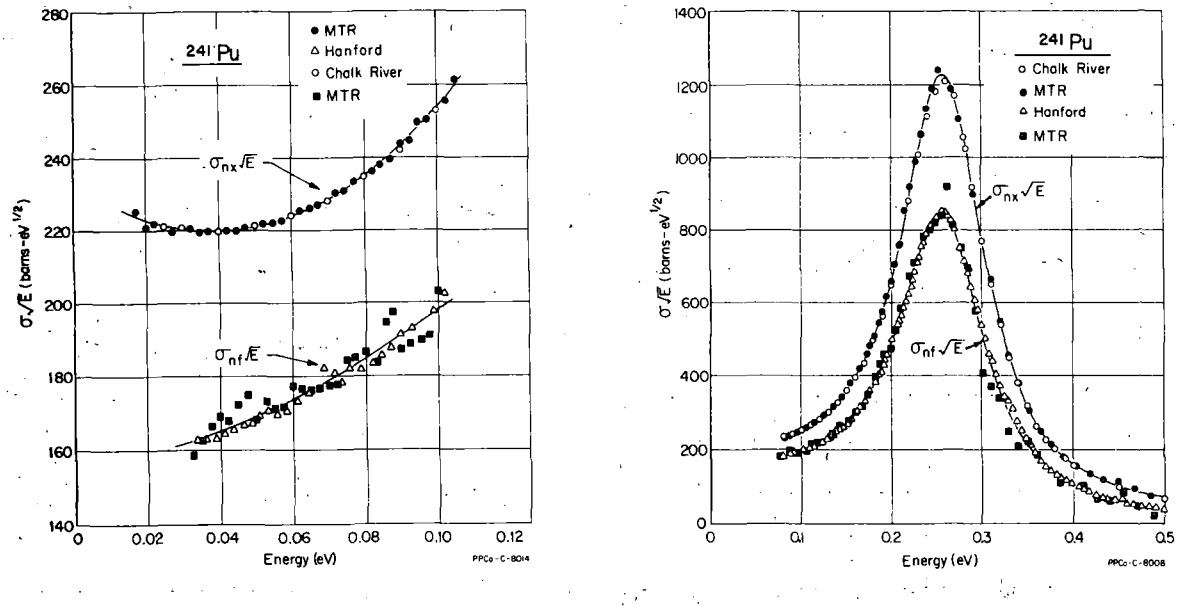

Figure 5 - Analytical fit to the ^{241}Pu absorption and fission cross sections ($\sigma\sqrt{E}$). The data shown were obtained at MTR [25,28], Hanford [26], and Chalk River [27].

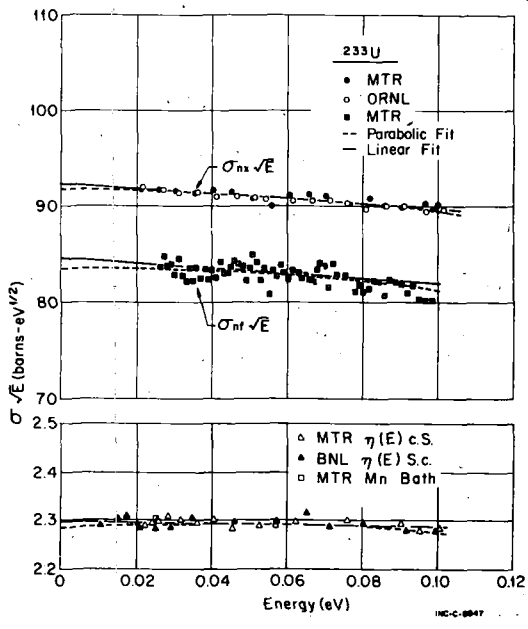

Figure 6 - Analytical fit to $\sigma_a\sqrt{E}$, $\sigma_f\sqrt{E}$, and η for ^{233}U below 0.1 eV. The three curves were obtained from the same least-squares analysis. Both linear and parabolic fits are shown. The data were obtained at MTR [12,13,14] and BNL [11].

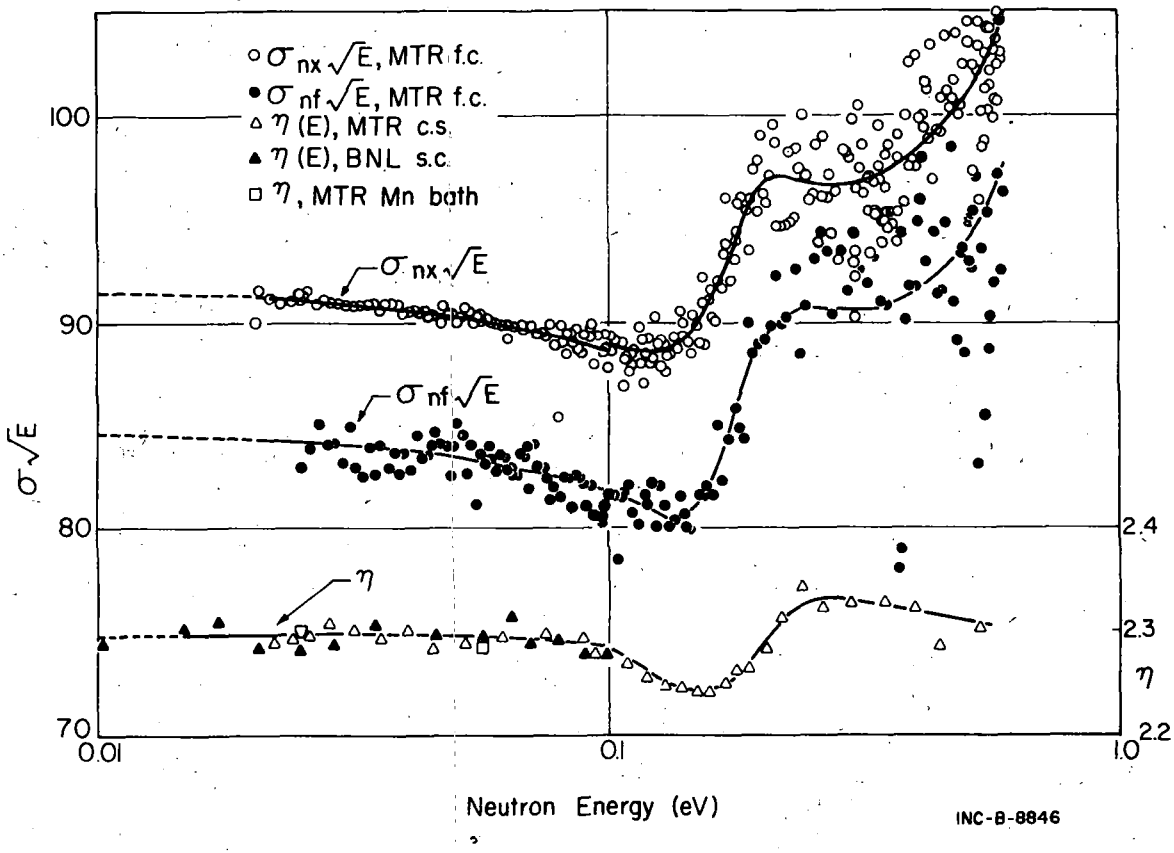

Figure 7 - Three-equation, Two region analytical fit to $\sigma_a\sqrt{E}$, $\sigma_f\sqrt{E}$, and η for ^{233}U. Data were obtained at MTR [12,13,14] and BNL [11].

NEUTRON CAPTURE BETWEEN 5 keV AND 3 MeV

Stupegia, D. C., Keedy, C. R., Schmidt, M., Madson, A. A.
Argonne National Laboratory, 9700 South Cass Avenue,
Argonne, Illinois 60439

INTRODUCTION

A series of radiative capture cross section measurements has been undertaken as a contribution to the collection of data necessary for reactor technology, and for the use of these data to test the statistical compound nuclear theory. The point of view taken in testing the theory is to choose a reasonable set of optical model and statistical parameters, and to attempt to fit the data by adjusting the value of the ratio of the radiation width and the observed level spacing. One can thus evaluate the usefulness of the theory in predicting cross section curves, given a set of parameters which are typically available from experimental sources.

METHOD

Neutron capture cross sections are being measured between a few keV and about 3 MeV by the activation method, in which a sample is irradiated in a neutron beam, and the radioactive capture product is measured by counting it in a beta counter or a gamma-ray spectrometer which has been calibrated with a 4π beta counter. Monoenergetic neutrons are produced by bombarding lithium or tritium targets with protons from the Van de Graaff accelerator, and neutron intensity is measured with a fission chamber. The data below about 150 keV are obtained by irradiating with neutrons at 120° with respect to the proton beam on lithium. The results are shown in Figures 1 to 8, along with data of other workers.

COMPARISON WITH THEORY

The experimental results are compared with calculations using the statistical model of the compound nucleus, which gives the energy averages of resonant or fluctuating compound nuclear cross sections. The model was first discussed by Wolfenstein [1] and by Hauser and Feshbach[2], and then was used by Lane and Lynn[3] to calculate capture cross sections. The curves given in this paper were calculated using the model in the form given by Moldauer[4,5,6] in which the average compound nuclear cross

section for capture of neutrons of energy E is given by

$$\sigma_{cap} = \pi^2 \lambda\!\!\!^{-2} \sum_{J\pi} \frac{2J+1}{2I_o+1} \left\langle \Gamma_o^{J\pi} \right\rangle \rho_{J\pi} \frac{\left\langle \Gamma_{cap}^{J\pi} \right\rangle}{\left\langle \Gamma^{J\pi} \right\rangle} S^{J\pi} \qquad (1)$$

where $\lambda\!\!\!^{-}$ is the rationalized deBroglie wavelength of the neutron, I_o is the spin of the ground state of the target nucleus, $\left\langle \Gamma^{J\pi} \right\rangle$ is the averge total width of compound states with spin J, parity π, and density, $\rho_{J\pi}$, at excitation energy U + E, where U is the neutron separation energy in the compound nucleus. Further, $\left\langle \Gamma_o^{J\pi} \right\rangle$ is the average partial width for emission of elastic neutrons, and $S^{J\pi}$ is the width fluctuation correction factor[3,5,6].

In equation (1), $\left\langle \Gamma_{cap}^{J\pi} \right\rangle$ is proportional to the number of captures ending in low-lying states of the product nucleus. The factor usually found in equation (1) is $\left\langle \Gamma_{\gamma}^{J\pi} \right\rangle$ which is proportional to the gamma-ray emission rate of the compound nucleus. This difference, then takes into account the possibility that a gamma-ray decay which leaves the compound nucleus at an excitation energy above the neutron emission threshold may emit a neutron. This process does not count as a capture. Details on the calculation of $\left\langle \Gamma_{cap}^{J\pi} \right\rangle$ and the relationship between $\left\langle \Gamma_{cap}^{J\pi} \right\rangle$ and $\left\langle \Gamma_{\gamma}^{J\pi} \right\rangle$ are given by Moldauer[4,7].

The calculations also take into account the variation of radiation width and level density with excitation energy and spin of the compound nucleus, and the variation of neutron widths from level to level (Porter-Thomas distribution)[8]. The Weisskopf[9] formula for electric dipole radiation is used for the energy variation of radiation width. Level densities, $\rho = D^{-1}$, are taken to have the form

$$\rho_{J\pi}(U+E) = K\left[e^{-J^2/2\sigma^2} - e^{-(J+1)^2/2\sigma^2}\right] e^{2\sqrt{a(U+E)}} \qquad (2)$$

where $\underline{\sigma}$ is the spin-dependence parameter and $\underline{a}$ is related to the sum of neutron and proton single particle spacings, δ, by $a = \pi^2/6\delta$.

The computations were performed with the Nearrex[4] computer code for compound nuclear cross sections, combined with the Abacus-2 code[10] for optical model transmission coefficients.

All of the fittings of theoretical curves to experimental points were arrived at using the optical model parameters given in Table I. In Table II are listed the values of the statistical parameters used for each nuclide. The values of $\underline{a}$ and $\underline{\sigma}$ were taken from the papers of Gilbert and

Cameron[11] or from Benzi and Bortolani[12]. Only one statistical parameter, the ratio of the radiation width to the observed level spacing, Γ_γ/Dobs, was varied to obtain the fittings. As a first choice for the value of the ratio, experimental Γ_γ and Dobs were taken from Hughes, et al.[13]. when available. When Γ_γ was not known experimentally, it was estimated from the systematics of its variation with nuclear mass. When Dobs was not known experimentally, it was calculated from the formula of Gilbert and Cameron[11]. First choice values of the ratio for which one or both of these terms was estimated in this way are given in parentheses.

The experimental data are accurately fitted for ^{41}K, ^{55}Mn, ^{85}Rb, ^{98}Mo, and ^{141}Pr, at least up to neutron energies at which the levels of the target nucleus are known. The same should also be true for ^{237}Np, when more experimental data become available. Further, if one makes a drastic change in the parameter a for ^{98}Mo in Figure 4, one gets an improved fit at the higher energies. The curves for ^{176}Yb and ^{175}Lu do not fit, probably because these are non-spherical nuclei, for which the transmission coefficients are not correctly calculated by the spherical optical model. There are no reasonable changes in the parameters that would make these curves fit the data.

Finally, it is seen by comparing the last two columns of Table II, that even when the shape of the curve has been predicted correctly, one cannot always get a good absolute fit using the first choice values of Γ_γ/Dobs which are available either experimentally or by estimate.

TABLE I

OPTICAL MODEL PARAMETERS

Real potential depth	46 MeV
Imaginary potential depth	14 MeV
Real well radius	$R = (1.16A^{1/3} + 0.5) \times 10^{-13}$ cm
Real spin-orbit potential depth	7 MeV
Real well diffuseness	0.62×10^{-13} cm
Imaginary well width	0.5×10^{-13} cm
Imaginary well radius	$(R + 0.5) \times 10^{-13}$ cm

TABLE II

STATISTICAL PARAMETERS

Nuclide	U(MeV)	σ	a $(MeV)^{-1}$	$\frac{\Gamma_\gamma}{D_{obs}} \times 10^4$ (first choice)	$\frac{\Gamma_\gamma}{D_{obs}} \times 10^4$ (used)
^{41}K	7.53	2	5.56	(1.0)	3.3
^{55}Mn	7.27	4	7.52	(2.5)	2.8
^{85}Rb	8.82	4	11.0	(62)	30
^{98}Mo (curve 1)	5.94	4	13	(1.2)	3.4
^{98}Mo (curve 2)	5.94	4	4.1	38	3.4
^{141}Pr	5.85	4	18	7.8(1960) 16.7(1961) 23.5(1964)	7.0
^{175}Lu	6.29	6	21	165	436
^{176}Yb	5.56	4	22	(14)	8.5
^{237}Np	5.38	6	28.5	310	880

REFERENCES

[1] WOLFENSTEIN, L., Phys. Rev. 82 (1951) 690.

[2] HAUSER, W. and FESHBACH, H., Phys. Rev. 87 (1952) 366.

[3] LANE, A. M. and LYNN, J. E., Proc. Phys. Soc. (London) A70 (1957) 557.

[4] MOLDAUER, P. A., ENGELBRECHT, C. A., and DUFFY, G. J., Nearrex, A Computer Code for Nuclear Reaction Calculations, ANL-6978 (1964).

[5] MOLDAUER, P. A., Rev. Mod. Phys. 36 (1964) 1079.

[6] MOLDAUER, P. A., Phys. Rev. 135 (1964) B642.

[7] MOLDAUER, P. A., Effects of (n, $\gamma n'$) Processes on Fast Neutron Capture and Non-Elastic Spectra, Conference on Neutron Cross Section Technology, Washington, D. C., March 1966.

[8] PORTER, C. E. and THOMAS, R. G., Phys. Rev. 104 (1956) 483.

[9] BLATT, J. M. and WEISSKOPF, V. F., Theoretical Nuclear Physics, Wiley, New York (1952) 649.

[10] AUERBACH, E. H., Abacus-2, unpublished.

[11] GILBERT, A., and CAMERON, A. G. W., A composite nuclear level density formula with shell corrections, Institute for Space Studies, NASA, New York.

[12] BENZI, V. and BORTOLANI, M. V., Nuovo Cimento 38 1 (1965) 216.

[13] HUGHES, D. J., MAGURNO, B. A., and BRUSSEL, M. K., Neutron Cross Sections, BNL-325, 2nd Edition (1960).

[14] BOOTH, R., BALL, W. P. and MACGREGOR, M. H., Phys. Rev. 112 (1958) 226.

[15] HUGHES, D. J., GARTH, R. C. and LEVIN, J. S., Phys. Rev. 91 (1953) 1423.

[16] STAVISSKY, YU. YA., and TOLSTIKOV, V. A., Atomnaya Energiya 10 (1961) 508.

[17] JOHNSRUD, A. E., SILBERT, M. G. and BARSCHALL, H. H., Phys. Rev. 116 (1969) 927.

[18] MACKLIN, R. L., LAZAR, N. H., and LYON, W. S., Phys. Rev. 107 (1957) 504.

[19] KAPCHIGASHEV, S. P., and POPOV, YU. P., Atommaya Energiya 15 (1963) 120.

[20] VERVIER, I., Nucl. Phys. 9 (1959) 569.

[21] KONKS, V. A., POPOV, YU. P. and SHAPIRO, F. L., Zhur. Eksp. Teor. Fiz. 46 (1964) 80.

[22] MACKLIN, R. L., GIBBONS, J. H. and INADA, T., Phys. Rev. 129 (1963) 2695.

[23] GIBBONS, J. H., MACKLIN, R. L., MILLER, P. D. and NEILER, J. H., Phys. Rev. 122 (1961) 182.

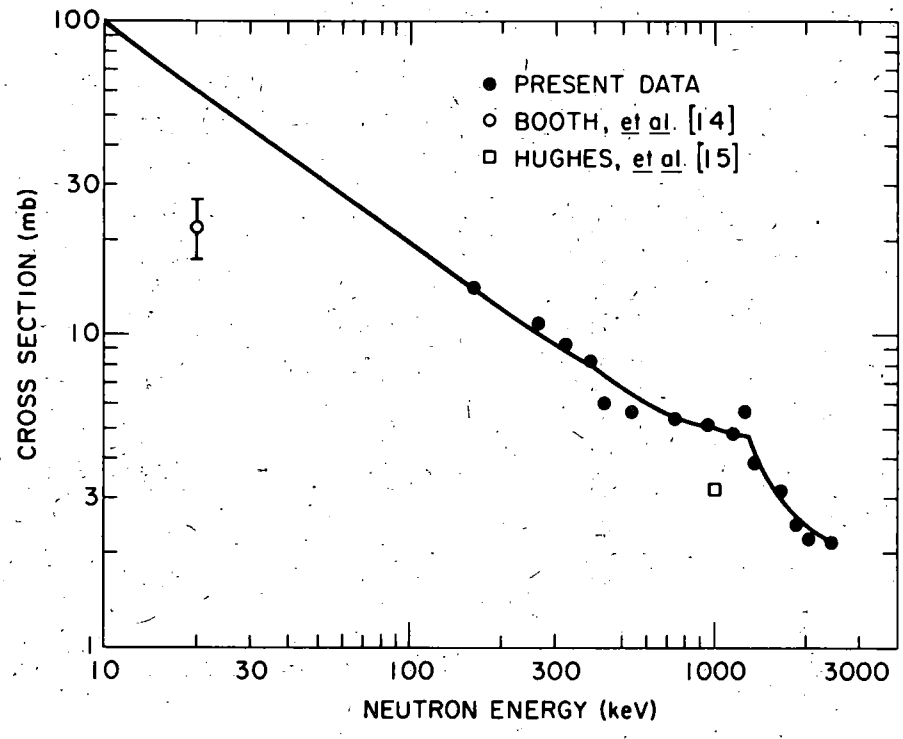

Fig. 1. Capture Cross Section of ^{41}K.

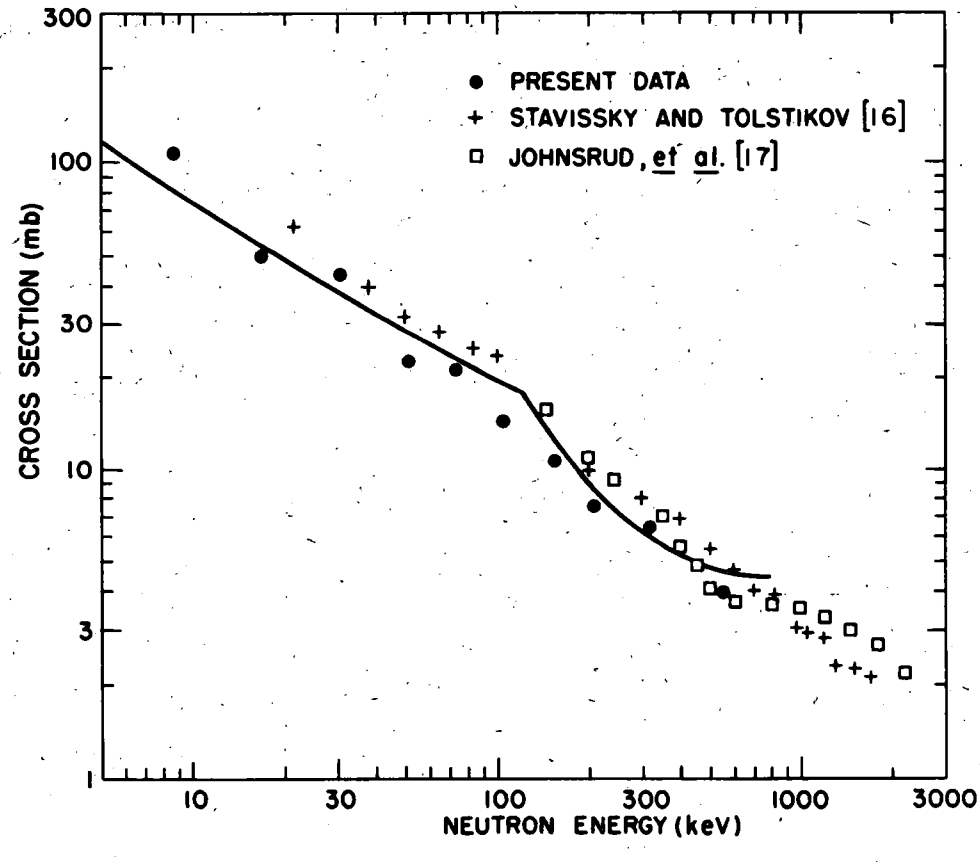

Fig. 2. Capture Cross Section of ^{55}Mn.

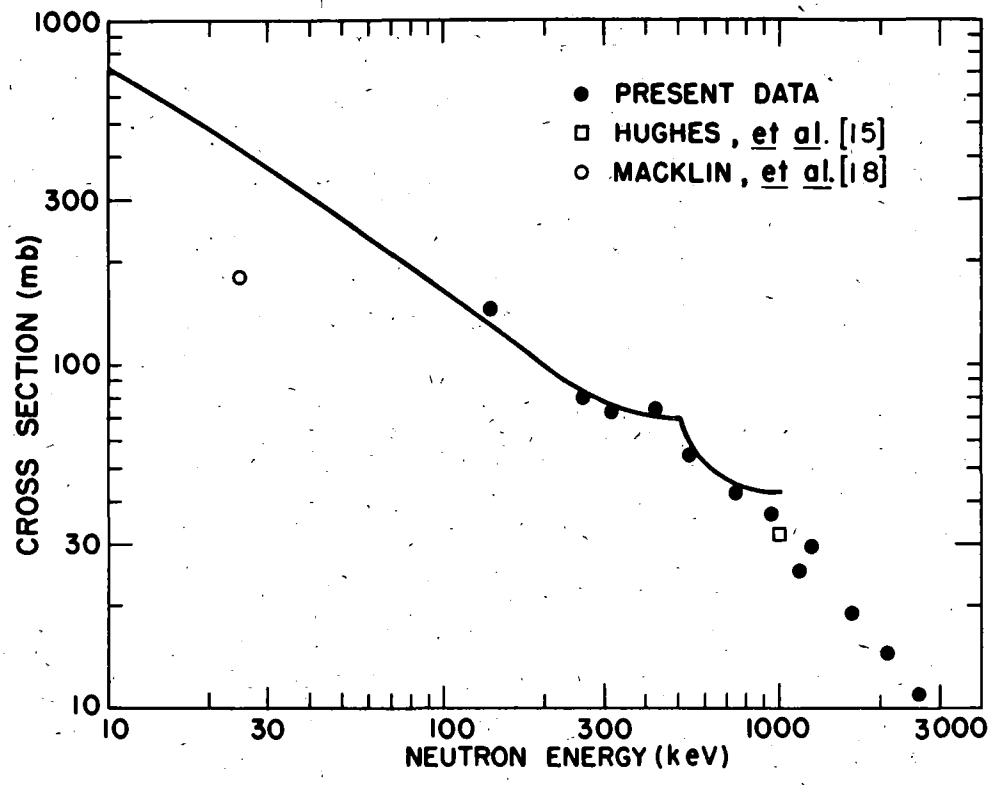

Fig. 3. Capture Cross Section of ^{85}Rb.

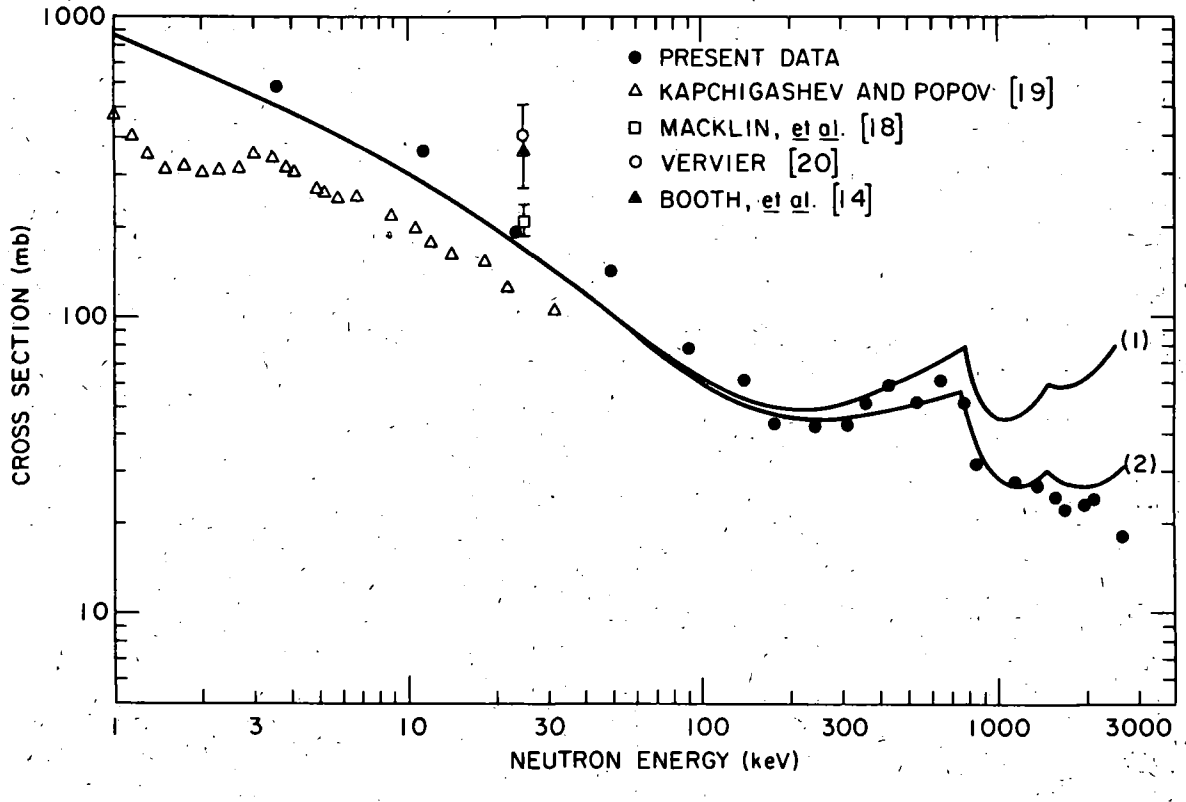

Fig. 4. Capture Cross Section of ^{98}Mo.

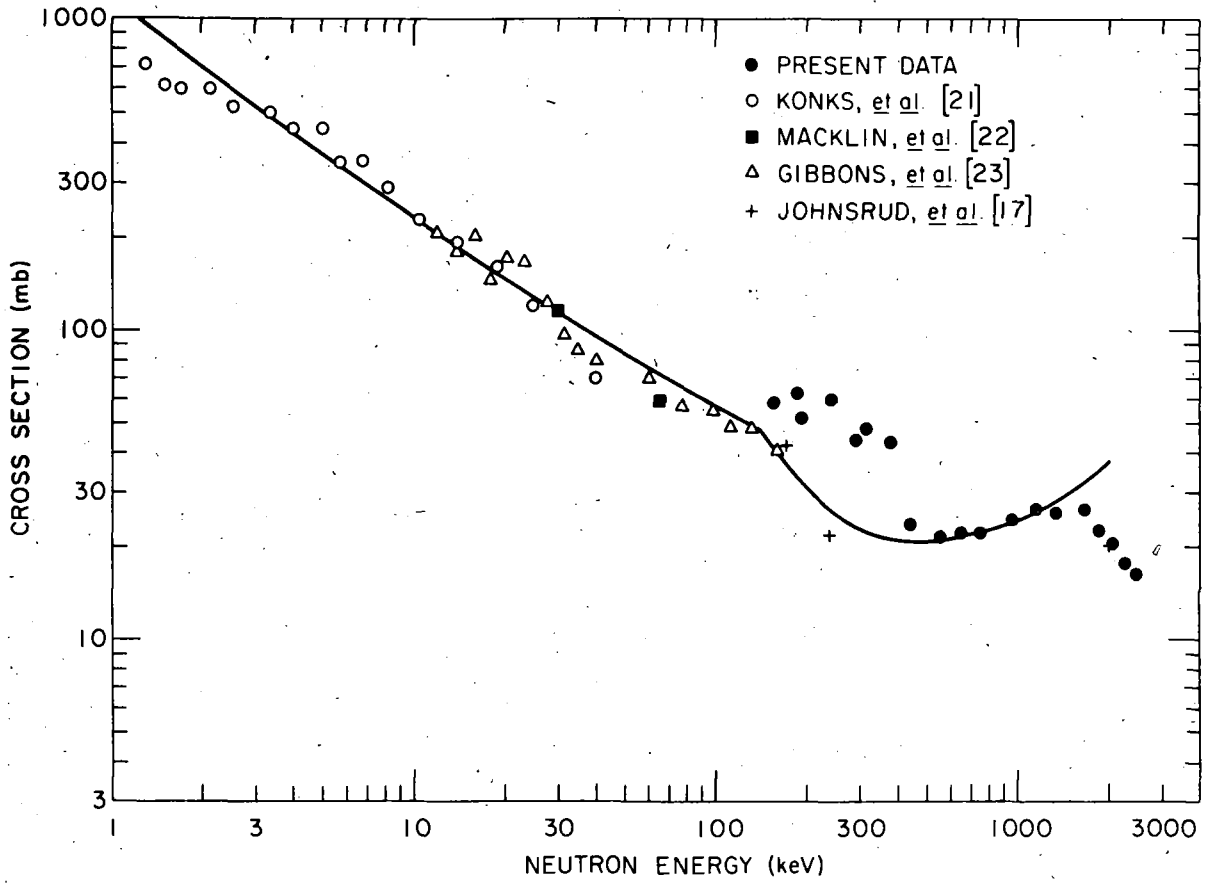

Fig. 5. Capture Cross Section of ^{141}Pr.

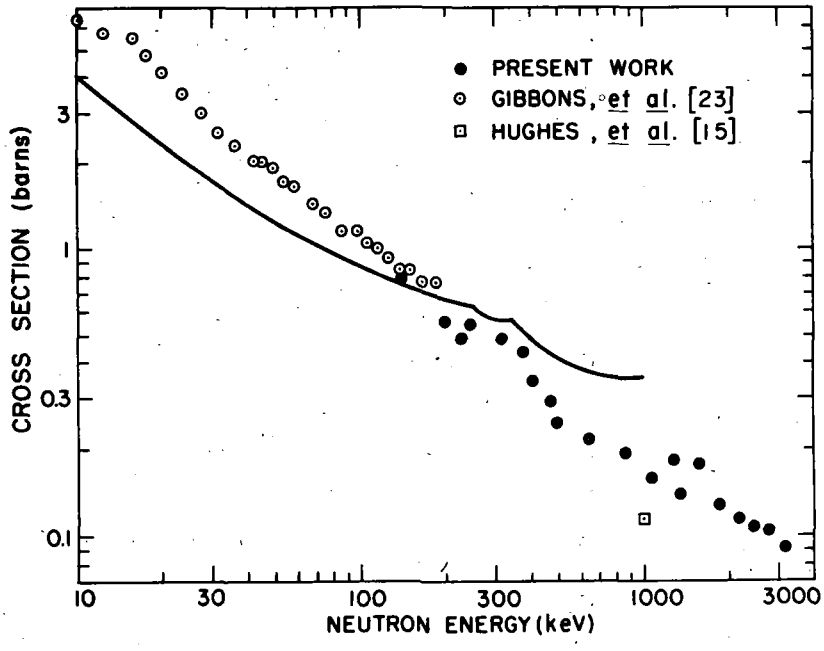

Fig. 6. Capture Cross Section for Production of 3.7 Hour State of ^{176}Lu.

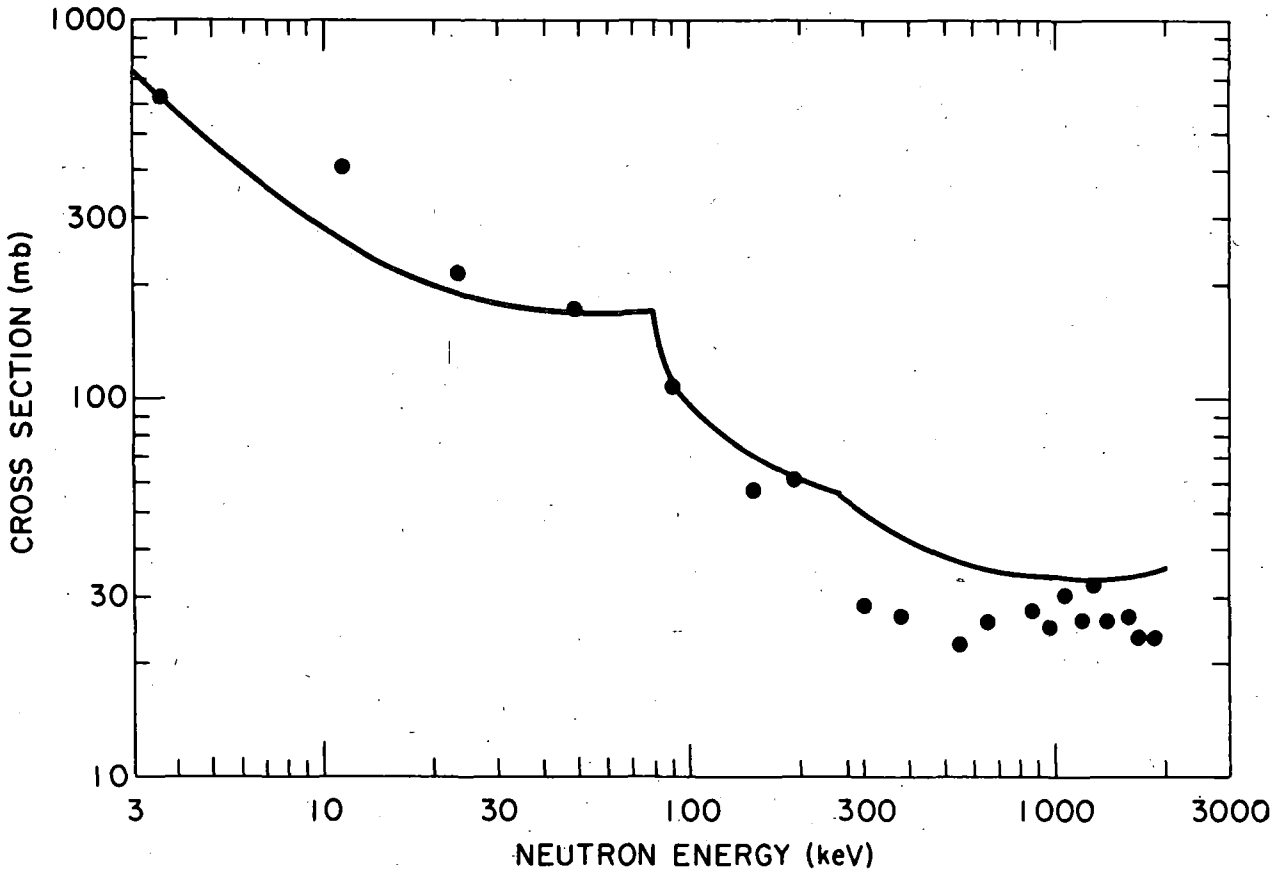

Fig. 7. Capture Cross Section of ^{176}Yb.

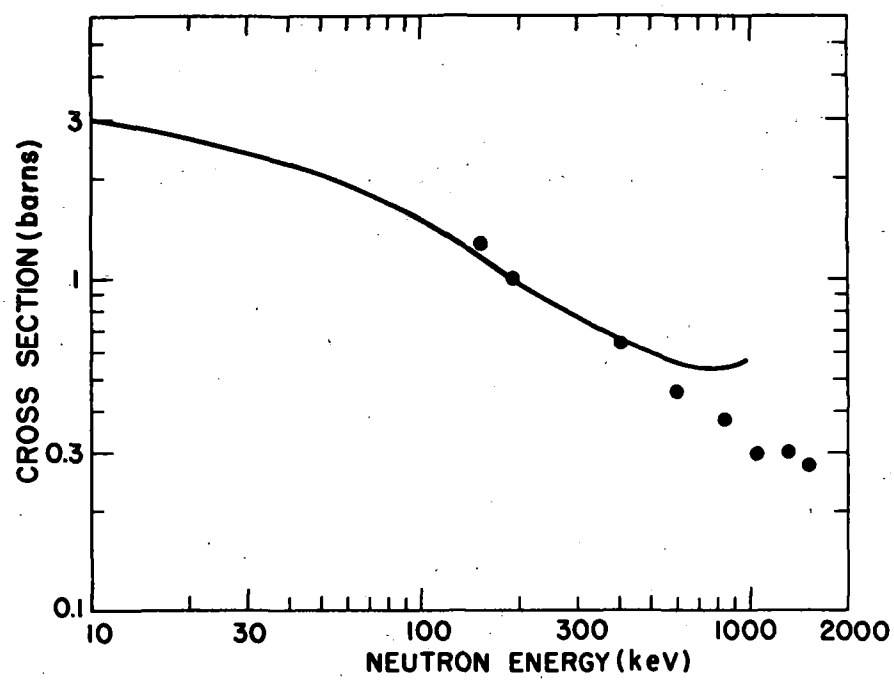

Fig. 8. Capture Cross Section of ^{237}Np.

CN-23/59

Gamma rays from neutron inelastic scattering in germanium

J. F. Barry

A.W.R.E., Aldermaston, Berkshire, England.

1. Introduction

The advent of lithium-drifted germanium detectors has resulted in a considerable increase of interest in gamma ray measurements. The high resolution coupled with fairly high efficiency of these detectors means that they can replace sodium iodide spectrometers and give improved performance in almost all applications.

In the measurement of gamma rays associated with neutron induced reactions there is always a background present due to neutron interactions in the detector itself. These reactions, such as $(n,n'\gamma)$ and (n,γ) give rise to unwanted background peaks whose positions and intensities need to be known before an unknown spectrum can be successfully analysed. Little information is available for these reactions. Chasman et al [1] report spectra obtained from the bombardment of a germanium detector with neutrons at a few isolated energies but the results are mainly of a qualitative nature. Malik et al [2] have observed gamma rays emitted from ^{70}Ge using a sodium iodide detector and quote gamma ray energies obtained following irradiation with 1.0 - 2.7 MeV neutrons.

The present paper gives results of a measurement of excitation functions of the more prominent gamma rays resulting from inelastic neutron scattering in the germanium of a crystal. The crystal itself acts as both target and detector. The neutron flux at each energy was measured with a fission counter containing a known mass of ^{237}Np. The curves were normalized to the data of Smith [3] who has measured the cross section for inelastic scattering to the pair of levels near 580 keV using a neutron detection method. Combining this with knowledge of the γ-ray decay schemes for germanium isotopes leads to cross sections for the excitation of individual levels by inelastic scattering.

Cross sections can be obtained by the gamma ray detection method in the neutron energy region immediately above threshold for excitation of a level. This is in contrast to the neutron detection method which fails at energies close to threshold due to the difficulty of detecting the low energy neutrons emitted.

It is of interest to compare the cross sections obtained, especially in the threshold region, with the results of optical model calculations. The theory of Hauser and Feshbach [4] was used and also a version corrected for level width fluctuations as described by Moldauer [5] and programmed by Wilmore [6].

2. Experimental details

2.1 The detector

The germanium crystal used as both target and detector in the measurements had an area of ≈ 1.5 cm^2 and a thickness of ~ 1 cm. Lithium was drifted in from one face to a depth of ≈ 0.6 cm. The crystal was mounted in a stainless steel container, 6 cm in diameter by 1.8 cm long and wall thickness 0.04 - 0.08 cm. A light spring supported the crystal against the centre of one face of the container and indium pads served to maintain good thermal and electrical contact with the crystal. The container was evacuated and sealed off before mounting on the end of a copper cold finger filled with liquid nitrogen. The whole cylinder was surrounded with an aluminium vacuum vessel continuously pumped to a pressure $< 10^{-5}$ mm to provide thermal insulation. The vacuum vessel was 7.9 cm in diameter by 12 cm long with a wall thickness of 0.10 - 0.3 cm. The assembly is shown in the irradiation geometry in figure 1.

2.2 Neutron flux

Neutrons were obtained from the $T(p,n)^3He$ reaction. Protons from a 3 MV Van de Graaff entered a tritium gas cell through a 2 mgm/cm^2 nickel window which was supported on a gold grid. The gas cell was 2.5 cm long and contained tritium at a pressure of 1 atmosphere. A Long Counter [7] 1.5 m from the target monitored neutrons from the reaction at 45°. The response of the Long Counter was related to neutron flux at the detector position by performing subsequent calibrations with the germanium assembly removed and replaced with a fission chamber. The latter was identical in design to those described by White [8] and contained a foil of ^{237}Np of known mass (0.5 mg/cm^2) deposited over an area of 8 cm^2. The fission rate in the counter was determined as a function of neutron energy and converted to neutron flux by using the known values of the ^{237}Np fission cross section [9], [10].

Corrections were made to the neutron flux deduced at the detector position to allow for neutron attenuation and scattering. The attenuation of neutrons in the aluminium vacuum container was calculated to be 4.5%, scattering from the cold finger materials 4%,

and scattering from the stainless steel crystal container 5%. The latter correction was however cancelled out since an almost identical correction applied to the ^{237}Np fission counter results. Neutron scattering from the germanium crystal assembly into the Long Counter was measured by observing the change in Long Counter rate when the assembly was removed from the neutron beam. The integrated proton current on target provided a monitor during this measurement. The scattering proved to be independent of energy within the accuracy of the measurement (1%) and equal to 3.5%. A similar experiment showed the scattering from the fission counter into the Long Counter to be negligible.

2.3 Gamma Ray Spectra

The pulses from the detector were recorded after amplification on a 400 channel pulse height analyser. The resolution obtained using a source of ^{22}Na was 7 keV (f.w.h.m.) at 0.51 MeV and of this about 5 keV was contributed by noise generated in the preamplifier. The resolution during neutron irradiations deteriorated to about 15 keV at 0.7 MeV due to the high overall counting rates involved ($\approx 10^3$/sec).

An example of the spectra obtained using neutrons of 1.5 MeV energy is shown in figure 3. The energy calibration is established with reference to known gamma ray lines at 0.51 and 1.277 MeV from a source of ^{22}Na. The assignment of the lines in the spectrum can be understood by reference to figure 2 which shows the known decay schemes of the isotopes of germanium together with their natural abundance [11], [12]. The most prominent feature is a very strong line at 695 keV which is attributed to detection of electrons from the decay of the 700 keV level in ^{72}Ge. This is a $0^+ - 0^+$ transition for which electromagnetic decay is forbidden and the internal conversion electrons are detected with essentially 100% efficiency. The decay from the second excited state in ^{72}Ge at 835 keV is not resolved from background gamma rays at 845 keV due to excitation of levels in iron and aluminium. The resultant broad peak is seen at 840 keV.

The peak at 595 keV due to decay of the first excited state of ^{74}Ge has a shoulder on the high energy side from the Compton distribution of the 840 keV γ-ray complex. The shape and magnitude of this distribution can be estimated for analysis of the 595 keV peak from spectra obtained with a ^{22}Na gamma ray source. The peak at 1.22 MeV is the ground state transition from the 2nd level in ^{74}Ge.

The lines at 565 keV and 1.125 MeV can be attributed to decay of the first two levels in ^{76}Ge and that at 1.04 MeV to decay of the first level in ^{70}Ge. The 1.215 MeV level in ^{70}Ge decays almost entirely through the 1.042 MeV level (Alburger [13]) consistent with the fact that the direct transition to the ground state would be $0^+ \rightarrow 0^+$ and therefore highly forbidden by comparison with the cascade decay. Hence the above assignment of the peak at 1.22 MeV to ^{74}Ge rather than ^{70}Ge. A gamma ray of energy 173 keV from the cascade decay could not be identified definitely in the present experiment.

Low intensity peaks at 365 keV and 1.125 MeV are due to levels in the low abundance isotope ^{73}Ge. There is no evidence for any cascade decay leading to a 760 keV gamma ray.

Background peaks due to neutron scattering in copper are present at 968 keV, 1.115 and 1.330 MeV and unidentified peaks at 145, 542(?), 982 keV and 1.295 MeV.

3. Results and discussion

The excitation functions of gamma rays with energies of 365, 565, 595, 695 keV (electron transition) and 1.04 MeV have been plotted in figures 4-8. The neutron energy spread is approximately ± 50 keV. The shapes of the curves were obtained by dividing the yields in the gamma ray peaks after subtraction of background (obtained by visual interpolation) by the neutron flux, corrected as described in 2.2.

To obtain absolute values of the cross sections requires further a knowledge of the sensitive volume of the germanium counter and of the efficiency for detection of internally-produced gamma rays. Because of the difficulty of obtaining these quantities the curves were normalized to the (n,n') cross sections of Smith [3] obtained by detection of the scattered neutrons. These measurements give the combined cross section for exciting the 565 and 595 keV levels between 1.0 and 1.5 MeV neutron energy. The value taken for the normalization was 0.36 b at 1.0 MeV. The only additional information required is the variation of "total absorbtion" efficiency with gamma ray energy in germanium and this was obtained from the photoelectric absorbtion cross sections tabulated by Chapman [14] and the ratio of total absorbtion to primary photoelectric absorbtion, calculated by Wainio and Knoll [15]. The normalization can then be extended to all the gamma rays of interest by the use of this total absorbtion efficiency curve.

Since the 695 keV peak is due to internal conversion electrons the above method of normalization is not applicable. The efficiency for electron detection is essentially 100% so that a calculation can be made, assuming the sensitive volume of the detector to be equal to the lithium-drift depth, to give an approximate value of the cross section. However the value obtained is only one fifth of that calculated by assuming the efficiency for the 595 keV gamma ray to be that measured by Ewan and Taverndale [16] using comparable size crystals and standardized gamma ray sources. In this calculation the efficiency value is used to relate the yield of the 695 keV peak to that of the previously normalized 595 keV peak. The discrepancy would disappear if the sensitive depth of the detector were changed from 6 to 3 mm in the calculations. The value of 6 mm was that observed by copper staining following the initial lithium drift, but subsequent displacement of the lithium could possibly have occurred during various servicing operations at room temperature. A value of 3 mm for the sensitive depth leads to a cross section of 100 mb for excitation of the 695 keV level, a value consistent with the rough figure of 80 mb deduced by Chasman et al [1] for 1.22 MeV neutrons. However in view of the above discrepancy the gamma ray yield curve in figure 7 is given in arbitrary units. It should be noted that the discrepancy in no way affects the normalization of the remaining cross section curves.

The cross sections obtained can be directly equated to (n,n') cross sections except where cascade gamma rays occur. This applies for each of the curves shown up to at least 1.1 MeV above which cascades may occur when the second or higher level becomes excited. The 835 keV second excited state in ^{72}Ge has essentially no decay through the 700 keV level (Landolt-Bornstein [11]).

The error in the shape of the curves is estimated to be 15% except for the 365 keV curve (40%) for which there was low statistical accuracy on the γ-ray counts. The main contributions to the error comes from neutron flux determination (10%) and γ-ray yield determination (2 - 10%). The absolute accuracy is difficult to estimate but a figure of 25% has been assigned except for the 695 keV decay which is discussed above.

Optical model calculations have been performed for comparison with the data using the theory of Hauser and Feshbach [4]. These were done for the four most abundant isotopes and lead to (n,n') cross sections to each level in the nucleus. The programme used for the calculations was that of Wilmore [6] which uses a Saxon-Woods real potential and Saxon-Woods derivative for the imaginary potential. Parameters used for the potential were the local equivalents for the non-local optical potential parameters calculated by Wilmore [17].

The results of the calculations are plotted as dotted lines in figures 5-8. The magnitudes of the peak cross sections agree with the experimental values within ~ 30% except for the 1.04 MeV level for which the theory is high by a factor of 2.8. The theoretical curves shown have been multiplied by the factors given on the graphs to enable the shapes of the excitation functions to be compared especially near to threshold. It is seen that in each case the theoretical curves rise somewhat more steeply than the experimental ones. The neutron energy spread (± 50 keV) in the measurements has been shown by calculation to make a negligible contribution to the slope of the observed excitation functions. Moldauer [5] has pointed out that close to reaction thresholds, where there are very few channels open, width fluctuations and correlations of levels in the compound nucleus can modify the simple Hauser-Feshbach idea of the reaction. Hence the calculations were repeated using the programme of Wilmore [6] incorporating a level width fluctuation factor calculated from the Porter-Thomas [18] distribution of levels. However the results, plotted as dashed curves in figures 5-8 and again adjusted in magnitude, showed only a marginal decrease in slope close to threshold.

It is possible that a more sophisticated calculation taking account of correlations amongst the compound nuclear levels may produce better agreement in the threshold region. It is also probable that the inflexion in the excitation function for the 695 keV gamma ray near to 1 MeV is due to compound nuclear level fluctuations since there is no evidence for level structure in the target nucleus at this energy.

Acknowledgments

The author is indebted to Dr. A. B. Smith, of Argonne National Laboratory, USA, for undertaking the neutron scattering measurements and supplying the data necessary for normalization. Also to Mr. A. Muggleton of A.W.R.E. for fabricating the germanium detector used in the experiments.

REFERENCES

[1] CHASMAN, C., JONES, K. W., RISTINEN, R. A., Nucl. Instr. and Methods 37 (1965) 1.

[2] MALIK, S. S., MANDEVILLE, C. E., NATH, N., ROTHMAN, M. A., VAN PATTER, E. M., Bull. Am. Phys. Soc. II 4 4 (1959) 259.

[3] SMITH, A. B., private communication.

[4] HAUSER, W., FESHBACH, H., Phys. Rev. 87 (1952) 366.

[5] MOLDAUER, P., Phys. Rev. 123 (1961) 968.

[6] WILMORE, D., UKAEA Rep. AERE-R5053 (1966)

[7] HANSON, A. O., McKIBBEN, J. L., Phys. Rev. 72 (1947) 673.

[8] WHITE, P. H., Journal Nucl. En. A/B 19 (1965) 325.

[9] STEHN, J. R., GOLDBERG, M. D., WIENER-CHASMAN, R., MUGHABGHAB, S. F., MAGURNO, B. A., MAY, V. M., Neutron Cross sections USAEC Report BNL 325, Second Edition, Supplement 2 (1965).

[10] WHITE, P. H., private communication.

[11] LANDOLT-BORNSTEIN, Energy levels of Nuclei, Ed. Hellwege K. H., Springer-Verlag, Berlin (1961).

[12] VAN PATTER, D. M., RIKMENSPOEL, R., TREHAN, P. N., Nuc. Phys. 27 (1961) 467.

[13] ALBURGER, D. E., Phys. Rev. 109 (1958) 1222.

[14] CHAPMAN, G. T., USAEC Report ORNL-TM 1237 (1966).

[15] WAINIO, K. M., Knoll, G. F., Nucl. Instr. and Methods, (In Press).

[16] EWAN, G. R., TAVENDALE, A. J., Can. J. Phys. 42 (1964) 2286.

[17] WILMORE, D., UKAEA Report AERE-R4649 (1966).

[18] PORTER, C. E., THOMAS, R. G., Phys. Rev. 104 (1956) 483.

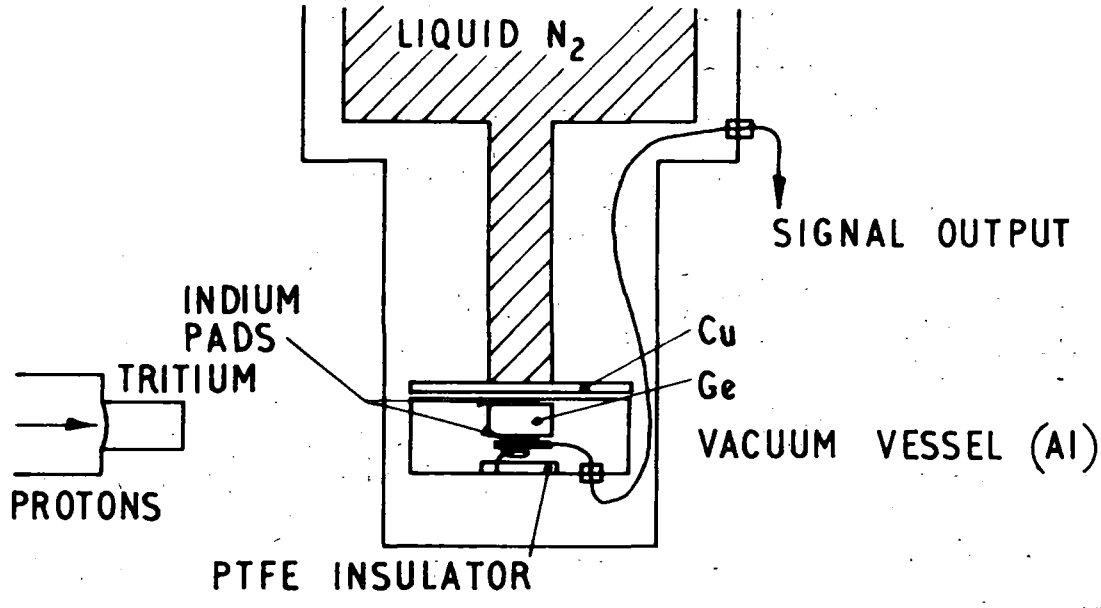

FIGURE 1. EXPERIMENTAL ARRANGEMENT

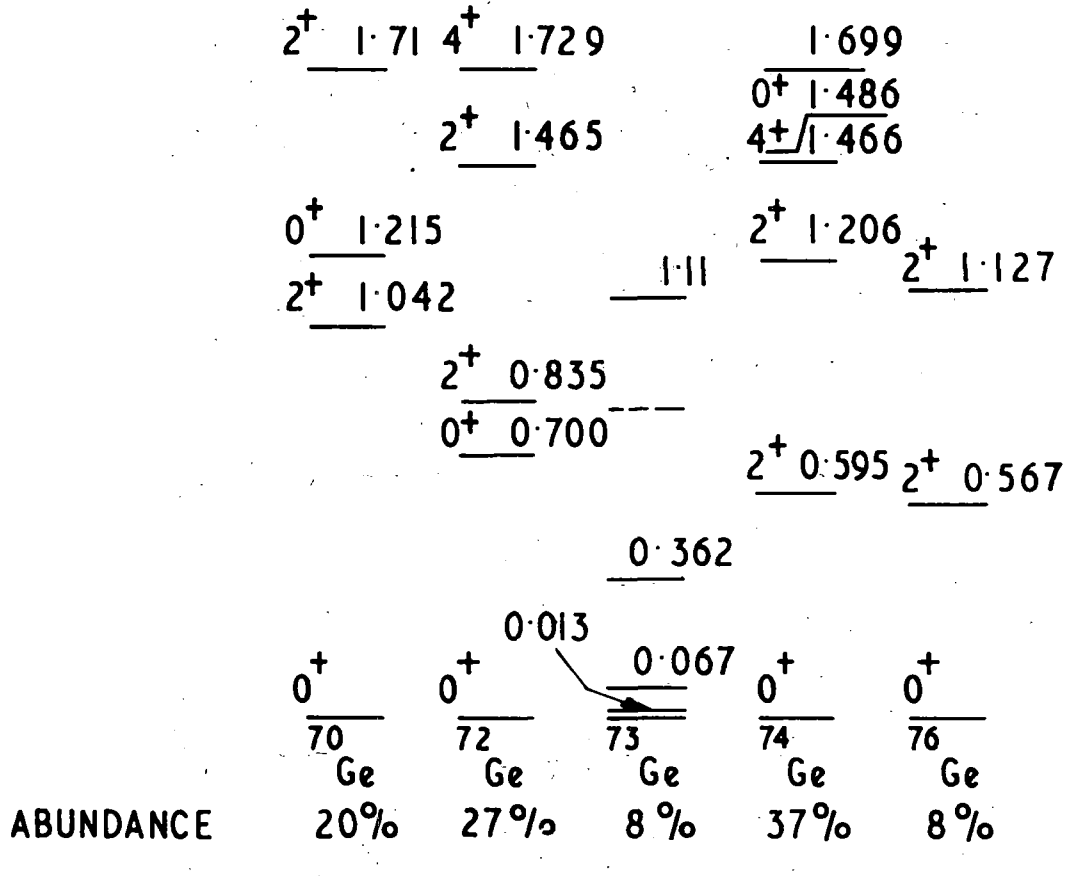

FIGURE 2. KNOWN ENERGY LEVELS OF GERMANIUM ISOTOPES

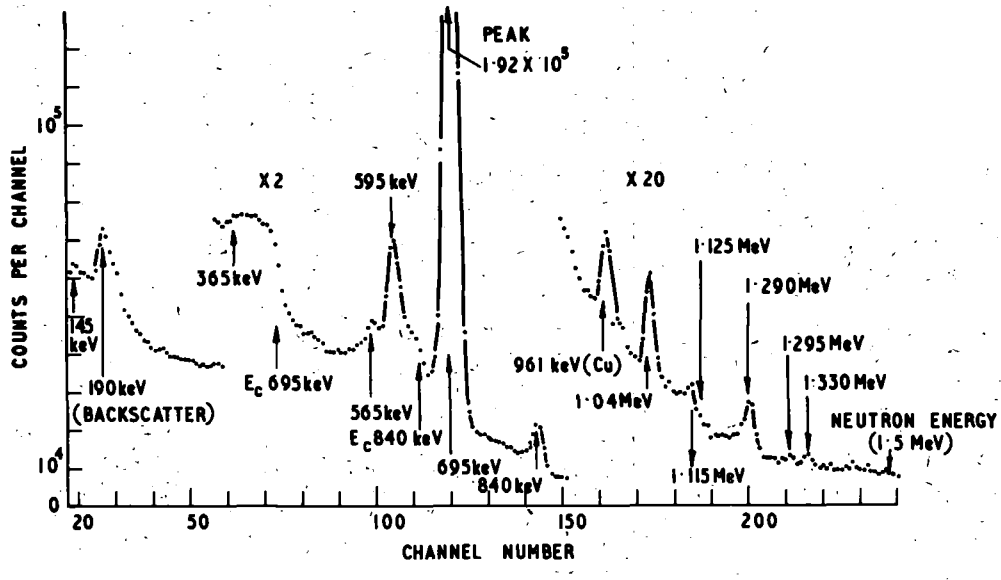

FIGURE 3. GAMMA RAY SPECTRUM FROM 1·5 MeV NEUTRON IRRADIATION

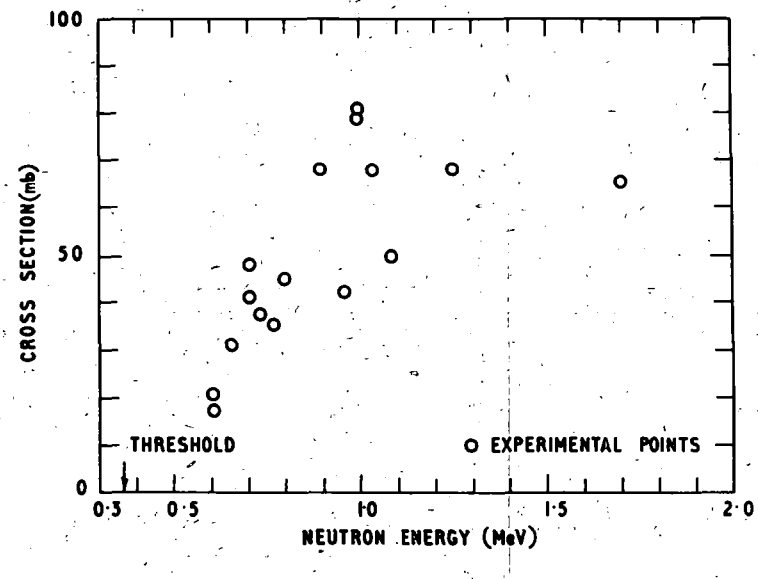

FIGURE 4. CROSS SECTION FOR EXCITATION OF 365keV LEVEL IN Ge-73

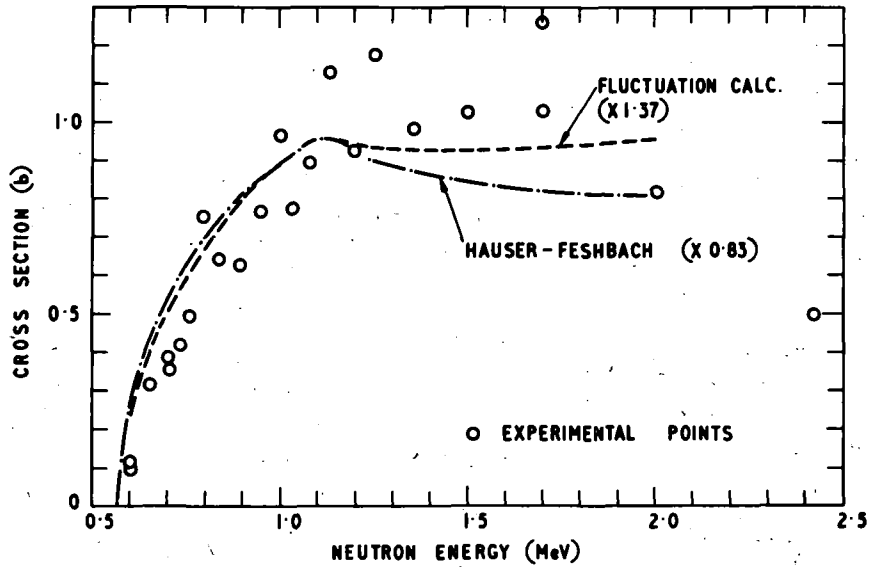

FIGURE 5. CROSS SECTION FOR EXCITATION OF 565keV LEVEL IN Ge-76

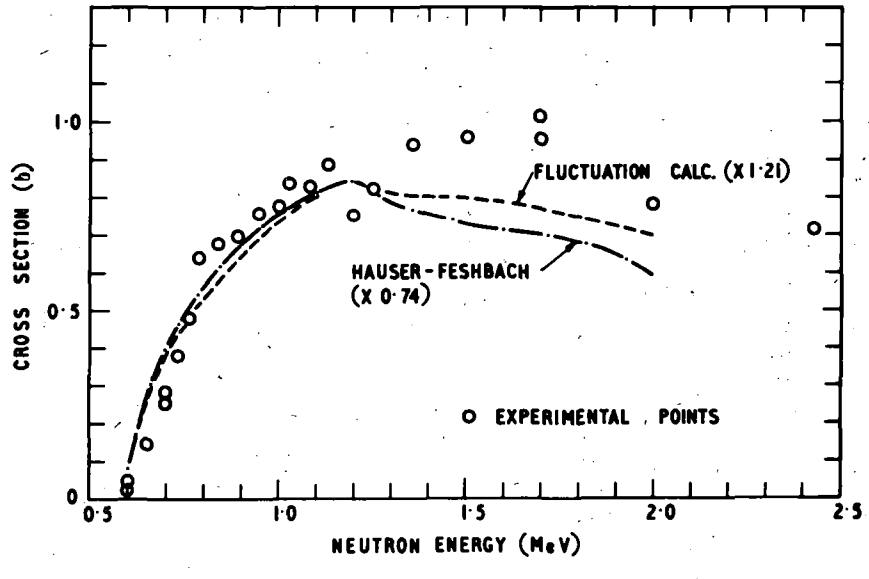

FIGURE 6. CROSS SECTION FOR EXCITATION OF 595keV LEVEL IN Ge-74

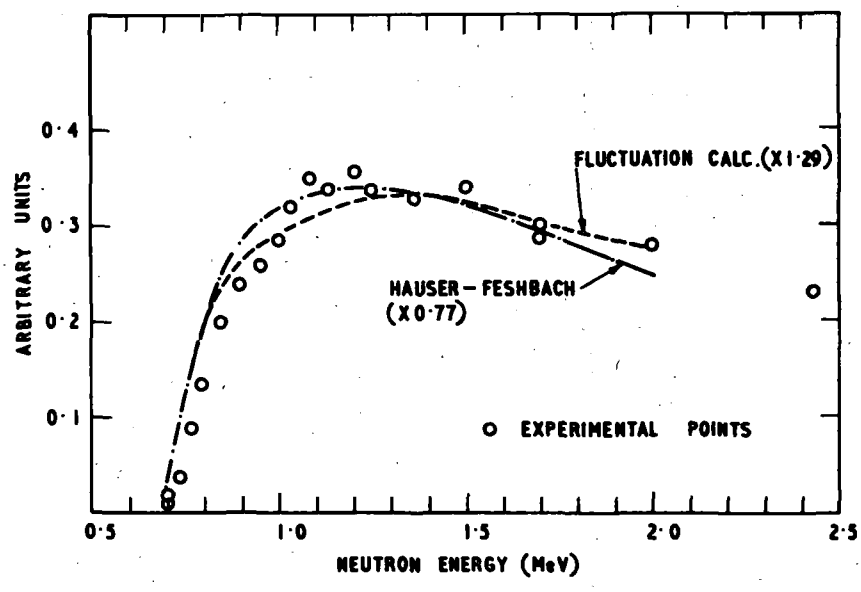

FIGURE 7. CROSS SECTION FOR EXCITATION OF 695keV LEVEL IN Ge-72

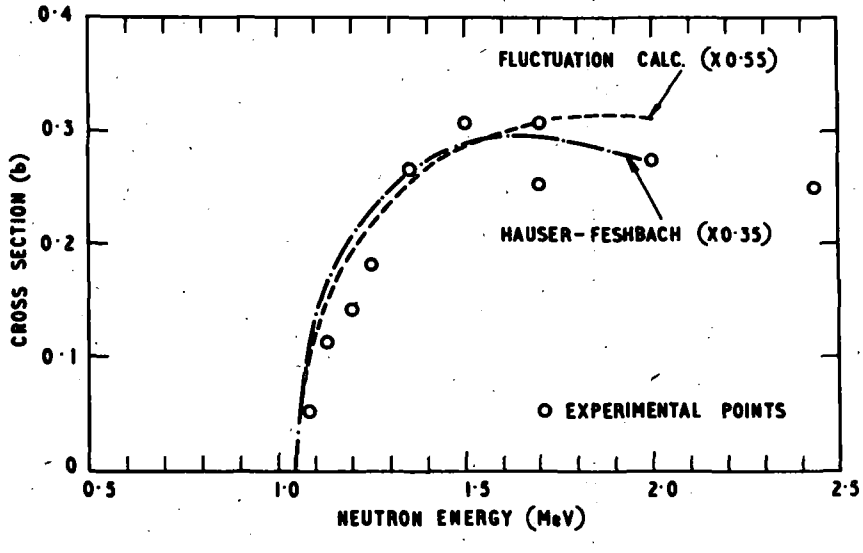

FIGURE 8. CROSS SECTION FOR EXCITATION OF 1·04 MeV LEVEL IN Ge-70

CN-23/64

DEPENDANCE DE LA FONCTION DENSITE S_o SUIVANT LA VALEUR DU SPIN.

J. JULIEN, S. DE BARROS*, P.L. CHEVILLON, V.D. HUYNH,
J. MORGENSTERN, F. NETTER et C. SAMOUR.

Centre d'Etudes Nucléaires de Saclay, France.

I - INTRODUCTION

La très bonne résolution obtenue à l'accélérateur linéaire de Saclay pour l'étude par la méthode du temps de vol des réactions nucléaires induites par les neutrons de résonance, a permis d'accroître le domaine d'énergie exploré, et d'analyser plusieurs dizaines

---

* Centre Brésilien des Recherches Physiques, Rio de Janeiro.

de résonances pour chaque élément étudié. Le spin a pu être donné pour un grand nombre de ces résonances (surtout pour les plus larges d'entre elles) par des méthodes que nous citons plus bas. On a pu faire une étude sur la dépendance de la fonction densité S_o suivant la valeur du spin pour les résonances induites par des neutrons "s" (de moment orbital $\ell = 0$).

II - ANALYSE DES EXPERIENCES

Pour trouver le spin de la résonance, nous avons utilisé trois méthodes :

Soient E_λ l'énergie d'une résonance de spin J, g_J le facteur statistique correspondant, $\Gamma_{n\lambda}$ sa largeur de diffusion et Γ_λ sa largeur totale.

a) La première méthode utilise uniquement une mesure de transmission. En effet, de cette mesure, on obtient la valeur de Γ_λ et de $g_J \Gamma_{n\lambda}$. Or si I est le spin du noyau cible, le spin J du noyau composé est égal soit à $J + = I + \frac{1}{2}$ soit à $J - = I - \frac{1}{2}$.

Donc pour une valeur de $g_J \Gamma_{n\lambda}$, il y a 2 possibilités pour $\Gamma_{n\lambda}$:

$$\text{soit } \Gamma^+_{n\lambda} = \frac{(g_J \Gamma_{n\lambda})}{g_+} \text{ , soit } \Gamma^-_{n\lambda} = \frac{(g_J \Gamma_{n\lambda})}{g_-}$$

Pour des résonances suffisamment larges, on peut avoir $\Gamma^-_{n\lambda} > \Gamma_\lambda$ ce qui exclut dans ce cas le spin $J = I - \frac{1}{2}$. On peut aussi avoir

$\Gamma^{+}_{n\lambda} \ll \Gamma_{\lambda}$ ce qui dans ce cas conduirait à une valeur exagérément grande de la largeur de radiation $\Gamma_{\sigma\lambda}$, ce qui permet d'exclure le spin $J = I + \frac{1}{2}$.

b) Une seconde méthode utilise aussi uniquement une mesure de transmission. On utilise le fait que pour des résonances de même spin, ce sont les amplitudes de diffusion correspondant aux différentes résonances qui s'ajoutent, tandis que pour des résonances de spins différents, ce sont les sections efficaces qui s'ajoutent. La formule de Bethe, par exemple, qui donne la section efficace de diffusion, illustre cela. On a :

$$\sigma_d = \pi \lambda\!\!\!^{-2} \sum_J g_J \left| \exp(2ikR')-1 + \sum_\lambda \frac{i\,\Gamma_{n\lambda}}{E-E_\lambda + \frac{i}{2}\Gamma_\lambda} \right|^2_J$$

On voit que les résonances de même spin présentent des termes d'interférence et donc, si l'on connaît le spin d'une résonance, on peut obtenir le spin de certaines autres.

Cette méthode a été employée dans un certain nombre de cas. Les figures 1 et 2 présentent une application de cette méthode.

c) Une troisième méthode, utilise une mesure de section efficace totale de capture en plus d'une mesure de section efficace totale. On obtient ainsi la valeur du rapport $\frac{\Gamma_{\sigma\lambda}}{\Gamma_\lambda} = \frac{\Gamma_\lambda - \Gamma_{n\lambda}}{\Gamma_\lambda}$ et on

peut ainsi choisir entre les deux valeurs $\Gamma^-_{n\lambda}$ et $\Gamma^+_{n\lambda}$ fournies par l'expérience de transmission. La figure 3 donne une illustration de cette méthode qui nous a permis d'attribuer le spin 2 à la résonance à 60 eV de ^{197}Au.

III - RESULTATS.

Les résultats obtenus sont représentés dans la table I qui donne pour chaque noyau étudié, le nombre de résonances détectées et le nombre de résonances attribuées à chaque état de spin.

a) Noyaux cible de spin $I = \frac{1}{2}$.

On ne trouve pas de variation de la fonction densité avec le spin. Une exception pour ^{77}Se. Là on trouve :

$$S_o(J=0) = 7\ S_o(J=1)$$

mais le nombre de résonances analysées est faible pour cet élément, toutefois ce rapport 7 est difficilement explicable pour un simple accident statistique.

b) Noyaux cible de spin I = 3/2.

Pour ces noyaux on trouve $S_o(J=2) \sim 2\ S_o(J=1)$. Le nombre de noyaux et de résonances étudiées écarte pour un bon nombre de ces noyaux l'hypothèse d'un accident statistique.

L'espacement moyen entre résonances de même spin est compatible avec une loi en $(2J+1)^{-1}$, ce qui montre que la différence des valeurs des fonctions densité n'est pas due à un manque de niveaux J=1.

c) Noyaux cible de spin I = 5/2.

Pour ^{55}Mn, on ne trouve pas de variation de S_o. Pour ^{141}Pr, on trouve $S_o(J=3) = 1,6\ S_o(J=2)$.

Ici la variation de S_o est due à ce que l'on n'attribue le spin 2 à aucune résonance entre 1 et 3,5 keV. Si on admet que les largeurs de diffusion obéissent à une loi en χ^2 à un degré de liberté et que les espacements obéissent à une loi de Wigner, ce manque de niveaux intenses J=2 est peu probable, toutefois l'hypothèse d'un accident statistique ne peut être écartée. Nous comptons poursuivre l'étude à plus haute énergie pour éclaircir ce point.

d) Noyaux cible I = 7/2.

Dans le cas de ^{59}Co, on trouve :

$S_o(J=3) = 1,8\ S_o(J=4)$ pour $0 < E < 80$ keV mais une attribution préliminaire des spins entre 80 et 120 keV diminue ce rapport et l'on trouve ;

$S_o(J=3) = 1,25\ S_o(J=4)$ pour $0 < E < 120$ keV

IV - <u>CONCLUSION</u>

La variation de la fonction densité suivant le spin ne paraît établie, pour le moment, que dans le cas des noyaux cible de spin I = 3/2.

REFERENCES

(1) J.JULIEN et al., Phys.Letters, 1962, 3, 67

(2) J.JULIEN et al., Phys.Letters, 1964, 10, 86

(3) G.LE POITTEVIN et al., Nucl.Phys., 1965, 70, 497

(4) J.JULIEN et al., Nucl.Phys., 1965, 66, 433

(5) J.MORGENSTERN et al., Nucl.Phys., 1965, 62, 529

(6) J.JULIEN et al., Nucl.Phys., 1966, 76, 432

+ points expérimentaux
• points calculés

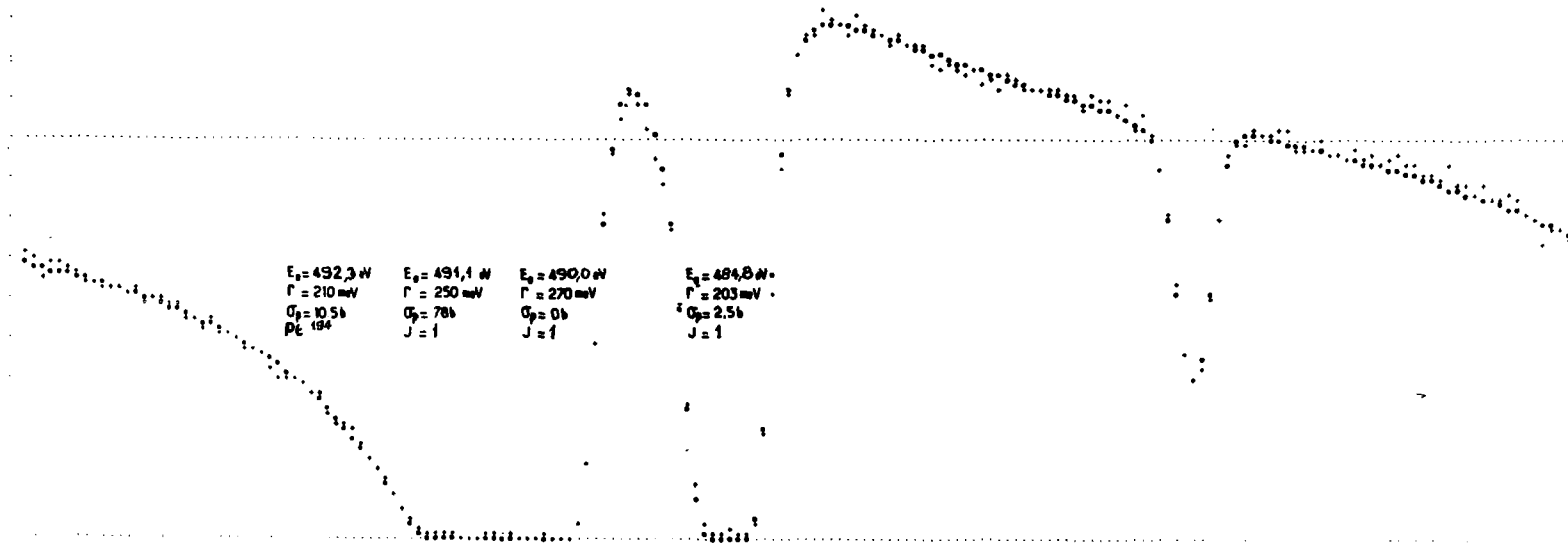

Fig. 1

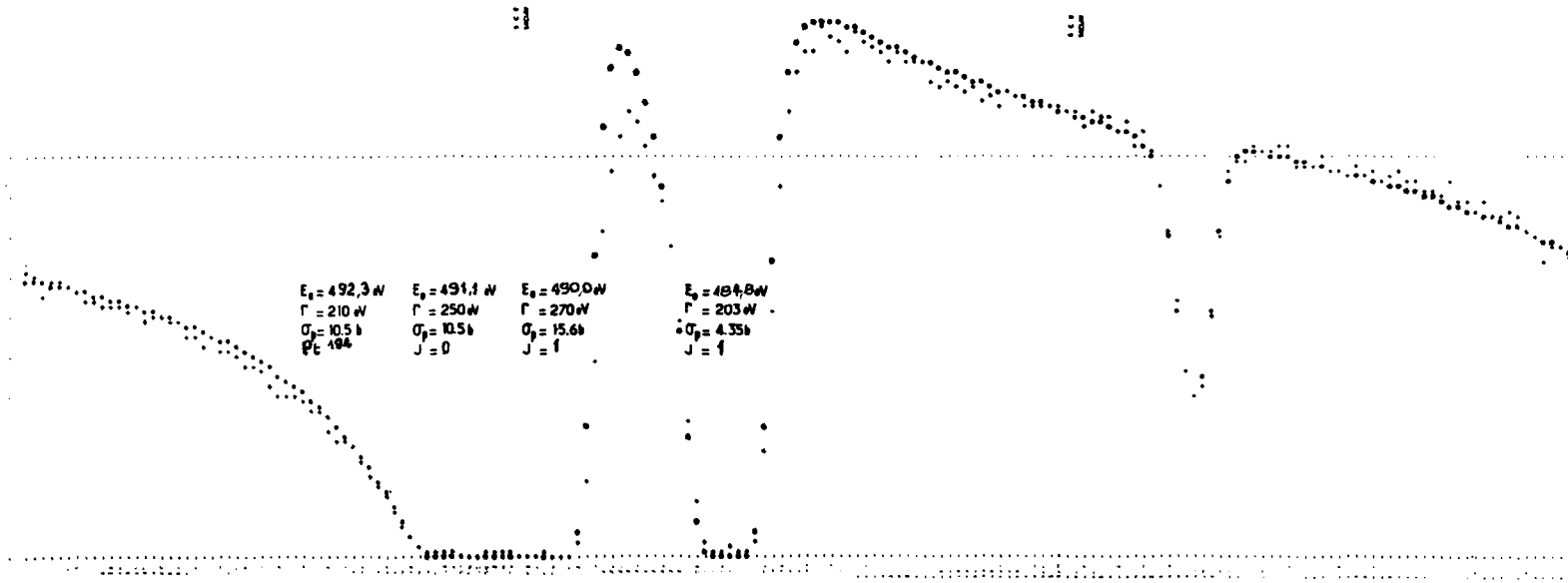

Fig. 2

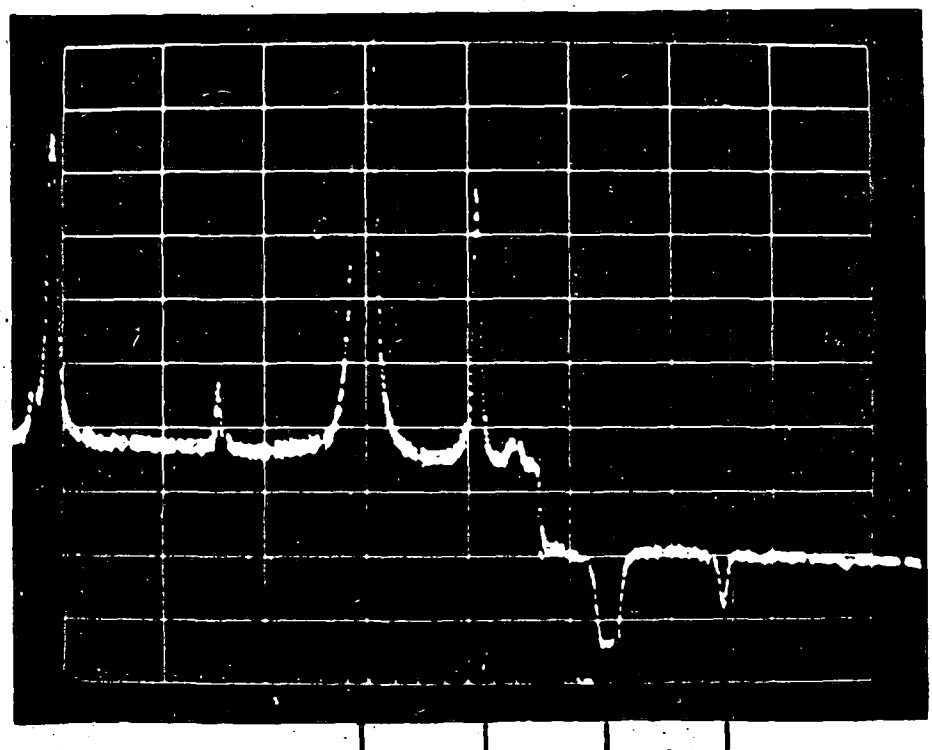

Pt Au Pt Au

65eV 60eV 65eV 60eV

Fig. 3

Table I

Target Nucleus	Spins	Number of detected and assigned levels	Energy range investigated	S_o values 10^{-4} $eV^{-\frac{1}{2}}$	Ratio r	Probability to find : $S_{o\,J'} \geqslant rS_{o\,J}$
^{77}Se	$\frac{1}{2}$	10 $\begin{matrix}3\\7\end{matrix}$ $\begin{matrix}J=0\\J=1\end{matrix}$	0 2000 eV	$\begin{matrix}2.1\\.3\end{matrix}$	7	~ 0.03
$^{107,109}Ag$	$\frac{1}{2}$	109 $\begin{matrix}26\\10\end{matrix}$ $\begin{matrix}J=0\\J=1\end{matrix}$	0 700 eV	$\begin{matrix}.63\\.62\end{matrix}$		
^{169}Tm	$\frac{1}{2}$	92 $\begin{matrix}16\\49\end{matrix}$ $\begin{matrix}J=0\\J=1\end{matrix}$	0 800 eV	$\begin{matrix}1.5\\1.5\end{matrix}$		
^{195}Pt	$\frac{1}{2}$	40 $\begin{matrix}9\\27\end{matrix}$ $\begin{matrix}J=0\\J=1\end{matrix}$	0 800 eV	$\begin{matrix}1.7\\1.8\end{matrix}$		
$^{63,65}Cu$	$\frac{3}{2}$	36 $\begin{matrix}8\\15\end{matrix}$ $\begin{matrix}J=1\\J=2\end{matrix}$	0 15000 eV	$\begin{matrix}1.3\\2.3\end{matrix}$	1.75	
^{75}As	$\frac{3}{2}$	55 $\begin{matrix}12\\16\end{matrix}$ $\begin{matrix}J=1\\J=2\end{matrix}$	0 4000 eV	$\begin{matrix}1\\2.5\end{matrix}$	2.5	~ 0.01
$^{79,81}Br$	$\frac{3}{2}$	80 $\begin{matrix}7\\16\end{matrix}$ $\begin{matrix}J=1\\J=2\end{matrix}$	0 2000 eV	$\begin{matrix}0.95\\1.9\end{matrix}$	2	0.07 for each isotope
^{135}Ba	$\frac{3}{2}$	23 $\begin{matrix}6\\13\end{matrix}$ $\begin{matrix}J=1\\J=2\end{matrix}$	0 1000 eV	$\begin{matrix}.47\\1.34\end{matrix}$	2.8	~0.06
^{197}Au	$\frac{3}{2}$	64 $\begin{matrix}12\\26\end{matrix}$ $\begin{matrix}J=1\\J=2\end{matrix}$	0 1000 eV	$\begin{matrix}1.17\\2.46\end{matrix}$	2.1	~0.02
^{141}Pr	$\frac{5}{2}$	15 $\begin{matrix}4\\5\end{matrix}$ $\begin{matrix}J=2\\J=3\end{matrix}$	0 1000 eV	$\begin{matrix}3.7\\3.8\end{matrix}$	1.6	
		80 $\begin{matrix}3\\12\end{matrix}$ $\begin{matrix}J=2\\J=3\end{matrix}$	1000 5700 eV	$\begin{matrix}0.9\\2.0\end{matrix}$		
^{55}Mn		56 $\begin{matrix}9\\10\end{matrix}$ $\begin{matrix}J=2\\J=3\end{matrix}$	0 80000 eV	$\begin{matrix}3.8\\4.4\end{matrix}$	1.1	
		32 $\begin{matrix}7\\12\end{matrix}$ $\begin{matrix}J=3\\J=4\end{matrix}$	0 40000 eV	$\begin{matrix}4.7\\2.9\end{matrix}$	1.6	
^{59}Co	$\frac{7}{2}$	29 $\begin{matrix}7\\5\end{matrix}$ $\begin{matrix}J=3\\J=4\end{matrix}$	40000 80000 eV	$\begin{matrix}2.6\\1.45\end{matrix}$	1.8	
		32 $\begin{matrix}12\\15\end{matrix}$ $\begin{matrix}J=3\\J=4\end{matrix}$	80000 120000 eV	$\begin{matrix}5.5\\5.9\end{matrix}$	0.93	

For each presented nucleus the quantity $\sum g\,\Gamma_n^o$ for both spin assignments is equal to or greater than 90 percent the quantity $\sum g\,\Gamma_n^o$ for all the detected levels. Calculated probability assumes that the neutron reduced widths Γ_n^o have a χ^2 distribution with one degree of freedom and that the detected levels obey to the law $(2J+1)^{-1}$.

ETUDE DES SPECTRES DE RAYONNEMENTS GAMMA DE CAPTURE A L'AIDE DE DETECTEURS Ge-Li.

H. JACKSON*, C. SAMOUR, A. BLOCH, J. JULIEN,
C. LOPATA et J. MORGENSTERN
Service de Physique Nucléaire à Basse Energie
Centre d'Etudes Nucléaires de Saclay, France

Depuis plusieurs années une étude systématique des propriétés statistiques des paramètres de résonances, induites par des neutrons lents dans des noyaux moyens et lourds, a été entreprise par la méthode du temps de vol auprès de l'accélérateur linéaire de Saclay. Des expériences de capture radiative ont, dès le début,[1] été associées aux expériences de transmission. Cependant, l'imperfection des détecteurs classiques utilisés (cristaux d'iodure de sodium) limitait l'efficacité de ces mesures dont l'intérêt est pourtant multiple.[2,3] En effet, l'analyse des spectres des rayons gamma, émis lors de la capture des neutrons de résonance, restait limitée, compte tenu de la résolution énergétique de ces spectromètres, aux niveaux excités voisins du niveau fondamental. Elle se heurtait au fait que les niveaux excités de basse énergie sont souvent trop proches pour que la résolution du détecteur permette d'isoler les composantes individuelles d'un spectre complexe. En outre, les rayonnements considérés, correspondant aux transitions vers ces premiers niveaux excités, ont une énergie voisine de l'énergie de liaison d'un neutron ; pour ces énergies, comprises entre 4 et 8 MeV, les pics d'échappement viennent, par leur intense contribu-

---

* En congé de Argonne National Laboratory.

tion, compliquer une situation déjà, pour le moins, confuse. Aussi avions-nous mis en oeuvre à Saclay un ensemble de détection comprenant un cristal NaI central 4" × 6" fonctionnant en coïncidence avec un cristal annulaire,[4] ce qui permettait de résoudre cette dernière difficulté ; mais la résolution demeurait de l'ordre de 300 keV à 8 MeV et les spectres devaient être analysés par une méthode de moindres carrés.[4]

Jusqu'à ces dernières années, les seules expériences de capture radiative à haute résolution furent effectuées à l'aide de spectromètres utilisant le principe de la diffusion cristalline ou de spectromètres magnétiques.[5] Bien qu'ayant une excellente résolution, ils furent exclusivement utilisés près des réacteurs, où l'on dispose de flux de neutrons très intenses, pour l'étude de la capture radiative de neutrons thermiques. Leur efficacité est beaucoup trop faible pour qu'ils puissent être exploitables près d'un accélérateur linéaire afin d'examiner le domaine des neutrons de résonance.

Le développement récent de la technique de diffusion du lithium dans le silicium[6] et le germanium[7] a permis d'étendre aux rayons gamma l'application des détecteurs à semi-conducteurs, déjà très utilisés pour détecter des particules chargées.[8,9] Les progrès considérables effectués dans le domaine de ces jonctions p-i-n laissèrent entrevoir dès le début des possibilités très séduisantes pour la spectrométrie gamma.[10] Leur excellente résolution et leur efficacité relativement élevée sont leurs qualités essentielles ; celles-ci ont été largement décrites dans la littérature et résumées dans plusieurs articles de synthèse[11] et en font, à l'heure actuelle et certainement pendant de nombreuses années, le détecteur idéal pour l'étude de la structure nucléaire.

Aussi un grand nombre de laboratoires ont-ils porté leurs efforts sur la réalisation de tels détecteurs, en particulier à Chalk-River,[10] Argonne[12] et Strasbourg.[13] La section efficace de l'effet photoélectrique étant proportionnelle à Z^5 et la section efficace du processus de matérialisation à Z^2,[14] le germanium a été très vite préféré au silicium. En contre partie, la faible largeur de la bande interdite du germanium rend nécessaire de refroidir le détecteur à la température de l'azote liquide afin de réduire le bruit.

Les performances des diodes au Ge-Li dépendent pour une large part de la qualité du germanium utilisé. La résolution est fonction de l'effet de "trapping", de la mobilité des porteurs, de l'intensité du champ électrique et des courants de fuite. Afin d'éviter toute condensation et toute contamination de la surface et de diminuer les échanges thermiques, les détecteurs doivent fonctionner sous vide. Deux structures différentes ont été développées, la structure planaire[10-13] et, plus récemment, la structure coaxiale.[15,16]

Nous avons utilisé, à Saclay, une jonction Ge-Li planaire de 6 cm^3 fabriquée par H. Mann au Laboratoire d'Argonne. La profondeur de la zone compensée était de l'ordre de 10 mm. Une tension de 1250 volts était appliquée à ses bornes. Elle était associée à un préamplificateur étudié par Sherman[17] à Argonne. La résolution de l'ensemble était de l'ordre de 5 keV à 1 MeV.

Dans la spectrométrie gamma et pour un tel détecteur, on doit considérer trois régions d'énergie, selon sa réponse.[11] En dessous de 1,5 MeV environ, l'interaction a lieu essentiellement par effet photoélectrique et l'interprétation des spectres reste simple. La figure 1 montre le spectre de ^{60}Co ; les deux pics photoélectriques (1173 et 1333 keV) sont très nettement séparés et les deux fronts

Compton ressortent aisément ; la résolution est de 4,7 keV à 1333 keV, soit environ 20 fois meilleure qu'avec un cristal d'iodure de sodium. Au dessus de 1,5 MeV, le processus de matérialisation devient vite prépondérant. Entre 1,5 et 3 MeV, le pic photoélectrique voit son intensité diminuer et celle du pic de double échappement devenir comparable. La figure 2 représente la réponse de notre détecteur aux rayons gamma de 2754 keV émis par ^{24}Na ; on voit apparaître un pic photoélectrique à 2754 keV, un faible pic à 2754-511 keV et un pic intense à 2754-1022 keV. L'interprétation d'un spectre complexe dans cette gamme d'énergie peut donc devenir délicate. Au dessus de 3 MeV, seul apparaît pratiquement le pic correspondant à l'échappement de deux photons de 511 keV et l'analyse est de nouveau aisée (fig. 4 et 5). Afin d'illustrer l'excellente résolution de ce type de détecteur à haute énergie nous présentons le spectre du fer, obtenu à Argonne par H.E. Jackson avec une diode identique, émis lors de la capture de neutrons thermiques par ^{56}Fe (fig. 3). Les deux transitions, aboutissant l'une à l'état fondamental de ^{57}Fe, l'autre au premier état excité situé 14 keV au dessus du précédent, sont totalement résolues ; la résolution était de l'ordre de 6 keV. A titre de comparaison nous donnons également le spectre obtenu par Groshev et al[18] avec un spectromètre magnétique Compton dont la résolution était de l'ordre de 0,3%. Le détecteur Ge-Li apparaît donc avoir une meilleure résolution. Nous avons entrepris près du réacteur de Saclay, avec un tel détecteur, une étude systématique des spectres thermiques de quelques éléments afin de calculer les intensités des différentes raies. Les figures 4b et 5 montrent deux essais effectués sur le nickel et le cuivre, en prenant 7 keV par canal ; la durée des expériences était de l'ordre d'une heure. Nous pren-

drons 4 keV par canal lors des mesures définitives. On compare en particulier le spectre du nickel obtenu avec notre ancien spectromètre NaI(Tl) à coïncidence (fig. 4a)[4] et une diode Ge-Li (fig. 4b) ; l'amélioration est évidemment spectaculaire.

La figure 6 présente la variation de l'efficacité relative du second pic d'échappement en fonction de l'énergie des rayons gamma obtenus lors de la capture thermique de ^{14}N. Elle est pratiquement constante dans le domaine qui nous intéresse c'est-à-dire entre 5 et 9 MeV. L'efficacité croît d'abord avec l'énergie comme la section efficace du processus de matérialisation puis passe par un maximum très large et décroît aux hautes énergies. Ceci est dû à deux effets.[11] Le plus important est qu'un grand nombre d'électrons s'échappent de la surface du cristal avant de perdre toute leur énergie cinétique ; le second est que ces électrons, ayant une énergie élevée, perdent, en se ralentissant, une certaine quantité d'énergie par émission de rayonnement de freinage, lequel peut ne pas être absorbé par le cristal. Ces deux effets de bord sont évidemment d'autant plus faibles que le détecteur est plus épais et le maximum d'autant plus haut en énergie. Avec une diode ayant une zone intrinsèque de 3,5 mm de profondeur le maximum est situé aux environs de 4 MeV,[11] alors qu'avec la diode utilisée dans notre travail, dont la zone s'étendait sur 10 mm, le maximum se présente aux environs de 8 MeV. L'efficacité de ce type de détecteur est 100 à 1000 fois supérieure à celle d'un spectromètre magnétique. On peut estimer que l'efficacité absolue de notre détecteur est de l'ordre de 0,3 à 0,8% à 8 MeV.

Le détecteur fut placé près de l'accélérateur linéaire de 45 MeV de Saclay, à 29 m de la source de neutrons et à 10 cm du centre du

faisceau et de la cible constituée par du platine naturel. Cette dernière, de 5 mm d'épaisseur, était disposée à 45° par rapport à l'axe du faisceau. La chaîne électronique fut stabilisée à l'aide d'un générateur de haute précision et d'un correcteur de dérive H.V.L. L'ensemble était particulièrement stable durant une semaine. Dans cet intervalle de temps la résolution globale était de 10 keV à 8 MeV. Cependant, le zéro du codeur d'amplitude n'étant pas stabilisé, les variations de la capacité de couplage et des capacités parasites du préamplificateur augmentaient la résolution, pour l'ensemble des données acquises en six semaines, jusqu'à 15 keV à 8 MeV. Afin de remédier à cet inconvénient nous avons depuis effectué l'étude de ^{238}U en stabilisant le spectre d'amplitude en deux points particuliers ; nous n'avons alors noté aucune évolution durant six semaines d'enregistrement. L'énergie des neutrons fut déterminée par l'intermédiaire de leur durée de parcours (méthode du temps de vol). Les événements furent enregistrés sur une chaîne multidimensionnelle Intertechnique fonctionnant en deux dimensions ; 12 digits binaires définissaient l'instant d'arrivée des neutrons sur la cible et 10 l'amplitude des rayonnements gamma émis. Le codeur en temps est du type accordéon HC 25 à largeurs de canaux variables de 50 ns à 1,6 μs,[19] et le codeur amplitude du type CA 25 à 4 Mc. Un circuit, déclenché par le signal de synchronisation de l'accélérateur, bloquait la chaîne électronique pendant un intervalle de temps de 20 μs. Ceci évitait la surcharge des amplificateurs due à la bouffée intense de rayonnements gamma émis instantanément à chaque cycle de l'accélération et permettait d'abaisser

la restitution de la chaîne à 50 μs environ. Dans toute la gamme d'énergie de neutron étudiée, soit de 12 à 700 eV, les pics correspondant aux différents rayons gamma étaient situés dans les mêmes canaux quelle que soit la résonance considérée. Nous avons analysé 22 résonances de spin $J = 1^-$ et 7 résonances de spin $J = 0^-$ du noyau cible ^{195}Pt, 2 résonances du noyau cible ^{192}Pt (situées à 46 et 53 eV) et une résonance du noyau cible ^{198}Pt (située à 96 eV).

Une expérience de capture radiative présente d'une façon générale de multiples intérêts. Elle offre, en effet, d'une façon directe, la possibilité d'une attribution isotopique et d'une détermination du spin des résonances d'un grand nombre de noyaux. L'examen détaillé des spectres des rayons gamma de capture permet surtout de mieux comprendre certains points du mécanisme de ce processus complexe, dont la loi de fluctuation, de résonance en résonance de même spin, des largeurs radiatives partielles n'est pas l'un des moindres aspects.[20,21] Le nombre de résonances de spin $J = 1^-$ de ^{195}Pt a permis de calculer une valeur absolue des intensités de cinq transitions $1^- \rightarrow 0^+$ ou $1^- \rightarrow 2^+$ d'énergies 7920, 7520, 7231, 6777 et 6516 keV aboutissant successivement à l'état fondamental de ^{196}Pt et aux états excités situés à 358, 689, 1143 et 1404 keV. Il suffit pour cela de déterminer l'intensité absolue pour une transition bien déterminée d'une résonance donnée, les intensités relatives étant toutes proportionnelles aux intensités absolues avec le même facteur de proportionnalité. Nous nous sommes normalisés sur la valeur absolue trouvée par Carpenter[22] pour la transition vers l'état fondamental de la résonance à 11,9 eV. Cette dernière se trouve en effet bien isolée et sa section efficace de capture est élevée ; les données ont donc une précision statistique

satisfaisante. D'autre part, la raie aboutissant à l'état fondamental est très intense et ressort nettement des deux raies voisines qui sont très faibles. Carpenter obtient 0,048 photon/capture avec une erreur de ± 30%. A partir de la valeur de Γ_γ trouvée à Saclay pour cette résonance (Γ_γ = 122 ± 7 meV) on a finalement obtenu les résultats présentés sur le tableau I. Nous avons comparé ceux-ci avec l'estimation de Weisskopf basée sur le modèle à une particule[23] et valable pour les transitions électriques dipolaires, dont la forme numérique s'écrit[2] :

$$\Gamma_{\gamma_i} = 0{,}11\ E_\gamma^3\ A^{2/3}\ \frac{D}{D_o}\ .$$

Dans cette expression E_γ désigne l'énergie de la transition en MeV, A le nombre de masse, D l'espacement des niveaux de capture en MeV. La quantité D_o est prise égale à 15 MeV. Γ_{γ_i} est exprimée en eV. Les valeurs obtenues sont également reportées sur le tableau I. L'accord peut être considéré comme bon étant donné les erreurs expérimentales et le caractère très approximatif de l'estimation.

Une telle expérience est également très riche de renseignements en vue de préciser les schémas de niveaux de plusieurs isotopes du platine. D'une façon générale l'étude des résonances de neutron offre, par rapport aux spectres thermiques, deux avantages précieux. D'abord, on peut obtenir, à partir d'une cible de l'élément naturel, les spectres des différents isotopes. En outre les fluctuations importantes des largeurs radiatives partielles accroissent la sensibilité spectrale lorsque l'on peut disposer, comme c'est notre cas, d'un grand nombre de résonances ; l'absence d'une transition dans une étude de capture thermique ne prouve pas, en effet, l'inexistence de cette transition.

Nous avons ainsi mis en évidence 18 niveaux nouveaux du noyau ^{196}Pt entre 0 et 2840 keV. Ils sont situés à 1143, 1404, 1610, 1683, 1810, 1829, 1858, 1925, 1978, 2077, 2104, 2181, 2240, 2381, 2504, 2585, 2747 et 2834 keV. La figure 7 est très explicite à cet égard. Certains spins ont pu être attribués ; en effet, si une transition est observée à la fois pour une résonance de spin $J = 1^-$ et une résonance de spin $J = 0^-$, le spin du niveau auquel aboutit la transition est nécessairement 1^+ si l'on admet que toutes les transitions qui apparaissent dans ces spectres sont du type E1. Ainsi le spin des niveaux situés à 1810, 1978 et 2181 keV a été attribué. Le fait essentiel est que nous n'ayons pu détecter de rayonnement gamma de 6802 keV et par conséquent, discerner le niveau situé à 1117 keV dont la présence avait été établie auparavent par Ikegami et al[24] ; ces auteurs ont pu lui attribuer le spin 2 et la parité + à l'aide de deux méthodes indépendantes, l'une par une mesure de corrélation angulaire, l'autre par une étude des spectres des électrons de conversion interne. La taille de notre échantillon peut remettre en doute l'existence de cet état. Par contre, nous avons observer un rayon gamma de 6777 keV qui implique la présence d'un état excité à 1143 keV, dont le spin peut être soit 0^+, 1^+ ou 2^+. L'isotope 196 du platine est un noyau sphérique pair-pair, dont on a jusqu'ici[24,25] essayé d'expliquer la structure à l'aide d'un modèle collectif phénoménologique à couplage faible.[26] Dans ce modèle on admet, en première approximation, pour de petites déformations autour de la forme sphérique d'équilibre, que les vibrations sont harmoniques et on se limite aux vibrations quadrupolaires. Les niveaux collectifs sont équidistants et de parité positive. Le modèle prévoit l'existence d'un premier état excité à 1 phonon (spin 2),

puis d'un triplet à 2 phonons (spin 0, 2, 4), un quintuplet à 3 phonons (spin 0, 2, 3, 4, 6) etc... Certains essais antérieurs pour trouver ces multiplets se sont révélés infructueux.[24,25] Cependant nos données suggèrent qu'il est vraisemblablement prématuré de nier leur existence. Il conviendrait par exemple de déterminer les caractères des niveaux à 1143 et 1404 keV.

Le spectre de capture de la résonance à 96 eV de l'isotope ^{198}Pt se trouve dominé par un rayon gamma très intense de 5456 keV. Une raie beaucoup plus faible, ayant une énergie supérieure de 47 keV à la précédente, ressort nettement (fig. 8). Nous avons observé quatre niveaux nouveaux de ^{199}Pt situés à 61, 114, 1126 et 1512 keV. Nous n'avons malheureusement pas d'autres résonances appartenant à cet isotope dans le domaine étudié.

Nous avons enfin analysé deux résonances à 46 et 52 eV de l'isotope ^{192}Pt. Mais seules deux transitions ressortaient, l'une de 6237 keV, l'autre de 6048 keV, qui aboutissent au niveau fondamental de ^{193}Pt et à l'état excité de 189 keV.

Dans le même but, nous avons entrepris l'étude de la capture radiative de ^{238}U, qui avait fait l'objet de plusieurs travaux antérieurs, tant dans le domaine des neutrons thermiques[27,28,29] que dans le domaine des neutrons de résonances.[30,31] Nos données sont en cours d'analyse.

Nous avons discuté, dans cette communication et dans une autre communication à cette conférence,[21] de quelques aspects qui peuvent être atteints par l'étude de la capture radiative des neutrons de résonance grâce aux détecteurs Ge-Li. Il est bon, pour conclure, d'insister sur le fait que l'application de ces diodes à la spectrométrie gamma est étroitement liée à la dimension de leur volume

utile. La structure coaxiale[15,16] permet dès maintenant d'obtenir des volumes sensibles importants, de l'ordre de 50 cm^3 et leur efficacité est comparable à celle d'un cristal NaI de 1,5" × 1". Cela conduit alors à entreprendre des expériences de coïncidences avec deux jonctions et même d'imaginer des mesures de corrélations angulaires, d'autant plus qu'il n'est pas déraisonnable de penser que l'on pourra disposer, dans un proche avenir, de détecteurs de 100 cm^3. Cependant, il faut rappeler que la limitation de ce type de spectromètre pour des rayons gamma de haute énergie reste l'épaisseur de la zone compensée et que la structure coaxiale ne permet pas de l'accroître. Une solution serait d'accoler deux structures planaires ; on pourrait ainsi espérer atteindre une profondeur d'environ 3 cm.[32] Le domaine d'application de ces détecteurs ne se restreint évidemment pas aux rayons gamma de capture de neutrons et ils ont déjà été appliqués avec succès à la détection des rayons X mumésiques.[33-36] On peut également envisager leur emploi dans les réactions photonucléaires.

Tableau I

Valeur absolue des intensités de 5 transitions de $^{195}Pt + n$

Energie transition (keV)	Energie niveau final (keV)	Intensité expérimentale (meV)	Intensité Weisskopf (meV)
7920	0	2,0 ± 1,2	3,4
7562	356	1,2 ± 0,7	3
7231	689	1,4 ± 0,8	2,6
6777	1143	0,7 ± 0,4	2,1
6516	1404	1,1 ± 0,7	1,9

REFERENCES

1. V.-D. HUYNH et al, Compt. Rend. 1959, 248, 2330.
2. G.A. BARTHOLOMEW, Ann. Rev. Nucl. Sci. 1961, 11, 259.
3. J. JULIEN, Neutron time of flight methods, Symp. Saclay, Edité par Spaepen, 1961, p. 139.
4. V.-D. HUYNH et al, Nucl. Instr. Methods 1965, 36, 29.
5. G.A. BARTHOLOMEW et al, Rept. Progr. Phys. 1960, 23, 453.
6. E.M. PELL, J. Appl. Phys. 1960, 31, 291.
7. D.V. FRECK et J. WAKEPEILD, Nature 1962, 193, 669.
8. J.W. MAYER, Electron. Nucl., Paris 1963, p. 129.
9. F.S. GOULDING, I.E.E. Trans. Nucl. Sci. 1964, NS 11, 3, 177.
10. A.J. TAVENDALE et G.T. EWAN, Nucl. Instr. Methods 1963, 26, 183.
11. G.T. EWAN et A.J. TAVENDALE, Can. J. Phys. 1964, 42, 2286.
F.S. GOULDING, UCRL-16 231.
F.S. GOULDING et J. HOLLANDER, Ecole d'Eté, Herceg-Novi 1965 (à paraître).
12. H. MANN, Communication privée.
13. L. STAB et al, Nucl. Instr. Methods 1965, 35, 113.
14. W. HEITLER, The quantum theory of radiation, 3ème édition, Oxford 1960.
15. H.L. MALM et al, Can. J. Phys. 1965, 43, 1173.
16. H.L. MALM et I.L. FOWLER, AECL-2504, 1965.
17. I. SHERMAN, non publié.
18. L.V. GROSHEV et al, Nucl. Phys. 1964, 58, 465.
19. J. THENARD et G. VICTOR, Nucl. Instr. Methods 1964, 26, 45.
20. C.E. PORTER et R.G. THOMAS, Phys. Rev. 1956, 104, 483.

21. C. SAMOUR et al, Cette Conférence.

22. R.T. CARPENTER, ANL-6589, 1962.

23. J.M. BLATT et V.F. WEISSKOPF, Theor. Nucl. Phys., Chap. XII, John Wiley, New York 1963.

24. M. IKEGAMI et al, Nucl. Phys. 1963, 41, 130.

25. P. MUKHERJEE, Nucl. Phys. 1965, 64, 65.

26. A. BOHR, Dan. Mat. Fys. Medd. 1952, 26, n° 14.

27. N.F. FIEBIGER, I.K.F. 1963, 8.

28. B.P.K. MAIER, T.H.M. 1964.

29. R.K. SHELINE et al, LA-DC-7915, 1966.

30. H.E. JACKSON, Phys. Rev. 1964, 134B, 931.

31. V.-D. HUYNH, Thèse, Paris 1965.

32. H. MANN, Communication privée.

33. R.D. ERLICH et al, Phys. Rev. Letters 1966, 16, 425.

34. T.T. BARDIN et al, Phys. Rev. Letters 1966, 16, 429.

35. H.L. ACKER et al, Nucl. Phys. (à paraître).

36. S. NILSSON (à paraître).

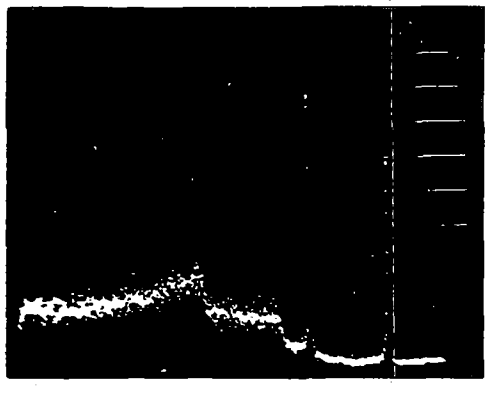

Fig. 1

Spectre d'une source de cobalt. Energies des deux rayons gamma : 1173 et 1333 keV. Détecteur Ge-Li : épaisseur 10 mm, volume utile 6 cm^3.

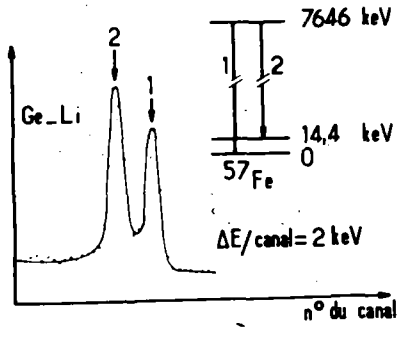

Fig. 3a

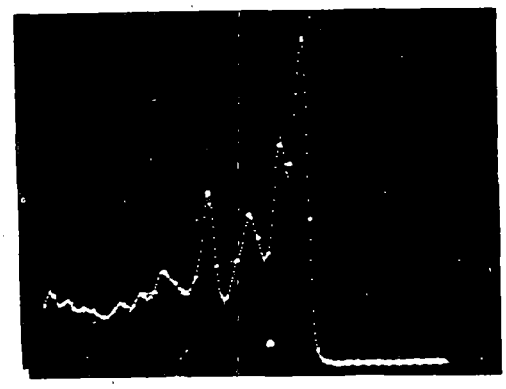

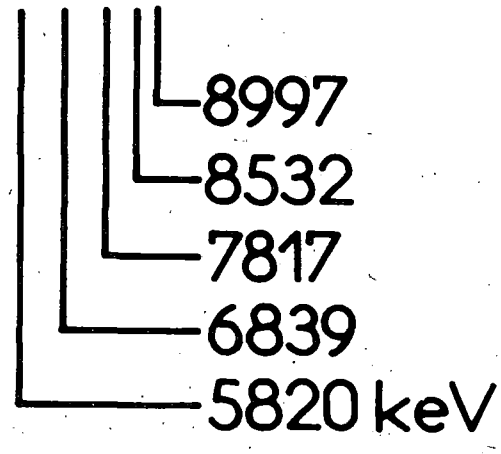

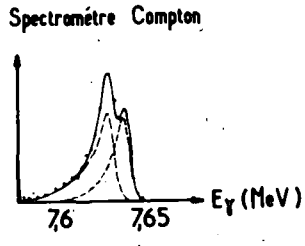

Fig. 3b

Fig. 4a

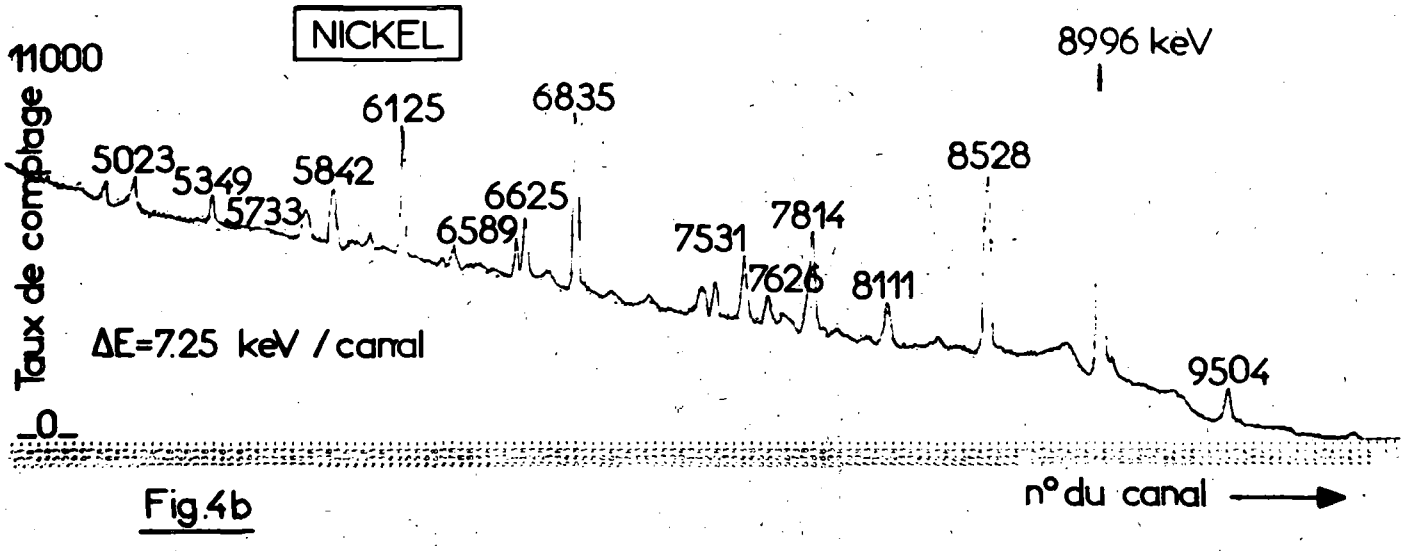

Fig.4b

Fig. 3 - Spectre thermique du fer obtenu avec un détecteur Ge-Li (fig. 3a) et un spectromètre Compton (fig. 3b).

Fig. 4 - Spectre thermique du nickel obtenu à l'aide d'un spectromètre à coïncidence NaI(Tl) (fig. 4a), (spectrométrie effectuée sur (E_γ - 511)keV) et d'un détecteur Ge-Li (fig. 4b).

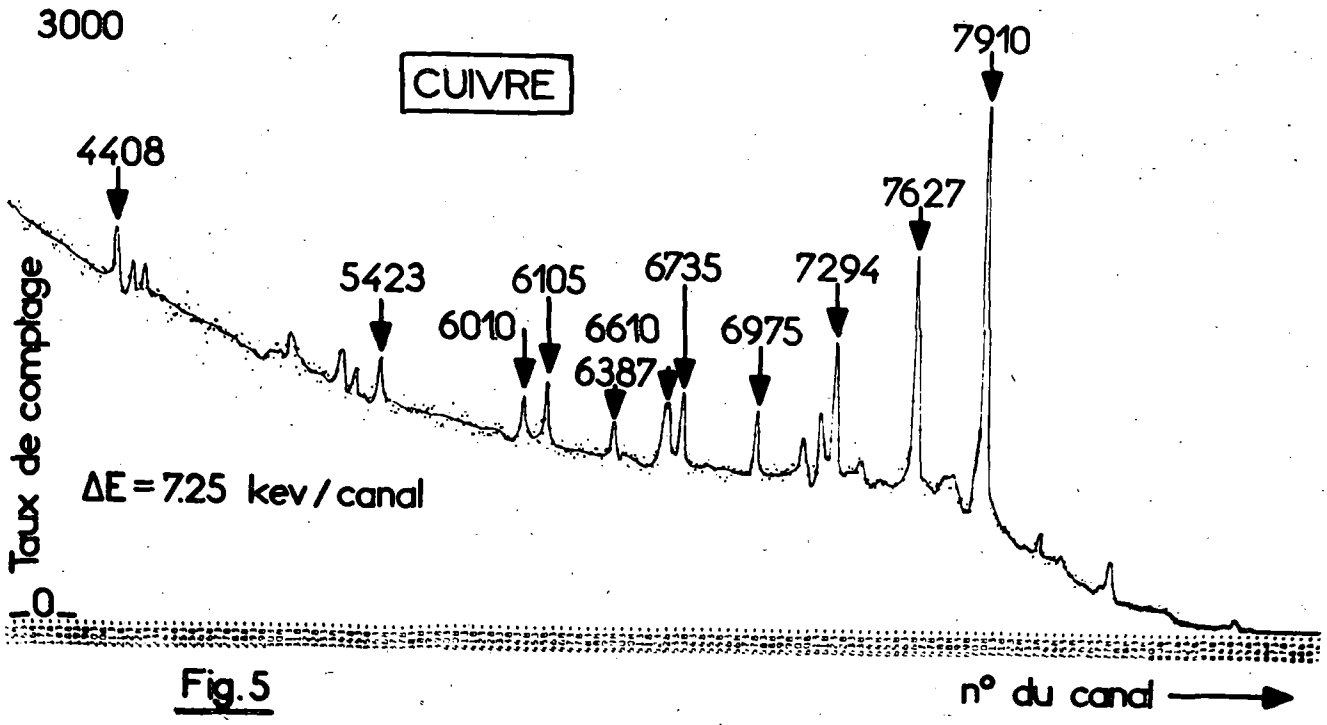

Fig. 5 - Spectre thermique du cuivre. Détecteur Ge-Li.

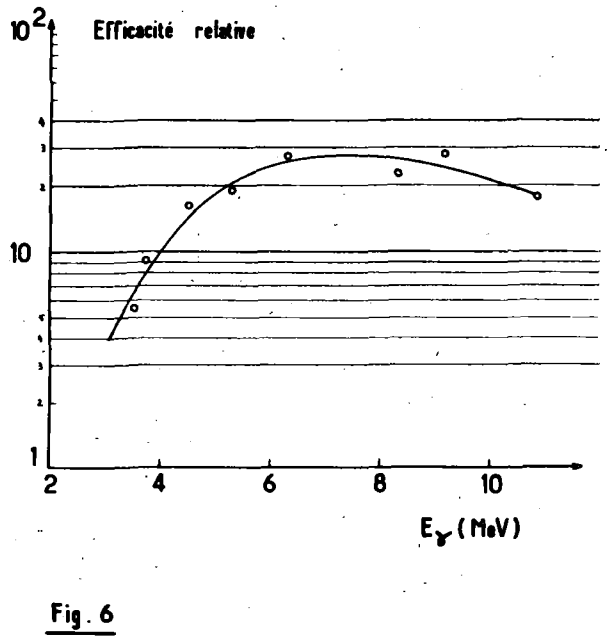

Fig. 6 - Efficacité relative de notre détecteur Ge-Li, épaisseur 10 mm, volume utile 6 cm^3.

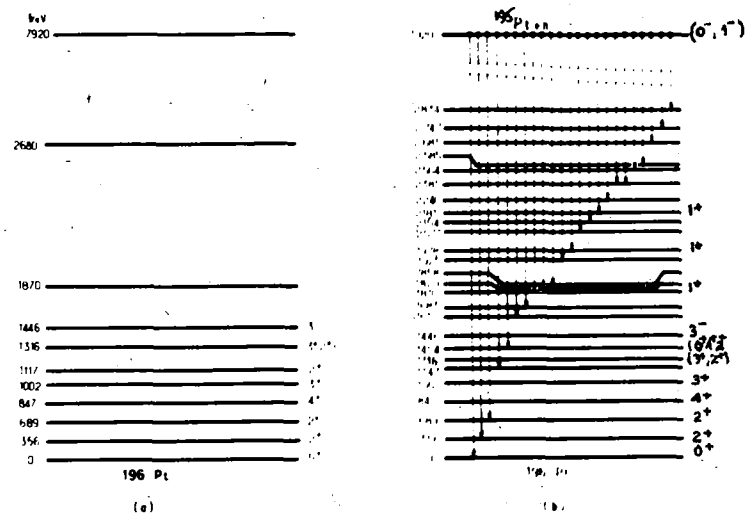

Fig. 7 - Schéma des niveaux excités de ^{196}Pt. On trouve en (a) le schéma tel qu'on le connaissait avant notre expérience et en (b) celui auquel nous conduit notre expérience.

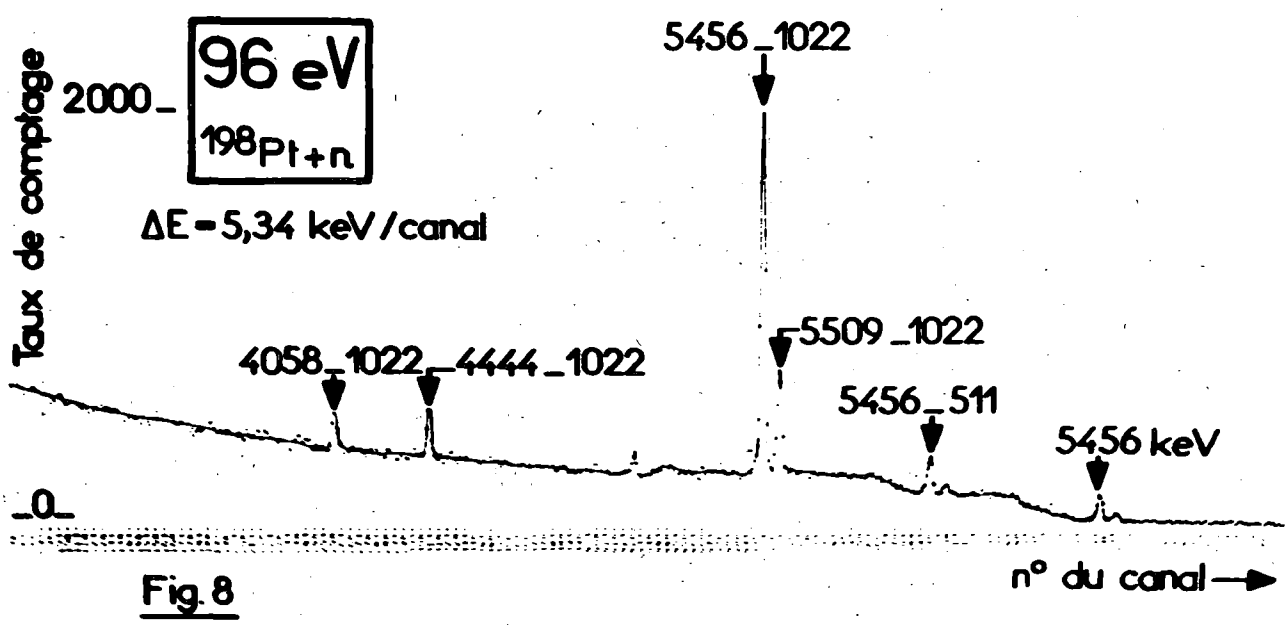

Fig. 8 - Spectre de la résonance à 96 eV de ^{198}Pt + n. La raie la plus intense est située à 5456 keV. Une raie plus faible située à 5509 keV est très nettement séparée. La spectrométrie est effectuée sur (E_γ - 1022)keV.

CN 23/69

SECTIONS EFFICACES TOTALE ET DE FISSION DU ^{237}Np

D. PAYA, H. DERRIEN, A. FUBINI(x), A. MICHAUDON, P. RIBON
Département de Recherche Physique
Section des Mesures Neutroniques Fondamentales
Centre d'Etudes Nucléaires de Saclay - BP n°2 - 91 - Gif-sur-Yvette
FRANCE

Le ^{237}Np est un noyau sur lequel on ne possède que très peu de renseignements. Les mesures les plus récentes sont celles de Slaughter [1] qui ne donne pas les largeurs totales et de Leonard [2] qui a étudié trois résonances de fission à basse énergie pour lesquelles il trouve des largeurs plus de cent fois plus petites que la largeur moyenne prévue par la théorie. Nous avons donc pensé qu'il pourrait être intéressant de l'étudier. Nous avons donc entrepris une série de travaux qui ont porté essentiellement sur la mesure de la section efficace totale et de la section efficace de fission dans la région des résonances. L'Accélérateur Linéaire d'électrons de 45 MeV de Saclay a été utilisé comme source de neutrons pulsée, les énergies de neutrons étant mesurées par la méthode du temps de vol.

1. Conditions expérimentales

1.1. Fission

Par suite de la présence du seuil de fission à 650 keV, on doit s'attendre à ce que la section efficace de fission du ^{237}Np soit très faible dans la région d'énergie qui nous intéresse et qui s'étend de 1 à 300 ev. Il s'agit alors de détecter des fragments de fission qui apparaissent en très petit nombre au milieu d'une activité α assez intense. Afin de pouvoir utiliser une quantité de matière fissile suffisamment importante sans être gênés par les empilements α, nous avons construit un scintillateur gazeux de grandes dimensions.

Le choix du gaz scintillant a posé quelques problèmes : on sait en effet que les résonances du xénon, et en particulier celles à 9,6 et 14,5 ev, perturbent les mesures faites avec le scintillateur. Cependant des comparaisons faites avec différents gaz ou mélanges de gaz nous ont convaincus que ses qualités comme gaz scintillant étaient telles qu'il valait la peine d'accepter ce défaut. Le scintillateur lui-même est constitué de douze cellules séparées optiquement et regardées chacune par un photomultiplicateur 56 UVP à travers une fenêtre de quartz (fig. 1). Chaque cellule contient un dépôt double de neptunium, sous forme d'oxyde, sur

(x) Stagiaire Euratom

un support d'aluminium situé dans un plan perpendiculaire au faisceau de neutrons et passant par l'axe du photomultiplicateur. L'épaisseur de dépôt est de 2 mg/cm^2 sur chaque face, la quantité totale est de 2 g répartis sur deux plans parallèles présentant aux neutrons du faisceau une différence de longueur de vol de 8 cm. En vue de la normalisation, l'une des douze cellules contient un dépôt réalisé à partir d'un mélange de ^{237}Np (99,2%) et de ^{235}U (0,8%).

Après discrimination et codage en temps, les impulsions issues des photomultiplicateurs sont enregistrées sur une bande magnétique de seize pistes dont trois servent à identifier la voie qui a compté et indiquent si le coup enregistré provient du premier plan de fission, du second ou de la cellule de normalisation. Au dépouillement, un programme permet d'ajouter les coups issus du premier plan à ceux issus du deuxième en tenant compte de la différence de distance de vol qui existe entre eux. La voie de normalisation dans laquelle se superposent les résonances du neptunium et de l'uranium est traitée séparément.

La forme du spectre de neutrons est mesurée à l'aide d'un compteur à BF 3. Le bruit de fond a été évalué en vidant complètement le scintillateur de son gaz. Nous nous sommes aperçu en effet que, dans ces conditions, et toutes choses égales par ailleurs, nous ne détections plus les fissions du Np en présence de faisceau, mais que nous continuions néanmoins à enregistrer un nombre de coups non négligeable, compte tenu du faible taux de comptage général de l'expérience. Des essais, en vue de déterminer l'origine de ce bruit de fond, ont montré que celui-ci était directement lié aux neutrons du faisceau. En effet, si on interpose dans le faisceau des écrans "noirs", on voit très distinctement se creuser dans le bruit de fond les ombres des résonances noires. Des recherches sont en cours actuellement afin de déterminer par quel processus on continue à compter des impulsions en l'absence de gaz scintillant, mais il est d'ores et déjà établi que la technique classique qui consiste à évaluer le bruit de fond en interposant des écrans noirs entre la source de neutrons et le détecteur et interpolant ensuite entre les fonds de résonances ne rend pas compte de ce phénomène et conduit à une section efficace résiduelle trop importante.

L'expérience principale a été effectuée sur une base de vol de 12,4 m inclinée à 18° par rapport à la normale au modérateur. Dans ces conditions, le taux de comptage était pour la résonance à 39,9 ev de 8 coups à l'heure par cellule dans un canal de 100 ns.

1.2. Transmission

La transmission a été faite à l'aide d'un détecteur de ^{10}B entouré de six cristaux de NaI (Tl) de 5" x 2 " montés sur des photomultiplicateurs XP 1040. Le neptunium était sous forme de NpO2, les principales impuretés étant le ^{232}Th (2100 ppm) et le ^{239}Pu (35 ppm). On a utilisé deux épaisseurs d'échantillons : 0,0066 et 0,002 atome/barn, les surfaces étant respectivement 9,6 cm^2 et 14,5 cm^2. Pour chaque épaisseur la mesure a été divisée en deux gammes à haute et basse énergie. Le tableau I résume les conditions générales de l'expérience. Le taux de comptage à 10 ev était pour l'échantillon épais à 16,7 m de 1400 coups par canal de 200 ns et par heure. Le bruit de fond était de 30% à la même énergie.

2. Analyse des résultats

2.1. Identification des résonances

La section efficace de fission s'est révélée plus importante que nous l'avions prévue mais seules les plus grandes résonances ont pu être détectées au moyen du scintillateur, les autres ont été noyées dans le bruit de fond. D'une manière générale, on estime que les résonances pour lesquelles $2\, g\, \Gamma_n^{\circ}\, \Gamma_f$ est supérieur à $50 \times 10^{-12}\, E^{3/2}$ ont été vues. Cette valeur définit en quelque sorte un "seuil de visibilité". La figure 2 montre à titre d'exemple la comparaison des sections efficaces totale et de fission entre 28 et 50 ev. Bien que dans cette zone la densité de résonance de fission soit particulièrement grande, on peut voir qu'on en manque un certain nombre. En réalité, entre 1 ev et 120 ev on voit en fission seulement 21 résonances contre plus de 140 en transmission. Sur la figure 3 on a porté le nombre de niveaux visibles en transmission et en fission. Il semble que la densité de niveaux identifiés au-dessus de 40 ev soit inférieure de 20% à la densité au-dessous de 40 ev. L'espacement moyen mesuré entre 0 et 40 ev est :

$$\langle D \rangle = 0{,}67 \text{ ev}$$

L'histogramme donnant le nombre de niveaux visibles en fission est très curieux. On peut y remarquer en effet que les résonances sont groupées par paquets. C'est ainsi que si l'on observe pratiquement tous les niveaux détectés en transmission au voisinage de 40 ev et une bonne partie de ceux qui se trouvent au voisinage de 26 ev, on n'en voit en revanche aucun entre 16 ev et 25 ev, ni entre 50 ev et 110 ev. Ce phénomène se reproduit à plus haute énergie où l'on compte 11 résonances entre 180 et 250 ev alors qu'on n'en voit aucune entre 120 ev et 180 ev. On se trouve donc en présence de fluctuations importantes de la section efficace moyenne de fission avec l'énergie.

Sur la figure 4 on a porté la distribution des espacements de niveaux entre 0 et 108 ev. Cette distribution est compatible avec une distribution de Wigner à deux familles de niveaux à condition d'admettre que l'on perd des petits espacements. C'est bien ce que l'on constate quand on observe une section efficace fictive construite à partir d'une distribution vérifiant au départ une loi de Wigner à deux populations.

2.2. Paramètres de résonance

Les résonances ont été analysées jusqu'à 110 ev à l'aide d'un programme d'analyse de forme à partir d'une formule de Breit et Wigner tenant compte de l'effet d'interférence entre résonances [3] . Le tableau I donne la liste des paramètres ainsi obtenus.

Pour toutes les résonances, sauf quatre, les largeurs partielles Γ_n et Γ_f sont inférieures au dizième de la largeur totale Γ . On peut donc considérer la plupart des résonances comme des résonances de capture. Les largeurs radiatives Γ_γ fluctuent très peu autour de la valeur moyenne :

$$\langle \Gamma_\gamma \rangle = 44 \text{ meV}$$

Cependant, si on ne considère que les résonances visibles en fission, on trouve :

$$\langle \Gamma_\gamma \rangle_{fiss} = 46 \text{ meV}$$

Cette valeur plus élevée est due principalement à la résonance à 39 eV pour laquelle Γ_γ = 74 meV. Il est possible qu'il y ait entre les Γ_γ et les Γ_f une certaine corrélation, analogue à celle déjà trouvée par Michaudon dans l'^{235}U [4] mais cela demande à être plus approfondi.

3. Distribution des largeurs partielles

La distribution des largeurs de fission (fig. 5) observées est compatible avec une distribution de Porter et Thomas à un degré de liberté avec une valeur moyenne de 0,37 meV. A titre de comparaison, on a calculé la valeur de $\langle \Gamma_f \rangle$ donnée par la formule de Hill et Wheeler [5]

$$\langle \Gamma_f \rangle = \frac{D}{2\pi} \exp - \frac{2\pi Es}{h w}$$

En prenant hw = 650 keV on trouve :

$$\langle \Gamma_f \rangle = 0,20 \text{ meV}$$

L'accord est donc très satisfaisant.

Nous avons porté sur la figure 6 la distribution des largeurs neutroniques réduites. A l'examen de ces deux distributions, on peut faire un certain nombre de remarques :

3.1. La distribution expérimentale des largeurs de fission présente une cassure au voisinage de 0,006 meV. Si d'autre part on considère que l'on manque essentiellement des petites valeurs de Γ_f , on doit s'attendre à ce que cet effet s'accentue et que la distribution expérimentale s'écarte encore plus d'une distribution de Porter et Thomas. On peut le voir d'une autre façon : si en effet on considère les 18 résonances pour lesquelles $2 g \Gamma_n^o \rangle$ 0,2 meV on constate que 9 d'entre elles ne sont pas vues en fission. Pour chacune de ces résonances, on peut calculer une valeur maximum de Γ_f (d'après l'estimation du "seuil de visibilité" donnée plus haut) ainsi que la probabilité d'avoir une telle valeur maximum (en supposant que cette probabilité est donnée par la distribution de Porter et Thomas de la figure 5). Cette probabilité varie de résonance en résonance mais reste comprise entre 0,1 et 0,3; d'où on peut déduire que la probabilité de manquer en fission 9 résonances sur 18 est inférieure à 1%.

On est donc amené à conclure que la distribution de Porter et Thomas de la figure 5 ne représente pas correctement la distribution des largeurs de fission. Par contre, celle-ci serait très bien représentée par deux distributions en χ^2, l'une avec un grand $\langle \Gamma_f \rangle$, l'autre avec un $\langle \Gamma_f \rangle$ très petit.

3.2. Les cinq résonances les plus basses en énergie ont toutes un $\Gamma_f <$ 0,006 meV. Si on suppose qu'il n'y a aucune corrélation et qu'on cherche la probabilité de trouver cinq niveaux successifs avec de telles largeurs de fission, on trouve (en utilisant toujours la distribution de la figure 5) une probabilité de 10^{-5}.

La distribution de ces petites valeurs de Γ_f n'est donc pas compatible avec une distribution de Porter et Thomas ayant un $\langle \Gamma_f \rangle$ aussi grand que celui de la distribution de la figure 5. S'il existe deux familles, la plupart de ces résonances à basse énergie appartiennent alors à la famille des petites largeurs de fission. On peut d'ailleurs s'attendre que les résonances de cette famille ne soient visibles qu'à très basse énergie (à cause du terme en $E^{3/2}$ qui intervient dans le seuil de visibilité) ou pour des grandes valeurs de $2\,g\,\Gamma_n^{\circ}$ (cas de la résonance à 25 eV, qui, d'ailleurs est peu visible).

REFERENCES

[1] SLAUGHTER G.G. et coll. ORNL 3085 (1961)

[2] LEONARD B.R., B.N.L. 325.

[3] RIBON P. et coll. Conférence sur les Constantes Nucléaires, Paris 17-21 octobre 1966, Mémoire CN 23/71.

[4] MICHAUDON A. et coll., Nuclear Physics 69 (1965) 545.

[5] HILL D.L. et WHEELER J.A., Physical Review 89 (1963) 1102.

Tableau I

Conditions expérimentales.

	Transmission		Fission
Zone d'énergie (eV)	1 - 20	15 - 300	1 - 300
Distance de vol (m)	16,7	53,7	12,4
Largeur de bouffée de neutrons (ns)	60	110	110
Fréquence de répétition (cycles/s)	500	500	500
Largeur de canal (ns)	100 (14,5 à 20 eV)	200 (15 à 40 eV)	1600 (1 à 2 eV)
	200 (7 à 14 eV)	100 (40 - 76 eV)	400 (2 à 20 eV)
	400 (1,7 à 7 eV)	50 (76 à 200 eV)	100 (20 à 100 eV)
	800 (1 à 1,7 eV)		50 (100 à 300 eV)
Résolution (ns/m)	22 (à 10 eV)	2,8 (à 100 eV)	25 (à 100 eV)
Durée d'accumulation (h)	10	100	350

TABLEAU DES RESONANCES

DU Np^{237}

E (ev)	$2g\Gamma_n$ (mev)	$\sigma_0 \Gamma_F$ (b. ev)	Γ (mev)	Γ_F (mev)	Remarque
23.97	0.171 ± 0.017		61. ± 18		
24.97	4.61 ± 0.07	0.029 ± 0.004	48.7 ± 4	0.0058 ± 0.001	
26.17	0.239 ± 0.016	0.020 ± 0.003	40.1 ± 10	0.066 ± 0.020	
26.54	2.84 ± 0.04	0.113 ± 0.012	44.7 ± 5	0.037 ± 0.007	
27.05	0.0247 ± 0.006				
28.48	0.146 ± 0.015				
28.92	0.11 ± 0.0121				
29.46	0.086 ± 0.013				
30.40	3.76 ± 0.05	0.52 ± 0.05	42.1 ± 5	0.135 ± 0.030	
30.72	0.327 ± 0.03		53.5 ± 13		
31.29	0.278 ± 0.016		36.3 ± 7.2		
31.65	0.0478 ± 0.012				
33.41	0.438 ± 0.02		28 ± 7		
33.90	0.456 ± 0.02		66 ± 10		
34.67	0.184 ± 0.014				
35.19	0.327 ± 0.019		37.2 ± 10		
36.36	0.159 ± 0.02		68.7 ± 23		
36.81	0.072 ± 0.014				
37.14	1.36 ± 0.04	0.22 ± 0.03	46.5 ± 9	0.239 ± 0.07	
37.86	0.064 ± 0.03				(a)
38.16	1.61 ± 0.06		61.9 ± 13		
38.92	1.24 ± 0.065	0.46 ± 0.06	57.5 ± 15	0.600 ± 0.180	
39.22	0.65 ± 0.045	0.41 ± 0.06	47.3 ± 14		
39.90	0.66 ± 0.027	1.74 ± 0.20	80.2 ± 14	6.35 ± 1.6	
41.34	2.26 ± 0.045	0.683 ± 0.085	40 ± 7	0.380 ± 0.1	
42.38	0.0907 ± 0.023				
42.81	0.117 ± 0.026	0.045 ± 0.007			
43.65	0.290 ± 0.05				
45.70	0.483 ± 0.06		62.8 ± 19		
46.01	0.659 ± 0.039	0.21 ± 0.03			
46.34	3.07 ± 0.06		46.8 ± 8		
47.31	2.40 ± 0.05		45.7 ± 8		
48.47	0.11 ± 0.022				
48.78	0.53 ± 0.026				
49.80	5.09 ± 0.09		46.4 ± 7		
50.58	0.93 ± 0.16	0.196 ± 0.026	48.3 ± 7	0.041 ± 0.014	
51.89	0.091 ± 0.033				

E (ev)	$2g\Gamma_n$ (mev)	$\sigma_0 \Gamma_F$ (b ev)	Γ (mev)	Γ_F (mev)	Remarque
0.489	0.0325 ± 0.01		34 ± 2	0.00075 ± 0.00015	ref. 1, 2
1.32	0.0374 ± 0.00037	0.0025 ± 0.0006	39.8 ± 0.8	0.0027 ± 0.0006	
1.48	0.145 ± 0.002	0.002 ± 0.0005	48.3 ± 1	0.00075 ± 0.0002	
1.97	0.0166 ± 0.00033		41.2 ± 1.3		
3.86	0.244 ± 0.0024	0.0089 ± 0.0012	41.6 ± 1.3	0.0045 ± 0.0007	
4.26	0.0264 ± 0.0007		37.5 ± 1.8		
4.85	0.0345 ± 0.0009		38.7 ± 1.9		
5.77	0.622 ± 0.006	0.019 ± 0.003	44.8 ± 2	0.006 ± 0.0008	
6.37	0.093 ± 0.0021		38.2 ± 1.9		
6.67	0.012 ± 0.0012		47.9 ± 12		
7.18	0.0078 ± 0.0012		35.4 ± 15		
7.42	0.146 ± 0.0025		39.9 ± 2		
8.30	0.107 ± 0.0023		37.8 ± 2.5		
8.97	0.121 ± 0.003		38.5 ± 2.5		
9.30	0.522 ± 0.0052		42.7 ± 2.6		
10.23	0.025 ± 0.0025		38.1 ± 12		
10.68	0.506 ± 0.02		36.1 ± 2.3		
10.84	0.88 ± 0.025		45.4 ± 2.7		
11.09	0.885 ± 0.011		43.9 ± 2.7		
12.20	0.0624 ± 0.003		49.7 ± 7.5		
12.61	0.795 ± 0.008		42.3 ± 2.5		
13.15	0.0197 ± 0.003				
15.83	0.102 ± 0.01				
16.11	0.924 ± 0.014		49.7 ± 3.5		
16.88	0.243 ± 0.006		34.6 ± 3.5		
17.02	0.006 ± 0.003				(a)
17.59	0.184 ± 0.07		39.6 ± 4		
17.88	0.018 ± 0.0036				
18.89	0.0366 ± 0.01				
19.11	0.106 ± 0.01				
19.92	0.075 ± 0.007		35.9 ± 1.2		
20.39	1.13 ± 0.022		41.7 ± 3.2		
21.09	0.516 ± 0.018		35.4 ± 4.8		
21.35	0.0229 ± 0.011				(a)
22.01	1.26 ± 0.025		41.6 ± 4		
22.66	0.447 ± 0.014		40.1 ± 6		
23.67	1.69 ± 0.034		41.7 ± 5		

TABLEAU II

TABLEAU DES RESONANCES DU Np^{237}

E (ev)	$2g\Gamma_n$ (mev)	$\sigma_0 \Gamma_F$ (b ev)	Γ (mev)	Γ_F (mev)	Remarque
52.19	0.375 ± 0.05				
52.62	0.703 ± 0.035				
53.03	0.062 ± 0.015				
53.86	0.387 ± 0.04				
54.20	0.131 ± 0.02				
55.01	0.317 ± 0.03				
56.03	1.99 ± 0.06		109 ± 22		(b)
58.35	0.463 ± 0.07				
58.60	2.01 ± 0.06				
59.48	2.70 ± 0.08		45 ± 9		
60.01	1.83 ± 0.055		45.9 ± 9		
60.92	0.523 ± 0.049		40.6 ± 8.8		
61.61	2.10 ± 0.1				
62.44	1.72 ± 0.1		82.2 ± 17		
62.89	0.276 ± 0.027		47.2 ± 12		
63.92	0.276 ± 0.028				
64.94	1.01 ± 0.06		44.7 ± 14		
65.68	4.55 ± 0.08		50.6 ± 9		
67.45	5.78 ± 0.1		44 ± 8		
67.93	2.93 ± 0.1		46 ± 10.5		
68.74	0.359 ± 0.032				
70.22	2.14 ± 0.09		68 ± 13		
70.65	0.5 ± 0.04				
71.18	2.30 ± 0.46				
71.44	2.68 ± 0.5				
73.85	0.31 ± 0.027				
74.26	1.47 ± 0.07				
74.54	0.51 ± 0.06				
75.09	0.11 ± 0.033				
76.53	0.186 ± 0.028				
76.97	0.375 ± 0.03				
78.33	2.45 ± 0.1		78.8 ± 16		
79.24	2.52 ± 0.075		54.1 ± 11		
80.35	0.157 ± 0.075				(a)
80.60	0.542 ± 0.065				
81.59	0.42 ± 0.021				
82.09	0.818 ± 0.04				
83.39	5.11 ± 0.6				
83.70	5.55 ± 1.1				

E (eV)	$2g\Gamma_n$ (mev)	$\sigma_0 \Gamma_F$ (b ev)	Γ (mev)	Γ_F (mev)	Remarque
85.19	1.19 ± 0.05		64.1 ± 16		
86.07	0.835 ± 0.12				
86.50	5.72 ± 0.23		49.0 ± 10		
87.65	3.700 ± 0.1				
88.13	1.03 ± 0.06				
88.90	1.85 ± 0.07				
89.43	4.29 ± 0.17				
90.84	4.98 ± 0.2				
91.32	0.158 ± 0.046				
91.95	0.51 ± 0.07				
92.75	0.189 ± 0.03				
93.36	1.8 ± 0.131		48.8 ± 17		
94.22	0.368 ± 0.055				
95.37	0.358 ± 0.055				
96.14	0.055 ± 0.027				(a)
96.61	0.35 ± 0.09				
97.72	3.48 ± 0.14		65.3 ± 13		
98.46	2.38 ± 0.9		77.4 ± 25		
98.99	0.1 ± 0.05				(a)
99.49	1.94 ± 0.14		51.7 ± 16		
100.19	5.30 ± 0.16		58.4 ± 12		
101.03	5.41 ± 0.16		62.5 ± 12		
101.62	1.23 ± 0.25				
101.92	1.67 ± 0.34				
102.15	0.30 ± 0.15				(a)
103.94	1.60 ± 0.06				
104.68	0.34 ± 0.068				
105.37	2.18 ± 0.21		79.7 ± 28		
105.89	3.29 ± 0.2		44.4 ± 13		
107.21	0.51 ± 0.06				

a) Résonance douteuse

b) Résonance pouvant être double.

TABLEAU II

suite

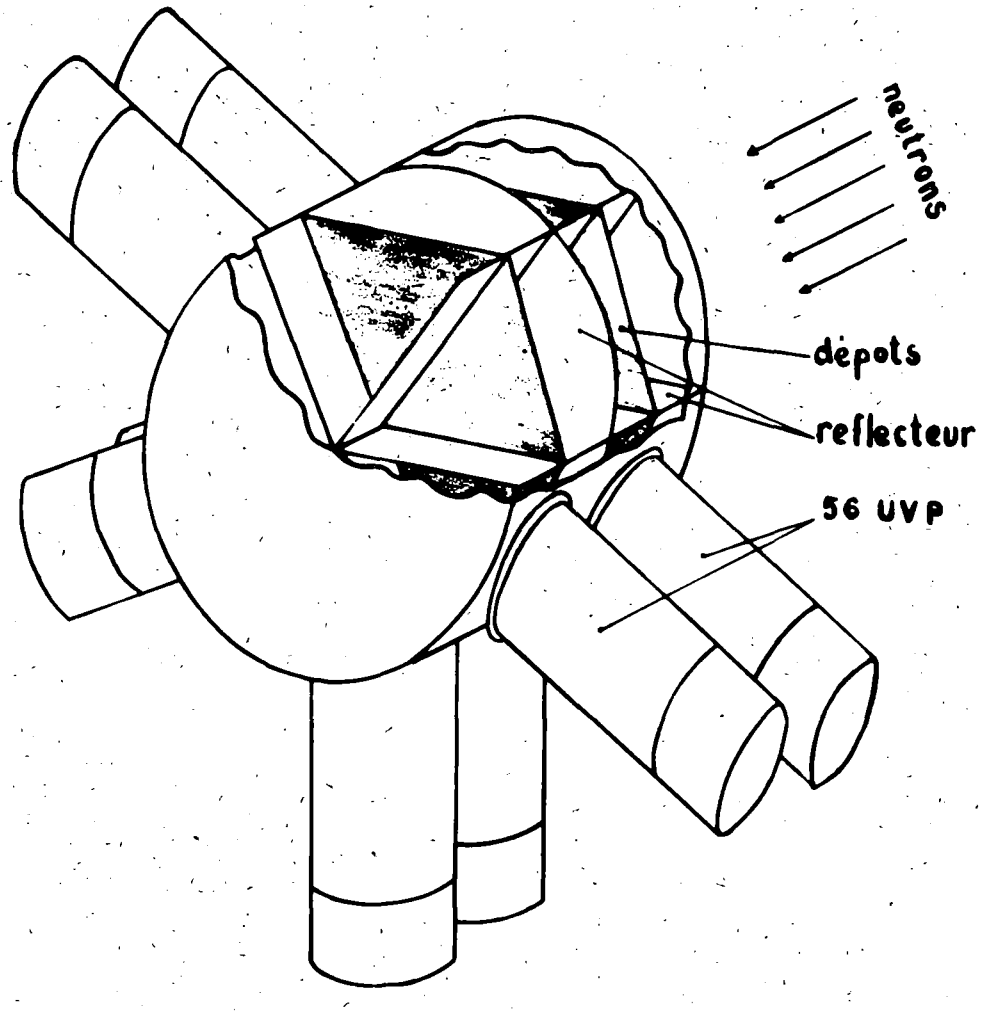

Figure 1 - Vue du scintillateur.

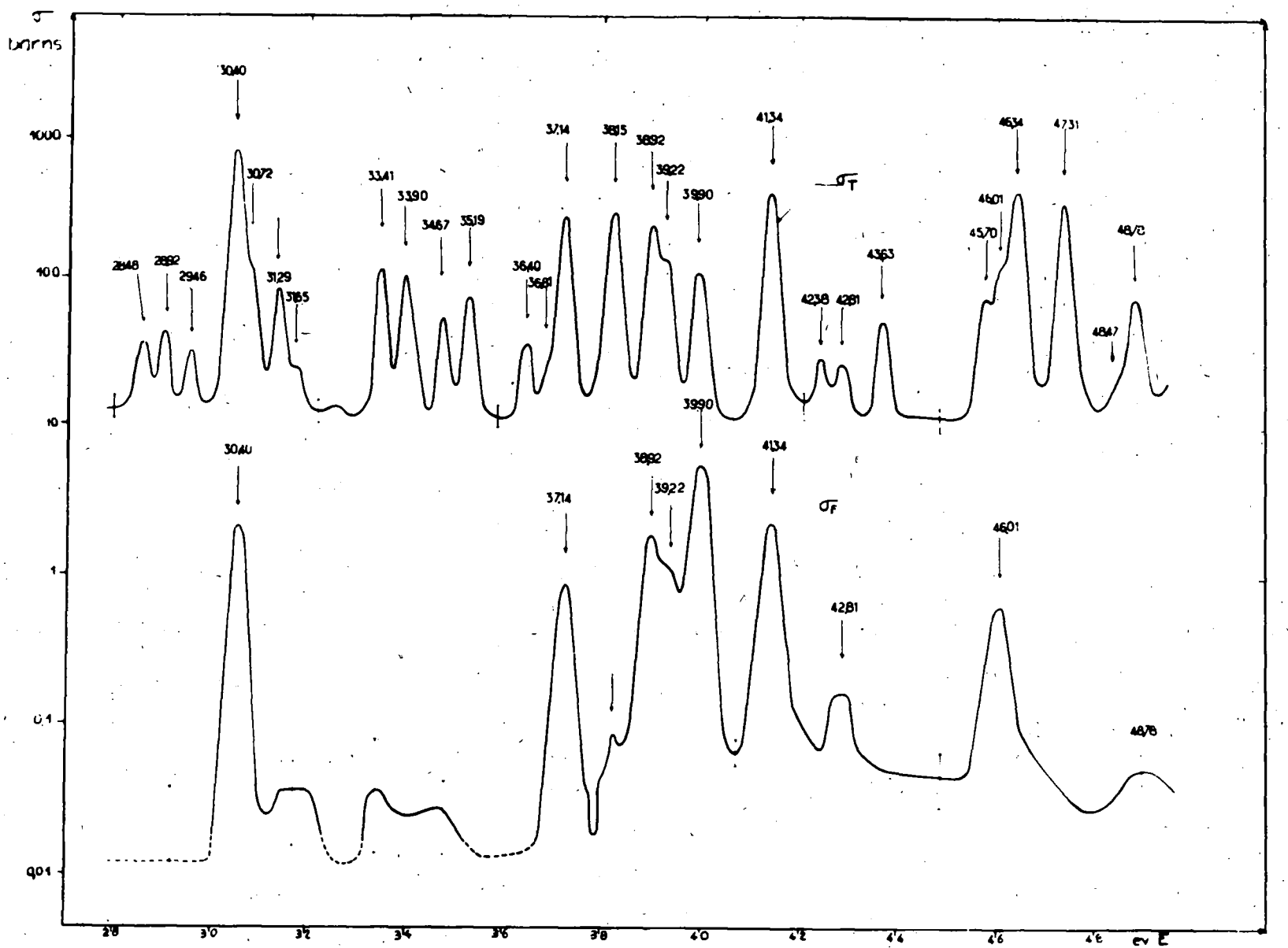

Fig. 2 - Sections efficaces totale et de fission du ^{237}Np

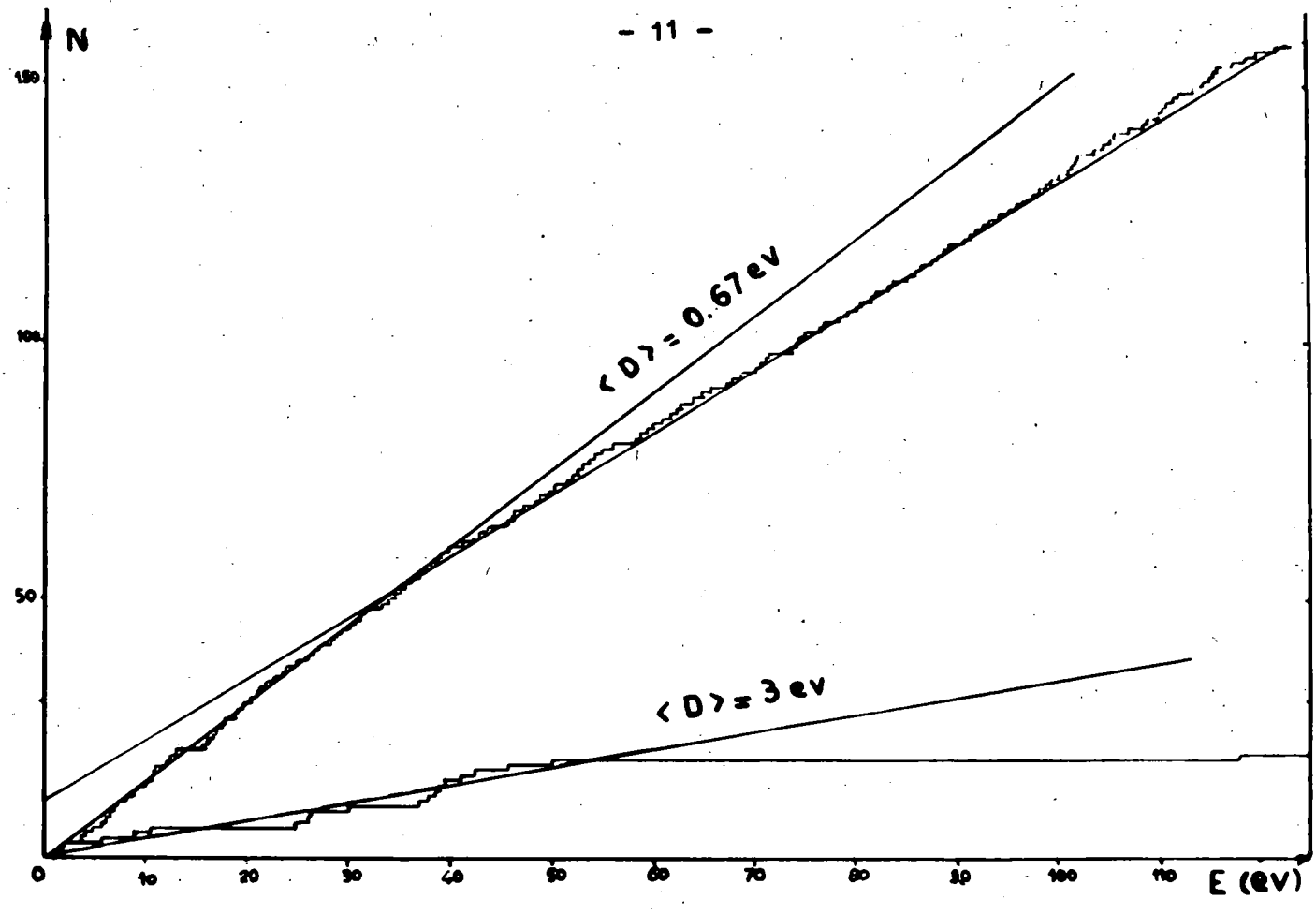

Fig. 3 - Nombre de niveaux en fonction de l'énergie.

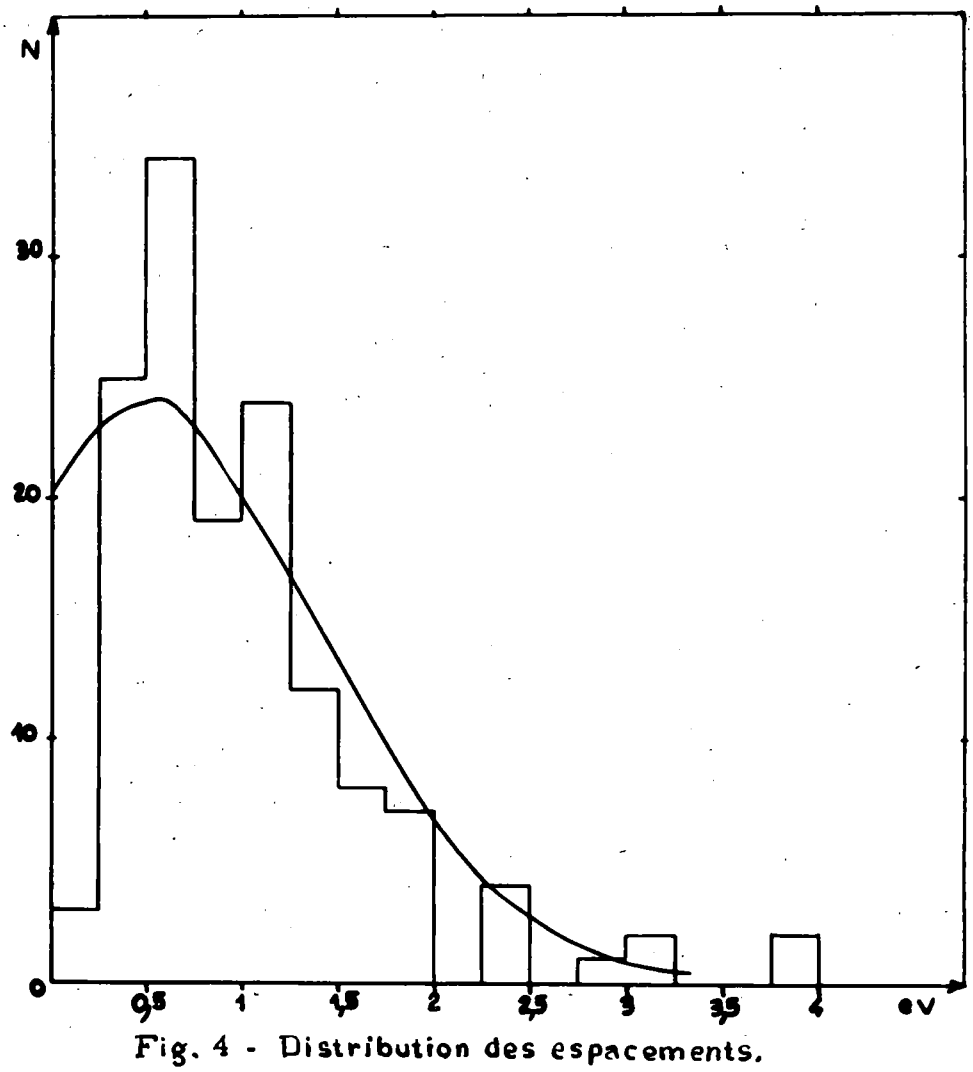

Fig. 4 - Distribution des espacements.

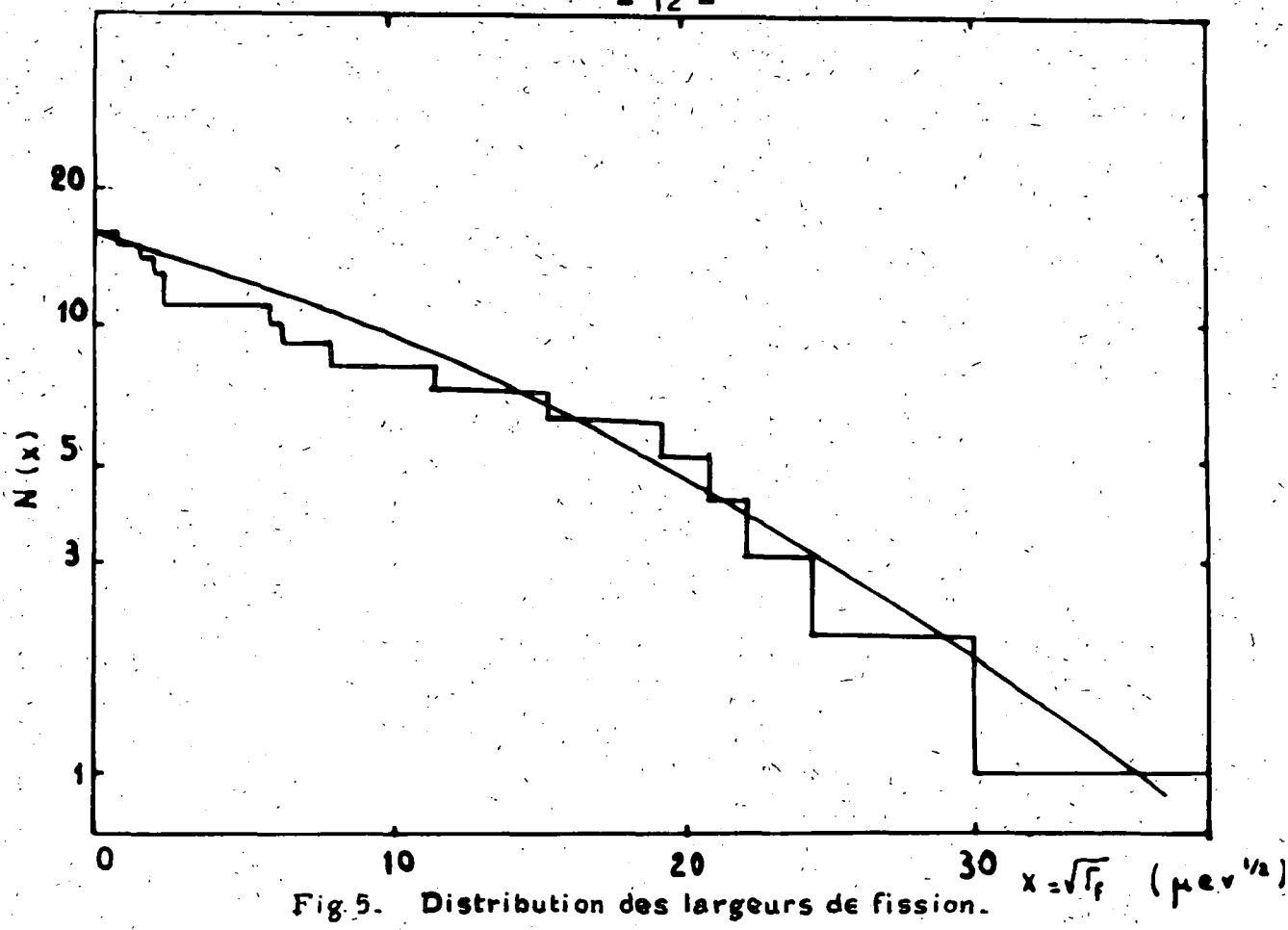

Fig. 5. Distribution des largeurs de fission.

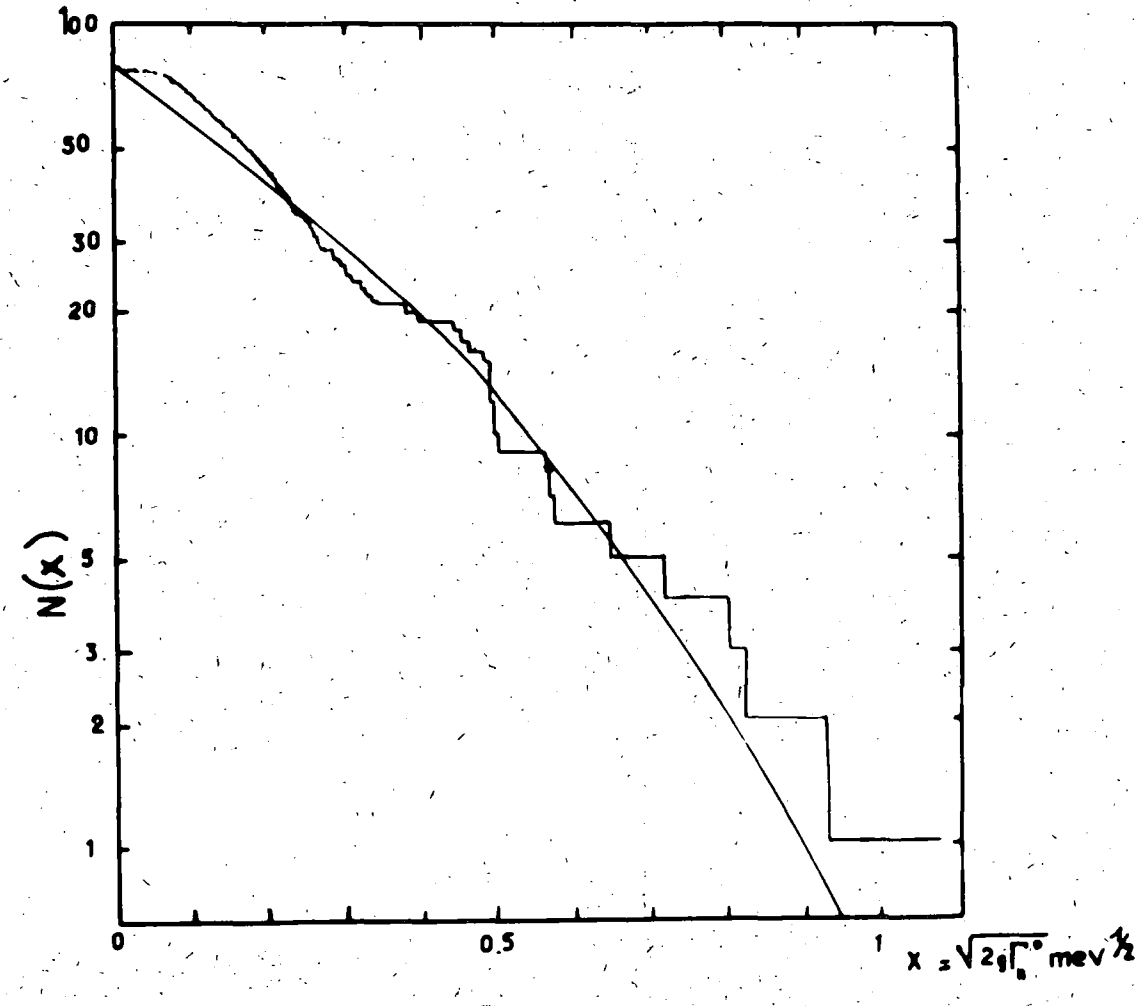

Fig. 6 - Distribution des largeurs neutroniques

TABLE DES INTEGRALES DE RESONANCE

R. VIDAL - F. ROULLIER

Centre d'Etudes Nucléaires de Fontenay-aux-Roses (France)

INTRODUCTION -

Nous nous proposons, en établissant cette table, de regrouper toutes les valeurs des intégrales de résonance mesurées après les avoir corrigées pour les ramener à une définition commune.

Pour les matériaux dont les paramètres de résonance sont connus avec une précision suffisante, nous indiquons la valeur calculée correspondant à la dilution infinie afin de les comparer aux valeurs mesurées.

De l'ensemble de cette comparaison, nous déduisons pour chaque corps les valeurs à adopter qui sont regroupées dans une table.

I - DEFINITION DE L'INTEGRALE DE RESONANCE

L'intégrale de résonance au-dessus de la partie 1/v, correspondant à la dilution infinie est définie par la relation :

$$\boxed{I = \int_{E_c = 0{,}55\,ev}^{\infty} \left(\sigma(E) - \sigma_0 \sqrt{\frac{E_0}{E}} \right) \frac{dE}{E} \qquad E_r \geqslant 1\,ev} \qquad (1)$$

$$\sigma_0 = \sigma(E_0) \qquad \text{avec } E_0 = 0{,}025\ ev$$

E_r : Energie de la résonance

E_c : Energie de coupure prise égale à 0,55 eV selon les recommandations de l'EANDC.

A partir de cette définition, on peut déduire l'intégrale de résonance totale :

$$\boxed{I_R = \int_{0,55}^{\infty} \sigma(E) \frac{dE}{E} \qquad E_r \geqslant 1\,eV} \qquad (2)$$

par la relation :

$$I_R = I + I_{1/v}$$

avec

$$I_{1/v} = 2\,\sigma_0 \sqrt{\frac{E_0}{E_c}} = 0{,}426\,\sigma_0 \qquad (3)$$

La limite inférieure d'intégration étant fixée à 0,55 eV, il est évident qu'on ne peut faire intervenir dans l'intégrale, que les résonances situées au-dessus de cette valeur et dont l'aile est éteinte à cette énergie. Dans ces conditions la section efficace réelle rejoint la valeur de la section efficace en 1/v.

Avec cette définition, on ne peut considérer que les résonances supérieures à 1 eV. Pour les matériaux dont les résonances sont inférieures à cette limite, l'intégrale sur un spectre en 1/E est sans intérêt, et il faut y substituer la section efficace effective, qui est l'intégrale de la section efficace microscopique rapportée au spectre réel.

II - CALCUL DES INTEGRALES DE RESONANCE A PARTIR DES PARAMETRES

L'intégrale de résonance correspondant à la dilution infinie s'obtient en utilisant les programmes "ZUT" et "TUZ".

1) Résonances résolues

Le programme "ZUT" traite individuellement les résonances résolues. Les sections efficaces sont obtenues à partir des paramètres par la formule de BREIT-WIGNER. Les bornes d'intégration sont choisies suffisament voisines de l'énergie de résonance, pour qu'on puisse considérer que

l'intégrale obtenue est celle au-dessus de la partie en 1/v, l'intégrale en 1/v étant alors négligeable.

2) Résonances non résolues

Les résonances non résolues sont obtenues à partir du programme "TUZ" en utilisant l'approximation NR, et une pondération de la largeur réduite suivant la distribution de PORTER-THOMAS.

Ces deux programmes permettent aussi le calcul des intégrales de résonance d'échantillons en dilution finie, lorsque celles-ci sont nécessaires.

III - VALEURS DES INTEGRALES DE RESONANCES MESUREES

Nous avons normalisé nos résultats en adoptant :

Pour le bore 10	σ_o = 3840 b	
Pour l'or	I = 1540 b	σ_o = 98,8 b

Afin de comparer l'ensemble des valeurs publiées, nous avons été conduit à effectuer sur certains résultats les corrections suivantes :

- Calcul de la partie en 1/v pour obtenir I à partir de I_R
- Modification de la coupure pour les mesures sous cadmium avec des boitiers de différentes épaisseurs et calcul de la nouvelle valeur pour la rapporter à E_c = 0,55 eV
- Normalisation pour rapporter les résultats aux valeurs de référence pour l'intégrale de résonance de l'or et la section efficace du bore 10, On adopte ainsi pour le bore naturel suivant sa teneur isotopique :
  - σ_o = 760 b (19,81 %)
  - σ_o = 771 b (20,12 %)
- Extrapolation à la dilution infinie en adoptant les coefficients d'auto-protection résonnante calculée à l'aide du programme ZUT.

- Calcul de la nouvelle valeur en adoptant pour les sections thermiques des matériaux mesurés les valeurs les plus récentes.
- Calcul de la valeur correspondant à la teneur naturelle à partir des valeurs de chacun des isotopes.

IV - NOTE DES AUTEURS

Nous citons pour chaque matériau toutes les valeurs dont nous avons eu connaissance à la date où nous effectuons cette étude, et nous nous excusons de ne pas avoir pris en compte tous les résultats publiés, notre bibliographie étant certainement incomplète. Dans les tableaux, les résultats précédés d'une astérisque (*) sont publiés dans des rapports où les renseignements sont insuffisants pour effectuer les corrections nécessaires à la comparaison, et nous n'en avons pas tenu compte pour définir la valeur recommandée.

Cette valeur recommandée est une pondération des valeurs les plus récentes et qui est en bon accord avec la valeur calculée.

Pour certains corps, les paramètres de résonance sont inconnus ou imprécis, et ne permettent pas d'obtenir une valeur calculée.

Dans certains cas, nous avons séparé les valeurs d'absorption et d'activation lorsqu'elles sont différentes, et nous donnons aussi les valeurs correspondant à chaque isotope.

Cette table comporte certainement des lacunes, et nous prions les lecteurs de bien vouloir nous aviser des omissions et des erreurs que nous aurions pu commettre dans l'interprétation de leurs mesures.

25 - MANGANESE

Valeurs recommandées : $I = 10,2 \pm 0,5$ b $I_R = 15,9 \pm 0,5$ b

Valeur calculée : I = 10,2 b

I corrigée	Date	Auteurs		Méthode
$10,0 \pm 1,9$	1966	LOUWRIER	[1]	Mesure avec solution de sulfate de Mn
$10,5 \pm 1$	1966	VIDAL	[2]	Oscillation sans cadmium Bore : σ_o = 760 b - Or : I = 1540 b
$12,7 \pm 1,8$	1964	BAUMANN	[3]	Activation sous cadmium
$7,5 \pm 0,8$	1962	BARDES	[4]	Activation et correction de la partie en 1/v avec le vanadium - Or : I = 1526 b
8,8	1962	BERRETH	[5]	Activation sous cadmium - Or : I_R = 1558 b
$11,7 \pm 0,4$	1961	FEINER	[6]	Activation sous cadmium - Or : I_R = 1534 b
$8,15 \pm 0,6$	1961	DAHLBERG	[7]	Activation sous cadmium
$8,8 \pm 0,3$	1961	JACKS	[8]	Activation sous cadmium - Or : I = 1513 b
$7,8 \pm 0,8$	1960	WALKER	[9]	Activation sous cadmium - Or : I = 1525 b
$9,5 \pm 5$	1960	TATTERSALL	[10]	Oscillation sans cadmium Bore : σ_o = 767 b - Or - I = 1513 b
*$(4,5 \pm 2,5)$	1958	ROSE	[11]	Oscillation sans cadmium
*$(5,8 \pm 1,5)$	1957	KLIMENTOV	[12]	Absorption
*(4,9)	1955	MACKLIN	[13]	Oscillation sous cadmium - Or : I = 1513 b
*(5,9)	"	"	[13]	Activation sous cadmium - Or : I = 1513 b

26 - FER

Valeurs recommandées : $I = 1,1 \pm 0,2$ b $I_R = 2,2 \pm 0,2$b

I corrigée	Date	Auteurs		Méthode
$1,1 \pm 0,3$	1966	VIDAL	[2]	Oscillation sans cadmium Bore : = 760 b - Or : I = 1540 b
$1,0 \pm 0,4$	1959	TATTERSALL	[10]	Oscillation sans cadmium Bore : = 767 b - Or : I = 1513 b
*$(0,5 \pm 0,3)$	1958	ROSE	[11]	Oscillation sans cadmium
*$(1,2 \pm 0,4)$	1957	KLIMENTOV	[12]	Absorption
*$(1,2 \pm 0,25)$	1955	SPYVAK	[14]	Absorption
*(1)	1955	MACKLIN	[13]	Oscillation sous cadmium : Or : I = 1513 b

27 - COBALT

Valeurs recommandées : $I = 55 \pm 3$ b $\quad I_R = 71 \pm 3$ b

Valeur calculée : $I = 50 \pm 5$ b

I corrigée	Date	Auteurs	Méthode
$50,5 \pm 4$	1966	VIDAL [2]	Oscillation sans cadmium Bore : $\sigma_0 = 760$ b - Or : I = 1540 b
53 ± 5	1964	VIDAL [15]	Oscillation sans cadmium - Co = 37,8 b Bore : $\sigma_0 = 760$ b - Or : I = 1540 b
$55,2 \pm 3,5$	1963	EASTWOOD [16]	Activation sous cadmium - Or : $I_R = 1535$ b
60,1	1962	BERRETH [5]	Activation sous cadmium - Or : $I_R = 1558$ b
$55,2 \pm 4,5$	1961	DAHLBERG [7]	Activation sous cadmium
$67,9 \pm 4$	1960	FEINER [17]	Activation sous cadmium - Or : $I_R = 1534$ b
$58,9 \pm 5$	1960	JOHNSTON [18]	Activation sous cadmium - Or : $I_R = 1564$ b
*(32 ± 4)	1957	KLIMENTOV [12]	Absorption
*(31,7)	1955	MACKLIN [13]	Oscillation sous cadmium - Or : I = 1513 b

28 - NICKEL

Valeur recommandée : $I = 1,0 \pm 0,4$ b $\quad I_R = 3,0 \mp 0,4$ b

I corrigée	Date	Auteurs	Méthode
$1,0 \pm 0,4$	1966	VIDAL [2]	Oscillation sans cadmium Bore : $\sigma_0 = 760$ b - Or : I = 1540 b
$< 1,1$	1959	TATTERSALL [10]	Oscillation sans cadmium Bore : $\sigma_0 = 767$ b - Or : I = 1513 b
*$(1,1 \pm 0,5)$	1957	KLIMENTOV [12]	Absorption
*(2)	1955	MACKLIN [13]	Oscillation sous cadmium - Or : I = 1513 b

29 - CUIVRE

Valeurs recommandées :

$I = 2,55 \pm 0,20$ b $I_R = 4,15 \pm 0,20$ b

Cu 63 : $I = 3,0 \pm 0,2$ b

Cu 65 : $I = 1,4 \pm 0,1$ b

I corrigée	Date	Auteurs	Méthode
$2,2 \pm 0,3$	1966	VIDAL [2]	Oscillation sans cadmium Bore : $\sigma_0 = 760$ b - Or : I = 1540 b
2,75	1963	BAUMANN [19]	Activation sous cadmium - Or : I = 1490 b
$2,56 \pm 0,15$	1961	DAHLBERG [7]	Activation sous cadmium
$1,62 \pm 0,07$	1961	BENNETT [20]	Activation sous cadmium
2,7	1959	TATTERSALL [10]	Oscillation sans cadmium Bore : $\sigma_0 = 767$ b - Or : I = 1513 b
*$(2,1 \pm 0,8)$	1957	KLIMENTOV [12]	Absorption
*$(1,6 \pm 0,3)$	1955	SPYVAK [14]	Absorption
*(2,4)	1955	MACKLIN [13]	Oscillation sous cadmium - Or : I = 1513 b
*(2,1)	1955	MACKLIN [13]	Activation sous cadmium - Or : I = 1513 b

40 - ZIRCONIUM

Valeurs recommandées : $I = 1,05 \pm 0,10$ b $I_R = 1,13 \pm 0,10$ b

Valeur calculée : $I = 1,1 \pm 0,1$ b

I corrigée	Date	Auteurs	Méthode
$1,1 \pm 0,15$	1966	VIDAL [2]	Oscillation sans cadmium Bore : $\sigma_0 = 760$ b - Or : I = 1540 b
$0,85 \pm 0,15$	1961	HELLSTRAND [21]	Oscillation sans cadmium Bore : $\sigma_0 = 758$ b - Or : I = 1500 b
0,99	1959	TATTERSALL [10]	Oscillation sans cadmium Bore : $\sigma_0 = 767$ b - Or : I = 1513 b
1,03	1959	TATTERSALL [22]	Oscillation sans cadmium
*(1,12)	1959	HONE [23]	Absorption
*$(3,6 \pm 0,5)$	1957	KLIMENTOV [12]	Absorption
*(3,0)	1955	MACKLIN [13]	Oscillation sous cadmium - Or : I = 1513 b

42 - MOLYBDENE

Valeurs recommandées : $I = 23 \pm 1$ b $I_R = 24,6 \pm 1$ b

Valeur calculée : I = 23 b

I corrigée	Date	Auteurs	Méthode
$23,2 \pm 1$	1966	VIDAL [2]	Oscillation sans cadmium - Mo : = 3,65b Bore : $\sigma_0 = 760$ b - Or : I = 1540 b
$19 \pm 2,5$	1959	TATTERSALL [10]	Oscillation sans cadmium Bore : $\sigma_0 = 767$ b - I = 1513 b
*(14 ∓ 2)	1958	ROSE [11]	Oscillation sans cadmium
*(12,6 ∓ 1,7)	1957	KLIMENTOV [12]	Absorption
*(11,9)	1955	MACKLIN [13]	Oscillation sous cadmium - Or : I = 1513 b

47 - ARGENT

Valeurs recommandées : $I = 710 \pm 30$ b $I_R = 740 \pm 30$ b

Valeur calculée : I = 730 b

I corrigée	Date	Auteurs	Méthode
670 ± 20	1964	VIDAL [15]	Oscillation sans cadmium Bore : $\sigma_0 = 760$ b - Or : I = 1540 b
810 ± 30	1959	TATTERSALL [10]	Oscillation sans cadmium Bore : $\sigma_0 = 767$ b - Or : I = 1513 b
*(435 ± 70)	1957	KLIMENTOV [12]	Absorption
*(> 620)	1955	MACKLIN [13]	Oscillation sous cadmium - Or : I = 1513 b
*(575)	1955	MACKLIN [13]	Activation sous cadmium - Or : I = 1513 b

49 - INDIUM

Valeurs recommandées :

$I = 3250 \pm 50$ b $I_R = 3330 \pm 50$ b In_{115} : $I = 3390 \pm 50$ b

Valeur calculée : $I = 3050$ b

I corrigée	Date	Auteurs		Méthode
3200 ± 70	1964	VIDAL	[15]	Oscillation sans cadmium Bore : $\sigma_0 = 760$ b - Or : $I = 1540$ b
3400 ± 150	1963	BECKURTS	[24]	Activation sous cadmium
3200 ± 100	1963	BAUMANN	[19]	Activation sous cadmium - Or : $I = 1490$ b
3200	1962	BROWN	[25]	Activation sous cadmium - Or : $I_R = 1558$ b
3250 ± 133	1961	JACKS	[8]	Activation sous cadmium - Or : $I_R = 1558$ b
3450 ± 100	1960	WALKER	[9]	Activation sous cadmium - Or : $I = 1525$ b
3160	1960	NILSSON	[26]	Activation sans cadmium - Or : $I = 1490$ b
3600 ± 350	1959	TATTERSALL	[10]	Oscillation sans cadmium Or : $I = 1513$ b - Bore : $= 767$ b
*(2490)	1955	MACKLIN	[13]	Activation sous cadmium - Or : $I = 1513$ b
*(2133 ± 330)	1957	KLIMENTOV	[12]	Absorption

Intégrales d'activation de In_{115} :

En adoptant : $I_2/I_1 = 0{,}276$ (BECKURTS) [24]

I_1^{115} (T : 54 mn) = 2660 ∓ 40 b

I_2^{115} (T : 14 s) = 730 ∓ 10 b

55 - CESIUM

Valeurs recommandées : $I = 410 \pm 20$ b $I_R = 420 \pm 20$ b

Valeur calculée : $I = 380 \pm 60$ b

I corrigée	Date	Auteurs		Méthode
450 ± 15	1964	VIDAL	[15]	Oscillation sans cadmium Bore : $\sigma_0 = 760$ b - Or : I = 1540 b
320 ± 50	1961	BROWN	[27]	Activation sous cadmium Co : $\sigma_0 = 36,65$ b et $I_R = 74$ b.
430 ± 25	1960	EILAND	[28]	Activation sous cadmium
490 ± 80	1959	TATTERSALL	[10]	Oscillation sans cadmium Bore : $\sigma_0 = 767$ b - Or : I = 1513 b
*(420 ± 40)	1958	ROSE	[11]	Oscillation sans cadmium
*(146 ± 28)	1957	KLIMENTOV	[12]	Absorption

72 - HAFNIUM

Valeurs recommandées : $I = 2100 \pm 50$ b $I_R = 2145 \pm 50$ b

Valeur calculée : $I = 1900 \pm 100$ b

I corrigée	Date	Auteurs		Méthode
2080 ± 50	1964	VIDAL	[15]	Oscillation sans cadmium Bore : σ_0 760 b - Or : I = 1540 b
2850 ± 350	1959	TATTERSALL	[10]	Oscillation sans cadmium Bore $\sigma_0 = 767$ b - Or : I = 1513 b
*(2100 ± 480)	1962	SCOVILLE	[29]	Absorption
*(1950)	1961	FEINER	[6]	Réactivité sous cadmium
*(1425 ± 200)	1957	KLIMENTOV	[12]	Absorption
*(1255)	1955	MACKLIN	[13]	Oscillation sous cadmium - Or : I = 1513 b
*(1705)	1955	MACKLIN	[13]	Activation sous cadmium - Or : I = 1513 b
*(2750 ± 600)	1955	SPIVACK	[14]	Absorption

90 - THORIUM

Valeurs recommandées : $I = 83 \pm 2$ b $I_R = 86 \mp 2$ b

Valeur calculée : $I = 87 \pm 6$ b

I corrigée	Date	Auteurs		Méthode
78 ± 4	1965	FOELL	[30]	Réactivité sous cadmium - Or : $I_R = 1579$ b
$80,6 \pm 3$	1965	HARDY	[31]	Activation sous cadmium - Or : $I_R = 1555$ b
87 ± 4	1964	VIDAL	[15]	Oscillation sans cadmium Bore : $\sigma_0 = 760$ - Or : $I = 1540$ b
86,5	1964	BROSE	[32]	Activation sous cadmium - Or : $I_R = 1461$ b
$84,6 \pm 6$	1962	TIREN	[33]	Activation sans cadmium - Or : $I = 1510$ b
79 ± 5	1962	BARDES	[4]	Activation sans cadmium - Or : $I = 1526$ b
83	1960	JOHNSTON	[18]	Activation sous cadmium - Or : $I_R = 1565$ b
106 ± 10	1959	TATTERSALL	[10]	Oscillation sans cadmium Bore : $\sigma_0 = 767$ b - Or : $I = 1513$ b
*$(58,4 \pm 12)$	1957	KLIMENTOV	[12]	Absorption
*(67 ± 5)	1955	MACKLIN	[13]	Activation sous cadmium - Or : $I = 1513$ b

TABLEAU DES INTEGRALES DE RESONANCE

Eléments naturels

N° at	ELEMENT	I_{barn}	Référence	N° at	ELEMENT	I_{barn}	Référence
11	Sodium	0,072 ± 0,01	[7][3]	53	Iode	180 ± 30	[10]
12	Magnésium	0,045 ± 0,020	[10]	55	Césium	410 ± 20	[45]
13	Aluminium	< 0,08	[10]	59	Praséodyme	11 ± 3	[28]
25	Manganèse	10,2 ± 0,5	[45]	61	Prométhium	3200 ± 500	[35]
26	Fer	1,1 ± 0,2	[45]	65	Terbium	610 ± 24	[36]
27	Cobalt	55 ± 3	[45]	67	Holmium	830 ± 26	[36]
28	Nickel	1,0 ± 0,4	[45]	68	Erbium	800 ± 26	[36]
29	Cuivre	2,55 ± 0,20	[45]	69	Thulium	1680 ± 54	[36]
30	Zinc	1,18 ± 0,16	[10]	70	Ytterbium	180 ± 10	[36]
40	Zirconium	1,05 ± 0,10	[45]	72	Hafnium	2100 ± 50	[45]
41	Niobium	11 ± 3	[6][10][34]	73	Tantale	1100 ± 400	[10]
42	Molybdène	23 ± 1	[45]	74	Tungstène	330 ± 60	[10]
43	Technétium	60 ± 20	[10]	75	Rhénium	810 ± 65	[37]
47	Argent	710 ± 30	[45]	82	Plomb	0,050 ± 0,030	[10]
49	Indium	3250 ± 50	[45]	83	Bismuth	0,050 ± 0,012	[10]
50	Etain	8,5 ± 2	[10]	90	Thorium	83 ± 2	[45]

Isotopes

N° at.	Isotope	% dans l'élément naturel	I_{barn}	Référence	N° at.	Isotope	% dans l'élément naturel	I_{barn}	Référence
18	A^{40}	99,6	0,08 ± 0,04	[38]	44	Ru^{106}	-	1,9 ± 0,6	[42]
23	V^{51}	99,76	0,38 ± 0,16	[4]	49	In^{115} (54 mn)	95,77	2660 ± 40	[45]
26	Fe^{58}	0,31	0,58 ± 0,16	[39]	49	In^{115} (14 s)	95,77	730 ± 10	[45]
29	Cu^{63}	69,1	3,1 ± 0,2	[45]	58	Ce^{140}	88,48	0,23 ± 0,05	[43]
29	Cu^{65}	30,1	1,4 ± 0,1	[45]	58	Ce^{144}	-	2,15 ± 0,26	[44]
30	Zn^{64}	48,89	0,67 ± 0,14	[39]	60	Nd^{143}	12,32	< 50	[10]
30	Zn^{68}	18,56	0,17 ± 0,03	[39]	60	Nd^{145}	8,29	130 ± 15	[10]
42	Mo^{98}	23,75	9 ± 2	[10] [40][6]	61	Pm^{147} (5,3 j)	100	1645 ± 250	[35]
42	Mo^{100}	9,62	3,85 ± 0,20	[41][3]	61	Pm^{147} (42 j)	100	1470 ± 230	[35]
						Hg^{202}	29,80	2,1 ± 0,5	[39]

REFERENCES

[1] LOUWRIER,P.W.F., Thèse Amsterdam (1966)
[2] CARRE,J.C., VIDAL,R., Ce Congrès
[3] BAUMANN,N.P., Rep. WASH 1046 (1964) 49
[4] BARDES,R.G., LANE,R.K., SAMPSON,J.B., TODT,L.J., Rep. GA 3069 (1962)
[5] BERRETH,J.R., SCHUMAN,R.P., Rep. WASH 1041 (1962) 37
[6] FEINER,F., Rep. KAPL 2000.16 (1961) I.3
[7] DAHLBERG,R., JIRLOW,K., JOHANSSON,E., J.Nucl.En. 14 (1961) 53
[8] JACKS,G.M., Rep. DP 608 (1961)
[9] WALKER,N.H., WESTCOTT,C.M., ALEXANDER,T.K., Can.J.Phy. 38 (1960) 57
[10] TATTERSALL,R.B., ROSE,H., PATTENDEN,S.K., JOWITT,D., Rep. AERE 2887 (1959)
[11] ROSE,H., COOPER,W.A., Actes 2ème Conf.Int. ONU sur UPEA (1958) P/14
[12] KLIMENTOV,V.B., Atomnaya Energiya 3 (1957)507, J.Nucl.En.9 (1959)20
[13] MACKLIN,R.L., Actes 1ère Conf.Int. ONU sur UPEA (1955) P/833
[14] SPYVACK,P.E., EROZOLIMSKY,B.G., Actes 1ère Conf.Int. ONU sur UPEA (1955)P659
[15] VIDAL,R., Rapport CEA R.2486 (1964)
[16] EASTWOOD,T.A., WERNER,R.D., Can.J.Phys. 41 (1963) 1263
[17] FEINER,F., ESCH,L.J., KAPL 2000.12 (1960) I.37
[18] JOHNSTON,F.J., HALPERIN,J., STOUGHTON,R.W., J.Nucl.En. 11 (1960) 95
[19] BAUMANN,N.P., Rep. DP 817 (1963)
[20] BENNETT,R.A., Rep. HW 68389 (1961) 50, Rep. HW 63576 (1960) 26
[21] HELLSTRAND,E., LINDAHL,G., LUNDGREN,G., Rep. AE 59 (1961)
[22] TATTERSALL,R.B., Rep. RPI 62 (1959)
[23] HONE, CRITOPH, Rep. RPI 59
[24] BECKURTS,K.H., BROSE,M., KNOCHE,M., PONITZ,W., Nucl.Sci.Eng. 17 (1963) 329
[25] BROWN,H.L.,Jr., CONNOLLY,T.J., FOELL,W.K., Trans.Am.Nucl.Soc. 5 2 (1962) 375
[26] NILSSON,R., Rep. RSA 47 (1960)
[27] BROWN,F., CAMPION,P.J., OLIVER,B.H., J.Nucl.En. 13 (1961) 141
[28] EILAND,H.M., FEHR,E.B., HANSEN,E.C., Rep. KAPL 2000.11 (1960) III.30
[29] SCOVILLE,J.J., ANL Newoletter n° 10
[30] FOELL,W.K., Rep. IDO 16986 (1965)
[31] HARDY,J., Nucl.Sci.Eng. 22 (1965) 121
[32] BROSE,M., Nucl.Sci.Eng. 19 (1964) 244
[33] TIREN,L.I., JENKINS,J.M., Rep. AEEW R 163 (1962)
[34] HELLSTRAND,E., LUNDGREN,G., Rep. AE 81 (1962)
[35] SCHUMAN, Nucl.Sci.Eng. 12 (1962) 519
[36] SCOVILLE,J.J., ROGERS,J.W., Rep. WASH 1056 (1965) 96
[37] SHER,R., LESAGE,L., CONNOLLY,T.J., BROWN,H.L., Trans.Am.Nucl. 9 1 (1966) 248
[38] FRENCH,R.L.D., BRADLEY,B., Nuclear Physics 65 (1965) 225
[39] BRUNE,D., JIRLOW,K., Nucl.Sci.Eng. 17 (1963) 350
[40] CABELL,M.J., Rep. AERE R.3647 (1961)
[41] CABELL,M.J., Rep. AERE R.3239 (1960)
[42] WERNER,R.D., EASTWOOD, T.A., Nucl.Sci.Eng. 21 (1965) 20
[43] LANTZ,P.M., BALDOCK,C.R., IDOM,L.E., Nucl.Sci.Eng. 20 (1964) 302
[44] LANTZ,P.M., Nucl.Sci.Eng. 13 (1962) 289
[45] Ce rapport

The Influence of Chemical Binding on Neutron-Cross-Sections at Higher Energies

K. Drittler
Institut für Reaktorphysik of the Gesellschaft für Kernenergieverwertung in Schiffbau und Schiffahrt mbH., Geesthacht, Federal Republic of Germany

I. Introduction

The scattering of thermal neutrons of chemically bound atoms is well known. But for atoms with heavier masses no investigations about the chemical binding effect at higher neutron energies could be found. The common opinion is that there is no effect above the neutron energy of a few eV. Unfortunately, most of the arguments which lead to this result are classical and they do not regard wave aspects. In order to get rough estimates some simple rules of quantum mechanics are used. From the width of Bragg reflexions follows that the coherence-length of the neutron is more than 10^4 wave-length units. However, at 100 eV it takes more than 10^{-13} sec for such a wave group (with the velocity of a classical neutron) to pass a fixed point. On the other hand, if neutrons are elastically scattered there will be an energy transfer to the target atoms. In the case of 100 eV neutrons scattering on free copper atoms, the target atom receives up to 6.3 eV, moving during the time of 10^{-13} sec a distance of up to 5 Å. Since the wave length of the neutron is 0.0286 Å there are in general interference effects due to the moving scattering centers

(similar to the scattering of thermal vibrating atoms). Since the threshold energy for the knock-off displacement of an atom is about 20 eV for noble metals*, there will be an influence of the binding forces on the cross-sections. Exact calculations have to use quantum mechanics and details of chemical binding. Therefore, a theoretical approach to the problem is made which leads to approximate formulae.

The results are discussed and some estimates are done for copper single crystals. Measurements on copper single crystals are presented and as far as possible compared with the theoretical result. Finally, the significance for reactor calculations is discussed.

II. Derivation of equations for the cross-section

The differential scattering cross-section of thermal neutrons is commonly calculated using the Born approximation tion. Since there are no restrictions in the magnitude of the neutron energy the Born approximation can be taken for the present purpose. Using the formalism of van Hove [2] the following expression gives the differential scattering cross-section:

$$\frac{\partial^2 \sigma}{\partial \vec{\Omega} \partial E} = |a|^2 \frac{1}{\hbar} \frac{k}{k_o} S(\vec{\kappa},\omega) \qquad (1)$$

where a is the scattering length.

If more than one type of atoms are present in the scattering substance, an average of $|a|^2$ is to be used. $\vec{k}_o$ and $E_o = \hbar^2 k_o^2/2m$ are respectively the wave number and energy of

---

* For references up to 1964 see [1].

the incident neutrons, and $\vec{k}$ and $E = \hbar^2 k^2/2m$ of the neutrons scattered in the direction of $\vec{\Omega}$. The change in wave vectors in a single collision is given bei $\vec{\kappa} = \vec{k}_o - \vec{k}$, and ω is defined as $\omega = (E_o - E)/\hbar$, where $\hbar$ is Planck's constant divided by 2π. The function $S(\vec{\kappa},\omega)$ is:

$$S(\vec{\kappa},\omega) = \frac{1}{2\pi} \int_{-\infty}^{+\infty} G(\vec{r}^*,t) \exp(i(\vec{\kappa}\vec{r}^* - \omega t))\, d\vec{r}^* dt \qquad (2)$$

where, for scattering which can be regarded as purely incoherent* (i.e. no Bragg reflexion and similar)

$$G(\vec{r}^*,t) = \delta(\vec{r}^* - \vec{r}(t)) \qquad (3)$$

In general the correlation function in space and time $G(\vec{r}^*,t)$ is an operator. However, under classical conditions, i.e. if quantum effects of the scattering atom can be neglected, this operator is reduced to a simple delta function.

We restrict ourselves to the scattering of substances in which the mass of the different atoms is nearly the same. Then the path of the scattered atom, $\vec{r}(t)$, after the collision is approximately the same for given energy and momentum transfer. If the average energy transfer is much larger than the average thermal energy, the thermal motion of the atom can be neglected. Therefore, no expectation value of the delta function is to be taken in equation (3). Inserting equations (3) and (2) into (1) one finds:

$$\frac{\partial^2 \sigma}{\partial \vec{\Omega}\, \partial E} = |a|^2 \frac{1}{\hbar} \frac{k}{k_o} \frac{1}{2\pi} \int_{-\infty}^{+\infty} \exp(i(\vec{\kappa}\vec{r}(t) - \omega t))\, dt \qquad (4)$$

Chemical binding effects on the differential cross-section are evident only on the behavior of $\vec{r}(t)$. Since the integral

---

* A derivation without this restriction will be published elsewhere. There are only slight changes.

in (4) is valid only for classical conditions, the function $\vec{r}(t)$ is like that of the classical model. Thus, the collision time is so short that the atom nearly remains stationary relative to the distances between atoms in the molecule or the lattice structure. If $\vec{K}$ is the binding force and M the mass of the atom, $\vec{r}(t)$ is the solution of Newton's equation:

$$M \frac{d^2\vec{r}}{dt^2} = \vec{K}(\vec{r}, \frac{d\vec{r}}{dt}, t) \qquad (5)$$

where the initial conditions can be found from the collision parameters;

$$\vec{r}(t) = \vec{r}_o = 0 \text{ at } t = 0 \qquad (6)$$

$$\frac{d\vec{r}(t)}{dt} = \vec{v}_o \qquad \text{at } t = 0 \qquad (6')$$

If we neglect thermal motion before the collision, all atoms are essentially at rest, i.e. at equilibrum positions, binding forces are equal to zero. Therefore, the collision <u>itself</u> is like the one between a neutron and a free atom. Since the scattering of neutrons on free atoms is elastic up to 100 keV, $d\vec{r}/dt$ at $t = 0$ has to be calculated from the energy and momentum transfer equations;

$$\left(\frac{d\vec{r}(0)}{dt}\right)^2 = \vec{v}_o^{\,2} = 2(E_o - E)/M \qquad (7)$$

$$\frac{d\vec{r}(0)}{dt} = \vec{v}_o = (\vec{k}_o - \vec{k})\hbar/M = \vec{\kappa}\hbar/M \qquad (8)$$

Inserting (8) into (4) one finds that;

$$\frac{\partial^2\sigma}{\partial\vec{\Omega}\,\partial E} = |a|^2 \frac{1}{\hbar}\frac{k}{k_o}\frac{1}{2\pi}\int_{-\infty}^{+\infty} \exp(i(\frac{M}{\hbar}\vec{v}_o\vec{r}(t) - \omega t))\, dt \qquad (9)$$

Equation (9) cannot be integrated in a close form, except in a few cases of no interest in this discussion. Therefore, an approximation of (9) will be derived. Rough estimates show that, generally, the argument of the exponential function in (9)"oscillates" very quickly. Thus, only if the argument is equal to zero the contribution to the value of the integral is of importance. Let $\vec{v} = d\vec{r}/dt$, and t_n be the values where the argument in (9) is equal to zero:

$$\frac{M}{\hbar}\vec{v}_o r(t_n) - \omega t_n = 0 \qquad (10)$$

$$(\omega = (E_o - E)/\hbar \text{ and } \vec{v}_o^{\,2} = 2(E_o - E)/M)$$

Then, the following equations give the linear expansions around t_n:

$$\frac{M}{\hbar}\vec{v}_o\vec{r}(t) - \omega t \approx \frac{M}{\hbar}\vec{v}_o\vec{v}(t_n)(t-t_n) - \omega(t-t_n) \qquad (11)$$

Inserting (11) into (9) and assuming that the argument in (9) "oscillates" very quickly between t_n and t_{n+1} we obtain integrals where the boundaries can be approximately made equal to $\pm\infty$. Since

$$\int_{-\infty}^{+\infty} \exp(iyt)dt = 2\pi\delta(y)$$

it follows that

$$\frac{\partial^2\sigma}{\partial\vec{\Omega}\partial E} = |a|^2 \frac{1}{\hbar}\frac{k}{k_o} \sum_n \delta\left(\frac{M}{\hbar}\vec{v}_o\vec{v}(t_n) - \omega\right) \qquad (12)$$

where the t_n are the solutions of equation (10).

When $t \to 0$, $\vec{r}(t) \to \vec{v}_o t$ and from (7) and (10) it follows that $t_o = 0$. Obviously this includes the case $E_o = E$ as a limit. Then, (12) becomes

$$\frac{\partial^2 \sigma}{\partial \vec{\Omega}\, \partial E} = |a|^2 \frac{1}{\hbar} \frac{k}{k_o} \left\{ \delta\left(\frac{1}{\hbar}(E_o - E)\right) + \sum_{t_n > 0} \delta\left(\frac{M}{h} \vec{v}_o \vec{v}(t_n) - \omega\right) \right\} \tag{13}$$

Since the collision between a neutron and an atom can be regarded as elastic, in this analysis, the energy of the neutron after the collision has a range from $E_o(1 - 4 \times m \times M/(m+M)^2)$ to E_o. Therefore, the total cross section is;

$$\sigma = 4\pi |a|^2 + |a|^2 \frac{1}{\hbar} \sum_{t_n > 0} \iint_{E_{min}}^{E_o} \sqrt{E/E_o}\, \delta\left(\frac{M}{\hbar} \vec{v}_o \vec{v}(t_n) - \omega\right) dE\, d\vec{\Omega} \tag{14}$$

$$E_{min} = E_o(1 - 4mM/(m+M)^2)$$

In sum, the proposed method for calculating cross-sections is as follows. $\vec{r}(t)$ is found from Newton's equation for a given binding force, with a given set of initial conditions.

Then, solutions t_n for the differential cross-section, with a zero complex argument, have to be determined. Finally these t_n values and the energy transfer equation are inserted into the rearranged expression for the differential or total cross-section.

For a free atom $\vec{r}(t)$ is equal to $\vec{v}_o t$. Equation (10) has no solution when $t_n > 0$, thus, arriving at the well known result: $\sigma_{free} = 4\pi |a|^2$. Therefore, the second term in (13) and (14) can be regarded as correction terms to account for the chemical binding effect.

III. General discussion of the formulae for the cross-section

From (10) it follows that;

$$\vec{v}_o\vec{r}(t_n)\frac{1}{t_n} = \frac{\hbar}{M}\omega \quad \text{for } t_n > 0 \tag{15}$$

For cross-sections which are not equal to that of free atoms the argument of the delta functions in (13) and (14) have to be equal to zero. Therefore, we have;

$$\vec{v}_o\vec{v}(t_n) = \frac{\hbar}{M}\omega \quad \text{for } t_n > 0 \tag{16}$$

A combined condition can be used in place of (15) and (16):

$$\vec{v}_o\left(\frac{\vec{r}(t_n)}{t_n} - \vec{v}(t_n)\right) = 0 \text{ for } t_n > 0 \tag{17}$$

If r^* and v^* denote the components of $\vec{r}$ and $\vec{v}$ in the direction of $\vec{v}_o$ we have that;

$$\frac{r^*(t_n)}{t_n} = v^*(t_n) \qquad \text{for } t_n > 0 \tag{18}$$

Since

$$\vec{r}(t) = \int_o^t \vec{v}(t)dt$$

equation (18) has a simple interpretation. The average value of $v^*(t)$ up to t_n has to be equal to $v^*(t_n)$ itself. Since $\vec{v} \to \vec{v}_o$ for $t \to 0$, $v^*(0) = |\vec{v}_o|$. Then, in the case of not free atoms, that is $v^*(t) \neq |\vec{v}_o|$, some values of $v^*(t)$ must be larger and smaller than $v^*(t_n)$, (Fig. 1). Except for special cases, such behavior of a collided atom, is the result of two modes of movement.

The first one is that for $0 \leqslant t \leqslant t_n$, in which there is a relative large back and forth movement of the atom, perpendicular to the direction of $\vec{v}_o$. (For an example see section IV and Fig. 2.) The other mode arises when there is no movement perpendicular to the direction of $\vec{v}_o$, in which case the binding-force can be well described by a potential U (non-conservative forces are neglected). Then, from the energy transfer equation we have;

$$\frac{M}{2}\vec{v}^{\,2} = \frac{M}{2}v^{*2} = E_o - E - U(\vec{r}(t_n)) - U(0)$$

In order to get values of v^* which are larger and smaller than $v^*(t_n)$ the potential U must have at least one maximum and one minimum for $t \leqslant t_n$.

Neither case of movement is done by an isotropic and harmonic oscillator.

Equation (16), as second condition, has also a simple interpretation when a potential U is used. Let Θ denote the angle between the direction of $\vec{v}_o$ and $\vec{v}$, and insert (7) and $\omega = (E_o - E)/\hbar$ into (16), then;

$$2\sqrt{E_o - E}\sqrt{E_o - E - U(\vec{r}(t_n)) + U(0)} \times \cos\Theta = E_o - E \qquad (19)$$

Solutions of this equation for $E \neq E_o$ are obtained from

$$U(\vec{r}(t_n)) - U(0) = (1 - 1/(4\cos^2\Theta))(E_o - E) \qquad (20)$$

The interpretation of (20) is that at time t_n the atom has to be at a position, $\vec{r}_n = \vec{r}(t_n)$, where the potential is $1 - 1/(4\cos^2\Theta)$ times the total transferred energy.

IV. Application of the cross-section formulae on copper crystals

Calculated cross-sections of single crystals do not need to be averaged over the direction of the incident neutrons in order to be compared with experimental cross-sections. That is one of the reasons why single crystals are used to study the predicted effects. The present knowledge about the binding forces is not sufficient for accurate calculations of cross-sections, and so only some estimates are given in this section.

Copper was chosen because some of the details of the binding forces are better known than for other metals. J.B. Gibson et al. [3] have calculated the threshold value of the kinetic energy of knock-off atoms. Since these results compare reasonably with experiments ([4], [5], references up to 1964 in [1]), some estimates can be made from the expression used for the binding forces. An atom at the position zero has the potential;

$$U(R) = A \times \exp(-R/c) \qquad (23)$$

with respect to another atom at a distance R. In (23), $A \sim 22500$ eV, and $c \sim 0.2$ Å when U and R have the dimensions eV and Å.

Copper crystals have a face centered cubic structure. A collided atom leaving the twelve nearest neighbour atoms, i.e. getting over the first maximum of the potential, must have a certain energy transfer ΔE_{min}. Assuming that the neighbour atoms are at rest we have

$$\Delta E_{min}(\langle 100 \rangle) = 5 \text{ eV} \qquad [1] \qquad (24)$$

that is the smallest value of ΔE_{min}.

From the energy and momentum transfer equation, (7) and (8), for a given energy transfer $\Delta E = E_o - E$ in the case $m \ll M$, it follows that;

$$E_o = \Delta E \times M/(4 m \cos^2 \vartheta) \tag{25}$$

where ϑ is the angle between the directions of the incident neutron and the outgoing atom. If ΔE is only slightly larger than ΔE_{min}, the conditions discussed in section II can be fulfilled beyond the maximum of the potential.

Some examples are given here. The incident direction of the neutron is $\langle 110 \rangle$ or $\langle 111 \rangle$ and the outgoing direction of the collided atom $\langle 100 \rangle$. The symmetry implies that in (20) $\cos\Theta = 1$. Then from (24) and (25) it follows that;

$$\begin{aligned} E_o &\sim 160 \text{ eV for } \langle 110 \rangle \\ E_o &\sim 240 \text{ eV for } \langle 111 \rangle \end{aligned} \tag{26}$$

If the behavior of the outgoing atom near $\langle 100 \rangle$ is approximately the same as in $\langle 100 \rangle$, i.e. within a discrete solid angle, there should be a peak in the cross-section curve at values of E_o given in (26). Similar behavior is observed in the $\langle 111 \rangle$ direction of the outgoing atom, where $\Delta E_{min} = 25$ eV. Then, there would be peaks at

$$\begin{aligned} E_o &\sim 600 \text{ eV for } \langle 110 \rangle \\ E_o &\sim 400 \text{ eV and } 1200 \text{ eV for } \langle 111 \rangle \end{aligned} \tag{27}$$

The potential in (23) neglects the interaction of the electron shells of the atoms (mainly the d-shells). This can lead to peaks in the cross-section curve below 100 eV.

Peaks in the total cross-section curve also occur when the back and forth movement is perpendicular to the direction of $\vec{v}_o$, as described in section III; obviously in this way there could be many peaks. One of the simplest examples of this mode is the movement of an atom towards two other atoms, (for a case where there is only movement in one plane see Fig. 2). It is apparent that there is only a discrete set of directions in which such movements can happen.

V. Experiments

If we restrict ourselves to incident neutron energies above a few eV, the average transferred energy is much larger than the thermal energy. Therefore, unlike the thermal region, there is only a very weak temperature effect. (C.F. section II.) Experiments with gases of noble metals and other materials which are crystalline at room temperature, are very difficult to carry out. The cross-sections of single crystals are in general functions of the direction of the incident neutrons. Therefore, one of the best ways of proving the predicted effects is by comparing the cross-sections measured at different directions for incident neutrons. Instead of the cross-section one can use the transmission-ratio, which is defined as the ratio of the counting rate of neutrons with scattering substance to that without it, at the same conditions. Let D denote the thickness of the sample: Then for the transmission ratio T* we have;

$$T^* = \exp(-D\sigma) \qquad (28)$$

Transmission ratios for copper single crystals (99.999 % Cu) were measured with the fast chopper at the reactor

station Geesthacht*. The direction of the incident neutrons were ⟨110⟩ and ⟨111⟩. (The angular deviation was ± 8 degrees.) In order to reduce the statistical error an average value of the transmission ratio for the channel i of the multi-analyzer was plotted in Fig. 3. That is possible because of the large resolution, compared to the distance between two channels. This average value T was calculated from the following equation;

$$T(i) = \frac{1}{16}(4T^*(i)+3(T^*(i+1)+T^*(i-1))+2(T^*(i+2)+T^*(i-2)) +T^*(i+3)+T^*(i-3)) \qquad (29)$$

The peaks of the cross-section curves become valleys in the transmission ratio curves. In Fig. 3 there are valleys due to resonances at about the following value of E_o: 227 eV, 580 eV and 1980 eV [7]. Inspite of the fact that the statistical error is relatively large it is apparent that there are many valleys not due to Bragg reflexions, in addition to the resonance valleys. From the Bragg equation and the equation for the neutron wave length it follows that the maxima of the Bragg reflexions are at values E* given by the equation

$$E^* = 8.2\times10^{-2}(h^2+k^2+l^2)/(4a_o^{\,2}\sin^2\alpha) \text{ eV} \qquad (30)$$

Here, h, k, and l are the Miller indices of the reflecting plain, a_o is the lattice constant in Å, and α is the scattering angle. Since in the chopper $2\alpha = 5\times10^{-3}$ disturbance of Bragg reflexions is not possible

---

* Measurements were performed by the chopper group of the Institut für Reine und Angewandte Kernphysik, Universität Kiel, under the direction of Dipl.-Phys. H.H. Jung and Dr. W. Biel. Details of the experiments will be published elsewhere.

beneath 500 eV. Above this value the maxima of the Bragg reflexions are relatively narrow and the valleys are "smeared" over a large region. Therefore, the valleys in the curves of Fig. 3 are most probably due to the effects described in sections III and IV, except for those which are resonances. Estimates show that the height of the peaks in the cross-sections is up to 2 barn. (The cross-section of copper beneath the resonance region is about 8 barn.)

The locations for valleys predicted in (26) and (27) correspond to locations of valleys in the curve of Fig. 3. In the case of 240 eV and 600 eV the resonance valleys are shifted and slightly increased. A certain separation of effects due to the chemical binding forces from those due to the interactions between neutrons and nuclei can be obtained by plotting the ratio of the transmission ratios. (See Fig. 4, lower curve). If the binding forces are isotropic or if there are only neutron-nucleus interactions there is only a constant value within the statistical error. The locations of valleys predicted in (26) and (27) are thus better recognized. The upper curve in Fig. 4 is from an early measurement [8]. Here, only the neutron counting rates with scattering substance were measured. The plotted ratio of the counting rates is averaged, like T* in (29). (The resolution of the chopper was not as accurate as in the lower curve.) Therefore, only maxima and minima can be compared; all those in the upper curve can be found in the lower curve. However, in the lower curve there are some additional peaks, which may be due to larger deviations of the ⟨110⟩ and ⟨111⟩ directions. (The angular deviation in the upper curve was

± 3 degrees.) Then, a peak may be splitted because the transferred energy depends on the angle between the directions of the incident neutron and the outgoing atom, as described in (25).

VI. The significance of these effects for reactor calculations

As described in sections IV and V, the location of a cross-section peak due to chemical binding, in single crystals, depends on crystallographic orientation. Therefore, the cross-section of polycrystalline substances as an average over all orientations do not have such peaks. They are "smeared" over a broad region. In the case of copper, estimates show that this region is larger than the distances between neighbouring peaks. Then, the total cross-section curve is smooth, but greater than that of free atoms. In order to get the absolute value of the scattering length from measurements of the cross-section, as a nuclear parameter, corrections have to be evaluated. For reactor calculations corrections are not needed when the material under study is used as reactor material, except when the chemical binding conditions are different. But at the present, there is no quantitative estimate of these corrections.

VII. Conclusion

From the presented theory and from the reported experiments it can be concluded that with great probability there is an influence of the chemical binding on

neutron cross-sections at energies above a few eV. That is in contradiction with the common opinion. However, the presented results have consequences for reactor calculations and for nuclear physics. Therefore, further investigations should be pursued.

Acknowledgements

The author wishes to thank Prof. Dr. E. Bagge, Prof. Dr. E. Fischer and Dr. D. Bünemann for their interest in this work and Dipl.-Phys. H.H. Jung, Dr. W. Biel, and the chopper group for performing the measurements. The assistance in the preparation of this paper by Dipl.-Phys. A. Mendez is acknowledged.

References

[1] LEIBFRIED, G., Bestrahlungseffekte in Festkörpern, Teubner, Stuttgart (1965).

[2] VAN HOVE, L., Phys.Rev. 95 1 (1954) 249.

[3] GIBSON, J.B., GOLAND, A.N., MILGRAM, M., VINEYARD, G.H., Phys.Rev. 120 4 (1960) 1229.

[4] KAMADA, K., et al., phys.stat.sol. 7 (1964) 231.

[5] WOLLENBERGER, H., WURM, J.,phys.stat.sol. 9 (1965) 601.

[6] DRITTLER, K., Atomkernenergie, in print.

[7] HUGHES, D.J., SCHWARTZ, R.B., BNL 325 (1958).

[8] DRITTLER, K., Atomkernenergie, in print.

August 9th, 1966

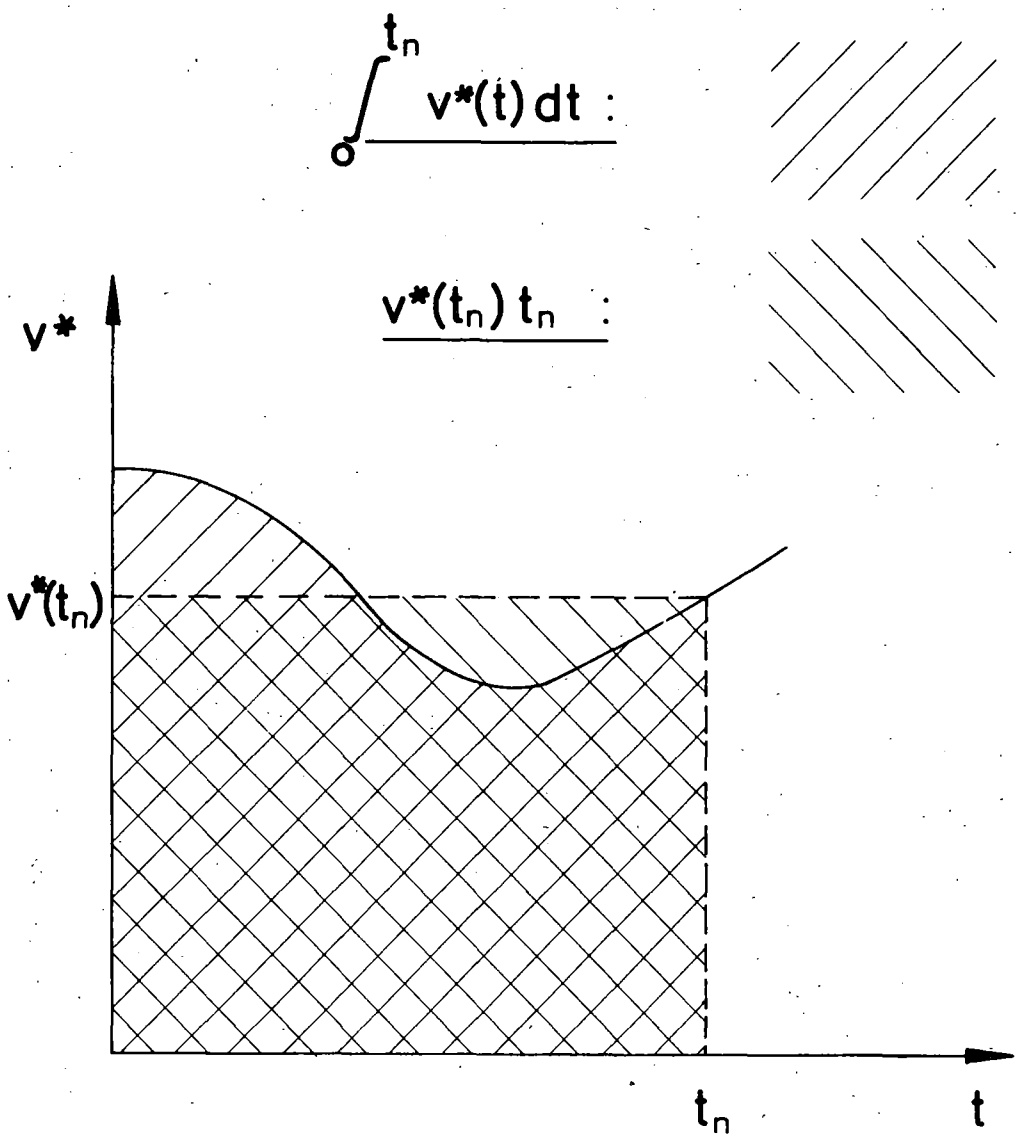

Fig. 1

Component v* of the velocity of the collided atom in the direction of the movement just after the collision plotted against time t (schematically). If the two different shadowed areas are equal, one of the conditions for increasing the cross-section is fulfilled.

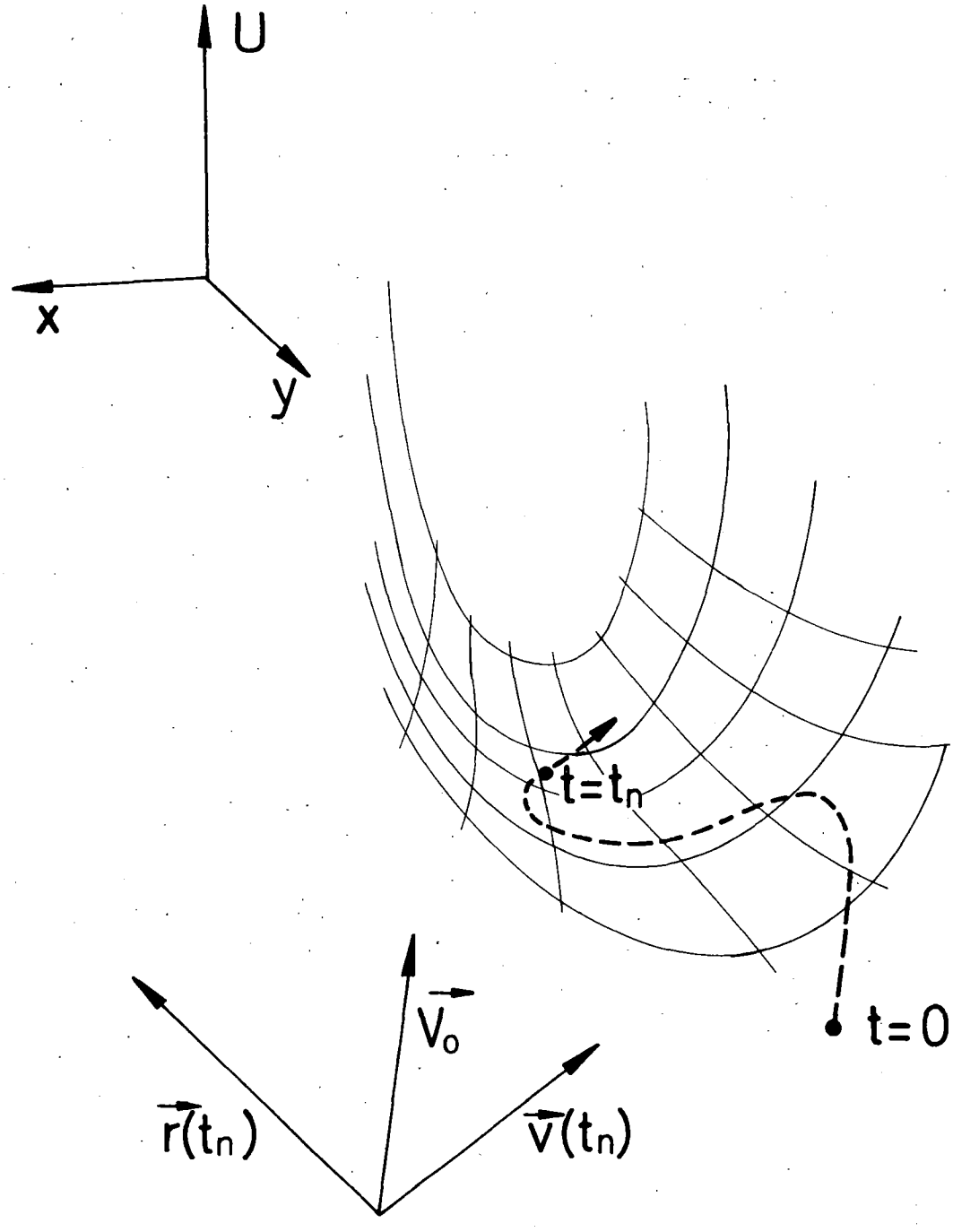

Fig. 2

A two dimensional example of the movement of a collided atom in a potential U (schematically). If certain quantitative conditions are fulfilled a larger cross-section is obtained.

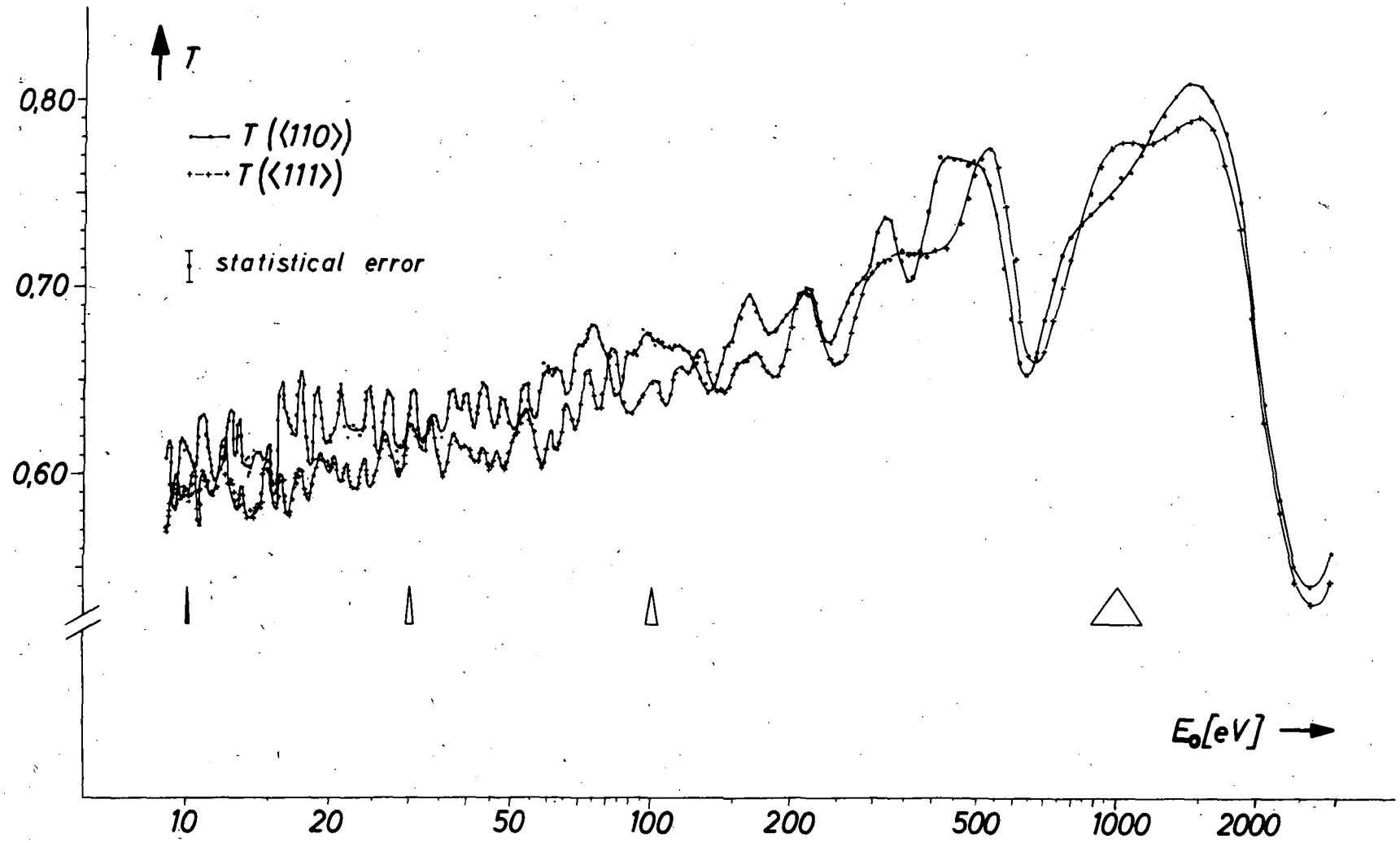

Fig. 3

Transmission ratios, T, of copper single crystals plotted against the energy of the incident neutrons, E_o. The incident directions are ⟨110⟩ and ⟨111⟩. The triangles indicate the resolution of the chopper.

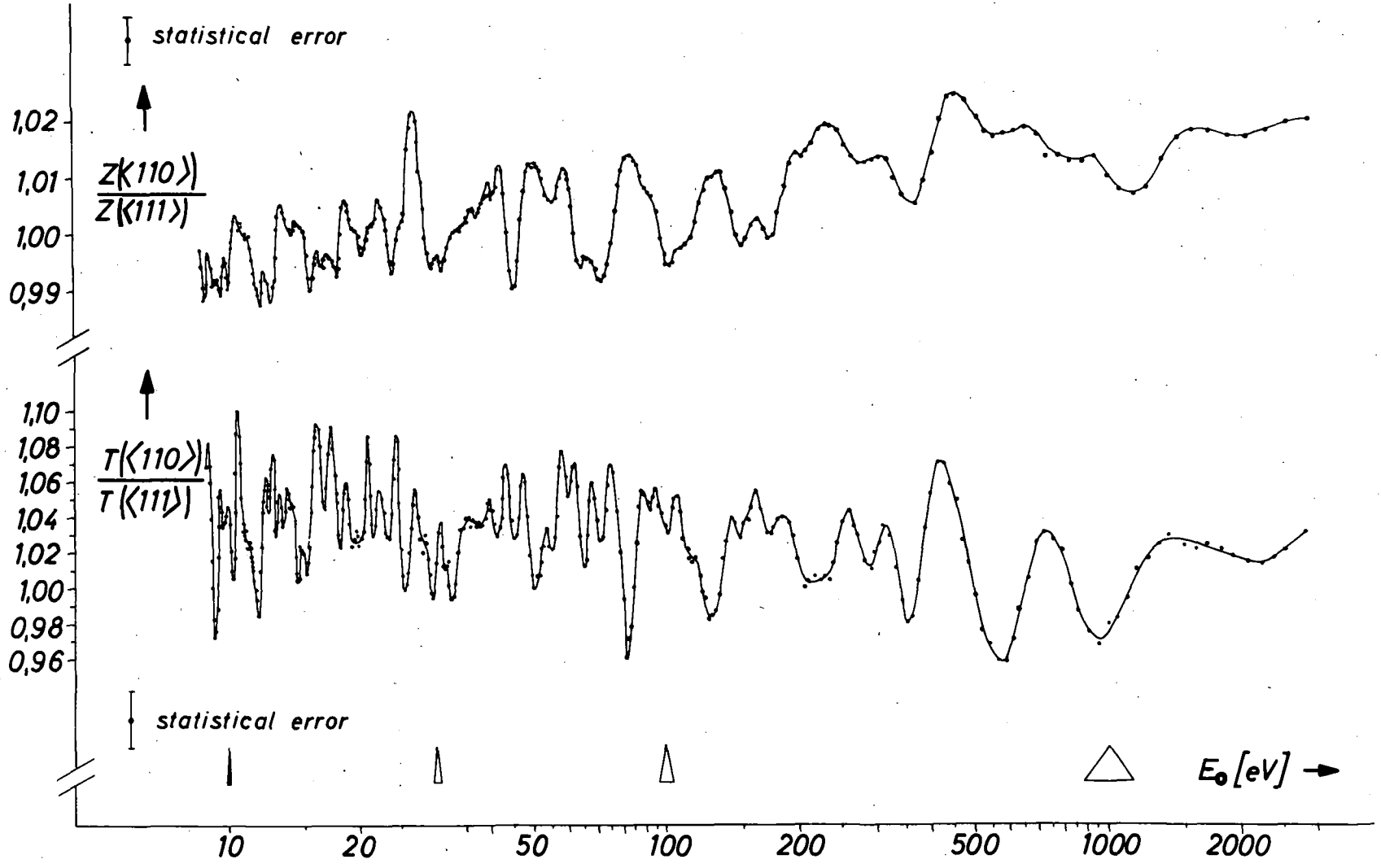

Fig. 4

Early measurement of the neutron counting ratios (upper curve), and ratios of the transmission ratios for copper single crystals plotted against the energy of the incident neutrons. The triangles indicate the resolution of the chopper.

THE ROLE OF ISOTOPIC COMPOSITION MEASUREMENTS IN CROSS SECTION EVALUATION

P. G. Aline
General Electric Company
Atomic Power Equipment Department
San Jose, California
June 6, 1966

ABSTRACT

The use of operating power reactor data rather than laboratory measurements to test the adequacy of cross section evaluations is described. Isotopic composition measurements from exposed fuel, test data in an environment not readily accessible in the laboratory, but under conditions which the data and methods must simulate. The significance and impact on data compilation is discussed.

INTRODUCTION

The purpose of this paper is to demonstrate how isotopic composition measurements, made on fuel irradiated in operating power reactors, have provided a valuable input to define the most accurate set of evaluated cross sections for reactor design application. The sensitivity of isotopic compositions to small differences in evaluated cross sections results in significant uncertainties in the predicted fuel cycle economics for the nuclear power industry. This great sensitivity of fuel cycle costs to predicted isotopic compositions places considerable emphasis on development of analytical models and data for precise prediction of power reactor performance.

The term "evaluated cross sections" in this paper refers to cross sections evaluated on the basis of integral measurements using a given model. Evaluators and users of such data have in the past established the validity of a cross section compilation by analysis of resonance integral measurements [1] and critical experiments [2]. This type of approach is being followed more frequently as data and methods become more accurate [3, 4] . Experimental data obtained from operating power reactors can provide a more sensitive test of the adequacy of cross section sets than the above approaches. As long-term irradiation of power reactor fuel continues, a large volume of data is becoming available which provides a good statistical sample to evaluate cross section data.

It is necessary to define the meaning of evaluator, evaluated data, and basic nuclear data to clarify the significance of isotopic composition measurements and put

them in proper perspective. An evaluator of basic nuclear data determines the most probable value of basic nuclear data by reviewing the experimental measurement techniques and selecting the "best" current data by weighting the experiments and using various fitting procedures such as least squares. This is independent of the application for which the resulting data may be used. Evaluated reactor cross sections are developed utilizing critical experiments, resonance integral measurements as well as evaluated basic nuclear data with an interest in the practical application to which the data are to be used. Hence, evaluated cross sections as used here refer to the best data to most precisely calculate a desired quantity. If the evaluation does not provide the user with data which will predict reality most precisely, then the user will empirically determine the best set of data which agrees with operating experience. Evaluators must point out why such alteration may not be justified and provide the user with what he needs. An important test of cross section sets may rest on using experimental data obtained from operating reactors, where a large portion of evaluated data in conjunction with design methods will eventually be used. Because these cross sections influence reactor design so significantly, it is important to have feedback from the interpretation of such experiments and for evaluation work. The difference of degree in such definitions may very well be unnecessary due to the automated processing of experimental data, least-squares fitting, weighting experimental results, and the improvement in methods which utilize such data. In the past, one had to distinguish between the "best" theory and simpler design models which were frequently called theory [5] . With today's automated computer capability, there is no clear boundary between the two classes. The application of both basic data and evaluated data in practice is primarily for nuclear energy associated programs. The purpose of cross sections in daily use is to design reactors of various types, optimize fuel cycle economics, and to indicate differences between reactor types.

The determination of cross section sets for use in the design of large commercial power reactors cannot be made completely independent of other considerations such as models and data accuracy, computer costs, and composite evaluation trends. Predictions of isotopic compositions in fuel discharged from operating reactors are sensitive to small differences in cross sections. Thus, the cross sections utilized have a significant impact on the predicted economics for the nuclear industry. Isotopic composition measurements provide more sensitive information about relative reaction rates, for various cross sections covering a wider range of conditions which actually occur in a reactor, than are available in the laboratory from critical experiments and resonance integral measurements. A large amount of isotopic information is accumulating for cross section ratio evaluation, while similar data from critical experiments or activation measurements covering this wide a range of conditions would be very expensive to develop. Critical experiments provide information on eta [6] . Analysis of such experiments should clarify the wide differences in the value of nu for U-235 which has varied from 2.385 [7] to a value a few years ago of 2.47 [8] . Another area of concern to evaluators and users alike is the differences in alpha values obtained by resonance integral measurements and basic cross section data [9] . This difference is even more perplexing when the evaluator must advise the user of how alpha changes with concentration, as it does in actual practice. Measurements with varying concentration or shielding are not available. Precise measurements with varying fissile concentration and geometry to account for shielding are necessary to reduce such uncertainties. Isotopic measurements help to indicate what epithermal data are significant when used in design models.

The sensitivity of results and conclusions obviously depends upon the analytical models chosen for such a study. To obtain precise agreement with isotopic measurements, it has been demonstrated that space-dependent thermalization with transport or Monte Carlo solutions are necessary [10] . Typical analytical methods [11] are used to test the relative adequacy of cross section sets for use in such models for

reactor design. To infer significant trends, consistent data and models are used to test cross section compilations for differences between measurement and analysis for data from reactors [12, 13, 14] .

PROCEDURES TO VERIFY CROSS SECTION EVALUATIONS

CRITICAL EXPERIMENTS

Critical experiments have been used to measure eta as well as to test evaluated cross section sets. Homogeneous critical experiments that provide valid data for eta of U-235 are not sufficient for eta of Pu-239 because of spectral and leakage corrections [15] . A comparison of experiment and analysis is given in Table I for two sets of data described more fully below. Heterogeneous critical experiments add the complication of geometrical effects and of fertile material such as U-238 or Th-232. It has been found that predictions of criticals are more sensitive to variations of fertile material reaction rates than fissile reaction rates [16] . The sensitivity of calculational results to different 2200 m/s cross section data for plutonium criticals [17] has been often demonstrated [2, 16] . As is evident from these comparisons only eta of Pu-239 can be selected even though different methods do not appreciably affect the conclusions.

RESONANCE INTEGRAL AND EPITHERMAL ALPHA EXPERIMENTS

Experiments to measure the epicadmium to subcadmium capture are performed in a less controlled environment than reactivity measurements in critical experiments because of: (1) perturbations caused by cadmium, (2) sensitivity to definition of cutoff, (3) uncertainty in spectrum, and (4) unknown high energy contributions. Nonetheless, evaluators rely on such data to test cross section compilations to determine their usefulness. It is possible to develop a cross section set which agrees with resonance integral data but does not agree with total activation measurements due to these unknowns. For instance, the cross section near the cadmium cutoff may be large and contribute significantly to the dilute integral because this is where the cadium has its major influence. The high energy contribution to the U-238 infinite dilute resonance integral is about 4b [18] which is small compared to the total of 270b. However, this is large when one considers an effective resonance integral of 20b in practical situations. Thus, the role of epicadmium measurements, even though useful, is limited for practical selection of cross section data.

ISOTOPIC COMPOSITION MEASUREMENTS

The term isotopic composition measurement refers to the determination of the atom concentration of the heavy isotopes present in irradiated fuel by the mass spectrometric method.

Accuracy of Measurements

The accuracy with which the isotopic content of a particular isotope can be determined is dependent on the abundance of that isotope, with about ± 0.5 percent for the higher concentration isotopes, to about 3 percent for isotopes having an atom fraction of 0.0001. Obtaining experimental isotopic composition data involves four types of

measurements. These measurements are listed below with their associated experimental uncertainties (one standard deviation) [19] .

Ratios of plutonium isotopic concentrations	±1%
Ratios of the isotopes of uranium	±1%
Determination of the Pu/U ratio	±0.8%
Determination of the concentration of burnup indicators	±1%

Since the experimental data are obtained from operating reactors, they possess the advantage of being associated with the actual reactor neutron spectrum. These data provide a means of directly testing methods and data under conditions not easily obtainable in laboratory mock-up experiments. Isotopic composition measurements are primarily aimed at obtaining experimental data to test analytical methods and evaluate effective microscopic cross sections for light water reactors. It has been found that analytical simplifications used in early analysis and basic cross section uncertainties for the higher plutonium isotopes account for many of the discrepancies between the large body of measured data presently available and the calculations [12].

The advantage of this type of measurement lies in the amount of data obtained for different isotopes at the same location under similar conditions. The magnitude of the concentration of one isotope relative to another will change with fuel irradiation and, hence, the significance of the production, fission, and capture process for that isotope will vary. The contribution to the total activation of thermal and epithermal capture will change as a function of concentration due to resonance self-shielding as in Pu-240. The sensitivity of the thermal and epithermal cross sections will thus change and may provide a sensitive test of cross section information. The usefulness of isotopic composition measurements made on fuel irradiated in operating reactors to determine the adequacy of evaluated cross sections lies in the relative reaction rates of all isotopes present. This reduces the possibility of systematic differences in experimental data for cross sections, made on various different samples and under various conditions. A vast amount of data for a wide range of conditions provides a statistically significant sample which exists for cross section evaluation. This ever increasing statistical sample provides a more sensitive test of relative reaction rates under less controlled conditions than those available in a laboratory but over a greater range of conditions than available in laboratory experiments. Similar data spanning this wide range of conditions and concentrations would be very expensive to obtain in controlled laboratory experiments.

Sensitivity to Cross Section Data

In reactor design the interplay between cross sections and methods is important. If methods and data are changed too often, their accuracy is likely to be unknown. If they are not changed when apparently better data or methods are available, economic penalties may ensue. To measure areas where changes in data appeared valid, a study was made of the sensitivity of isotopic compositions to changes in cross sections with a constant analytical method. A few of the results will be indicated here to demonstrate the testing procedure used for cross section changes.

In a light water reactor the ratio of thermal reaction rate to epithermal is different for different isotopes as shown in Table II.

These differences change a little depending on the isotopic composition and the water-to-fuel ratio. They do, however, give an indication of what energy region will be most sensitive to cross section improvements.

The sensitivity of isotopic composition measurement of U-235 for various exposures and epithermal fission rates is given in Table III. There is a difference of

about 2 percent in the composition of U-235 for epithermal fission data which reproduces measured cadmium ratios (295b) and the measured fission integral (270b). The isotopic composition can be as much as 6 percent larger if the self shielding of resonances and corrections for cadmium cutoffs are considered. The sensitivity of isotopic composition for Pu-240 and Pu-241 for changes in resonance data for Pu-239 is shown in Table III. In this instance the Pu-240 and Pu-241 are more sensitive at low exposures where the data should be compared to isotopic measurements. Resonance absorption data for Pu-242 have been relatively scarce as compared to other plutonium isotopes. Isotopic composition measurements for fuel containing detectable amounts of Pu-242 are now becoming available. In Table III the marked difference occurring when a major change in data takes place is indicated. The uncertainty in the Pu-242 epithermal and thermal cross sections in relation to isotopic measurements will be considered in the following paragraphs.

The influence on isotopic compositions for different published values of plutonium data in the thermal region is given in Table IV. The decrease in alpha of Pu-239 from 0.389 [2] to 0.358 [20] has its major influence on the isotopes heavier than Pu-239. The increased thermal absorption rate for a change in the Pu-240 cross section from 265b to 286b leads to decreased Pu-240 and increased composition for isotopes heavier than Pu-240. Decreasing the thermal Pu-242 cross section from 30b to 18.6b has a negligible effect on Pu-242 and Cm-242 because the epithermal contribution of Pu-242 is dominant as shown in Table II. Finally, the consistent set of 2200 m/s data is compared in Table IV to indicate the sensitivity of isotopic compositions to changes in these parameters. Some of the differences are negligible compared with uncertainties in isotopic composition measurements. Others are sufficiently different to help select a cross section set for practical application. Sets II [1, 20] and III [21] are much closer together than that indicated for Set I [2, 22]. Sets I and II will be compared to measurements in the following paragraphs.

USE OF ISOTOPIC COMPOSITION MEASUREMENTS

Isotopic composition measurements have improved in accuracy over the last several years and in addition measurements of americium, curium, and Np-237 [23] are available. The early comparisons of isotopic compositions indicated quite large uncertainty in the measurements and appreciable scatter in the data. However, useful information was obtained as reviewed in the following paragraphs [12] .

Since the rate of change of Pu-239 concentration may be expressed as a difference between U-238 capture rate and Pu-239 absorption rate, an error in the Pu-239/U-238 atom ratio may be associated with reactor effective values of Pu-239 absorption cross sections and U-238 capture cross sections. At extended exposures of about 10,000 MWd/T the Pu-239 is very close to its equilibrium concentration and thus a measure of the 49/28 atom ratio is a direct measure of the effective 49/28 cross section ratio. If the experiment is conducted at low exposures (0-300 MWd/T), then the loss term due to Pu-239 absorption may be neglected and the 49/28 atom ratio is only a function of the effective U-238 capture cross section and exposure level. This type of approach provides a check of the effective capture cross section of U-238 before inferring other information about cross section ratios.

By using such a procedure it was found that the U-238 capture rate was calculated 5 percent too low in relation to the isotopic data. This was traced to the lack of the high energy contribution in U-238 capture [17] . For exposure ranges above 1000 MWd/T an error in the Pu-239 absorption cross section materially affects the computed 49/28 atom ratio. This is because the destruction rate of Pu-239 due to neutron absorption is approximately one-half as great as the formation rate through U-238 capture. Although the absorption cross section at 2200 m/s for Pu-239 is known quite accurately, the effective cross section at energies above this are not well

verified. In considering the formation of Pu-240 at exposures around 3500 MWd/T the formation rate is four times greater than the destruction rate. Thus, when measured and computed 40/49 isotope ratios are compared at a given exposure the accuracy of the comparison between experiment and analysis may be principally due to the accuracy of the effective Pu-239 capture cross section. Using the data in Set I for fuel irradiated in the Vallecitos Boiling Water Reactor (VBWR) the mean relative difference for 20 samples between measured data and the analysis is 2 percent low. Analysis of the fuel irradiated in the Dresden reactor using 40 samples shows a mean relative difference of 15 percent, the calculations being higher than the measured data [12] .

Similar to the Pu-240, the Pu-241 is produced at a rate approximately four times greater than its destruction rate at about 3500 MWd/T. Thus, since the Pu-241 is essentially only made and not destroyed, an error in the computed 41/40 atom ratio can be assigned to an error in the Pu-240 effective cross section. The calculations tend to underpredict the 41/40 isotopic ratio by approximately 20 percent in the VBWR and 35 percent in the Dresden reactor [12] . The use of more precise cross section data for Pu-240 significantly reduces this error. The calculated 42/41 atom ratio is overpredicted by 20 to 25 percent. This discrepancy is most probably due to the effective capture cross section of Pu-241 being too large and influences the 41/40 ratio [12] . At low exposure levels the Pu-242 has a production rate 14 times greater than its destruction rate and, thus, the difference in the 42/41 atom ratio may be assigned to errors in the effective capture cross section of Pu-241. At high exposure both cross sections are important. These differences stimulated a review of cross section data which made significant improvement between theory and experiment.

The use of these isotopic composition measurements indicated a change was necessary in the value of alpha for Pu-239 [2] . Prior to changing the capture cross section from 293b to 282b, the computed plutonium atom concentrations were low compared to measurement. This change corresponded to a Pu-239 fission cross section change from 715b to 726b. After changing the cross sections in 1962, about one-half of the data points were higher and one-half were lower than computed. In Table V is shown mean square error defined as $\sqrt{\Sigma Xi/n}$) where Xi is (measured-computed)/ computed for the twenty data points [12] .

As fuel exposures increased above a few thousand MWd/T, increased accuracy in the measurements of isotopic compositions of the higher isotopes became possible. Improved techniques in mass spectrometric analysis also were developed. These more recent isotopic composition measurements were used to test the selection of new cross section compilations described under the discussion of sensitivity to cross section differences. All of the changes in data were included to test the composite effect. Set I [2, 22] is based on analysis of plutonium- and uranium-fueled criticals as well as resonance integral comparisons. Set II [1, 20] is based on more recent cross section compilations. The comparison between measurement and calculation for isotopic composition is shown in Table VI. As previously indicated (Table I) comparison with criticals favors Set I. This situation is quite different, however, when recent isotopic measurements from several light water reactors are considered in the evaluation process. Set II shows a decided improvement in the agreement between experiment and analysis for isotopic compositions of 1.5-percent-enriched boiling water reactor fuel irradiated in a 20 percent voided location to a local exposure of 12,000 MWd/T. The comparison shown in Table VI is for a representative sampling having the last three isotopics available. The general agreement is similar to that shown when 60 recent samples are considered. The original 40 samples [12] are being remeasured with the more accurate mass spectrometric techniques now available. The comparisons with criticals show slightly poorer agreement, but only eta is tested in the critical comparisons.

It would appear that the compositions at other exposures should be used to test the cross sections for Np-237 which is produced by an (n,γ) reaction in U-236. The accuracy of Np-237 production in power reactors is well predicted. The cross

section data for Am-243 and Cm-244 apparently is not accurate enough, even though at these low concentrations the differences are primarily due to the production rate. The Am-243 is produced by beta decay from Pu-243. Uncertainties in the Am-243 data may be due to uncertainties in Pu-242 absorption cross section being too low and not producing sufficient Pu-243 to beta decay to Am-243. Likewise, Cm-244 is produced from beta decay of Am-244. Thus, an error in the Cm-244 production rate due to an absorption cross section of Am-243 which is too small, is a likely possibility. Further analysis is needed to establish the magnitude of these necessary changes.

CROSS SECTIONS FOR REACTOR DESIGN

The reactor designer needs to obtain from evaluations the most probable values of $\sigma_t, \sigma_s, \sigma_a, \sigma_f, \sigma_c, \eta, \nu$, and α. These are necessary to determine: (1) isotopic composition, (2) local and gross power distributions, (3) reactivity, and (4) coefficients of various types. In the past, different empirical sets of cross sections and methods were used for different reactor types. With the advent of large, high-speed computers and more sophisticated computational techniques the reactor designer has need for more cross section information. The development of accurate design models for light water reactors has reached the point at which data uncertainties are a major limitation to practical applications [24] . However, more compilations and cross section libraries are not what is necessary. More precise data without sysematic unknowns are necessary. The feedback from user to evaluator to determine the adequacy of evaluated data is desirable. The testing of evaluated data prior to its release provides for greater confidence by the users to adopt the more fundamental cross section evaluations and discard the many scores of empirically determined cross section sets in use today.

Isotopic composition measurements provide a sensitive test of cross section compilations where the low U-235 initial concentration emphasizes the influence of the plutonium isotopes. In this case, the U-235 atom fraction discharged is about 0.6 percent and the fissile plutonium is about 0.4 percent. This leads to a greater utilization of the plutonium produced and more sensitivity to cross section ratios. One advantage or disadvantage is the void variation which changes the spectrum and provides a test of the energy dependence of the cross section. The sensitivity to differences in plutonium and U-235 fission rates is much less pronounced when higher initial enrichments are used. For plutonium recycle fuel, which has an initial amount of plutonium, the change in isotopic composition is less pronounced. Thus, the BWR fuel isotopic composition measurements can provide particularly useful information to arrive at a usuable evaluated compilation.

CONCLUSIONS

If cross section evaluating is to be kept in proper perspective, the evaluation process cannot be considered independently of the cross section applications. The use of only critical experiments or resonance integrals to test an evaluated set of data and models is not sufficient to arrive at the best set for general application. Ratios of reaction rates, inferred from isotopic composition measurements, should be included. For light water power reactor design application, as for other reactor types, the intereaction between cross section data uncertainties and approximations used in the models is sufficient to significantly affect final results and conclusions. For these reasons, it is important to make use of all sources of data, including data from operating power reactors, to select evaluated cross section sets for general use in reactor design calculations. Such cooperation between users and evaluators will highlight deficiencies in methods used in applying the data and in the evaluated data itself. This would indicate when better analytical methods were needed and what additional cross section measurements were necessary for the evaluations process.

TABLE I

COMPARISON BETWEEN MEASUREMENTS AND CALCULATIONS OF REACTIVITY

	Experiment	Set I	Percent Difference	Set II	Percent Difference
Uranium-235 Criticals	1.0	0.998	-0.2	0.996	-0.4
Uranium-233 Criticals	1.0	0.999	-0.1	0.997	-0.3
Plutonium Criticals	1.0	1.01	+1	1.026	+2.6

TABLE II

RATIO OF THERMAL TO EPITHERMAL REACTION RATE

Isotope	Ratio
U-235	3.5
Pu-239	11
Pu-240	0.37
Pu-241	6.5
Pu-242	0.41

TABLE III

SENSITIVITY OF ISOTOPIC COMPOSITIONS IN ATOM PERCENT TO CHANGES IN VARIOUS CROSS SECTIONS

Sensitivity of U-235 composition to resonance fission with constant alpha.

Exposure (MWd/T)	U-235 I_f=295b	U-235 I_f=270b	U-235 I_f=250b	U-235 I_f=230b
10,000	1.421	1.427	1.432	1.437
20,000	0.809	0.818	0.827	0.835
27,000	0.500	0.510	0.519	0.528

Sensitivity of Pu-240 and Pu-241. Isotopic composition for changes in Pu-239 resonance data.

Exposure (MWd/T)	Set II I_a = 472b, I_f = 288b, α = 0.639		Set I I_a = 535b, I_f = 288b, α = 0.858	
	Concentration of			
	Pu-240	Pu-241	Pu-240	Pu-241
10,000	0.0943	0.0358	0.0968	0.0364
20,000	0.202	0.0880	0.207	0.0895
27,000	0.256	0.116	0.262	0.118

Sensitivity of Pu-242 and Cm-244 isotopic compositions to changes in the resonance data of Pu-242.

Exposure (MWd/T)	Set II I_a = 1100b		Set I I_a = 2423b	
	Pu-242	Cm-244	Pu-242	Cm-244
10,000	0.006	0.3×10^{-4}	0.0056	0.7×10^{-3}
20,000	0.035	0.9×10^{-3}	0.030	0.17×10^{-2}
27,000	0.071	0.4×10^{-2}	0.056	0.71×10^{-2}

TABLE IV

SENSITIVITY OF ISOTOPIC COMPOSITIONS IN ATOM PERCENT TO CHANGES IN VARIOUS CROSS SECTIONS

Sensitivity of isotopic compositions to changes in thermal data for Pu-239 and Pu-240. For exposures in the range of 27,000 MWd/T.

Set II, $\alpha^{Pu-239} = 0.358$						Set I, $\alpha^{Pu-239} = 0.389$					
U-235	Pu-239	Pu-240	Pu-241	Pu-242	Cm-244	U-235	Pu-239	Pu-240	Pu-241	Pu-242	Cm-244
0.51	0.394	0.250	0.114	0.0536	0.67×10^{-2}	0.50	0.395	0.262	0.118	0.0559	0.71×10^{-2}
$\sigma_a^{Pu-240} = 286b$						$\sigma_a^{Pu-240} = 265b$					
0.50	0.396	0.258	0.119	0.0564	0.72×10^{-2}	0.50	0.395	0.262	0.118	0.0559	0.71×10^{-2}

Sensitivity of isotopic composition to 2200 m/s cross section data for exposures in the range of 27,000 MWd/T.

	U-235	Pu-239	Pu-240	Pu-241	Pu-242	Cm-244
Set I	0.500	0.395	0.262	0.118	0.0559	0.71×10^{-2}
Set II	0.509	0.394	0.250	0.113	0.0457	0.57×10^{-2}
Set III	0.507	0.393	0.255	0.117	0.0523	0.66×10^{-2}

TABLE V

CHANGE IN MEAN SQUARE ERROR FOR THE CHANGED CAPTURE CROSS SECTION

	293b	282b
Pu-239	9%	6%
Pu-240	11%	7%
Pu-241	22%	15%

TABLE VI

COMPARISON BETWEEN MEASUREMENT AND CALCULATION FOR ISOTOPIC COMPOSITION

	Composition (atom percent)			Percent Difference	
Isotope	Experiment	Set I	Set II	(Set I)	(Set II)
U-235	0.57	0.555	0.562	- 2.6	- 1.4
U-236	0.158	0.158	0.158	0	0
Pu-239	0.364	0.337	0.339	- 7.4	- 6.8
Pu-240	0.134	0.156	0.143	+ 16.4	+ 6.7
Pu-241	0.051	0.0585	0.0565	+ 14.7	+10.8
Pu-242	0.013	0.0175	0.0135	+ 35	+ 3.8
Np-237	0.012	0.0108	0.0107	- 10	-11
Am-243	0.0015	0.0027	0.0010	+ 80	-33
Cm-244	0.00016	0.00026	0.0001	+ 63	-38

REFERENCES

[1] Drake, M. K., Dyos, M. W., USAEC Rep., GA-6576 (1965).

[2] Aline, P. G., McWhorter, R. J., Trans. Am. Nucl. Soc. 5, 2 (1962) 369.

[3] Liikala, R. C., et al., Neutron Cross Section Conf., Washington, D. C. (1966).

[4] Weinstein, S., et al., Neutron Cross Section Conf., Washington, D. C. (1966).

[5] Hellens, R. L., IAEA, Vienna,(May 1962).

[6] Hellens, R. L., and Honeck, H. C., IAEA, Vienna, (May 1962).

[7] Colvin, D. W., and Sowerby, N. G., Proc. 3rd UN Int. Conf. PUAE, 16 (1958) 121.

[8] Hughes, D. J., and Schwartz, R. B., USAEC Report, BNL-325 (1958).

[9] Feiner, F., ANS National Topical Meeting, (1966).

[10] Aline, P. G., Trans. Am. Nucl. Soc., 8, 2 (1965) 510.

[11] Snyder, T. M., APED-4038 (1962).

[12] Hackney, M. Rachel, et al., USAEC Report, TID-7672 (1963) 288.

[13] Robkin, M. A., USAEC Report, GEAP-4907 (1965).

[14] Chajson, L., USAEC Report, WCAP-6061 (1964).

[15] Gwin, E., and Magnusson, D. W., USAEC Report, ORNL-60-4-12 (1960).

[16] Liikala, R. C., and Stinson, W. P., Trans. Am. Nucl. Soc., 9, 1 (1966) 127.

[17] Gast, P. F., IAEA, Vienna (May 1962).

[18] Chernick, J., and Vernon, R., Nuclear Science and Engineering, 4, 649 (1958).

[19] Rider, B. F., et al., USAEC Report, GEAP-5174 (1966).

[20] Westcott, C. H., et al., Atomic Energy Review, 3, 2 (1965).

[21] Sher, R., and Felberbaum, Joan, USAEC Report, BNL-918 (1965).

[22] Safford, G. J., and Havens, W. W., "Fission Parameters for U-235," Nucleonics, 17, 11 (1959) 135.

[23] Ruiz, C. P., et al., APED-5016 (1966).

[24] Hellens, R. L., Neutron Cross Section Conf., Washington, D. C. (1966)

CN-23/106

ПЛОТНОСТЬ УРОВНЕЙ И СТРУКТУРА АТОМНЫХ ЯДЕР

Шубин Ю.Н., Малышев А.В., Ставинский В.С.
Физико-энергетический институт, г.Обнинск

I. Статистические свойства атомных ядер представляют особый интерес, поскольку атомные ядра состоят из небольшого числа сильно взаимодействующих частиц, и флуктуационные явления играют фундаментальную роль в поведении ядер при низких энергиях возбуждения. Изучение этих уникальных объектов может не только выяснить границы применимости известных положений статистики, установленных на основании анализа свойств макросистем, но также глубже понять их физическое содержание.

В этой связи особенно важным становится исследование одной из основных статистических характеристик атомных ядер - плотности их энергетических уровней. Оно может дать важную информацию о характере элементарных возбуждений атомных ядер и, следовательно, пролить свет на их структуру, о которой наши знания еще весьма ограничены.

Представление об элементарных возбуждениях, высказанное Ландау [I] , заключается в том, что слабовозбужденное состояние любой квантовой системы взаимодействующих частиц можно представить как состояние почти идеального газа элементарных возбуждений (квазичастиц), движущихся в самосогласованном потенциале. Малое остаточное взаимодействие между квазичастицами является естественной причиной установления равновесия в системе по отношению к "квазичастичным" степеням свободы.

Успех модели оболочек и оптической модели, показавших, что модель почти независимых частиц в состоянии объяснить многие факты, говорит о том, что представление об элементарных возбуждениях применимо и к такой системе как атомное ядро. Этот вопрос рассмотрен в большом числе работ Мигдала и сотрудников [2]. Поэтому при анализе плотности уровней мы будем исходить из этой картины ядерной структуры.

II. В модели независимых частиц плотность уровней ядра с данной энергией возбуждения U и моментом количества движения J имеет вид:

(I) $$\rho(U,J)=\frac{2J+1}{24\sqrt{2}\,a^{1/4}U^{5/4}\sigma^3}\exp\left\{2(aU)^{1/2}-\frac{(J+\frac{1}{2})^2}{2\sigma^2}\right\},$$

где:

(2) $$a=\frac{\pi^2}{6}g(\mu);$$

$g(\mu)$ – плотность одночастичных состояний вблизи поверхности Ферми μ;

(3) $$\sigma^2=\frac{6}{\pi^2}\langle m^2\rangle(aU)^{1/2};$$

$\langle m^2\rangle$ – средний квадрат проекции полного момента отдельных частиц; усреднение ведется по одночастичным состояниям вблизи поверхности Ферми.

Показатель экспоненты в выражении (I) слабо зависит от полного момента J в большинстве случаев и, следовательно, плотность уровней определяется, в основном, одним параметром a, что характерно для вырожденных ферми-систем. Таким образом, плотность уровней атомных ядер должна быть чувствительной к расположению одночастичных состояний вблизи поверхности Ферми.

При сравнении формулы (I) с опытом обычно принимают во внимание два важных эффекта. Во-первых, анализ экспериментальных данных показал необходимость учета остаточных взаимодействий в ядрах с четными Z и N путем введения характеристического уровня Бете-Гурвица [3]. Это означает, что в (I) под энергией возбуждения U нужно понимать эффективную энергию возбуждения U^*:

$$U^* = U - \begin{cases} \delta_p + \delta_n & \text{- для четно-четных ядер,} \\ \delta_p & \text{- для четно-нечетных ядер,} \\ \delta_n & \text{- для нечетно-четных ядер,} \end{cases} \tag{5}$$

а энергии спаривания протонов δ_p и нейтронов δ_n можно вычислить, зная массы ядер, согласно, например, Немировскому П.Э. и Адамчуку Ю.В. [4].

Во-вторых, основной параметр теории a оказывается чувствительным к оболочечной структуре, которая является следствием конечных размеров ядер. Ньютон [5] впервые обратил внимание на свя зь между величиной параметра a и мультиплетностью одночастичных уровней модели оболочек. Рассматривая ядро как ферми-газ, заключенный в сферическом объеме с радиусом $\sim A^{1/3}$ (A - полное число частиц), он получил следующее выражение для величины a :

$$a = \alpha A^{2/3}(\bar{j}_Z + \bar{j}_N + 1) \quad , \tag{6}$$

где $\bar{j}_Z$ и $\bar{j}_N$ - средние значения полного момента протонных и нейтронных состояний вблизи поверхности Ферми в интервале порядка ядерной температуры. $\bar{j}_Z$ и $\bar{j}_N$ определялись Ньютоном на основании схемы последовательного заполнения одночастичных состояний, которая, как известно, нарушается из-за наличия остаточного взаимодействия. Использование экспериментальной схемы заполнения улучшило количественное согласие формулы (6) с экспериментом [6].

При получении формулы (6) предполагалось, что среднее расстояние между вырожденными одночастичными уровнями, пропорциональное $\alpha A^{2/3}$, не зависит от числа протонов и нейтронов в ядре. Известно, однако, что в модели оболочек наблюдается расслоение этих уровней на группы, расстояние между которыми больше, чем среднее расстояние между уровнями в пределах группы. Верхние границы этих групп по числу частиц определяют магические числа протонов и нейтронов. Таким образом, параметр α должен увеличиваться к середине оболочек и спадать между ними. На это обстоятельство ранее обращалось внимание в работах Маргенау [7] и Эриксона [8], однако, при этом эффект снятия вырождения по j не выделялся и не проводилось количественного сравнения с опытом.

В настоящей работе показано, что этот эффект является существенным при анализе плотности уровней ядер. Расслоение вырожденных уровней на группы приводит как к изменению структуры выражения (6), та к и к изменению процедуры усреднения при нахождении $\bar{j}_Z$ и $\bar{j}_N$. В самом деле, вблизи магических чисел усреднение величин j_Z и j_N следует проводить лишь по состояниям той оболочки, которой принадлежит ферми-уровень данного ядра, поскольку расстояние между границами соседних оболочек значительно больше температуры ядра при умеренных энергиях возбуждения ($T \sim 0{,}7$ Мэв). Усредненные с учетом этого обстоятельства величины $2\bar{j}_Z+1$ и $2\bar{j}_N+1$ даны в таблицах I и 2, где приведены также $2j_N+1$ и $2j_Z+1$ последнего заполненного состояния (вторые колонки). В качестве $\bar{j}_Z$ и $\bar{j}_N$ брались средние арифметические значения с $\Delta Z = 3$ для $Z < 50$ и $\Delta Z = 5$ для $Z \geqslant 50$; $\Delta N = 3$ для $N < 70$, $\Delta N = 5$ для

$70 \leqslant N \leqslant 110$ и $\Delta N = 7$ для $N > 110$. Экспериментальная схема заполнения одночастичных уровней была взята, в основном, из работы [6]. В соответствии с новыми данными были сделаны следующие изменения. Во-первых, как показывает опыт, 39, 40, 43 нейтроны и 39 и 40 протоны находятся в состоянии $1g_{9/2}$. Это означает, по-видимому, что в том случае, когда состояния с сильно отличающимися полными моментами близки по энергии, предпочтение отдается большему моменту. С учетом этого обстоятельства были получены средние значения $\bar{j}_Z$ и $\bar{j}_N$ в областях $45 \leqslant Z \leqslant 62$ и $56 \leqslant N \leqslant 88$ (состояния $3s_{1/2}$ и $1h_{11/2}$ в первом случае и $1g_{9/2}$ и $2p_{1/2}$ - во втором). Кроме того, опыт показывает [9], что 124-й нейтрон находится в состоянии $3p_{3/2}$, а не в $2f_{5/2}$, как это полагалось в работе [6].

Для того, чтобы учесть эффект группировки вырожденных одночастичных уровней, положим:

$$a_Z = [\alpha_0 + \beta \cos(\omega_Z Z + d)] A^{2/3} (2\bar{j}_Z + 1) \tag{7}$$
$$a_N = [\alpha_0 + \beta \cos(\omega_N N + d)] A^{2/3} (2\bar{j}_N + 1)$$

Выражения в квадратных скобках учитывают отклонение распределения одночастичных уровней от равномерного, которое получится, если $\beta = 0$. ω_Z и ω_N определяются числом состояний в протонных и нейтронных оболочках. В области $A < A_0 = 80$ среднее число состояний в оболочке порядка 20, так что $\frac{2\pi}{\omega_Z} \simeq \frac{2\pi}{\omega_N} \simeq 20$. С ростом A число состояний в оболочках растет приблизительно линейно, поэтому можно написать:

$$\omega_Z = \frac{2\pi}{T_0 [1 + \gamma (Z - Z_0)]}$$
$$\omega_N = \frac{2\pi}{T_0 [1 + \gamma (N - N_0)]} \tag{8}$$

где T_0 - период, соответствующий области легких ядер ($N \approx Z$),

а γ - параметр, учитывающий изменение периода, одинаковый для протонов и нейтронов.

Из (7) и (8) получим:

$$a = a_Z + a_N = 2\alpha_0 A^{2/3}(\bar{j}_Z + \bar{j}_N + 1) +$$

(9) $$+\beta A^{2/3}\left[(2\bar{j}_Z + 1)\cos(\omega_Z Z + d) + (2\bar{j}_N + 1)\cos(\omega_N N + d)\right]$$

В области $A < 80$ $N \sim Z \sim \frac{A}{2}$, $\omega_Z \simeq \omega_N \simeq 0$ и схемы заполнения мало отличаются. Поэтому вместо (9) в этой области можно написать:

(I0) $$a = \left[2\alpha_0 + 2\beta\cos\left(\omega\frac{A}{2} + d\right)\right]A^{2/3}(\bar{j}_Z + \bar{j}_N + 1)$$

На рис. I приведены значения параметра a в зависимости от массового числа A, использованные в настоящей работе. Как и ранее [I0], они получены из анализа плотности нейтронных резонансов на основании соотношений (I) и (5) с привлечением новейших экспериментальных данных. Энергии спаривания δ_p и δ_n принимались согласно [4].

На рис. 2 представлено отношение $\alpha = \frac{a}{A^{2/3}(\bar{j}_Z + \bar{j}_N + 1)}$. Отчетливо видна периодическая структура в зависимости α от A, особенно в области легких ядер. Из сравнения экспериментальных точек с (I0) получаем $d \approx \frac{\pi}{2}$, $T \approx 20$, что позволяет записать (9) в виде:

$$a = A^{2/3}(\bar{j}_Z + \bar{j}_N + 1)\Big\{2\alpha_0 -$$

(II) $$-\frac{2\beta}{1+\varepsilon}\left[\sin\frac{\pi Z}{10[1+\gamma(Z-Z_0)]} + \varepsilon\sin\frac{\pi N}{10[1+\gamma(N-N_0)]}\right.,$$

где $\varepsilon = \frac{2\bar{j}_N + 1}{2\bar{j}_Z + 1}$ - величина, мало отличающаяся от I для большин-

ства рассматриваемых ядер.

Полагая $\mathcal{E}$ = I и пренебрегая членами порядка $\left(\frac{N-Z}{A}\right)^2$, получим вместо (II)

$$a = A^{2/3}(\bar{j}_Z + \bar{j}_N + 1)\left\{2\alpha_0 - \right.$$

$$\left. -2\beta \sin\left[\frac{\pi}{20}\frac{A}{1+\gamma\frac{A-A_0}{2}}\right]\cos\left[\frac{\pi}{20}\frac{(1-\gamma\frac{A_0}{2})(N-Z)}{\left[1+\gamma\frac{A-A_0}{2}\right]^2}\right]\right\} \tag{I2}$$

Экспериментальные данные во всей исследуемой области лучше всего описываются при следующем выборе параметров:

$$\begin{aligned} \alpha' = 2\alpha_0 &= 0{,}076 \\ 2\beta &= 0{,}025 \\ \gamma &= 0 \qquad A<80 \\ \gamma &= 0{,}00667 \qquad A \geqslant 80 \\ Z_0 = N_0 = \frac{A_0}{2} &= 40 \end{aligned} \tag{I3}$$

Необходимо отметить, что полученное значение γ соответствует наблюдаемому увеличению числа состояний в оболочках с ростом полного числа частиц.

Из выражения (I2) видно, что параметр a зависит не только от полного числа частиц в ядре A, но также от избытка числа нейтронов над протонами $N-Z$. Этот эффект, обнаруженный ранее для ядер с $A < 65$ [II], получает, таким образом, естественное объяснение.

На рис. 3 показана величина $\alpha - \alpha_0'$ для разных значений $N-Z$. Видно, что в разных областях A эта величина с ростом $N-Z$ изменяется различным образом, что проявляется также в экспериментальных данных на рис. 2. Так, в области $A \sim 50$ меньшим значениям $N-Z$ соответствуют меньшие значения α, в то время как в об-

ласти $A \sim 70$ наблюдается обратная картина. С ростом A различие в величине α для соседних $N-Z$ уменьшается, так что этот эффект становится менее отчетливо выраженным. На рис. 2 пунктирными кривыми даны вычисленные с помощью (I2) и (I3) величины α лишь для крайних значений $N-Z$. Видно, что подавляющее большинство точек расположено в областях, ограниченных этими кривыми, что оправдывает принятую здесь аппроксимацию (7).

Проведенный анализ показал, что отклонения экспериментальных значений α от формулы (I2) следуют нормальному закону со среднеквадратичной ошибкой, близкой к средней экспериментальной ошибке отдельных точек. Следует отметить, что использование схемы последовательного заполнения в предположении $\alpha = const$ приводит к распределению, несимметричному относительно среднего значения, а экспериментальная схема заполнения [6] без учета расслоения вырожденных одночастичных состояний на группы - симметричную, но отличную от нормальной функции распределения.

IУ. Из вышеизложенного следует, что группировка вырожденных одночастичных уровней в оболочки влияет на величину a почти в такой же степени, как и мультиплетности одночастичных состояний вблизи поверхности Ферми. Полученная полуэмпирическая формула (I2) для параметра a позволяет предсказывать эту величину с хорошей точностью, что важно для решения широкого круга задач ядерной физики низких энергий. Обнаруженная явная зависимость плотности уровней от $N-Z$ позволяет надеяться на дальнейшее уточнение этого важного параметра статистической теории ядра. Для этого, однако, необходимы новые экспериментальные данные, относящиеся к нейтронно-избыточным и нейтронно-дефицитным ядрам.

ЛИТЕРАТУРА

I. Л.Д.Ландау, ЖЭТФ 35, 97 (I958).

2. А.Б.Мигдал, Теория конечных ферми-систем, I965.

3. H.Bethe, H.Hurwitz, Phys. Rev. 81 (1951) 898.

4. Немировский П.Э., Адамчук Ю.В., Nucl. Phys. 39 (1962) 553.

5. Newton T.D. Can. J. Phys. 34 (1956) 804.

6. N.N.Abdelmalek, V.S.Stavinsky, Nucl. Phys. 58 (1964) 601.

7. H.Margenau, Phys. Rev. 59 (1941) 627.

8. T.Ericson, Nucl. Phys. 8 (1958) 265.

9. G.H.Fuller, W.W.Cohen, Nucl. Moments, App. 1 to NDS, 1965.

I0. А.В.Малышев, ЖЭТФ 45 (I963) 3I6.

II. A.V.Malyshev, Int. Congr. de Phys. Nucl. 4a(1)/C394, Paris, 1964.

ТАБЛИЦА № I

Порядок заполнения протонных уровней.

Z	$2j_z+1$	$2\bar{j}_z+1$	Z	$2j_z+1$	$2\bar{j}_z+1$	Z	$2j_z+1$	$2\bar{j}_z+1$
I	2							
I	2	2	3I	6	6	64	8	6.4
2	2	2.67	32	6	5.33	65-66	6	7.6
3	4	3.33	33	4	5.33	67	I2	6.8
4-5	4	4	34	6	4.67	68	6	6.4
6	4	3.33	35	4	5.33	69	4	6.8
7	2	2.67	36	6	4.67	70	4	6
8	2	3.33	37	4	5.33	7I	8	6.4
9	6	4.67	38	6	6.67	72	8	8
I0-I3	6	6	39	I0	8.67	73	8	8.4
I4	6	4.67	40-50	I0	I0	74	I2	9.2
I5	2	3.33	5I	8	8.8	75	6	8.4
I6	2	2.67	52	8	8.4	76	I2	7.6
I7	4	3.33	53-56	8	8	77	4	6
I8-I9	4	4	57	8	8.2	78	4	5.6
20	4	5.33	58	8	8.4	79	4	3.6
2I	8	6.67	59	6	8.6	80	4	3.2
22-28	8	8	60	6	8.8	8I	2	3
29	4	5	6I-62	6	9	82	2	2.67
30	6	5.33	63	6	6.4	83	I0	6.8

ТАБЛИЦА №2

Порядок заполнения нейтронных уровней.

N	$2j_n+1$	$2\bar{j}_n+1$	N	$2j_n+1$	$2\bar{j}_n+1$	N	$2j_n+1$	$2\bar{j}_n+1$
I	2	2	49	2	7.0	I00	8	7.6
2	2	2.67	50	6	8.0	I0I	4	8
3	4	3.33	5I-54	6	6	I02	4	7.2
4-5	4	4	55	6	6.67	I03	I0	7.6
6	4	3.33	56	6	7.6	I04	I0	8.8
7	2	2.67	57	8	8.4	I05	I0	I0.8
8	2	3.33	58	8	9.2	I06	I0	I0.4
9	6	4.67	59-64	8	I0	I07	I4	9.6
I0-I3	6	6	65-74	I2	I0	I08	8	8.8
I4	6	4.67	75	I2	8.8	I09	6	7.6
I5	2	3.33	76	I2	7.6	II0	6	6
I6	2	2.67	77	4	8.8	III	4	6.29
I7	4	3.33	78	I2	8.4	II2	6	6.57
I8-I9	4	4	79	4	7.2	II3	I4	7.I5
20	4	5.33	80	I2	8.8	II4	I0	8
2I	8	6.67	8I	4	8	II5	I0	9.43
22-28	8	8	82	I2	9.33	II6	I0	8.86
29	4	4	83	8	5.6	II7	2	8.86
30	4	4.67	84	8	6.8	II8	I4	8
3I	6	5.33	85-88	8	8	II9	2	8.57
32	6	5.33	89	I4	II.2	I20	I4	8
33	4	5.33	90	I4	II.6	I2I	4	8.29
34	6	4.67	9I	I0	II.6	I22	I4	6.59
35	4	5.33	92	I0	I0.8	I23	6	6.59
36	6	5.33	93	I0	9.6	I24	4	5.33
37	6	6	94	I0	9.2	I25	2	5.6
38	6	7.33	95	8	8.8	I26	2	3.5
39	I0	8.67	96	8	8.4	I27	I0	7.I4
40-47	I0	I0	97-98	8	9.2			
48	I0	7.33	99	I4	8.4			

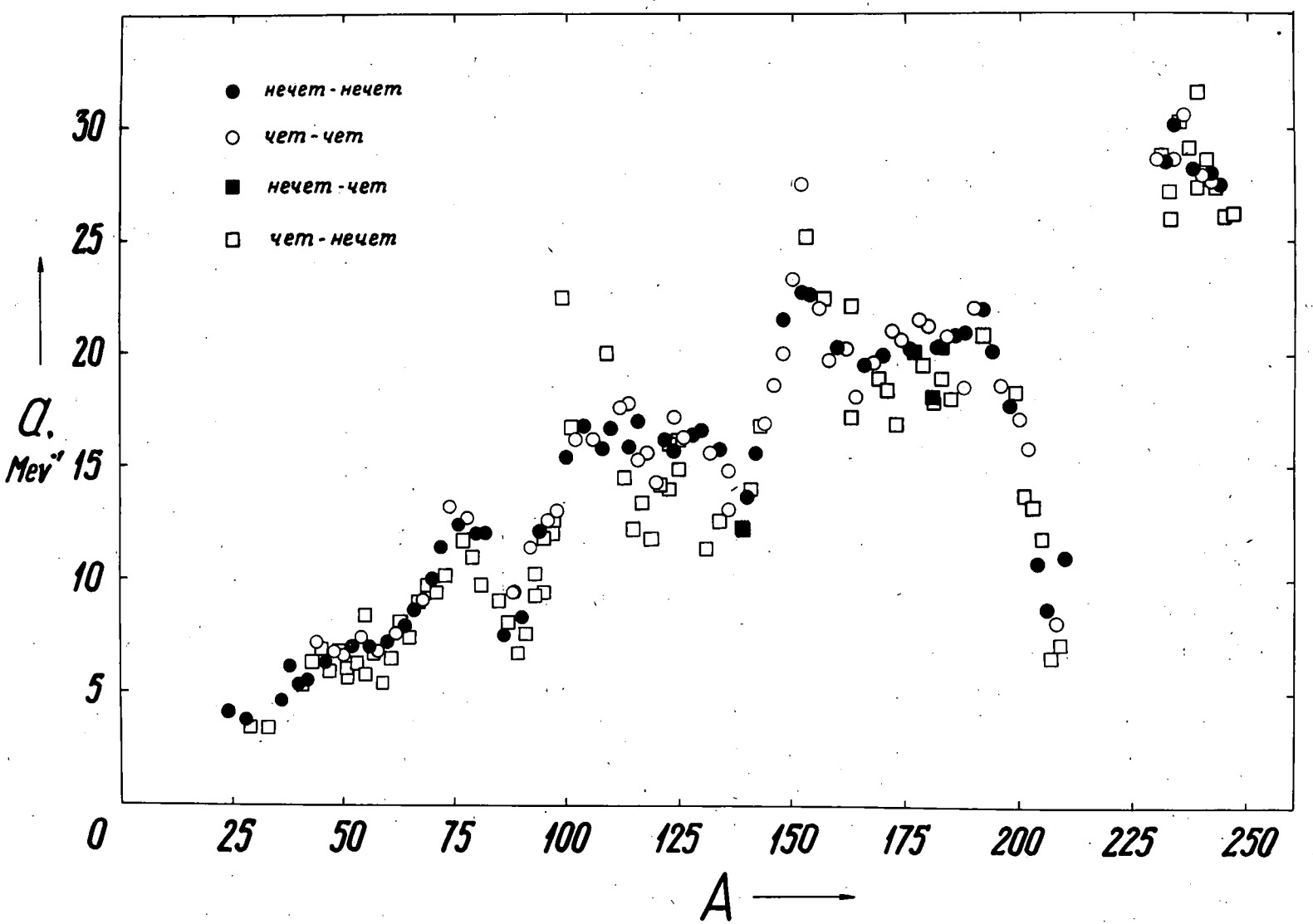

Рис. 1 Экспериментальная зависимость параметра a от атомного веса.

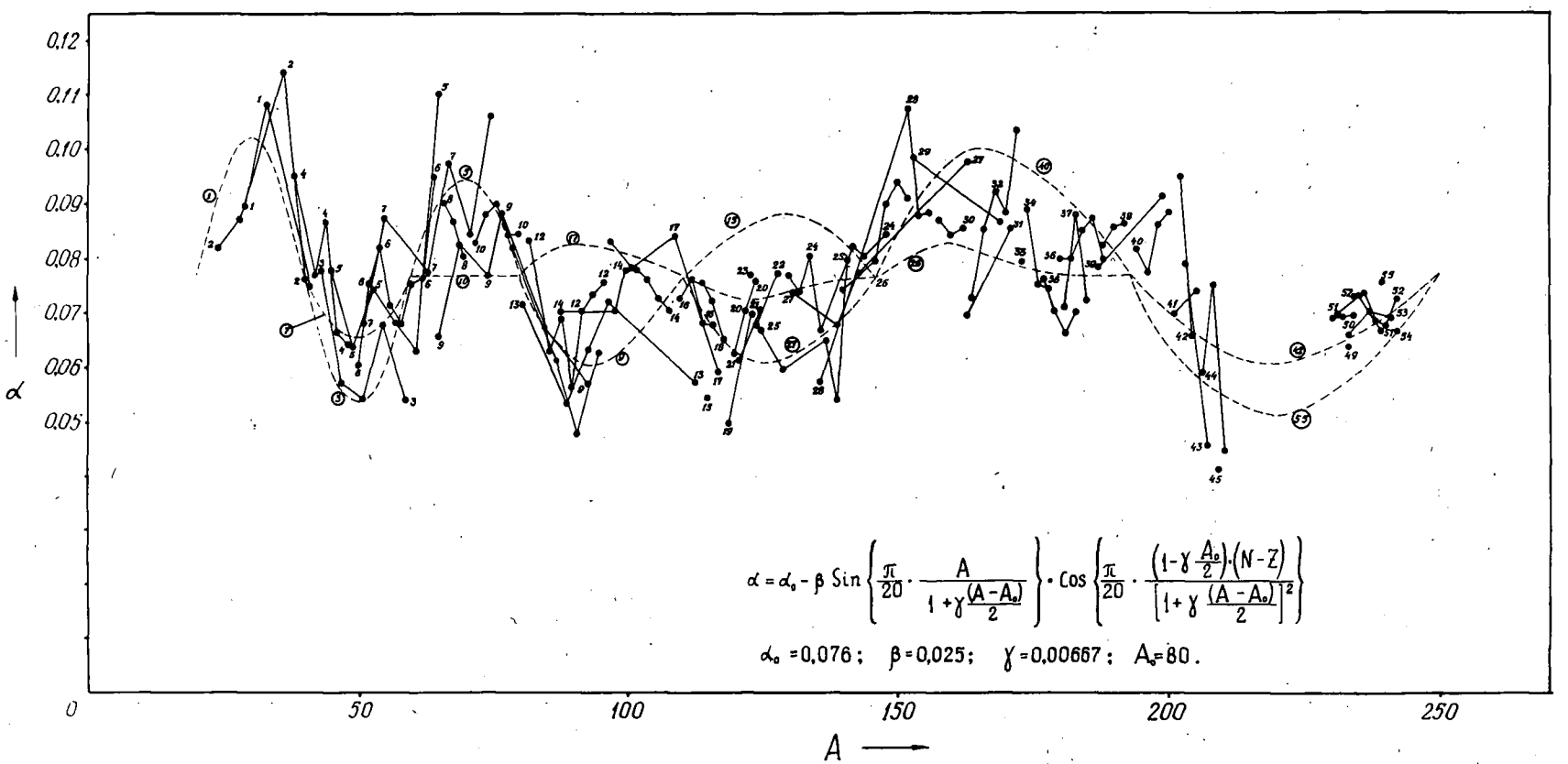

Рис. 2 **Изотопическая зависимость параметра** α .

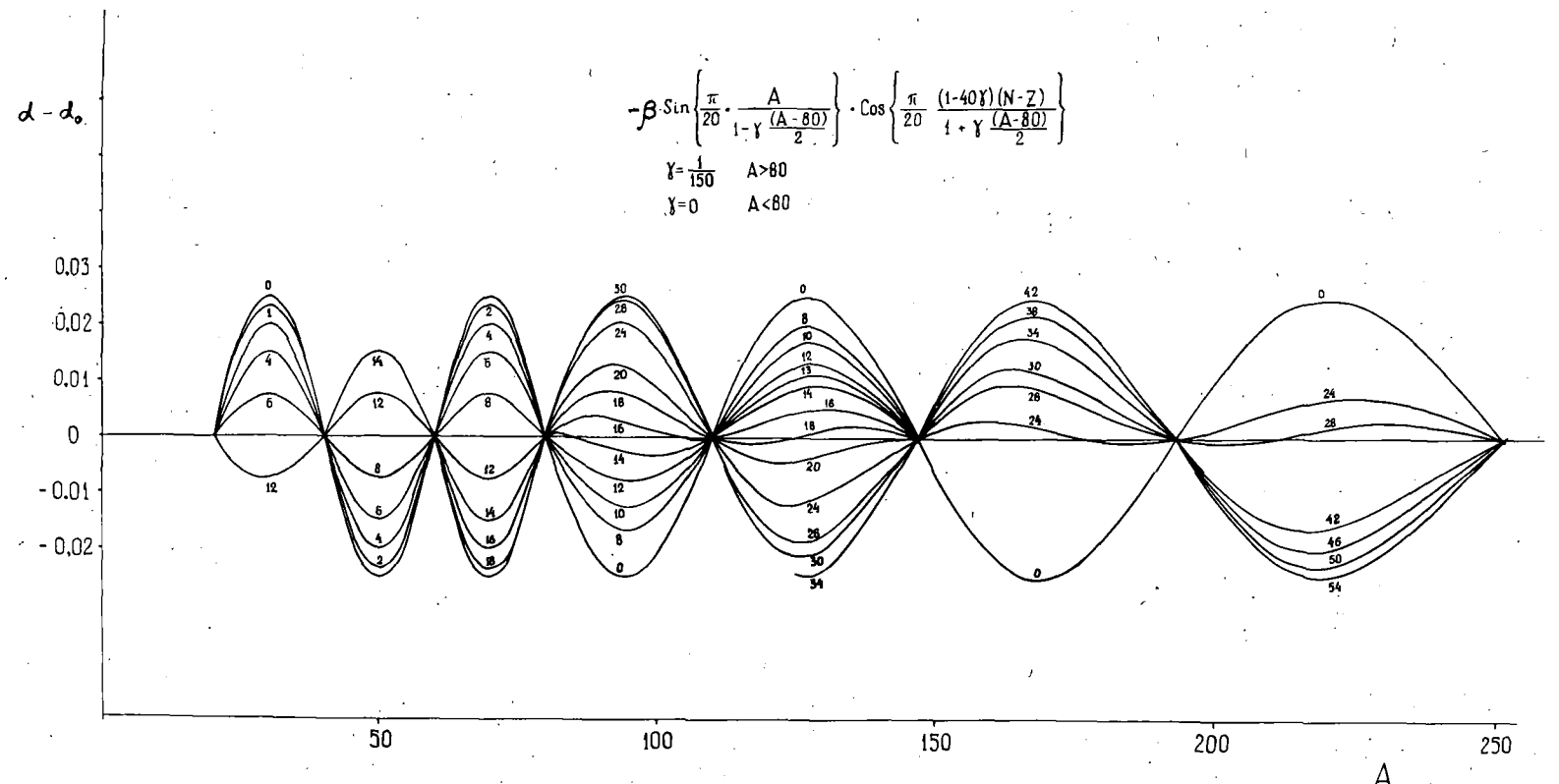

Рис. 3 Изменение разности $\alpha - \alpha_0$ в зависимости от $N - Z$.

CN-23/113

ЗАВИСИМОСТЬ СЕЧЕНИЯ СИММЕТРИЧНОГО ДЕЛЕНИЯ U^{238} ОТ ЭНЕРГИИ НЕЙТРОНОВ

Н.И.Борисова, С.М.Дубровина, В.И.Новгородцева,
В.А.Пчелин, В.А.Шигин, В.М.Шубко

ИНСТИТУТ АТОМНОЙ ЭНЕРГИИ им.И.В.КУРЧАТОВА
Москва, СССР

А Н Н О Т А Ц И Я

Радиохимическим методом сравнивались выходы некоторых продуктов симметричного и асимметричного деления U^{238}. Деление вызывалось моноэнергетическими нейтронами. Измерения проведены при энергиях нейтронов I,5 ; 2 ; 3 ; 4 ; 5 ; I3 ; I5 ; I6,5 ; I8 Мэв. Выход продуктов симметричного деления по отношению к выходу продуктов асимметричного деления при энергиях нейтронов I,5 ; 5 ; I3 и I8 Мэв соответственно равен I/800 ; I/90 ; I/9 ; I/7.

Результаты эксперимента сравниваются с предсказаниями статистической теории деления.

Малая вероятность деления ядра на осколки с равными массами, наблюдающаяся при небольших энергиях возбуждения делящегося ядра, и быстрое увеличение этой вероятности с ростом энергии возбуждения до сих пор не находят окончательного объяснения в теории деления и остаются узловым вопросом физики деления.

Со времени открытия асимметрии деления ядер появилось несколько разных объяснений этого явления / I /. Не останавливаясь на них подробно, отметим, что одной из причин, затрудняющих выбор между ними, является скудность экспериментального материала, особенно по зависимости выходов симметричного деления от энергии возбуждения.

Для ряда ядер выход осколков симметричного деления изучался при делении тепловыми нейтронами и нейтронами с энергией $E_n \simeq 14$ Мэв и только для U^{235} имеются также данные при $E_n = 1; 5; 8$ Мэв, а для U^{238} при 8 Мэв / 2 /. Систематического изучения выходов симметричного деления с изменением E_n в широком интервале энергий, начиная от порога деления, не проводилось. (Некоторым началом в этой области можно считать работу / 3/).

Вместе с тем, изучение распределения осколков деления по массам при разных энергиях возбуждения, особенно при делении нейтронами, имеет и прикладное значение.

В настоящей работе измерены выходы некоторых ядер при симметричном и асимметричном делении U^{238} моноэнергетическими нейтронами в широком интервале изменения энергии нейтронов, на-

чная от порога деления до 5 Мэв, а также в интервале от I3 до I8 Мэв.

Методика

Моноэнергетические нейтроны получались в одной из ядерных реакций: $p+T$, $d+d$, $d+T$ на электростатическом ускорителе /4/. Выбор реакции, а также угла облучения и энергии ускоренных протонов или дейтонов определялся требующейся энергией нейтронов. Как правило, одновременно облучались четыре образца U^{238} в геометрии, изображенной на рис. I. Образцы состояли из порошка закиси-окиси U^{238} с содержанием $U^{235} \sim 0,I\%$, заключенного в тонкостенные контейнеры. Вес образцов I-2 грамма. Выделение осколков из облученных образцов производилось радиохимическим путем, который подробнее описывается ниже. Выделялись Mo^{99}, Ag^{III}, Cd^{II5}, Ba^{I40}.

При измерениях на пучке дейтонов для уменьшения фона от нейтронов, появляющихся в результате $d+d$ реакции на набитых самим же пучком дейтонах, мишень менялась через каждые 6 часов работы, а коллимирующая диафрагма была сделана так, что не прошедший через нее пучок обеспечивал нагрев диафрагмы, достаточный для удаления из нее дейтерия. Проведенные контрольные измерения показали, что указанный фон лежит за пределами ошибок измерений и может не учитываться. Фон от нейтронов, рассеянных соседними образцами и материалом конструкции, как показали оценки, также меньше ошибок измерений и нами не учитывался.

Каждое облучение продолжалось ~ 20 часов. При этом поток нейтронов через образец составлял от 10^7 до 10^8 нейтр /см^{2}сек в зависимости от энергии нейтронов.

Было проведено несколько серий измерений. Результаты отдельных серий совпадают в пределах ожидаемых ошибок.

Очистка урана и выделение осколков

Исходный препарат U^{238} (99,9%) очищался экстракцией диэтиловым эфиром / 5/. Азотнокислый раствор урана выпаривался в кварцевом стакане досуха и прокаливался затем при 800°С до

закиси-окиси урана. Полученный препарат помещался в никелевые контейнеры и облучался.

После облучения образцы растворялись в концентрированной азотной кислоте с носителями (в количестве 15-30 мг по металлу) определявшихся изотопов. Для обеспечения изотопного обмена полученные растворы кипятились в течение получаса. Растворы выпаривались почти досуха, разбавлялись водой до 30 мл и добавлением 0,5 мл 2N HCl и 0,5 мл 2N H_2SO_4 осаждались $AgCl$ и $BaSO_4$.

К растворам после отделения сульфатов бария и хлоридов серебра добавлялось по 5 мл концентрированной H_2SO_4 и растворы выпаривались до паров серной кислоты. После разбавления водой осаждались сероводородом сульфиды кадмия и молибдена. Сульфид кадмия растворялся в 6N HCl.

Дальнейшая очистка изотопов проводилась общепринятым методом /6/. Полученные образцы весом от 5 до 20 мг просчитывались на проточном метановом счетчике с геометрией 4π и фоном 1 имп /мин /7/. Для перехода к абсолютному счету использовались градуировочные кривые зависимости эффективности счета от веса образца, полученные экспериментально для каждого изотопа. Активности приводились к бесконечному облучению.

Результаты и обсуждение

Результаты измерений представлены в таблице. При каждой энергии нейтронов - E_n - строка 1, нами определялись соотношения между выходами разных осколков. В строке 2 приведены значения среднеквадратичного разброса в энергиях нейтронов - ΔE_n. В строке 3 приведено отношение выхода Mo^{99} к выходу Ba^{140}.

В строке 4 приведено значение γ_ε -отношения выхода симметричного деления к выходу асимметричного деления. Выход асимметричного деления нами определялся как полусумма выходов Mo^{99} и Ba^{140}, а в качестве выхода симметричного деления взят выход Cd^{115}. Строго симметричному делению U^{239} отвечает масса 117, поскольку осколок, образующийся при делении ядра приблизительно на равные массы, теряет около двух нейтронов.

В строке 5 приведено отношение выхода Ag^{111} к полусумме выходов Mo^{99} и Ba^{140}.

Таблица

№ № п/п	Величина	Размерность	Значения								
I	E_n	Мэв	I,5	2,0	3,0	3,9	4,8	I3,0	I5,0	I6,4	I7,7
2	ΔE_n	Мэв	0,I	0,I	0,I5	0,I5	0,I	0,I5	0,25	0,25	0,I5
3	Y_{Mo}/Y_{Ba}	Отн.ед.	I,03	I,I3	I,20	I,I4	I,I6	I,I6	I,22	I,22	I,29
4	γ_{Σ}	Отн.ед.	$\frac{I}{825}$	$\frac{I}{452}$	$\frac{I}{238}$	$\frac{I}{I29}$	$\frac{I}{89}$	$\frac{I}{8,8}$	$\frac{I}{6,5}$	$\frac{I}{5,8}$	$\frac{I}{6,8}$
5	$2Y_{Ag}/Y_{Mo}+Y_{Ba}$	Отн.ед..	$\frac{I}{29I}$	$\frac{I}{I93}$	$\frac{I}{II9}$	$\frac{I}{68}$	$\frac{I}{48}$	$\frac{I}{7,0}$	$\frac{I}{5,9}$	$\frac{I}{5,3}$	$\frac{I}{6,3}$
6	σ_{Σ}	барн	0,30	0,57	0,57	0,57	0,57	I,08	I,35	I,45	I,47
7	$\Delta\sigma_c$	мбарн	0,02I	0,07I	0,I36	0,249	0,364	7,0	II,8	I4,I	I2,2

В таблице приведены средние значения из серий измерений. Суммарная ошибка в определении отношений ~10%.

Величина γ_{Σ} есть не что иное, как отношение парциального сечения симметричного деления - $\Delta\sigma_c$ (с образованием одной массы) к парциальному сечению асимметричного - $\Delta\sigma_a$: [1] $\gamma_{\Sigma} = \frac{\Delta\sigma_c}{\Delta\sigma_a}$. Поэтому парциальное сечение симметричного деления будет $\Delta\sigma_c = \gamma_{\Sigma} \cdot \Delta\sigma_a$. Значения $\Delta\sigma_a(E_n)$ легко получить из полного сечения деления, приведенного в строке 6 /8/, поскольку вклад выходов Mo^{99} и Ba^{140} в полное сечение известен /2/. Практически он не меняется в исследуемом интервале E_n. Величина $\Delta\sigma_c$ приведена в строке 7.

Отметим, что единственные имеющиеся в литературе данные при E_n, совпадающей с E_n наших измерений (~15 Мэв), согласуются с полученными нами /2/.

Из рассмотрения результатов измерений видно, что выходы осколков подчиняются следующим закономерностям.

1. Выходы Mo^{99} и Ba^{140} мало различаются, а их отношение остается, в пределах ошибок измерений, постоянным во всем интервале изменения энергий нейтронов. Наблюдаемое поведение, видимо, объясняется тем, что Mo^{99} и Ba^{140} образуются при делении ядра на близкие пары осколков, отличающиеся друг от друга всего на 2-5 нуклонов (в зависимости от E_n) в каждом из осколков, а свойства осколков, влияющие на вероятность деления, слабо меняются с изменением масс осколков в этой области масс.

2. Выход симметричного деления быстро увеличивается с ростом энергии нейтронов от 1/800 выхода асимметричного деления вблизи порога деления до 1/90 при E_n = 4,8 Мэв и достигает 1/9 при E_n = 13 Мэв. При дальнейшем увеличении энергии нейтронов выход симметричного деления меняется слабо, находясь вплоть до 17,7 Мэв на уровне 1/6 ÷ 1/7 от выхода асимметричного деления.

3. Выход Ag^{111} качественно ведет себя аналогично выходу Cd^{115}. По абсолютной величине выход Ag^{111} вблизи порога деле-

---

1) В физических интерпретациях обычно используют терминологию сечений, однако в радиохимических исследованиях предпочитают пользоваться терминологией выходов.

ния в 2,8 раза больше, чем Cd^{115}, тогда как при E_n=13÷18 Мэв эти выходы приблизительно равны.

С целью физической интерпретации полученных результатов из экспериментальных данных выделим ту часть выходов осколков, которая связана только с делением составного ядра U^{239}, отбросив часть, связанную с делением U^{238} и U^{237}, образующихся в результате испускания одного-двух нейтронов из сильно возбужденного ядра U^{239}. Последние дают вклад в деление в нашем случае при E_n= 13-18 Мэв.

Для этого воспользуемся тем, что доля выходов Mo^{99} и Ba^{140} в полном сечении деления остается приблизительно постоянной. Тогда:

$$\gamma_\Sigma \cdot \sigma_\Sigma = \gamma_9 \cdot \sigma_9 + \gamma_8' \cdot \sigma_8 \cdot \gamma_7'' \sigma_7 .$$

Индекс 9,8,7 Σ показывает, что γ или σ -сечение деления относится к делению соответственно только U^{239}, U^{238}, U^{237} или к делению через все эти ядра. Величины с одним и двумя штрихами относятся к энергиям нейтронов, меньшим E_n на энергию, уносимую одним или двумя вылетевшими нейтронами. Отсюда:

$$\gamma_9 = \gamma_\Sigma \frac{\sigma_\Sigma}{\sigma_9} - \gamma_8 \frac{\sigma_8}{\sigma_9} - \gamma_7 \frac{\sigma_7}{\sigma_9} \approx \gamma_\Sigma \frac{\sigma_\Sigma}{\sigma_9} - \gamma_9' \frac{\sigma_8}{\sigma_9} - \gamma_9'' \frac{\sigma_7}{\sigma_9} .$$

Мы приняли: $\gamma_9 = \gamma_8 = \gamma_7$. Это упрощение в нашем случае не приводит к большим ошибкам.

Выражение позволяет получить последовательным приближением $\gamma_9(E_n)$, по экспериментальным значениям $\gamma_\Sigma(E_n)$, при условии, что сечения деления известны. Значение $\sigma_\Sigma(E_n)$ известно из измерений / 8 /. Сечения σ_9, σ_8, σ_7 , как следует из работы / 9 /, выше порогов деления приблизительно постоянны вплоть до $E_n \approx 40$ Мэв.

Полученные значения $\gamma_9(E_n)$ вместе с использованными значениями сечений деления изображены на рис. 2.

На этом же рисунке приведена расчетная зависимость $\gamma_9^P(E_n)$, полученная в предположении, что между осколками в момент, предшествующий их отрыву, имеется тепловое равновесие. Это предположение лежит в основе весьма общего статистического подхода к

процессу деления /10/

$$\gamma_g^P = c\,\exp\left(2\sqrt{2a_c E_c^*} - 2\sqrt{2a_a E_a^*}\right)$$

Здесь: C - предэкспоненциальный множитель порядка единицы; E^* - энергия возбуждения пары осколков; индексы c и a означают симметричное и асимметричное деления; a - коэффициент, характеризующий плотность уровней осколка и [illegible] одинаковым для обоих осколков пары, в соответствии с экспериментальными значениями этих коэффициентов /11/. При этом a_c = 18 Мэв$^{-1}$, a_a = 16 Мэв$^{-1}$.

Анализ выражения показывает, что экспериментальной зависимости $\gamma_g(E_n)$ удовлетворяют только значения $E_c^* = E_n$ +1,95 Мэв, $E_a^* = E_n$ +5,1 Мэв. Отметим также, что выбор других a_c и a_a ухудшает согласие с экспериментом.

Полученный результат позволяет сделать ряд выводов.

1. Энергия возбуждения осколков в момент, предшествующий их отрыву, при асимметричном делении превосходит энергию возбуждения при симметричном делении на ~3 Мэв. Потенциальная энергия делящегося ядра перед разрывом - $P = (E_n + B_n + W) - E^* - K$, где W - энергия связи осколков, B_n - энергия связи, вносимая в ядро нейтроном, K - кинетическая энергия осколков. Так как $(W_c - W_a) \approx 5$ Мэв для U^{239} /12/, а $(K_c - K_a) \approx 0$ ($K \ll E^*$ /10/), то $P_c - P_a \approx 8$ Мэв. Таким образом, потенциальная энергия в момент, предшествующий отрыву осколков, для симметричного деления значительно больше, чем для асимметричного деления.

Поскольку определяющую роль в величине потенциальной энергии в момент, предшествующий отрыву осколков, играет жесткость осколков по отношению к деформации [2], а жесткость симметричных осколков значительно меньше, чем асимметричных /13/, естественно связывать большую величину потенциальной энергии для симметричного деления с малой жесткостью симметричных осколков. В та-

---

[2] При одинаковой жесткости симметричных и асимметричных осколков $P_c \approx P_a$ /13/.

ком случае, причина асимметрии деления заключается в трудности отрыва легко деформируемых симметричных осколков (например, из-за большей толщины шейки между легко деформируемыми осколками. Этот эффект не учитывался в работе / I3 /).

2. При делении нейтронами вблизи порога деления ($E_n \approx$ I,5 Мэв) энергия возбуждения осколков невелика: $E^*_{c\,o} \approx$ 3,5 Мэв ; $E^*_{a,o} \approx$ 6,5 Мэв. В момент, предшествующий отрыву, осколки являются "холодными".

3. Увеличение выхода симметричного деления с ростом энергии нейтронов можно описать только при выборе $a_c > a_a$. Это означает, что заполнение провала в массовом распределении осколков происходит вследствие того, что плотность уровней возбуждения у симметричных осколков возрастает с ростом энергии возбуждения быстрее, чем у асимметричных. Действительно, если $a_c > a_a$, то

$\rho_c \sim exp\, 2\sqrt{2a_c(E_n + \text{I,95 Мэв})}$ растет быстрее с E_n,

чем $\rho_a \sim exp\, 2\sqrt{2a_a(E_n + \text{5,I Мэв})}$.

Итак, статистический подход к делению объясняет результаты наших измерений и позволяет определить из них энергию возбуждения осколков в момент, предшествующий их отрыву.

Авторы выражают признательность Б.М.Гохбергу, Б.В.Курчатову и Г.А.Пик-Пичаку за полезные советы и обсуждения.

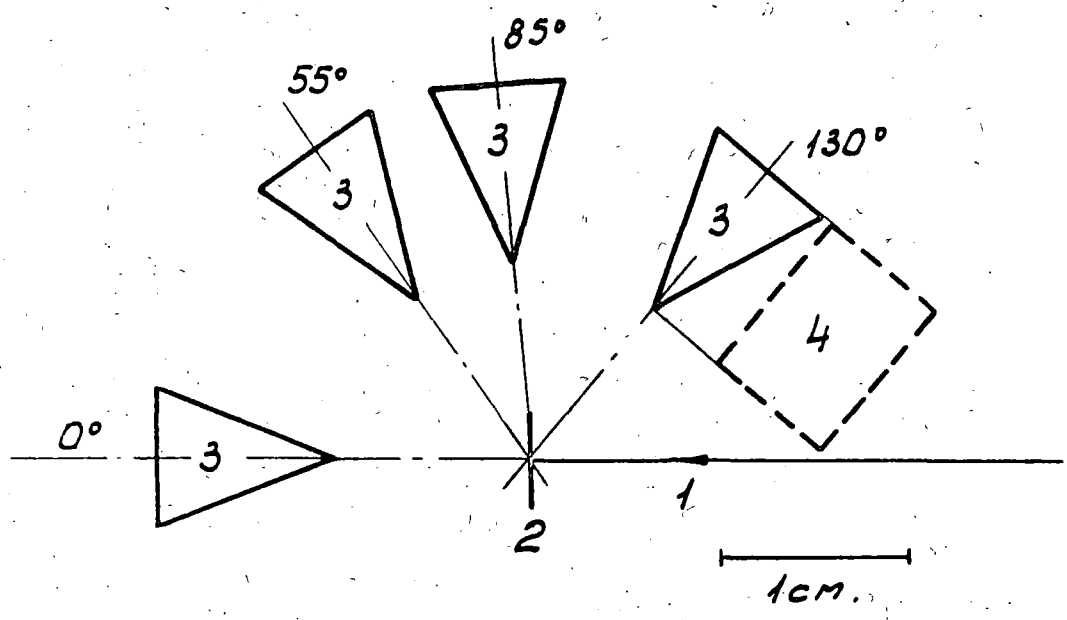

Рис.I. Геометрия облучения.

I. Коллимированный пучок ускоренных протонов или дейтонов.

2. Твердая дейтериевая или тритиевая мишень диаметром 0,5 см.

3. Образцы U^{238}.

4. Сечение одного из образцов плоскостью симметрии перпендикулярно чертежу.

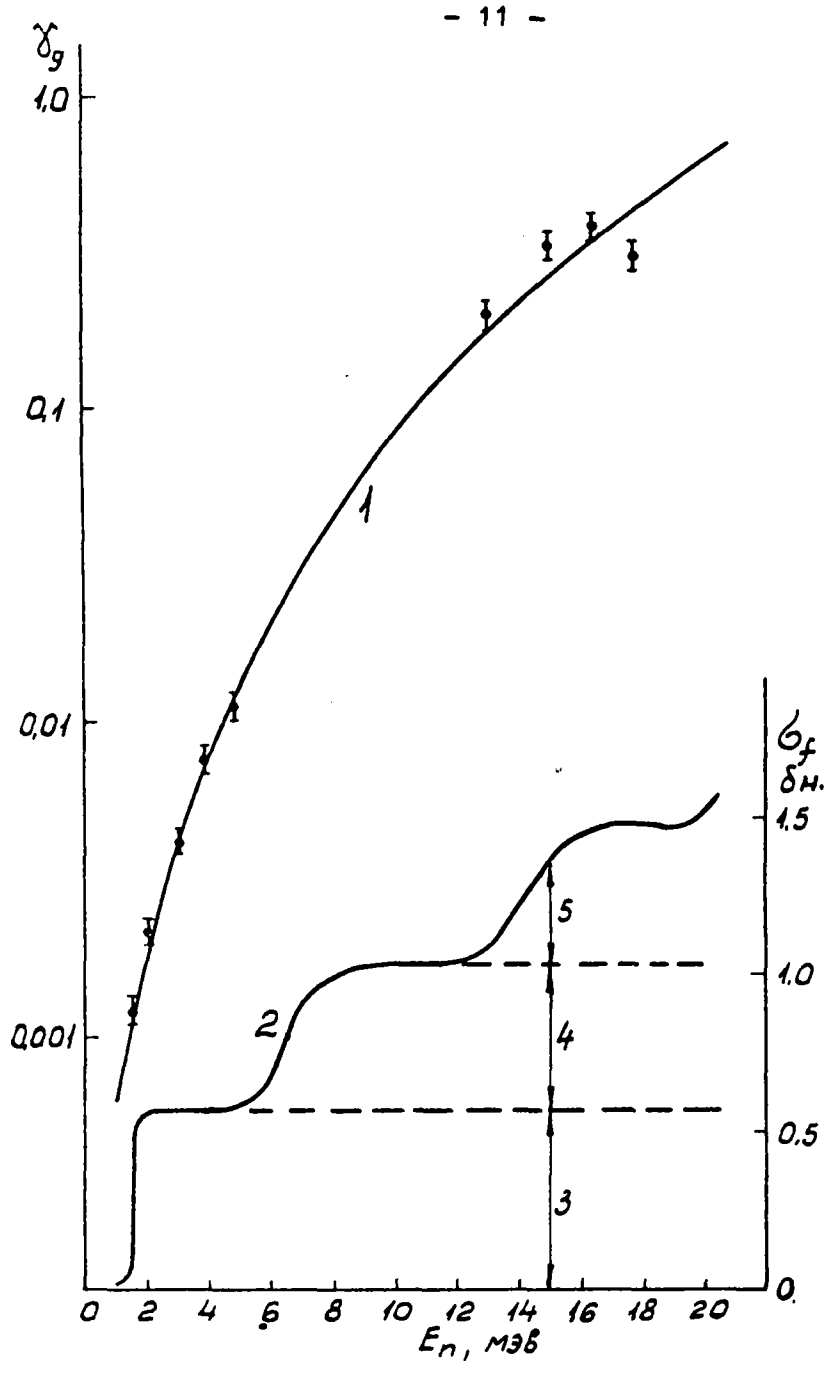

Рис.2.

1 - γ_g^P - отношения выходов симметричного и асимметричного делений U^{239} без предварительного испускания нейтронов согласно статистической теории деления.

I - значения γ_g, полученные из наших измерений. Указана ошибка измерений.

2 - полное сечение деления U^{238} нейтронами.

3,4,5 - сечения деления соответственно U^{239}, U^{238}, U^{237} без предварительного испускания нейтронов.

ЛИТЕРАТУРА

1. A. Turkevich, J.B Niday Phys. Rev. 84 (1951) 52.
P. Fong Phys. Rev. 102 (1956) 434
H. Faissner, K. Wildermuth, Nucl. Phys. 58 (1964) 177
Б.Т.Гейликман. "Атомная энергия" 6 (1959) 290,
В.А.Шигин. "Ядерная физика" 3 (1966) 756.
2. S. Katcoff, Nucleonics, 18, N11 (1960) 201.
Ю.А.Зысин, А.А.Лбов, Л.И.Сельченков. "Выходы продуктов деления и их распределение по массам". Сборник. Госатомиздат. Москва, 1963.
3. Борисова Н.И., Новгородцева В.И., Пчелин В.А., Шигин В.А. Ядерная физика 2, № 2 (1965), 243.
4. Б.М.Гохберг, Г.А.Отрощенко, В.А.Шигин. ДАН СССР 128 № 5 (1959) 911,
J.L. Fowler, J.E. Brolley, Rev. Modern Phys. 28 (1956) 103
5. В.К.Марков, Е.А.Верный, А.В.Виноградов, С.В.Елинсон, А.Е.Клыгин, И.В.Моисеев. Уран. Методы его определения. Атомиздат. Москва, 1964.
6. Radiochemical studies the fission products Book 3, Charles D. Coryell, Nathan Sugarman New York. 1951.
7. Р.М.Полевой, В.А.Пчелин. ПТЭ 1 (1963) 82.
8. В.М.Панкратов. "Атомная энергия" 14 (1963) 177.
D.J. Huges, Neutron Cross Sections, B.N.L.-325, 1958.
9. R. Vandenbosch, J.R. Huizenga, Proc. 2nd Conf Peaceful Uses Atomic Energy Geneva 1958, vol 15, p 284
10. P. Fong. Phys. Rev. 135, N6 B (1964) B 1338
P. Fong. Phys. Rev. 102 (1956) 436.
11. E. Erba, U. Facchini, E.S. Menichella, Nuovo Cimento, 22 (1961) 1237
12. J.C.D. Milton "Fission energy tables and an application to nuclear charge division", U.C.R.L. - 9883 Rev. 1962.
13. R. Vandenbosch, Nucl. Phys. 46 (1963) 129.

ИАЭ-1146. Зак.3936. Тир.515. 25.6.66г.
Отв.за выпуск Шигин В.А.

EVALUATION OF THE ELASTIC AND INELASTIC SCATTERING CROSS SECTIONS OF 14 MEV NEUTRONS FOR EVEN - EVEN NUCLEI.

L. Zuffi

Centro di Calcolo del C.N.E.N. - Bologna (Italy)

1. Introduction

In this paper some experimental results on the elastic and inelastic scattering of 14 MeV neutrons by collective nuclei are analysed in terms of a generalized optical model, with the target state described by phenomenological collective coordinates.

We assume weak coupling between the excited and the ground--state channels, i.e., the elastic scattering is assumed to be the most important process that occurs, so that the inelastic events can be treated as a perturbation.

In addition we use the adiabatic approximation, which is valid for the energies of the excited states, low compared to the energy of the incident beam.

2. The interaction potential

We describe the collective nature of the considered excited states in terms of rotational or vibrational deformations of the nuclear shape. The particle-nucleus interaction is described by an optical model potential $V(r,\vartheta,\varphi)$ of the following form

$$V(r,\vartheta,\varphi) = -(V+iW)\frac{1}{1+\exp\left[(r-R)/a\right]}$$

$$- 4iW_D \frac{\exp\left[(r-\bar{R})/\bar{a}\right]}{\left\{1+\exp\left[(r-\bar{R})/\bar{a}\right]\right\}^2} - V_{SO}(\vec{\sigma}.\vec{\ell})\lambda\!\!\!^{-}_{\pi}{}^2 \frac{1}{ar} \cdot$$

$$\frac{\exp\left[(r-R)/a\right]}{\left\{1+\exp\left[(r-R)/a\right]\right\}^2} \qquad (1)$$

($\lambda\!\!\!^{-}_{\pi}$ = π -meson Compton wave lenght)

where R and $\bar{R}$ depend on the polar angles ϑ and Φ .
We shall consider only a quadrupole deformation of the nucleus.
For vibrational nuclei R and $\bar{R}$ are given by

$$R = R_o(1+\sum_\mu a_{2\mu} Y_{2\mu}(\vartheta,\varphi))$$

$$\bar{R} = \bar{R}_o(1+\sum_\mu a_{2\mu} Y_{2\mu}(\vartheta,\varphi)) \qquad (2)$$

whereas for axially symmetric deformed nuclei

$$R = R_o(1+\beta_2 Y_{20}(\vartheta'))$$

$$\bar{R} = \bar{R}_o(1+\beta_2 Y_{20}(\vartheta')) \qquad (3)$$

Inserting the expressions (2) or (3) in (1), and expanding the potential to the first order in powers of $\sum_\mu a_{2\mu} Y_{2\mu}(\vartheta,\varphi)$ or $\beta_2 Y_{20}(\vartheta')$ respectively, we obtain

$$V(r,\vartheta,\varphi) = V_{diag} + V_{coupl} \qquad (4)$$

where

$$V_{diag} = -(V+iW)(1+e)^{-1} - 4iW_D\ \bar{e}(1+\bar{e})^{-2}$$
$$-V_{SO}(\vec{\sigma}\cdot\vec{\ell})(\lambda\!\!\!^{-2}/ar)\ e\ (1+e)^{-2} \tag{5}$$

$$V_{coupl} = V_{cp}^{(v)}(r)\sum_{\mu} a_{2\mu}\ Y_{2\mu}(\vartheta,\varphi) \tag{6}$$

or

$$V_{coupl} = V_{cp}^{(r)}(r)\ \mathcal{E}_2\ Y_{20}(\vartheta') \tag{6'}$$

and

$$e = \exp\left[(r-R_o)/a\right]$$
$$\bar{e} = \exp\left[(r-\bar{R}_o/\bar{a})\right] \tag{7}$$

$$V_{cp}^{(v)}(r) = V_{cp}^{(r)}(r) = -\left(\frac{\delta V}{\delta r}\right)_{\substack{R=R_o\\ \bar{R}=\bar{R}_o}} \tag{8}$$

Eqs.(6) and (6') refers to a vibrational and a rotational nucleus respectively. In (6') the angle ϑ' refers to the body--fixed system.

3. Scattering formalism

Let us consider now the Hamiltonian

$$H = T+H_t+V(r,\vartheta,\varphi) = T+H_t+V_{diag}+V_{coupl} \tag{9}$$

where T is the kinetic energy of the incident particle and H_t is the Hamiltonian for the internal motion of the target nucleus.

Since we use the adiabatic approximation, the term H_t will be neglected.

It is convenient to write the Hamiltonian of the Schrödinger equation

$$H\psi = E\psi \tag{10}$$

as a sum of two terms, namely an imperturbed Hamiltonian

$$H_o = T + V_{diag} \tag{11}$$

and a perturbation term

$$\lambda H_1 = V_{coupl} \tag{12}$$

where λ is a real parameter.

Then we have

$$H = H_o + \lambda H_1 \tag{13}$$

Expanding ψ to the second order

$$\psi = \psi_o + \lambda\psi_1 + \lambda^2\psi_2 \tag{14}$$

one has, as usual

$$\begin{cases} (H_o-E)\,\psi_o = 0 \\ (H_o-E)\,\psi_1 = -H_1\psi_o \\ (H_o-E)\,\psi_2 = -H_1\psi_1 \end{cases} \tag{15}$$

From the solution of Eqs.(15), explicit expressions for the elastic and inelastic scattering cross sections can be obtained in the usual way.

In particular, we have solved the Eqs.(15) in a fixed-body coordinate system, in which the z-axis is along the symmetry axis of the nucleus, to avoid coupling between partial waves with different projections of the angular momentum. Such a tecnique can be applied to β-vibrational or axially symmetric rotational nuclei.

It can be noted that for even-even vibrational nuclei the reduced matrix element [1], which appears in the expressions for the cross sections, is identical to those obtained for rotational nuclei.

For odd nuclei, if they can be considered to have a pure rotational or vibrational level structure, the scattering cross sections can be obtained in a very simple manner from the calculations performed for adiacent even-even nuclei, as it has been pointed out by Stelson [2].

This extension to odd nuclei is very useful if we want to compare the theoretical cross sections with the experimental ones, when even and odd isotopes are present in the target.

4. Analyses of experimental data

The following standard parameters [3],[4] for the interaction potential have been used for computations:

$$r = \bar{r}_o = 1,25 \text{ F} \qquad a = 0,65 \text{ F} \qquad \bar{a} = 0,47 \text{ F}$$

$$V_{SO} = 7.5 \text{ MeV} \qquad W = 0.0 \text{ MeV}$$

$$V = 46 \text{ MeV} \qquad W_D = 9.5 \text{ MeV}$$

The values of the quadrupole deformation β_2, used in analyses of the elastic and inelastic scattering cross sections (from the first excited states) for the elements considered, are given below

Element	β_2	Element	β_2
S^{28}	0.38	Ni	0.19
S^{32}	0.36	Zn	0.22
Cr	0.18	Sn	0.12

Results of calculations are shown in Figs. 1-3.
The source of the experimental data is Ref. [5].
As one can see the agreement between theory and experiments is rather good
Similar computations have been carried out by Stelson et al. [2], using the DWBA [6].
A comparison between the two methods is shown in Fig. 1, where the full line curves represent the results of our calculations for Si and S, in which the β-values were chosen to fit the data of Stelson [2] and Martin [7] respectively. The dashed line curves for the shape elastic cross section have been obtained assuming $\beta = 0$, so that they are identical to those which would be obtained by means of DWBA calculations.

ACKNOWLEDGMENTS - Our grateful thanks are due to Miss F. FABBRI who wrote the programme for the IBM 7094 computer.

REFERENCES

[1] Rose M.E., Elementary Theory of Angular Momentum (John Wiley and Sons, New York, 1957)

[2] Stelson P.H. et al., Nucl. Phys. 68 (1965) 97

[3] Perey F.G., Phys. Rev. 131 (1963) 745

[4] Tamura T., Rev. Mod. Phys. 37 (1965) 679

[5] CINDA - An Index to the Literature on Microscopic Neutron Data - EANDC 60 "U" + NYO-72-107 (1966)

[6] Bassel R.H. et al., Phys. Rev. 110 , (1958) 1080

[7] Martin P.W. et al., Nucl. Phys. 61 (1965) 524

This work has been performed under the auspices of EURATOM-CNEN Association for Fast Reactors.

The EURATOM-CNEN permission for the publication of this work is gratefully acknowledged.

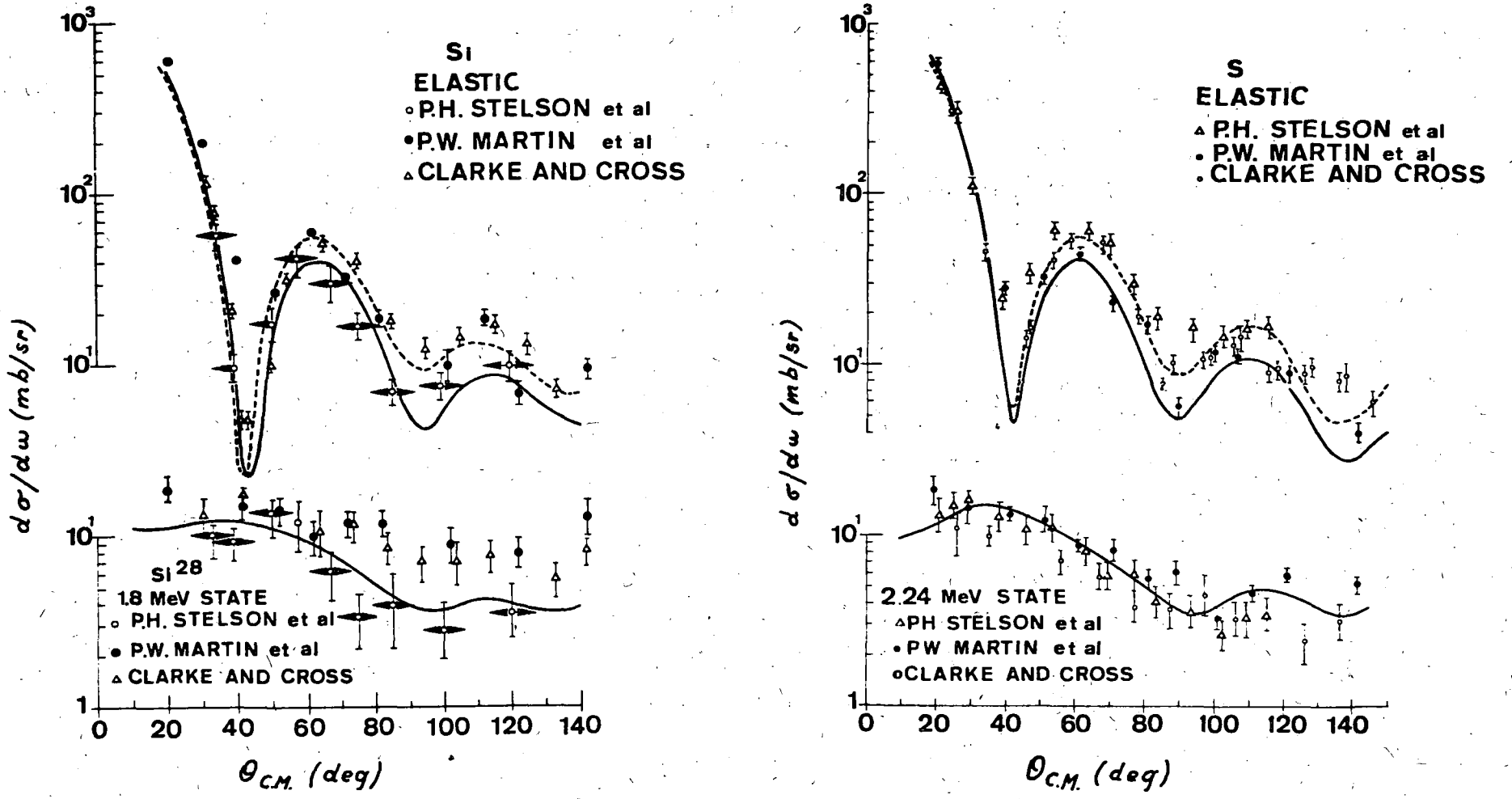

Fig. 1 Differential cross sections for the elastic and inelastic scattering to the 2^+ state in ^{28}S and ^{32}S. The full line curves represent the result of our theoretical calculations. The dashed line curves have been obtained assuming $\beta = 0$.

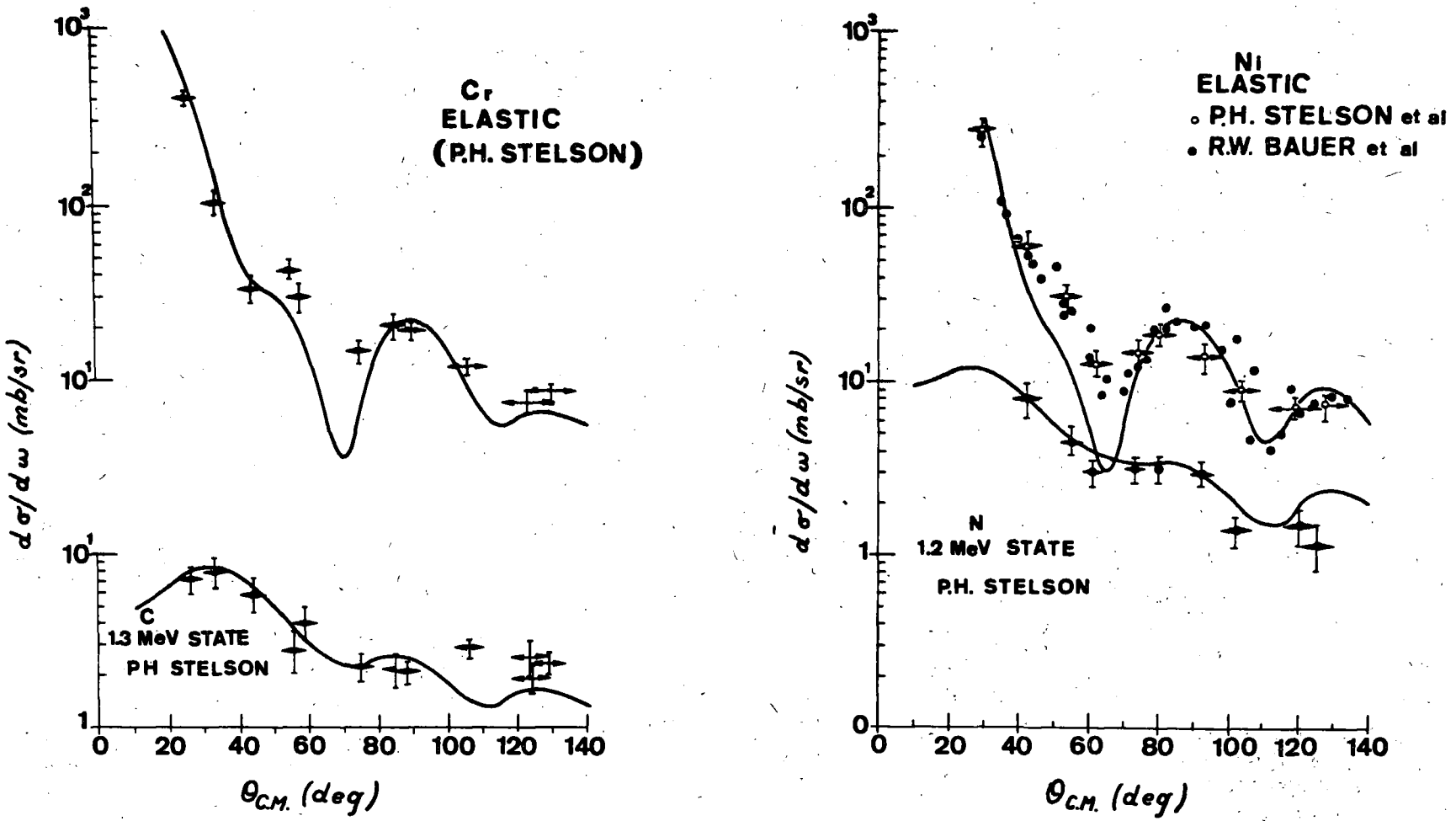

fig. 2 Differential cross sections for the elastic and inelastic scattering to the first excited state in Cr and Ni. The curves are the result of our theoretical calculations.

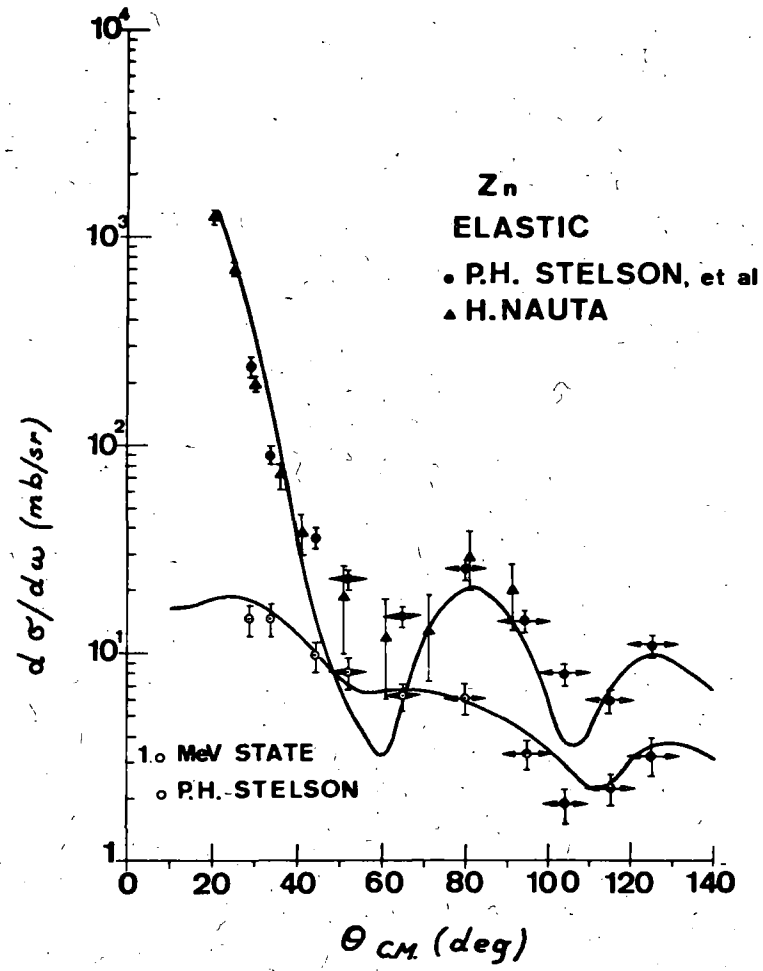

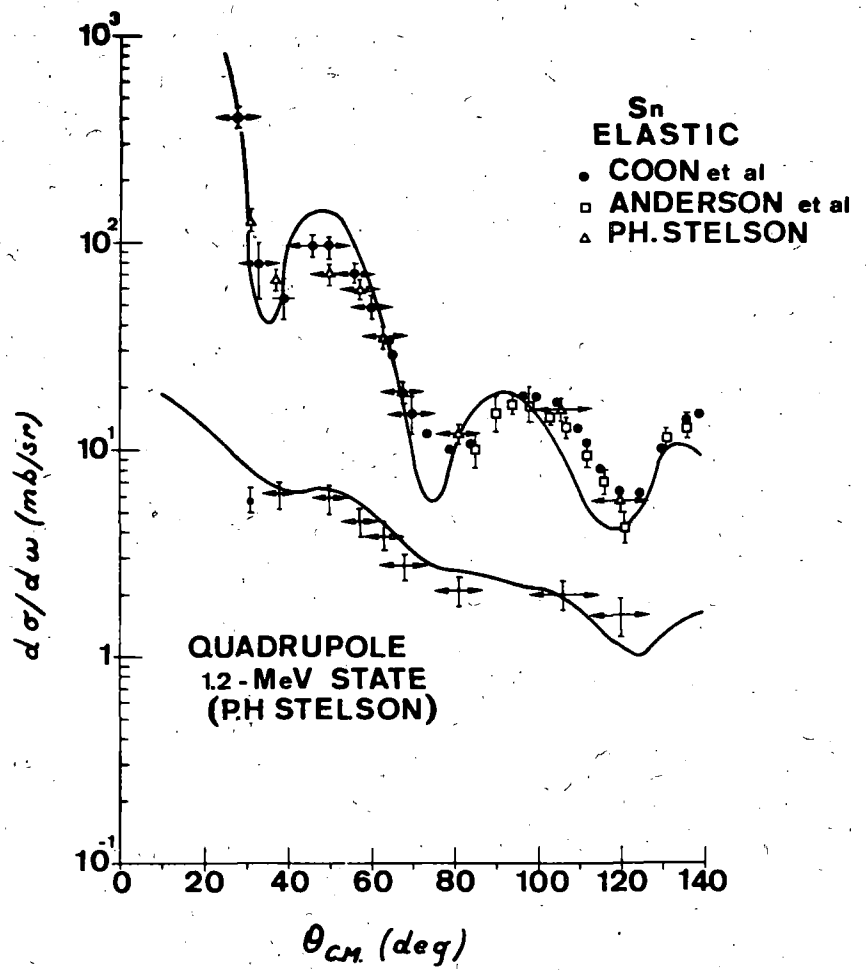

Fig. 3 Differential cross sections for the elastic and inelastic scattering to the first excited state in Zn and Sn. The curves are the result of the theoretical calculations.

ИНТЕГРАЛЬНЫЕ И ДИФФЕРЕНЦИАЛЬНЫЕ СЕЧЕНИЯ ДЕЛЕНИЯ Th^{232} НЕЙТРОНАМИ

С.Б.Ермагамбетов, Л.Д.Смиренкина, Г.Н.Смиренкин

ВВЕДЕНИЕ

Энергетическая зависимость сечений деления $\sigma_f(E_n)$ под действием нейтронов, как правило, обнаруживает довольно сложную структуру, которая особенно отчетливо проявляется у нечётных делящихся ядер в окрестности порога. Происхождение её было связано Уилером [1] с дискретностью спектра состояний переходного ядра и ядра-мишени, т.е. спектра каналов деления и неупругого рассеяния нейтронов. Из анализа интегральных σ_f и дифференциальных $\sigma_f(\vartheta)$ сечений деления для многих ядер удалось получить представление о характеристиках нижайших каналов деления [1 ÷ 6]. Каналовый анализ состоит в сопоставлении наблюдаемых сечений σ_f и угловых распределений осколков $W(\vartheta)=\frac{\sigma_f(\vartheta)}{\sigma_f}$ с теоретическими и подборе характеристик нижайших каналов деления, которые бы обеспечивали согласие между расчетом и экспериментом. В наиболее простой форме дифференциальное сечение деления $\sigma_f(\vartheta)$ может быть представлено для чётно-чётных ядер-мишеней, обладающих нулевым спином основного состояния:

$$\sigma_f(\vartheta)=\frac{\lambda\!\!\!^{-2}}{4}\sum_{J,\pi}(2J+1)\,T_\ell^J\,\frac{\sum\limits_{K\le J}\Gamma_f^{J,K,\pi}}{\sum\limits_{K\le J}\Gamma_f^{J,K,\pi}+\Gamma_n^{J,\pi}+\Gamma_\gamma}\,W_{JK}(\vartheta)\quad,\qquad(1)$$

где $\lambda\!\!\!^{-}$ – длина волны нейтрона, Γ_f, Γ_n, Γ_γ, – делительная, нейтронная и радиационная ширины, соответственно, ℓ –орбитальный момент нейтрона, J,K,π –полный угловой момент, его проекция

на ось ядра и четность состояния, через которое происходит деление, T_ℓ^J -коэффициент прилипания нейтронов, $W_{JK}(\vartheta)$ - угловое распределение осколков в канале с характеристиками J, K. $W_{JK}(\vartheta)$ и результирующее угловое распределение $W(\vartheta)$ нормированы так, что $\int W_{JK}(\vartheta)\sin\vartheta\, d\vartheta = 1$ и $\int \sigma_f(\vartheta)\sin\vartheta\, d\vartheta = \sigma_f$. Формула (1) упрощается дальше если делимость ядра, т.е. Γ_f/Γ_n, мала по сравнению с единицей. В этом случае в знаменателе (1) ширинами Γ_f и Γ_γ по сравнению с Γ_n можно пренебречь, а $\sigma_f(\vartheta)$ представить в форме :

$$\sigma_f(\vartheta) = \frac{\lambda^2}{4}\sum_{J,\pi}(2J+1)\frac{\sum\limits_{K\le J} P_{J,K,\pi}}{\sum\limits_{\ell' J'} T_{\ell'}^{J'}} \qquad (2)$$

Здесь использовано выражение $\Gamma_f^J = \frac{\bar{D}_J}{2\pi} P$ и $\Gamma_n^J = \frac{\bar{D}_J}{2\pi}\sum\limits_{\ell' J'} T_{\ell'}^{J'}$ через проницаемость соответствующего канала и $T_{\ell'}^{J'}$ -коэффициенты прилипания нейтронов неупругого рассеяния на доступные уровни ядра-мишени. Для барьера параболической формы

$$P = \frac{1}{1 + e^{\frac{2\pi}{E_{curv}}(B-E_n)}} \approx e^{\frac{2\pi}{E_{curv}}(E_n - B)}, \text{ если } B - E_n > \frac{E_{curv}}{2\pi} \qquad (3)$$

где B - высота барьера для данного канала деления, а E_{curv} -параметр, характеризующий его кривизну в максимуме.

В качестве объекта исследования было избрано ядро-мишень Th^{232}, для которого условия пригодности приближения (2) из всех доступных и удовлетворительно делящихся ядер выполнены лучше всего. Для Th^{233} канальный анализ производился Вилетсом и Чейзом [2], Хиттмайером [4], Струтинским [7], Люмиром [5], но с использованием весьма ограниченной информации. Авторы работ [2,4, 7] располагали данными о $W(\vartheta)$ всего

лишь для одного значения энергии нейтронов $E_n = 1,6$ Мэв [8]. В распоряжении Лэмфира имелись данные только для угловой анизотропии деления, т.е. отношения $\frac{W(0^0)}{W(90^0)}$. Во всех случаях анализ не затрагивал хода сечения деления, которое было известно при $E_n > 1,2$ Мэв, и не учитывая конкуренции нейтронов (предполагалось, что Γ_n от Y не зависит). Характеристики возбужденных уровней Th^{232} известны до 1,1 Мэв. В связи с этим в настоящей работе основное внимание было обращено на низкоэнергетический участок σ_f и $\sigma_f(\vartheta)$. Некоторые результаты измерения этих величин, а также следствия из их анализа сообщаются в данном докладе.

ИЗМЕРЕНИЯ

Измерения производились на электростатических генераторах Физико-энергетического института с использованием реакции $T(p,n)$ и твердых мишеней на титановой подложке. Малая величина измерявшихся сечений деления потребовала применения в опыте больших количеств делящегося вещества и умеренного энергетического разрешения. В опыте использовалась многослойная ионизационная камера деления, в которую было загружено около 4 грамм ThO_2. Полный энергетический разброс ΔE_n (ширина спектра нейтронов у основания) с увеличением E_n изменяется от 70 до 100 кэв. Экспериментально определялось отношение актов деления Th и естественного урана R в одинаковом потоке нейтронов. Ошибки результатов относительных измерений ΔR падают от 15% при $E_n \simeq 0,6$ Мэв до 3% в области "плато". Более подробно методика измерений описана в [9].

Абсолютизация зависимости от E_n $\sigma_f^{Th} \sim R \cdot \sigma_f^{V}$ производилась путём сравнения с данными [10]. Вследствие того, что энергетическое разрешение, достигнутое в данном опыте и в [10] различаются существенно, для привязки потребовались измерения σ_f в области E_n, достаточно удалённой от порога, где наблюдается относительное плавное изменение σ_f (E_n= 1,8÷2,0 Мэв и 2,5 ÷ 3,0 Мэв) и несоответствие в ΔE_n сказывается незначительно. На рис. 1 изображена полученная в данной работе зависимость σ_f от E_n в миллибарнах, нормированная таким образом, чтобы в указанных областях E_n отклонения от результатов работы [10] были бы минимальными.

Измерение угловых распределений осколков $W(\vartheta)$ производилось с помощью методики стекол [11, 12]. Схема опыта практически совпадает с применявшейся в работе [12] с той лишь разницей, что в настоящем опыте детектирование осколков производилось в 20 интервалах угла ϑ между 0° и 180° (вместо 14 в [12]) . На рис. 2 и 3 приведены некоторые результаты этих измерений (здесь числа отсчетов для углов ϑ и $180^o-\vartheta$ объединялись). Угловое и энергетическое разрешение в измерениях $W(\vartheta)$ составило : $\sqrt{\overline{(\vartheta-\bar{\vartheta})^2}} \simeq 4^o$, $\Delta E_n \simeq$ 90 кэв ($E_n \leq 1,3$ Мэв), $\Delta E_n \simeq 40$ кэв ($E_n > 1,3$ Мэв)

ОБСУЖДЕНИЕ

Наиболее примечателен с точки зрения каналового анализа участок E_n = 0,9÷1,2 Мэв, где наблюдается перегиб в ходе $\sigma_f(E_n)$ и резкое падение угловой анизотропии с ростом E_n. Это явление естественно связать с "насыщением" средней делительной ширины для нижайшего канала, которому следует

приписать характеристику $K = 1/2$, поскольку только $W_{J,1/2}(\vartheta) \neq 0$ при $\vartheta = 0^0$. По той же причине каналам, преобладающим в области нового подъёма σ_f / $E_n > 1,2$ Мэв / и ведущим к уменьшению $\frac{W(0^0)}{W(90^0)}$, отвечает характеристика $K > 1/2$. На рис. 2 с экспериментальными данными сравниваются распределения $W(\vartheta)$, рассчитанные с участием полос $K^{\pi} = 3/2^+$ и $3/2^-$. В расчётах, производившихся по формуле / 2 /, предполагалось, что вероятность деления от J не зависит / $P_{J,K,\pi} = P_{K,\pi}$ /, и игнорировалось расщепление по J между уровнями одной полосы, поскольку для переходного ядра $\frac{\hbar^2}{2J_\perp} \ll \frac{E_{curv}}{2\pi}$. Коэффициенты прилипания были рассчитаны с параметрами оптической модели Ауэрбаха и Мура [13], которые обеспечивают хорошее согласие с экспериментальными функциями возбуждения отдельных уровней в реакции Th^{232} / n, n' /. Отношения парциальных проницаемостей $\frac{P_{3/2;\pi}}{P_{1/2;\pi}}$, которым соответствует ход изображенных на рис.2 кривых, приведены в таблице 1. Характерные признаки угловых распределений осколков при делении через полосы $K = 3/2^+$ и $3/2^-$ при рассматриваемых E_n:

а/ $W(\vartheta)$ для $K = 3/2^+$, форму которого в основном определяет компонента $W_{5/2\,3/2}(\vartheta)$, имеет максимум при $\vartheta = 30 \div 40^0$

б/ у $W(\vartheta)$ при $K = 3/2^-$, форму которого в основном определяет компонента $W_{7/2\,3/2}(\vartheta)$, максимум смещается к $\vartheta \simeq 60^0$, а в области $60^0 < \vartheta < 90^0$ образуется провал, где $\frac{W(\vartheta)}{W(90^0)} < 1$.

Эксперимитальные распределения при $E_n = 1,1$ и $1,2$ Мэв, где вклад полос $K = 3/2$ ёще невелик, из-за ошибок опыта не позволяют отдать предпочтение какой-либо из комбинаций $K^{\pi} = 1/2^{\pm}$ и $K^{\pi} = 3/2^{\pm}$. Однако, данные при больших $E_n = 1,3$ и $1,4$ Мэв значительно лучше согласуются с качественными особенностями $W(\vartheta)$ для $K^{\pi} = 3/2^-$, хотя общее согласие расчёта с экспериментом ухуд-

шается. Последнее обстоятельство можно связать как с отсутствием сведений о каналах неупругого рассеяния нейтронов при $E_n > 1,1$ Мэв, так и с возможной неточностью приближения / $\frac{\hbar^2}{2J_1} \to 0$ /, принятого в расчётах. Однако, мы полагали, что на идентификацию K^{π} каналов, преобладающих в области $E_n = 1,2 \div 1,4$ Мэв, отмеченные факторы сколько-нибудь существенно повлиять не могут.

При ещё больших $E_n = 1,5$ и 1,6 Мэв характер $W(\vartheta)$ снова изменяется - максимум смещается в область больших углов. Такой ход $W(\vartheta)$ типичен для полосы $K = 3/2^+$. Интересно, что он проявляется в области нового подъема σ_f / см. рис. 1 /. Результаты наших измерений при $E_n = 1,6$ Мэв существенно отличаются от данных Хенкеля и Бролли [8]. Соответственно и идентификация преобладающих каналов приводит к иному результату : анализ прежних результатов давал $K^{\pi} = 3/2^-$ [2,4].

Определить чётность нижайшего канала, доминирующего при $E_n < 1,2$ Мев, пользуясь имеющимися данными о $W(\vartheta)$ трудно / см. рис.2/ : результаты эксперимента в пределах точности опыта примерно одинаково согласуются с предположением $\pi = \pm 1$ для $K=1/2$. Это конечно не значит, что отсутствует принципиальная возможность установления чётности этой полосы по $W(\vartheta)$, для этой цели необходимы данные при $E_n < 1,1$ Мэв. Угловое распределение при $E_n = 1,1$ Мэв описывается в предположении только одной полосы $K = 1/2^+$: $\frac{P_{3/2}^{\pi}}{P_{1/2}^{+}} = 0$, $\frac{W(0^\circ)}{W(90^\circ)} = 2,4$, тогда как для чистой полосы $K = 1/2^-$ $\frac{W(0^\circ)}{W(90^\circ)} = 3,6$. Таким образом, если при $E_n < 1,1$ Мэв анизотропия заметно возрастёт, то $\pi = -1$, если наоборот, то $\pi = +1$.

Интересующую нас характеристику в принципе можно определить и путём сравнения средних делительных ширин на S - нейтронах с энергией E_n в той области, где ожидается преобладание нижайшего канала с $K = 1/2$. Деление чётно-чётного ядра-мишени S-нейтронами происходит через каналы с единственным набором / J, K, π /:

$J = K = 1/2$, $\pi = +1$. Тогда, если $\Gamma_f^{наблюд}(E_n)$ сравнима по величине с шириной, экстраполированной согласно /3/, $\Gamma_f^{экстр.}(E_n) = \Gamma_f^S e^{\frac{2\pi E_n}{E_{curv}}}$ то $\pi = +1$, если $\Gamma_f^{экстр.} \ll \Gamma_f^{наблюд.}$, то у нижайшего канала либо $\pi = -1$, либо $K \neq 1/2$, а каналы с $K = 1/2^+$ открываются при более высоких E_n. Для Th^{232} известно сечение деления тепловыми нейтронами $\sigma_f^T = 0{,}06 \pm 0{,}02$ мбарн [14], откуда $\Gamma_f^S = \Gamma_\gamma \frac{\sigma_f^T}{\sigma_\gamma^T} = 2{,}5 \cdot 10^{-7}$ эв, где $\Gamma_\gamma \simeq 3\ 10^{-2}$ эв -радиационная ширина и $\sigma_\gamma^T = 7{,}4$ барн -сечение радиационного захвата [15]. Принимая величину $\frac{E_{curv}}{2\pi} = 0{,}06$ Мэв [9], которую легко оценить на участке крутого роста σ_f, где Γ_f изменяется во много раз быстрее, чем Γ_n (см.рис.4), получим для $E_n = 0{,}7$ Мэв : $\Gamma_f^{экстр.} = 3 \cdot 10^{-2}$ эв. Можно показать, что вклад состояний $J = 1/2$ в предположении $K^\pi = 1/2^+$ при $E_n = 0{,}7$ Мэв составляет приблизительно половину наблюдаемого сечения $\sigma_f = 4$ мбарн. Тогда согласно (2), получим $\Gamma_f^{наблюд}(E_n) \simeq \frac{2\sigma_f}{\pi \lambda^2}\left(\sum_{l'J'} T_{l'}^{J'}\right)_{1/2^+} \cdot \frac{E_{1/2}}{2\pi} \simeq$ $\simeq 3 \cdot 10^{-6}$ эв. Получившееся расхождение $\Gamma_f^{наблюд.}$ и $\Gamma_f^{экстр.}$ объяснить трудно [9]. Ожидаемое в предположении для нижайшего доступного канала $K^\pi = 1/2^+$ значение σ_f^T оказалось в 10^4 раз меньше указанного в работе [14]. Для нас здесь важно лишь то, что предположение о любом другом K^π будет означать еще большее расхождение.

Наконец, представление о чётности нижайшего канала можно получить из сопоставления энергетических зависимостей сечения деления и нейтронной ширины. В этом плане большое значение приобретает излом σ_f в районе 0,75 Мэв, где ожидается вступление каналов реакции (n, n'), связанных с уровнями ядра Th^{232} 0,725 Мэв (0^+), 0,775 Мэв (2^+) и 0,788 Мэв (2^+) Такой эффект может возникнуть лишь в том случае, когда скорости изменения Γ_n и Γ_f сравнимы. Очевидно, что наблюдаемый

на опыте результат конкуренции Γ_n и Γ_f можно связать только с испусканием S - нейтронов. Но конкуренция процессов (n,f) и (n,n') с испусканием S - нейтронов и возбуждением уровней ядра-мишени положительной чётности возможна лишь в том случае, если деление происходит через полосу каналов также положительной чётности. Эти соображения, приведшие к установлению $K^{\pi} = 1/2^{+}$ нижайшего канала реакции Th^{232} (n,f), иллюстрируются на рис. 4 результатами расчётов величины $\frac{2\pi\Gamma_n^{J\pi}}{D_J} = \sum_{\ell' J'} T_{\ell'}^{J'}$ для состояний составного ядра $J = 1/2$, $3/2$, $5/2$, $7/2$ обеих четностей. Вкладом слагаемых с $J > 7/2$ в (2) из-за малости T_{ℓ}^{J} можно пренебречь. Характер приведенных на рис.4 кривых для $\pi = +1$ и $\pi = -1$ отличается очень сильно, что весьма существенно для определенности принятой идентификации.

Таким образом, предпринятый в настоящей работе анализ приводит к следующей последовательности K^{π} нижайших каналов переходного ядра Th^{233}, возбуждаемых в реакции Th^{232}(n,f) нейтронами с $E_n < 1,6$ Мэв : $1/2^{+}$, $3/2^{-}$, $3/2^{+}$. Кроме того на участке $E_n > 1,2$ Мэв наряду с каналами $K = 3/2^{-}$, по-видимому, включаются новые каналы с $K = 1/2$. Если мы предположим, что вероятность деления σ_f (0°) при $E_n > 1,2$ Мэв связана с той же полосой $K = 1/2$, которая преобладает при $E_n < 1,1$ Мэв, то получим дальнейшее возрастание $\Gamma_f^{1/2^{+}}$ вместо насыщения, предположенного нами для объяснения перегиба σ_f в районе $E_n \simeq 1,1$ Мэв. Объяснить происхождение последнего только конкуренцией неупругого рассеяния нейтронов на уровни 1,045 Мэв (1^{-}) и 1,095 (3^{-}) по причинам, обсуждавшимся выше,

не удается. Лемфир [5] ,располагавший меньшей информацией и производивший идентификацию каналов в основном эвристическим путём, на указанном интервале E_n выделил лишь две полосы $K^{\pi} = 1/2^+$ и $3/2^-$. Участие большего числа каналов в делении нечётного ядра разумно -оно лучше соответствует гипотезе О.Бора [16] о подобии спектра каналов деления спектру состояний равновесных ядер.

ТАБЛИЦА 1

E Мэв	$\frac{P_{3/2^+}}{P_{1/2^+}}$	$\frac{P_{3/2^+}}{P_{1/2^-}}$	$\frac{P_{3/2^-}}{P_{1/2^-}}$	$\frac{P_{3/2^-}}{P_{1/2^+}}$
1,100	0 *)	0,7732	0,3836	0 *)
1,200	0,8315	2,2980	1,0998	0,3914
1,300	1,5124	3,9022	1,7203	0,9430

*) при E = 1,1 Мэв эксперимент оказался в согласии с расчетом для чистой полосы с $K = 1/2^+$, соответствующая кривая на рис. 2 обозначена значком (e).

ЛИТЕРАТУРА

1 - J.A.Wheeler Channel Analysis of Fission. In „Fast Neutron Physics". Part II., N.Y. Interscience Publ., 1963, p.2057

2 - L.Wilets, D.M. Chase Phys.Rev. 103, 1296 (1956)

3 - R.W. Lamphere Nucl. Phys. 38, 561 (1962)

4 - O.Hittmair Nucl. Phys. 18, 346 (1960)

5 - R.W.Lamphere Symposium on the Physics and Chemistry of Fission. Salzburg, 1965, IAEA, SM-60/7

6 - П.Е.Воротников, С.М.Дубровина, Г.А.Отрощенко, В.А.Шигин Ядерная физика 3, 479 (1966)

7 - В.М.Струтинский ЖЭТФ 39, 781 (1960)

8 - R.L. Henkel, J.E.Brolley Phys. Rev. 103, 1292 (1956)

9 - С.Б.Ермагамбетов, В.Ф.Кузнецов, Г.Н.Смиренкин. Ядерная физика /в печати/.

10 - D.J.Hughes, R.B.Schwartz BNL-325 (1958)

11 - В.П.Перелыгин, С.П.Третьякова, И.Звара ПТЭ № 4 (1964) 78

12 - А.С.Солдатов, З.А.Александрова, Л.Д.Смиренкина, Г.Н.Смиренкин. Ядерная физика 1, 471 (1965)

13 - E.N.Auerbach, S.Moore Phys. Rev. 135, 413 (1964)

14 - Е.И.Корнеев, В.С.Скобкин, Г.Н.Флеров ЖЭТФ 37, 41 (1959)

15 - И.В.Гордеев, Д.А.Кардашев, А.В.Малышев. "Ядерно-физические константы". М, Госатомиздат. 1963.

16 - О.Бор. Материалы Международной конференции по мирному использованию атомной энергии. Женева, 1955г. т.2, М, Физматгиз, 1958 стр.175.

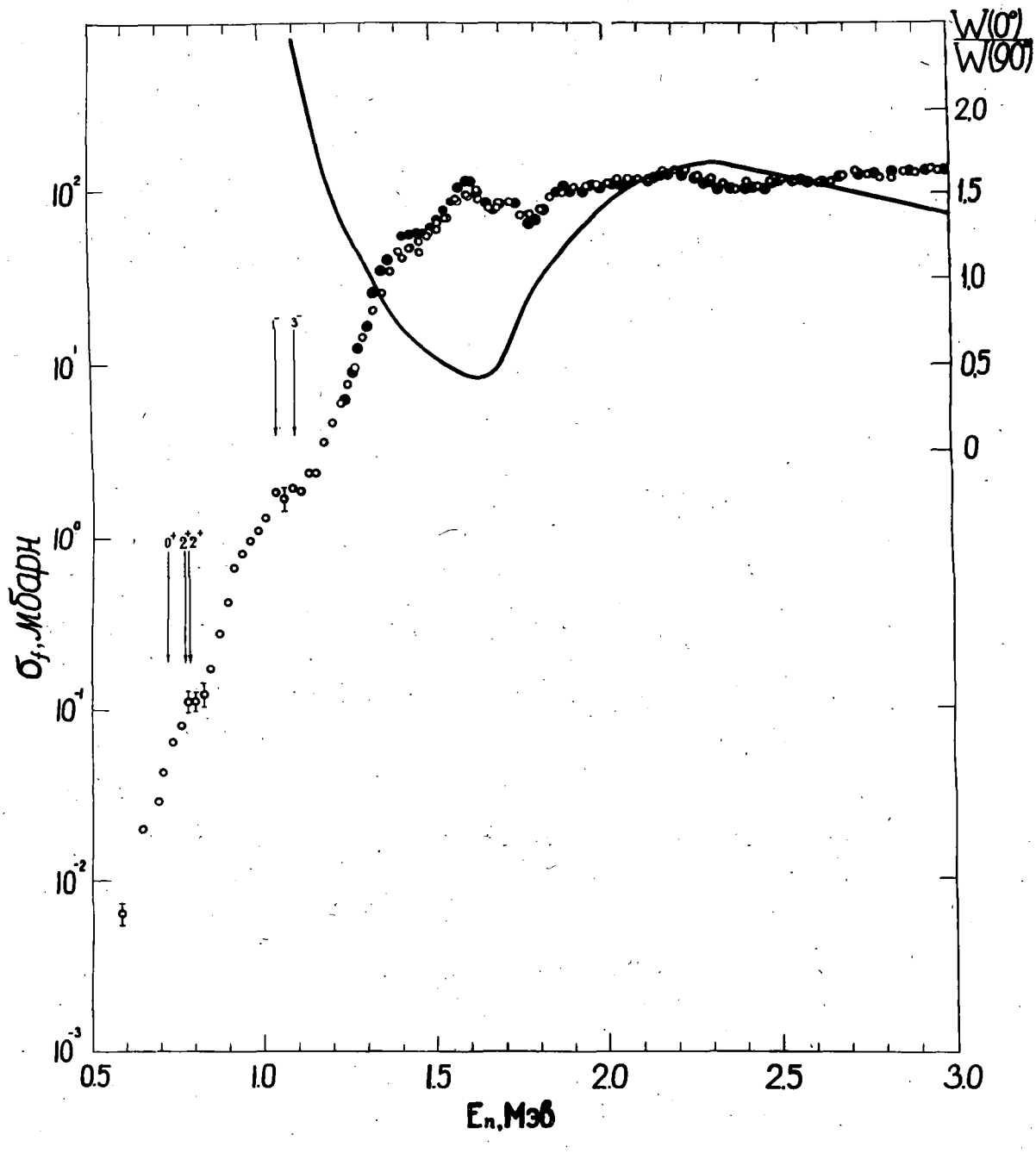

Рис. 1 Энергетические зависимости сечения σ_f и угловой анизотропии $W(0°)/W(90°)$ деления Th^{232} нейтронами ○ -данные σ_f настоящей работы, ● - [10]; сплошная кривая описывает данные $W(0°)/W(90°)$ [5], [8] и настоящего опыта.

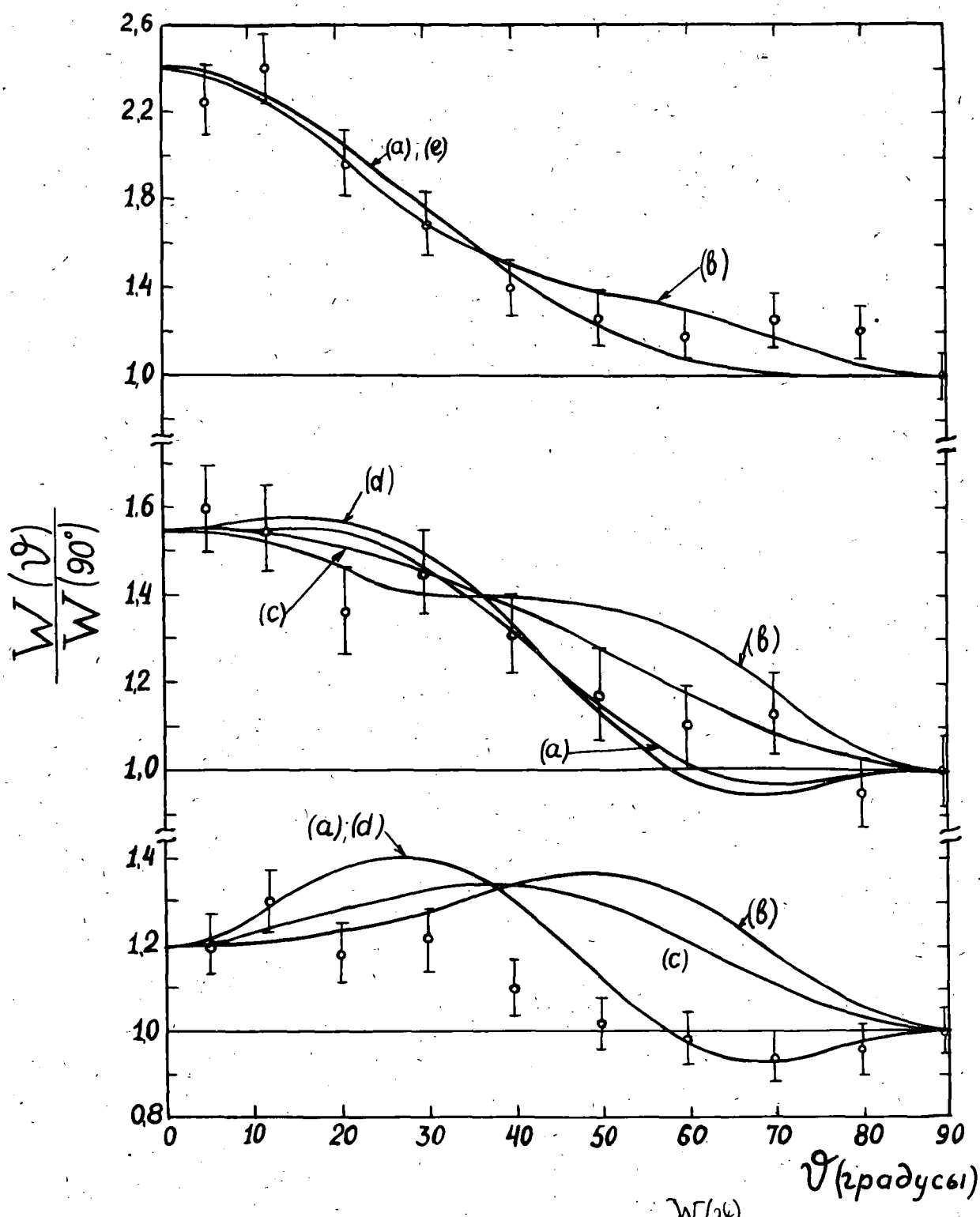

Рис.2 Угловые распределения осколков $\frac{W(\vartheta)}{W(90°)}$ при E_n=1,1Мэв (сверху), 1,2 Мэв (посередине), 1,3 Мэв (внизу). Кривыми показаны распределения, рассчитанные для различных комбинаций полос K^{π}, участвующих в делении: (a)-$1/2^-$ и $3/2^-$, (в) - $1/2^-$ и $3/2^+$; (c)-$1/2^+$ и $3/2^+$, (d) - $1/2^+$ и $3/2^-$, (e)-чистая полоса с $K=1/2^+$ в верхней части рисунка (см.текст и таблицу).

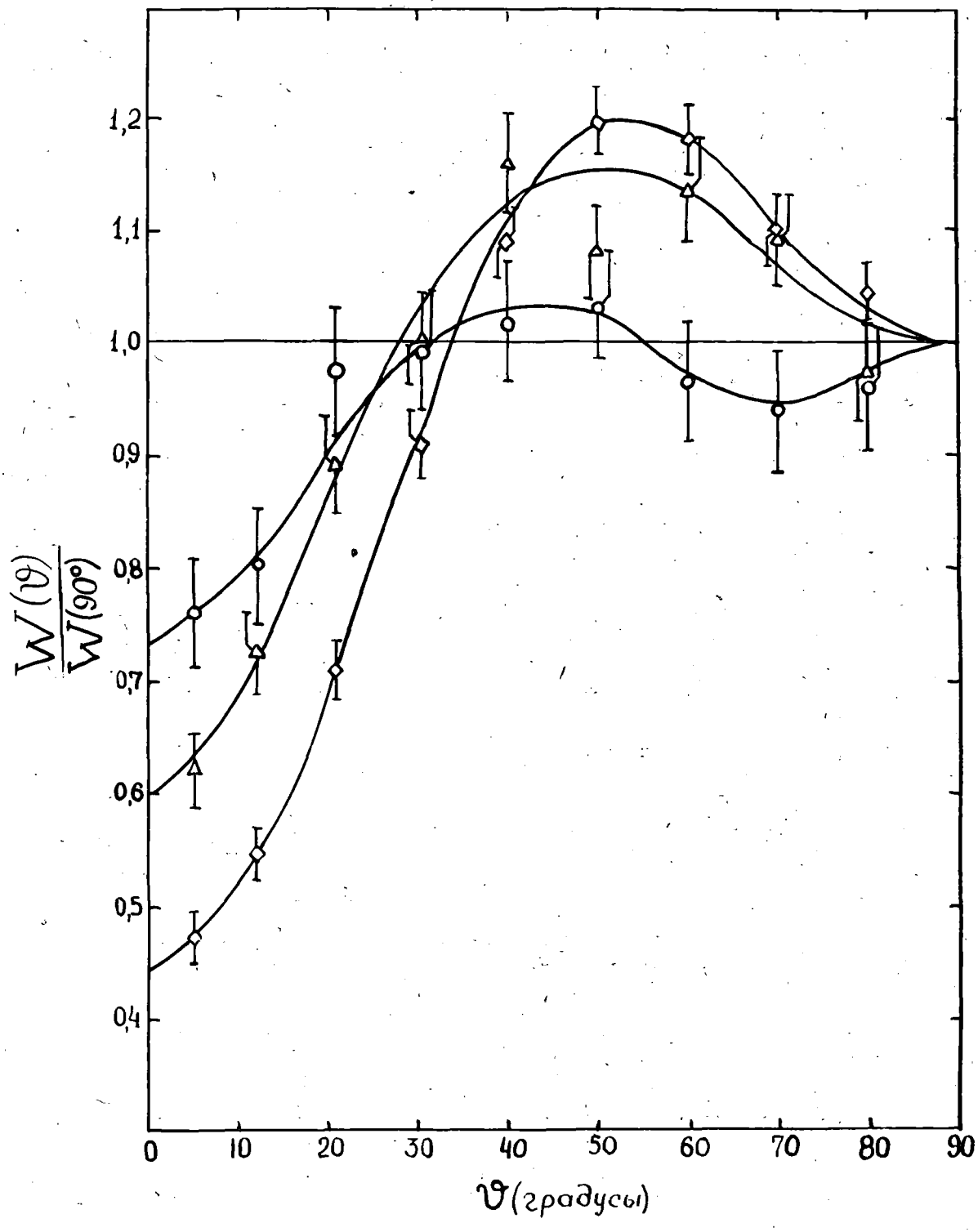

Рис.3 Угловые распределения осколков $\frac{W(\vartheta)}{W(90°)}$ при E_n=1,4Мэв - **O** ; E_n= 1,5 Мэв - Δ; E_n= 1,6 Мэв - ◊ .

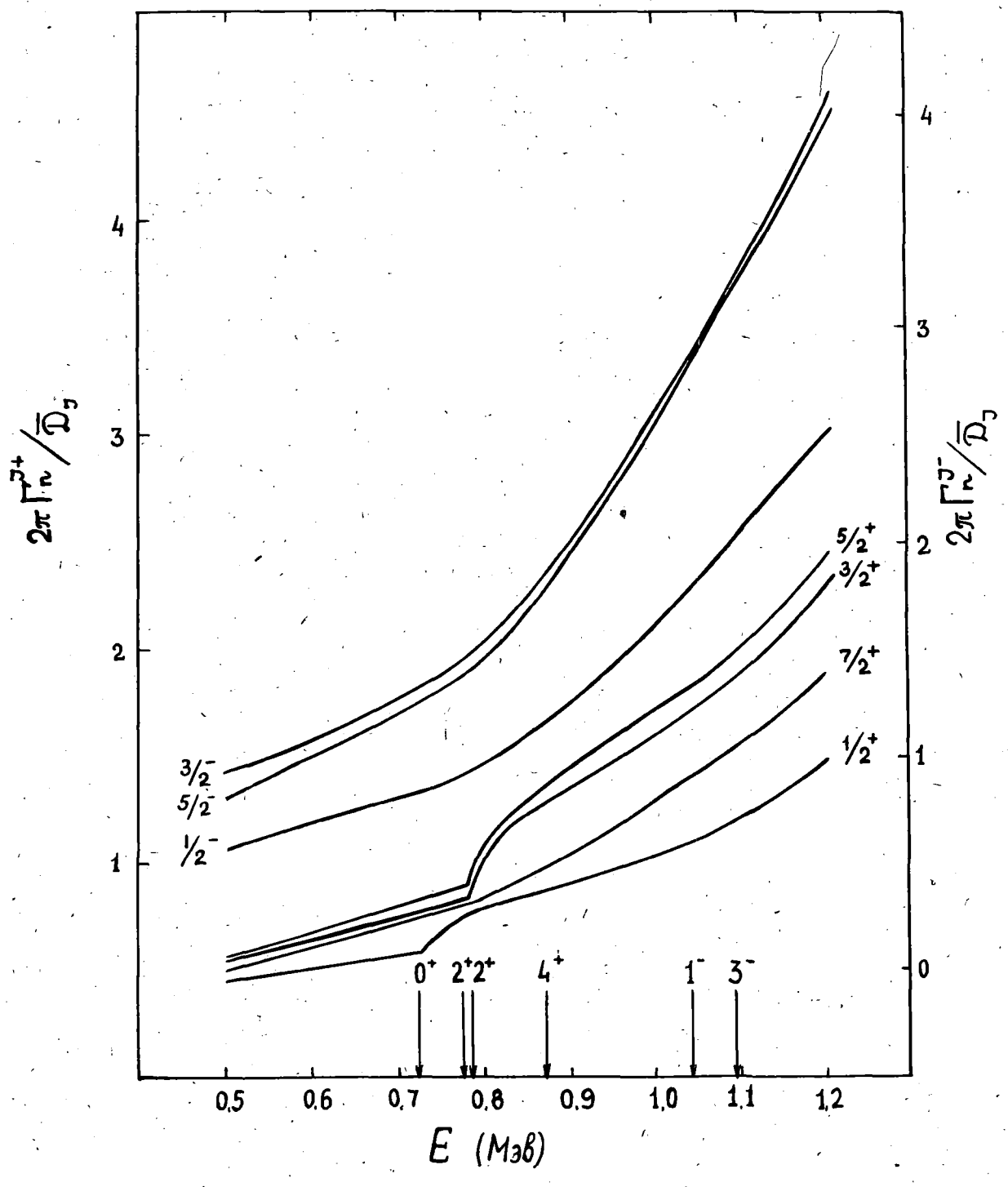

Рис.4 Энергетическая зависимость $2\pi\Gamma_n^{J\pi}/\bar{D}$ для обеих четностей состояний составного ядра Th^{233} Стрелками показаны возбужденные уровни ядра-мишени Th^{232}.